Studies of Bioactive Natural Products and Mechanism-Based Bioassays

Jason Anderson Clement

Dissertation submitted to the faculty of the Virginia Polytechnic Institute and State University in partial fulfillment of the requirements for the degree of

Doctor of Philosophy
In
Chemistry

Dr. David G. I. Kingston, Chairman
Dr. Paul R. Carlier
Dr. Harry C. Dorn
Dr. Richard D. Gandour
Dr. James M. Tanko

November 16, 2005
Blacksburg, VA

Keywords: isomalabaricane, triterpenoids, sesterterpenoids, dereplication, Chk1.

Copyright 2005 Jason Anderson Clement

Studies of Bioactive Natural Products and Mechanism-Based Bioassays

Jason Anderson Clement

ABSTRACT

An extract of the sponge *Rhabdastrella globostellata* was active in an assay measuring stabilization of the binding of DNA with DNA polymerase β. From this extract, four isomalabaricane triterpenoids were isolated and characterized, three of which were active in the binding assay. All compounds were active in the A2780 ovarian cancer cell line assay.

Bioassay-guided fractionation of an extract of a sponge of species *Dysidea* using the A2780 bioassay yielded the known scalarane sesterterpenoid heteronemin in good yield. Four derivatives of heteronemin were prepared semisynthetically from the natural product, tested for their bioactivity, and their structure-activity dependence was observed.

Bioassay guided-fractionation of an extract of a *Tuemoya* sp. green alga, using an assay for inhibitors of the enzyme Tie2 kinase, afforded a two sulfated cycloartanol triterpenoids. Both the major and minor compounds were identified by spectroscopic methods.

Bioassay-guided fractionation of an extract of *Petalonyx parryi* yielded three known oleanane triterpenoids which inhibited the lyase domain of DNA polymerase β. The structures were confirmed by NMR spectroscopic techniques. This is the first reported study of the chemical components of *Petalonyx parryi.*

As part of our antitumor natural product drug discovery efforts, several extracts were selected for bioassay-guided fractionation based on their activity in initial *in vitro* screens. A new dereplication method using aminopropyl SPE cartridges was applied to

six of these extracts, and four of the extracts were dropped due to the presence of long-chain fatty acids (LCFAs). We present results for the testing and application of this SPE-based method for LCFA dereplication.

The cell cycle kinase Chk1 is an interesting target for the development of agents which might potentiate DNA damaging agents. Typical assays for Chk1 involve the use of expensive or radioactive reagents. To facilitate the development of new assays using shorter peptide substrates, small libraries of peptides have been synthesized and tested for their activity as Chk1 substrates. Several of the substrates synthesized displayed activity in the Chk1 assay.

Acknowledgements

Many people have positively contributed to my endeavors here in Blacksburg. I would first like to thank my advisor, Dr. David G.I. Kingston, for giving me the opportunity to work in his laboratory here at Virginia Tech. I also thank Dr. Kingston for his guidance throughout my time here, both professional and personal. I am one of many people who has benefited in multiple ways from his influence and work both at Virginia Tech and in the community in Blacksburg.

I would also like to thank the other members of my committee, Professors Paul R. Carlier, Harry C. Dorn, Richard D. Gandour, and James M. Tanko, for their assistance and guidance during my time here. I would especially like to thank Dr. Sidney Hecht and his group at the University of Virginia for our collaborative effort through a National Cooperative Drug Discovery Group grant that has made this research possible. This collaboration has fostered in me the desire and commitment to improve the cancer chemotherapy arsenal. I am also grateful to the Department of Chemistry at Virginia Tech for their support of research and for providing me with teaching assistantships at various times. The faculty in this department genuinely care about the success of their graduate students, independently of group membership. I also thank Mr. Tom Glass, Mr. Bill Bebout, and Mr. Kim Harich for their assistance in acquiring spectroscopic data.

I would like to thank the members of the Kingston research group who have helped me over the years. This includes Dr. Bing-Nan Zhou, who taught me much about isolation work; Dr. Shugeng Cao, who has stirred me to aim higher in natural products research and has had many helpful conversations with me; Mr. Russell Williams, who has helped me to find better ways to do natural products research; Mr. Brent Yoder, who

has been a good friend and colleague during our time here; and Dr. Thota Ganesh, who has been of help with synthetic questions over the years. I also appreciate the work of Ms. Jeannine Hoch, Mrs. Jennifer Schilling, and Mr. Andrew Norris for their help with in-house bioassay work.

I also would like to thank my parents for their support over the years, and for preparing me for life. They provided an environment where I could learn, but they also taught me the importance of making a positive difference in the lives of people. I would like to thank my wife, Ella, who has supported me so much over the years. She has been a constant help and encouragement in all aspects of life and work since I have known her. I would like to thank the folks in the Graduate Christian Fellowship and at Blacksburg Christian Fellowship who have been good friends and have offered wise counsel over the years, especially Mr. Tom Oster, Dr. Jim Krouscas, and Mr. Kevin Duffy. Finally, I would like to give thanks to God for bringing me to Blacksburg. I have learned much about the importance of Christian community since I have been here, more than I ever imagined I would.

This work is dedicated to all people and families who have suffered from cancer.

…In the world ye shall have tribulation: but be of good cheer; I have overcome the world.

John 16:33

Authors who always refer to their works as "my book, my commentary, my history," sound like solid citizens with their own property who are always talking about "my house." They would be better to say: "our book, our commentary, our history," seeing that there is usually more of other people's property in it than their own.

Blaise Pascal

Table of Contents

List of Figures

List of Tables

List of Schemes

I. Introduction to Antitumor Natural Products Drug Discovery

1.1 Introduction

Long ago, people discovered that the natural setting around them yielded useful substances beyond those necessary for the diet. It was recorded in the book of Genesis how Noah made wine from grapes. Hippocrates gave his patients willow bark to chew, to soothe their pains. Even before primitive hunter-gatherers developed agriculture, there have been some people who have made a point to understand how to harness the power of the mysterious chemicals found all around. Thus, natural products chemistry was born. In the past two centuries, natural products chemistry has come into its own as a bounteous source of interesting and useful chemicals. Modern scientists have succeeded in treating many of the diseases of humanity by utilizing naturally occurring chemicals. As our knowledge of the intimate workings of chemicals and cell structures has grown, natural products chemistry continues to contribute to drug development.

This chapter will review the history of anticancer natural products drug discovery and the rationale for the continued investigation of natural products. We will review the most important natural products in clinical use for the treatment of cancer, as well as natural products which have entered clinical drug trials or have sparked significant interest as potential drugs. We will briefly describe the methods used to identify compounds with interesting biological activity, setting the stage for understanding the usefulness of the mechanism-based approach to natural products drug discovery.

As industrial cultures thrive, the common diseases of the agrarian past have been replaced by new threats. Cancer is one disease that has become a huge burden on

industrialized nations of the world. Cancer can attack in many different ways, and it varies in lethality. The suffering and pain of cancer patients is very serious, and exacts an emotional toll on both the patient and those around them. Cancer is a disease that can justifiably receive our full attention in efforts to eradicate it. Cancer strikes many cell types in the human body. The words tumor and cancer are often used interchangeably; the word tumor refers to a clump of abnormal cells. The word cancer refers more to the state of being of a patient having malignant tumors in their body. Thus, in drug discovery, potential drugs with *in vitro* cytotoxic effects in tumor cell line assays are often referred to as antitumor agents, since they have proven ability to kill tumor cells, but no proven *in vivo* activity. Drugs that have been shown to have good *in vivo* activity against tumors are often called anticancer agents.

Because of their inherent invasiveness, tumor masses can eventually take over an organ in which they are growing, impairing proper organ function.[1] Tumor cells can also break away from their point of origin and take hold in another organ of the body through the process of metastasis. This can lead to tumor growth in an otherwise healthy organ. Once a tumor is determined to be a threat to a patient, a range of treatment options are available. The ultimate goal of treatment is to hold the tumor in check or destroy the tumor. Thus, the patient's body will show a total response to therapy and the patient can live normally. Tumors may have a range of responses to therapy, and these responses can depend on the type of tumor involved and the treatment methods used. Likewise, potential antitumor agents and established anticancer drugs are often have selective activity towards some tumor types. Liver, pancreatic, and lung cancers are some of the more pernicious forms of cancer, with very low survival rates.

Currently, many antitumor compounds have already been discovered, and many have already entered clinical usage in treating cancer. Such chemotherapy is often ineffective in the long run. Many times, the toxicity of the chemotherapy is harmful to the patient. Tumors can relapse if a remission is not complete, leading to the death of the patient from what might be a more resistant tumor. In order to overcome the problems and shortcomings of current chemotherapy, the quest for more potent and selective drugs continues.

1.2 Rationale for Studying Natural Products

The term "natural product" is used to refer to compounds produced by living organisms as secondary metabolites. Primary metabolites include compounds required by an organism for survival and metabolic activity, such as glucose or DNA. Secondary metabolites are compounds that are not directly required by the organism to maintain functionality. Primary metabolites tend to be ubiquitous and do not offer novelty in structure or function. Secondary metabolites, on the other hand, are not as widespread. Potentially, so long as our knowledge of plant, animal, and microbial species continues to grow, our ability to discover novel secondary metabolites is likely to continue.

There are several principal reasons for studying natural product sources in a search for antitumor agents. The first reason is that Nature has a proven track record of yielding chemicals that are useful as treatments or cures for several diseases. The chemistry of natural products has given us such useful drugs as quinine, morphine, and penicillin. Quinine was the main tool in eradicating malaria in developed countries.

Morphine is a very powerful drug used in dulling pain. Penicillin is an antibiotic that revolutionized how infectious diseases were treated.

Secondly, many organisms are equipped with feeding deterrents that will discourage or kill predators that prey upon the organism. Because these feeding deterrents are able to interact with the predator's metabolism, there is a chance that they will be able to interact in some other type of cellular system. Since the deterrents are toxic, the compounds may have cytotoxicity towards other cell types, such as tumor cells.

Of course, simple cytotoxicity is not desirable for a drug lead. The toxicity must be selective. This is where another strength of natural products enters, the awesome variety of structure and function available in nature. Nature seems to effortlessly form chemicals of such unimaginable complexity that no synthetic chemist could have ever dreamed of them.[2] The complexity of the product of a synthesis is often proportional to the complexity of the synthetic scheme, and many natural products are produced by schemes that are much more complex than typical human-directed synthetic routes. Much complexity is required to generate molecules that can interact therapeutically with the human body.

As an extension of this, natural products can provide a clue about what an effective drug might look like. A simple derivatized natural product might retain the bioactivity of the original parent molecule, but possibly without high toxicity. A synthetic derivative might even have higher potency than the natural product. Overall, Nature provides investigators with a library of chemical leads from which to choose a useful compound.[3]

1.3 History of Anticancer Drug Discovery

Cancer is the Latin word for the Greek *karkinoma*, which in English means *crab*. This was how Hippocrates described the enlarged, elongated veins emanating from cancerous lumps in the female breast.[4] For centuries, from the ancient Egyptians up to the 1800's, the root cause of cancer was not known and was therefore not treatable. In the United States, very little substantial research or serious work was performed in attempting to treat cancer until 1930, when the National Institutes of Health was formed. In 1937, the National Cancer Institute (NCI) was formed, and serious thought was being given to causes and the possibility of treatments for cancer.[1] The Sloan-Kettering Institute was founded in 1945, and it quickly became the largest private cancer research body in the country. Research in chemical warfare during the Second World War had persuaded researchers that chemotherapy was the best method for treating cancer. In 1953, after pressure from the American Cancer Society and the Sloan-Kettering Institute, the U.S. Congress directed the NCI to explore the possibilities of chemotherapy as a means of treating leukemia. From then until 1955, many synthetic and fermentation products were screened, and six drugs were approved for the treatment of cancer, all of them synthetically derived.

Within the NCI, the Cancer Chemotherapy National Service Center (CCNSC) was created, and a chemist named Jonathan Hartwell was appointed director. Hartwell was interested in the bioactivity of plants, and he pursued an ethnobotanical approach to folk remedies reported from around the country. With this approach, chemical work was focused on plant species that were believed to have therapeutic effects based on local testimonials. Influenced by the discovery of bioactivity in the plant products colchicine

(**1.1**) and podophyllotoxin (**1.2**), Hartwell set about to unite the efforts of the NCI with the U.S. Department of Agriculture (USDA). The USDA could help with the collection of plant material, while the NCI could analyze the bioactivity and potential usefulness of

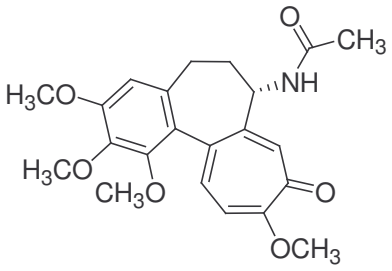

1.1

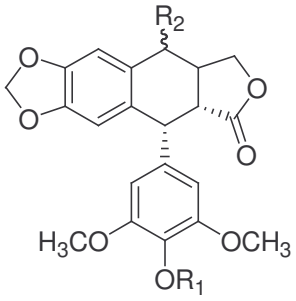

1.2 $R_1 = CH_3$ $R_2 = OH$ (α)

1.3 $R_1 = H$ $R_2 =$ 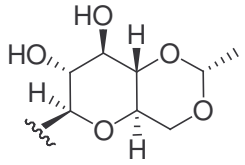 (β)

1.4 $R_1 = H$ $R_2 =$ 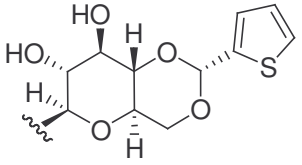 (β)

the plant extracts. This was the foundation of antitumor natural products drug discovery on a large scale in the United States, and eventually led to the discovery of the important antitumor compounds camptothecin (**1.5**) and paclitaxel (**1.8**).[5] It seemed that the

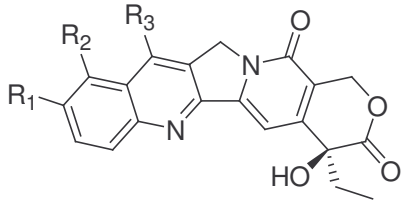

1.5 $R_1 = H$; $R_2 = H$; $R_3 = H$

1.6 $R_1 = OH$; $R_2 = CH_2NH(CH_3)_2$; $R_3 = H$

1.7 $R_1 =$ 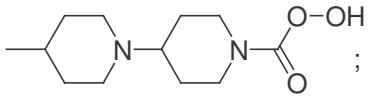 ;

$R_2 = H$; $R_3 = C_2H_5$

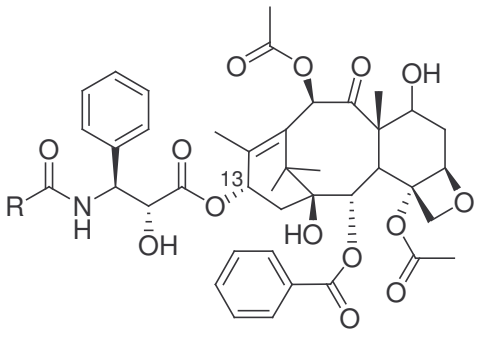

1.8 $R = C_6H_5$

1.9 $R = (CH_3)_3CO$

discovery of these agents justified the expense of all the programs involved. This progress promoted antitumor drug discovery with natural products to an important area of science.

1.4 Discovery and Action of New Antitumor Agents

1.4.1 Bioassays

To determine the potential efficacy of isolated compounds from a crude mixture, some sort of test must be employed to identify compounds that possess the type of activity that was present in the crude mixture. In the earlier days of natural products drug discovery, assays were carried out on mice with implanted tumors, and survival time measurements were recorded, as well as body mass and tumor changes.[6] These measurements were used to determine the potency and efficacy of potential drugs. Clearly, this sort of study was slow and expensive, and information about the mechanism of action was not normally obtained from such a crude system.

In later work, cell culture bioassays were developed, and these could be used for bioassay-guided fractionation. Early assays of this type were the P-388 (murine leukemia) and KB (human oral epidermoid carcinoma) cell culture tests. These assays measured cytotoxicity, or the ability of chemical samples to simply kill or inhibit the proliferation of cells in culture. With the bioassay-guided approach, each fractionation step is followed by biological evaluation of each fraction. Only fractions which display biological activity in the bioassay are selected for further fractionation. The cycle of fractionation and testing and further fractionation is repeated until a pure compound with the desired activity is isolated. One problem with cell-based assays is that there is often

little correlation between activity in these cytotoxicity models and *in vivo* tests.[7] This can be a result of problems with cell permeability or *in vivo* degradation of the potential drug. Also, it can be difficult or impossible to obtain definitive information on the mechanism of action just from cytotoxicity results from one cell line.

A refinement of the older methods which allows for the isolation of compounds with more selectivity is bioassay-guided fractionation using mechanism-based assays. As separations are performed on a crude mixture, an assay is employed to find potential antitumor agents which work by a specific mechanism in a selective manner.[8] Desirable mechanisms of action are those which might enable a drug to target tumor cells selectively or specifically. For example, the target for an isolation might be a compound which will damage DNA in a cell. Since tumor cells tend to replicate more frequently, and therefore replicate their genomes frequently, DNA damaging agents are somewhat selective to tumor cells. An assay may be designed that can quantify DNA damage, even specific kinds of DNA damage, and the assay can be used to guide fractionation efforts.

As mentioned above, mechanism-based bioassays are based on the identification of certain mechanisms of action that are believed to be potentially useful in treating tumors. There are many possible mechanisms for general cytotoxicity, but the mechanisms of action of the historically most successful cancer drugs are more limited in number. As our knowledge of the biochemical workings of cells becomes greater, our ability to identify new potential drug targets in cells increases. One shortcoming of the mechanism-based approach is that in the search for a treatment for cancer, one could come across a potential drug that operated by a different mechanism and not know it because of the specificity of the bioassay used. This specificity is also a benefit,

however, since it means that once an active agent is discovered, its mechanism of action is already known and development towards a clinical drug is thus greatly facilitated. Some examples of compounds isolated using mechanism-based assays are reported at the end of this chapter.

1.4.2 Mechanisms of Anticancer Drugs

The operation of a unique mechanism of action has been observed for each of the most successful anticancer drugs. One of the most important general mechanisms is the interference with the tubulin-microtubule equilibrium. Tubulin is a protein that forms fibers in a cell that allow for cell division and other cellular processes to occur normally. Microtubules are formed from the polymerization of the protein tubulin in a specific configuration. When a cell is ready to divide, spindle fibers made up of microtubules form and carry out the process of dividing the cytoplasm and the nucleus of the cell. The cell controls the equilibrium between tubulin and microtubules so that when it is time for the microtubules to dissociate, they can return to the tubulin form. Some chemical agents strongly bind microtubules together, and prevent tubulin depolymerization, while some other agents prevent tubulin polymerization altogether. The disruption of tubulin fiber function in the cell leads to the arrest of cell division, which leads to programmed cell death, or apoptosis.[9]

Another important mechanistic category is that of interaction with DNA topoisomerase I or II. Topoisomerases (topo) I and II are involved in maintaining the shape and structure of DNA. These enzymes assist with joining and breaking strands apart and with forming supercoils in DNA. It has been noted that in the presence of some

chemical agents, topo II actually carries out the cleavage of DNA, leading to an irreparable DNA break, which leads to cell death.[10] Topo I-mediated cleavage of a single strand of DNA has been observed as well.[11]

Direct DNA damage is responsible for the action of many anticancer natural products. The binding may be either covalent or noncovalent. Examples of mechanisms of DNA damage include alkylation, hydrogen abstraction, or oxidation of nucleotides in DNA. Irreparable DNA damage prevents proper protein synthesis, which leads to cell death.

1.4.3 Characterization of Natural Products

The characterization of natural products in the past few decades has taken advantage of spectroscopic techniques as well as chemical techniques to determine the structure of natural products. The use of nuclear magnetic resonance (NMR) spectroscopy, mass spectrometry (MS), high performance liquid chromatography (HPLC), and X-ray crystallography can yield complementary information that may be used to determine structures of relatively low molecular weight molecules (smaller than proteins). Other techniques used to characterize a structure include polarimetry, circular dichroism, and ultraviolet-visible and infrared spectrophotometry. Sometimes, a total synthesis and spectroscopic comparison between the synthetic and natural product is the easiest method for stereochemical determination and confirmation, when NMR data and degradative studies are inconclusive.[12]

1.4.4 Synthetic Approaches

Purely synthetic routes to drug discovery have yielded some important cancer treatments. Among the first examples of useful chemical agents in the treatment of cancer was nitrogen mustard, the second generation of synthetic poison gases for chemical warfare. Observed effects of nitrogen mustard on lymphocytes roused interest in the mustards as antitumor agents.[13] Eventually, the use of the DNA-alkylating nitrogens became a common part of cancer treatment.

The unexpected discovery of the antibacterial properties of platinum salts led to the investigation of antitumor applications of such salts. After numerous studies with many different ligands, *cis*-diaminetetrachloroplatinum, or cis-platin, was found to be very effective against L1210 leukemia in mice. Since the drug's significant side effects were circumvented by additional drugs, cis-platin has become a vital part of curative chemotherapy regiments. These cases demonstrate biological and chemical observations coming together to result in a synthetic anticancer agent.[13]

Chemical synthesis has another major contribution to offer to natural products drug discovery. Once a compound with a novel structure and interesting, selective, and potent activity is isolated, the compound will be selected for further study. This may require the total synthesis of the natural product. Also, synthetic studies may be performed where the biological activity of derivatives of a natural product is studied as a function of chemical modifications to the natural product skeleton. Referred to as structure-activity relationship studies, such studies have been employed to improve the efficacy or reduce the toxicity of several natural product lead compounds. This is

discussed further below. Overall, chemical synthesis and natural products drug discovery are important partners in the development of new antitumor agents.

1.5 Clinically Important Natural Products

The alkaloid camptothecin (**1.5**) was isolated from the stem wood of *Camptotheca acuminata*.[14] The isolation was guided by both *in-vitro* and *in-vivo* leukemia cell bioassays. Camptothecin and several derivatives have been isolated from a number of plant species.[15] The activity of the camptothecins is believed to be due to a stabilizing effect on the topo I-DNA complex.[16] Other evidence suggests a more complex mechanism, where collisions between topo I-DNA complexes and RNA polymerases in a cell lead to DNA transcription arrest and apoptosis.[17] A recent study demonstrated that DNA damage from camptothecins in intestinal cells is greater in proliferating cells than in differentiated cells, suggesting that the DNA templating that occurs in proliferating cells is one of the targets of the DNA damage from the camptothecins.[11] Though the water solubility of camptothecin is too low for clinical use, the derivatives topotecan (**1.6**) and irinotecan (**1.7**) are used clinically.

Podophyllotoxin (**1.2**) is a lignan isolated from *Podophyllum peltatum*, the May Apple of the eastern United States. The roots of *P. peltatum* were known to the indigenous people of North Carolina and Virginia to be toxic, and podophyllotoxin was isolated in 1880. It was later identified as an antitumor substance by bioassay-guided fractionation. The derivatives etoposide (**1.3**) and teniposide (**1.4**) have entered clinical use for the treatment of several cancers, including small-cell lung cancer, acute leukemia,

and breast cancer.[15] Due to extreme human toxicity, podophyllotoxin itself was never developed as an antitumor drug.

Podophyllotoxin inhibits microtubule assembly during the metaphase of cell division. The derivatives **1.3** and **1.4** have different mechanisms of action, however. The principal operation of these semisynthetic derivatives is inducing reversible cleavage of DNA by inhibition of topo II.[18] Structure-activity relationship studies have been performed on podophyllotoxin congeners, and it has been reported that etoposide and teniposide do not cleave DNA directly, but instead must be metabolized in a cell before DNA damage occurs. This sort of activity is similar to that of camptothecin, which can cleave cellular DNA but not purified DNA.

Paclitaxel (**1.8**), or Taxol®, was isolated via bioassay-guided fractionation from the bark of *Taxus brevifolia*, using leukemia cell lines in the testing.[19] Though **1.8** was active against several different cancer cell lines, its poor water solubility and scarcity reduced the initial interest in it. Interest was stimulated by good activity against several solid tumor xenografts in nude mice, and interest grew further when the mechanism of action was discovered by Horwitz in 1979.[9] The activity of **1.8** was found to be due to its promotion of microtubule assembly. The equilibrium between tubulin and microtubules was shifted towards the microtubules, and depolymerization to tubulin was inhibited. This led to the interruption of cell division and subsequent cell death. Further studies led to its introduction into clinical use in 1992.

Many structure-activity studies have been carried out for **1.8**.[20] Various additional natural products, including the epothilones and discodermolide, have been found to have the same mechanism of action as **1.8**. Our group has recently discovered

that a conformationally restricted analog of **1.8,** where the C-3' phenyl ring and C-4 acetate ester are connected through a short alkenyl tether, has activity better than that of **1.8**, while an analog where the same tether is broken has a thousandfold less activity than **1.8**. Therefore, it has been shown that the bioactive conformation of **1.8** likely involves the two sides of the molecule coming close together when **1.8** is bound to tubulin. This study could possibly aid in the development of simplified tubulin binding agents that might have the same effect as **1.8** without the overwhelming synthetic complexity. A synthetic derivative of **1.8**, docetaxel (**1.9**), has entered clinical use as well. Paclitaxel has become the best-selling cancer drug in the world, and has been the subject of

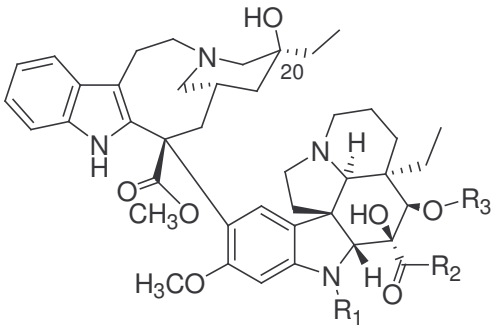

1.10 $R_1 = CH_3$; $R_2 = OCH_3$; $R_3 = CH_3CO$
1.11 $R_1 = CHO$; $R_2 = OCH_3$; $R_3 = CH_3CO$
1.12 $R_1 = CH_3$; $R_2 = NH_2$; $R_3 = H$

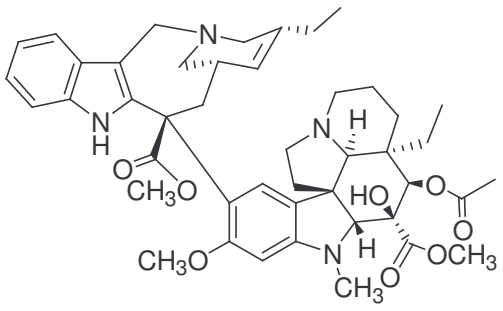

1.13

numerous synthetic studies and reviews. Paclitaxel was a center of debate and struggle between the pharmaceutical industry and environmentalists from the time of its isolation until a semi-synthetic approach to its production was developed.[5] As a symbol of the influence and importance of the discovery of **1.8**, it has been mentioned in more Chemical Abstracts Service abstracts than any other antitumor drug. Paclitaxel has been applied to the treatment of lung, ovarian, and breast cancers.

The vinca alkaloids **1.10**-**1.13** were isolated from the leaves of *Catharanthus roseus*, the Madagascar periwinkle (previously named *Vinca rosea*). Workers had begun studying the extract of *C. roseus* for its potential as a diabetes treatment, but its ability to destroy bone marrow cells in laboratory rats was eventually more pronounced, and bioassay-guided fractionation was performed to isolate the active agent. *C. roseus* contained both vinblastine (**1.10**) and vincristine (**1.11**), two similar bisindole compounds which differed in structure at one carbon. The discovery of these compounds was a result of simultaneous discoveries in Canada and in the United States.[21] Vinblastine has been clinically applied, in conjunction with other methods, to treat Hodgkin's disease, non-Hodgkin's lymphoma, and testicular and ovarian cancers. Vincristine has been used clinically for the treatment of childhood lymphocytic leukemia and Hodgkin's disease. Vindesine (**1.12**), a derivative of vinblastine, has shown significant activity against lung cancer.[22]

Total synthesis of the earlier vinca alkaloids has been reported by several routes,[21] and much work has been done in synthesizing new derivatives.[23] Thorough structure-activity studies have been performed.[15] Two vinca-type alkaloids, vinorelbine (**1.13**) and **1.12**, have been developed as a result of this work. Vinorelbine has been introduced recently for the treatment of advanced breast cancer and advanced non-small cell lung cancer.

The activity of the vinca alkaloids has been found to be due to their ability to inhibit tubulin polymerization in cells. A recent study demonstrated the effects of modifying the catharanthine portion of the bis-indole alkaloids. The vindoline portion of the drug molecules was left unchanged, since it was responsible for the binding effect to

tubulin. The workers demonstrated a correlation between cytotoxicity in L1210 cells and the size of spirals induced in tubulin for several vinca-type alkaloids. The spirals in tubulin induced by vinca alkaloids occurred at high drug concentrations, and the spirals were a result of the trapping of the drug between the α and β portions of microtubules. Their results showed that changes at the C-20' position had no effect on the tubulin binding affinity, but did affect the spiraling effect, which was correlated to cytotoxicity.[24]

Several effective anticancer compounds have been isolated from microbial sources. Actinomycin D (**1.14**) is a peptide derivative isolated from various *Streptomyces* species. The activity of the actinomycins is principally due to a sequence-specific binding to DNA, which inhibits the operation of RNA polymerases that transcribe DNA

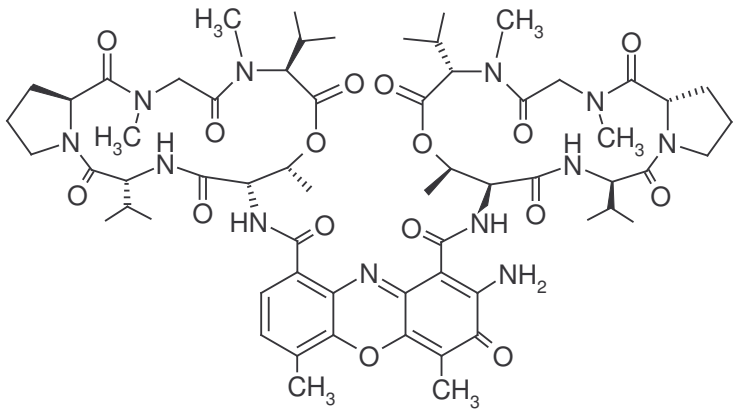

1.14

information to RNA.[25] There is evidence that actinomycins D, C_2, and VII also block oncogenic signal transduction pathways which are responsible for runaway cell growth in some cells.[26] The DNA-binding of **1.14** has been examined closely by fluorescence and ^{1}H-NMR methods,[25] as well as by a technique which cleaves a ligand-bound DNA fragment (actinomycin D attached to DNA) and allows for identification of the fragment. When the latter technique is applied to a combinatorial library of DNA sequences, the

specificity of the DNA binding of **1.14** is revealed.[27] Compound **1.14** is clinically used in conjunction with vinblastine and cyclophosphamide for the treatment of childhood leukemia.[3]

The bleomycins **1.15** and **1.16** are another group of antitumor antibiotics isolated from a *Streptomyces* species, *S. verticillus*. The structure and absolute configuration have been determined after spectroscopic and synthetic study. Typically, in clinical usage, the bleomycins are administered as a mixture of congeners, known collectively as blenoxane, which contains both bleomycins A_2 (**1.15**) and B_2 (**1.16**).[28] The antitumor function of

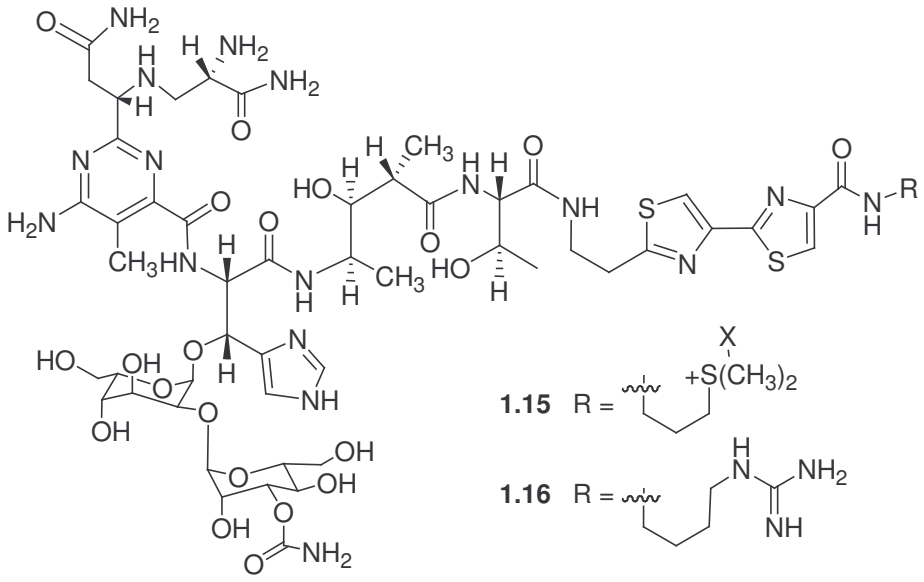

bleomycins is believed to lie in their ability to bind to specific sequences in DNA in the presence of iron(III) ion,[29] and to abstract a hydrogen atom from DNA at the C-4' position of a DNA base. In the presence of O_2 and a metal ion (Fe^{2+} or Co^{3+}), this leads to the formation of oxidation products of DNA, and the cleavage of DNA. Yet, these mechanistic arguments might be used to justify a RNA cleavage-based mechanism of action, since a crucial cellular RNA cleavage might be more destructive for a tumor cell.

Blenoxane is commonly used in the treatment of testicular cancer in conjuction with vinblastine.[15]

The anthracyclines doxorubicin (adriamycin, **1.17**) and daunomycin (**1.18**) are also antibiotic antitumor compounds that were isolated by Italian researchers using mouse tumor bioassay-guided fractionation from *Streptomyces* species: **1.17** from a mutant strain of *S. peucetius,* and **1.18** from the wild-type strain.[6,30] Compound **1.17** is able to induce single strand cleavages of DNA via a topo II-mediated cleavage.[31] It has been shown in structure-activity studies that the sugar portion of both **1.17** and **1.18** is

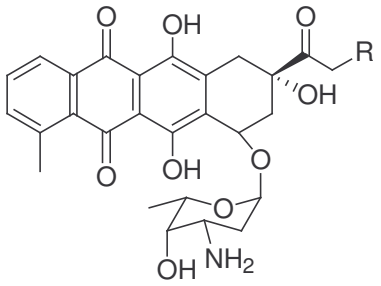

1.17 R = OH

1.18 R = H

crucial to the cytotoxicity of these two compounds.[32] Both **1.17** and **1.18** are used clinically as antitumor agents . However, the usefulness of **1.18** has been limited because of heart toxicity over extended dosage periods.[33]

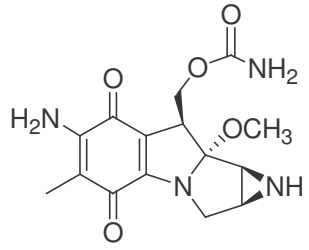

1.19

Mitomycin C (**1.19**) is the most active of the mitomycin antitumor antibiotics, which are derived from various members of the *Streptomyces* genus. Under reducing conditions, **1.19** is able to react with two DNA nucleotides, which can result in cross-

linked DNA. Compound **1.19** seems to have higher potency in cells with lower oxygen concentrations than normal, [13] and it is used against tumors where typical radiation treatments do not work, where poor vascularization around the tumor decreases oxygen levels in the cells.[34] Mitomycin C is considered one of the most toxic anticancer agents in clinical use.

1.6 Natural Products in Development or in Clinical Trials for Cancer

Now that we have examined several of the most important anticancer drugs that have emerged from natural products chemistry, we will briefly review several anticancer agents that have made progress through clinical trials and have generated interest for their good activity and interesting structures.

The alkaloid homoharringtonine (**1.20**) was isolated from the Chinese evergreen *Cephalotaxus harringtonia*.[35] Compound **1.20** was shown to bind to ribosomes in a cell,

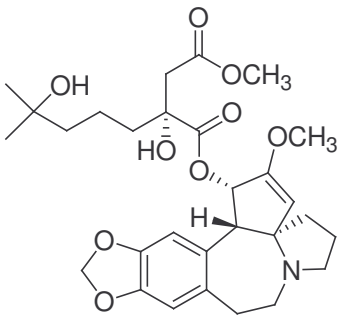

1.20

leading to the inhibition of protein synthesis.[36] The cytotoxicity of **1.20** was discovered using *in vivo* tests with P-388 leukemic mice. As it has turned out, **1.20** has shown the promise as a treatment for acute myelogenous leukemia.[37] Investigation of **1.20** for its clinical usefulness has remained a topic of interest.[38]

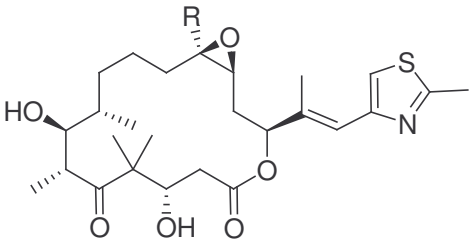

1.20 R = H

1.21 R = CH_3

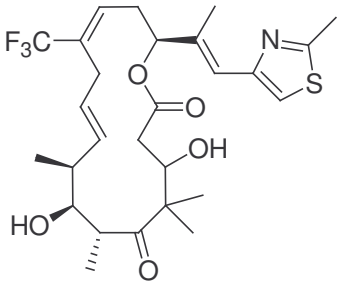

1.22

One other class of compounds that has stirred much investigation and is very promising is the epothilone class. Epothilones A and B (**1.20** and **1.21**) were isolated from a culture of the myxobacterium *Sorangium cellulosum*. The first isolation of **1.20** and **1.21** was guided by an antifungal assay, but they were isolated independently by another group based on a tubulin polymerization assay. The mechanism of action of the epothilones has been shown to be cytotoxicity due to the promotion of microtubule polymerization, just like paclitaxel.[39] The synthetic epothilone analog **1.22** has recently been shown to have nanomolar cytotoxicity in a multiple myeloma (MM) cell assay, and it was also found to have very good *in vivo* activity in a mouse MM model.[40] Because of the superior water solubility of the epothilones and because of the availability of material from bacterial culture, the epothilones are under intense study as lead compounds for the next generation of cancer drugs.

The area of drug discovery from marine organisms has been quite active for several years, and the isolation of several promising lead compounds for cancer treatments has been reported. Cyclic depsipeptides didemnins A and B (**1.23** and **1.24**) were isolated from a Caribbean tunicate of the family *Didemnidae*. They displayed both antiviral and antitumor properties in viral and L1210 assays.[41] The NCI developed **1.24** through phase II clinical trials, but it was withdrawn due to its high toxicity. However,

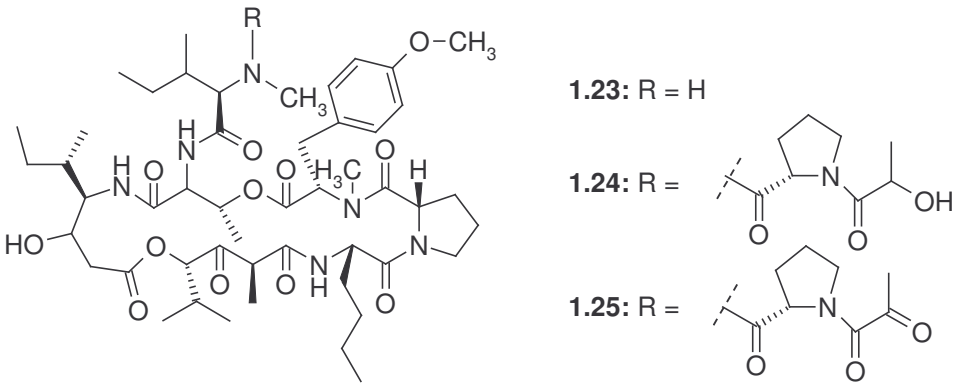

dehydrodidemnin B, or aplidine (**1.25**), has demonstrated anticancer activity that is superior to **1.24**,[42] but does not produce the same pernicious toxicity.[43] Compound **1.25** is currently in Phase II clinical trials.[44]

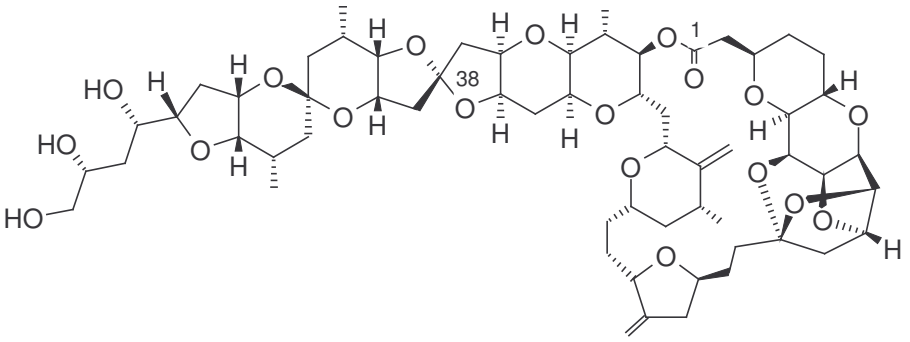

1.26

Halichondrin B (**1.26**) was isolated from a marine sponge, *Halichondria okadai*. A polyether macrolide, **1.26** was isolated along with several similar macrolides based on its toxicity to melanoma cells in culture.[45] The NCI has examined **1.26** in preclinical trials using material obtained from a sponge of the *Lissodendoryx* species. Structure-activity experiments have allowed researchers to identify the important pharmacophore of the natural product, the C1-C38 portion containing the polyether macrocycle. This knowledge has allowed for the synthesis of simpler structures which retain the high

antitumor potency of the natural product.[46] Along with all of the synthetic analogues, **1.26** operates by inhibiting tubulin polymerization.[47]

Bis-indole alkaloid topsentins were isolated from the Mediterranean sponge *Topsentia genitrix*.[48] Topsentin B1 (**1.27**) has also been isolated from several other sponge species. The topsentins showed weak activity in a fish assay and a mouse assay. It has been shown that **1.27** is a powerful mediator of neurogenic and imunogenic inflammatory response. The cytotoxicity has been shown to come from topsentin's ability to bind to DNA in the minor groove.[49]

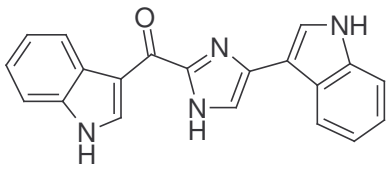

1.27

The pentapeptide dolastatin 10 (**1.28**) was first isolated from the sea hare *Dolabella auricularia*. Compound **1.28** demonstrated exceptional curative response in various tests with implanted tumors in mice.[50] A synthesis of **1.28** was developed, and

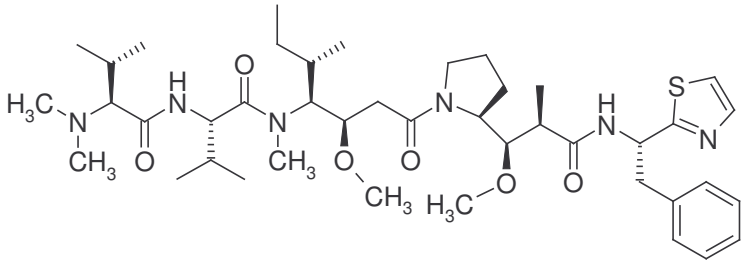

1.28

work toward understanding the drug's mechanism of action could commence. The antitumor action of **1.28** arises from its inhibition of tubulin polymerization, and it functions in much the same way as the vinca alkaloids,[51] though the binding is not at the

same site.[52] It has been reported that **1.28** is present in a cyanobacterium of the *Symploca* species.[53] This seems to suggest, as some workers have hypothesized, that **1.28** might be a product from a bacterial symbiont of *D. auricularia*. Unfortunately, **1.28** has not demonstrated promising *in vivo* activity in phase II testing with solid tumors.[43]

Ecteinascidin 743 (**1.29**) was isolated from the Caribbean tunicate *Ecteinascidia turbinata*, along with several other antitumor compounds. Compound **1.29** had a cytotoxicity value of IC_{50} = 0.5 ng/mL,[54] and it has been shown to alkylate DNA in the minor groove and bend DNA toward the major groove. This bending might lead to interaction between DNA and topo-I, possibly inhibiting DNA repair, making **1.29** potentially useful.[55] Compound **1.29** is currently in phase II trials in the United States.[44]

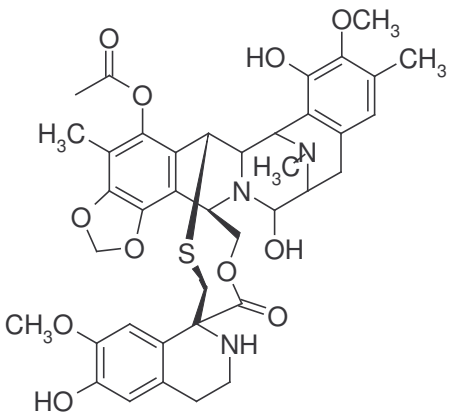

1.29

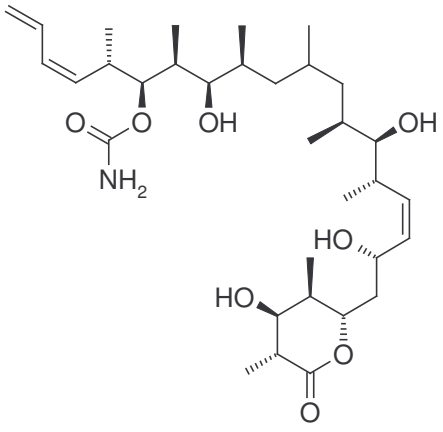

1.30

Discodermolide (**1.30**), a polyhydroxylated lactone, was isolated from the marine sponge *Discodermia dissoluta*. Discodermolide demonstrated cytotoxicity to P-388 cells and is also an immunosuppressant.[56] Mechanistic studies have shown that **1.30** disrupts the tubulin-microtubule equilibrium in much the same way as paclitaxel.[57] Based on 1D and 2D NMR studies, the solution structure of **1.30** was determined and found to be

remarkably similar to the solid state structure determined by X-ray crystallography.[58] As with the conformationally restricted analogs of paclitaxel, understanding the conformational profile of known antitumor agents might facilitate the design of new drugs. Compound **1.30** is currently in Phase I clinical trials for cancer.[44] As a testament to the interest of **1.30**, Novartis carried out an industrial scale multi-step synthesis of the compound to provide enough material for clinical trials,[59] but these have apparently been ended due to toxicity problems with **1.30**.[60]

Overall, these examples describe how many compounds discovered over the past 30 years are finally getting close to the clinic. Unfortunately, most compounds with good *in vitro* activity do not even make it to clinical trials. Natural products drug discovery is very labor-intensive, and many drug companies like GlaxoSmithKline and Bristol-Myers Squibb have discontinued their natural products discovery efforts, probably since it is so difficult to get a return on money invested. It should be clear, however, that natural products with good activity do offer medicinal chemists great scaffolds for use in discovering new drugs. Therefore, it seems that natural products chemists must find ways to make their work more productive in order to encourage investment. With investment in natural products, new treatments might be discovered, but with no investment in natural products fewer antitumor lead compounds will be found.

1.7 The Mechanism-based Approach to Natural Products Isolation

The previous examples of bioactive compounds were all discovered using cell-based assays, where the assay used to guide the isolation of the active compound was a cytotoxicity assay. As previously mentioned, this approach allows for the isolation of

compounds that will have known toxicity to tumor cells, while the exact mechanism of that toxicity is largely unknown. A different method that has been employed in the search for antitumor natural products is the mechanism-based approach. With this approach, an assay is designed to measure interaction with a single drug target, usually an enzyme or biological receptor protein. The assay is designed so that the activity or functionality of the target can be measured in the absence and presence of the potential drug, and this interaction is quantified by use of some detection method that depends on the activity of the target. For the discovery of potential antitumor agents, the target of interest is often an enzyme that plays a key role in the life of a cell. The major advantage of the mechanism-based approach to drug discovery is that once a bioactive component is detected and isolated, the mechanism of action is known; in terms of gaining governmental approval for a drug, this information is of utmost importance for new antitumor agents. A second advantage to mechanism-based assays is that they require only a few hours to set up and run; while cell-based assays require 1-2 days of incubation in order to detect the activity of samples tested. Because of this difference, mechanism-based assays are very amenable to high-throughput screening and automation. Thus, while cell-based assays are still a very important part of natural products drug discovery, the field is shifting more towards the selectivity and efficiency afforded by mechanism-based assays. Below are found some recent examples of natural products with interesting structures isolated by use of mechanism-based assays, some of which have entered clinical trials for cancer treatment.

The oxindole alkaloid speradine A (**1.31**) was isolated along with a similar compound from a culture broth of the fungus *Aspergillus tamarii,* [61] The compound was

found to inhibit Ca^{2+}-ATPase (IC_{50} 8 mM), histone deacetylase (HDA, IC_{50} 100 μg/mL), and it also showed antibacterial activity against *Mycrococcus luteus* (MIC 16.7 μg/mL). These activities are fairly weak, but perhaps this compound could serve as a scaffold for the development of HDA inhibitors.

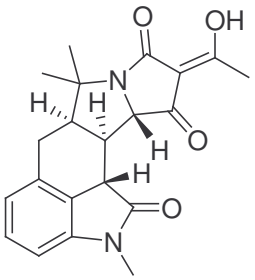

1.31

Psammaplins I and J (**1.32** and **1.33**) are sulfide bromotyrosine derivatives from the sponge *Pseudoceratina purpurea*: Using an assay screen of extracts and bioassay guided fractionation, these compounds were found to be potent HDAC inhibitors (nanomolar range) that also possess weak cytotoxicity. Novartis has also worked on the synthesis of derivatives with the psammaplin pharmacophore, and these have already entered clinical trials for cancer.[62]

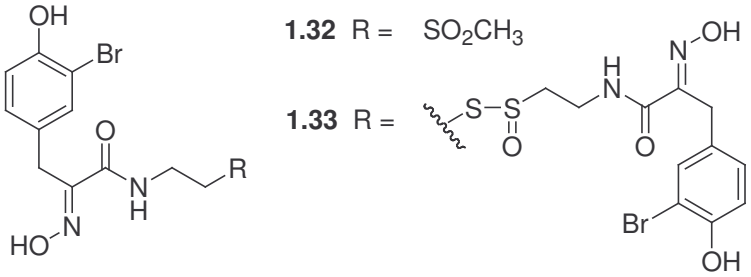

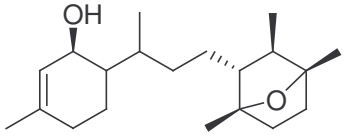

1.34

Tumors often grow in reduced oxygen conditions, and hypoxia-inducible factor-1 (HIF-1) helps promote survival under these conditions. Using a breast-cancer cell-based assay that monitors HIF-1 by use of a luciferase reporter gene (when the luminescence produced by luciferase is reduced, this means HIF-1 is being inhibited) laurenditerpenol (**1.34**) was isolated. Further study has shown that **1.34** selectively inhibits hypoxia-induced HIF-1 activation. This assay in an example of how a mechanism-based assay can be designed within a cell-based framework, which allows for the activity of the compound and its cell permeability to be simultaneously estimated.[63]

Berkeleydione I (**1.35**) was isolated from a fungus of *Penicillium* sp. found in the Berkeley Pit Lake of Butte, Montana. The crude extract showed antibiotic properties, and **1.35** (IC_{50} = 12 mM) was isolated along with a similar compound by use of enzyme inhibition assays for matrix metalloproteinase 3 (MMP-3) and caspase-1 (Casp-1), two enzymes that play a critical role in the spread of tumors. Compound **1.35** was tested in the NCI's 60-cell panel and found to be selectively cytotoxic to non-small cell lung carcinoma. Casp-1 and MMP-3 inhibitors might be useful in combination therapies for cancer, and may play a role in the treatment of other diseases as well.[64]

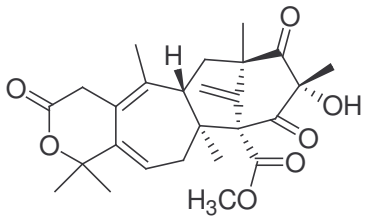

1.35

It should be evident that mechanism-based assays can lead to the isolation of compounds with interesting structure, activity, and activity against whole tumor cells.

Because enzyme assays make screening and assay work faster, mechanism-based assays are a key part of making natural products drug discovery competitive in the quest to find new drug candidates.

The following chapters will describe our efforts in discovering natural products with activity in mechanism based assays. Chapter 3 covers work using a cytotoxicity assay to discover a sesterterpenoid from a sponge extract that initially displayed activity in a mechanism-based assay. Chapters 2, 4, and 5 all cover mechanism-based bioassay-guided natural product isolations. Chapter 6 is a study of efforts to efficiently remove long-chain fatty acids from natural extracts in order to eliminate false positives in enzyme-based bioassays. Finally, Chapter 7 reports our efforts and understanding the substrate length and sequence requirements of the cell cycle enzyme Chk1, a potential target for antitumor drug development.

References for Chapter 1

1. Cancer Research UK. How Can Cancer Kill You? http://www.cancerhelp.org.uk/help/default.asp?page=2561. Accessed October 7th, 2005.

2. Preface. In *Biologically Active Natural Products: Pharmaceuticals*. Cutler, S.J.; Cutler, H.G.; Eds. CRC Press: Boca Raton, FL, 2000. Unnumbered pages.

3. Kingston, D.G.I.; Abdel-Kader, M.; Zhou, B.-N.; Yang, S.-W.; Berger, J.M.; van der Werff, H.; Evans, R.; Mittermeier, R.; Malone, S.; Famolare, L.; Guerin-McManus, M.; Wisse, J.H.; Miller, J.S. Biodiversity Conservation, Economic Development, and Drug Discovery in Suriname. In *Biologically Active Natural Products: Pharmaceuticals*. Cutler, S.J., Cutler, H.G., Eds. CRC Press: Boca Raton, FL, 2000, pp 39-59.

4. Patterson, J.T. *The Dread Disease: Cancer and Modern American Culture*. Harvard University Press: Cambridge, MA, 1987.

5. Goodman, J. ; Walsh, V. *The Story of Taxol*. Cambridge University Press: New York, 2001.

6. Di Marco, A.; Gaetani, M.; Scarpinato, B. Adriamycin (NSC-123, 127): A New Antibiotic with Antitumor Activity. *Cancer Chemother. Rep.* **1969**, *53*, 33-37.

7. Suffness, M.; Pezzuto, J.M. Assays Related to Cancer Drug Discovery. In *Methods in Plant Biochemistry*; Hostettman, K.; Dey, P.M.; Harborne, J.B., Eds. Academic Press Inc.: San Diego, CA., 1991; Vol. 6, p 84.

8. Johnson, R.K.; Bartus, H.F.; Hofmann, G.A.; O'Leary Bartus, J.; Mong, S.-M.; Faucette, L.F.; McCabe, F.L.; Chan, J.A.; Mirabelli, C.K. Discovery of New DNA-Reactive Drugs. In In Vitro *and* In Vivo *Models for Detection of New Antitumor Drugs*, Proceedings of a workshop at the 14th International Congress of Chemotherapy, Kyoto, Japan, 1985; Hanka, L.J.; Kondo, T.; White, R.J. Eds.; Organizing Committee of the 14th International Congress of Chemotherapy: Kyoto, 1986. 16-26.

9. Kingston, D.G.I. Taxol, a Molecule for All Seasons. *Chem. Comm.* **2001**, 867-880.

10. Ross, W.E. DNA Topoisomerases as Targets for Cancer Therapy. *Biochem. Pharmacol*. **1985**, *34*, 4191-4195.

11. Ulukan, H.; Muller, M.T.; Swaan, P.W. Downregulation of Topoisomerase I in Differentiating Human Intestinal Epithelial Cells. *Int. J. Cancer* **2001**, 94, 200-207.

12. Lipton, M. "Solid Phase Synthesis of the Cyclic Depsipeptide Callipeltin B." Highlands in Chemistry Seminar Series, Department of Chemistry, Virginia Tech, February 16, 2001.

13. Pratt, W.B.; Ruddon, R.W.; Ensminger, W.D.; Maybaum, J. *The Anticancer Drugs*. Oxford University Press: New York, 1994.

14. Wall, M.E.; Wani, M.C.; Cook, C.E.; Palmer, K.H. Plant Antitumor Agents. I. The Isolation and Structure of Camptothecin, a Novel Alkaloidal Leukemia and Tumor Inhibitor from *Camptotheca acuminata*. *J. Am. Chem. Soc.* **1966**, *88*, 3888-3890.

15. Kuo, Y.-H.; King, M.-L.; Antitumor Drugs from the Secondary Metabolites of Higher Plants. In *Bioactive Compounds from Natural Sources*; Tringali, C. Ed.; Taylor and Francis Inc.: New York, 2001, pp 189-281.

16. Hsiang, Y.H.; Hertzberg, R.; Hecht, S., Liu, L.F. Camptothecin induces protein-linked DNA breaks via mammalian DNA topoisomerase I. *J. Biol. Chem.* **1985**, *260*, 14873-14878.

17. Wu, J.;Liu, L.F. Processing of topoisomerase I cleavable complexes into DNA damage by transcription. *Nucleic Acids Res.* **1997**, *25*, 4181-4186.

18. Loike, J.D.; Horwitz, S.B. Effect of VP-16-213 on the Intracellular Degradation of DNA in HeLa Cells. *Biochemistry*, **1976**, *15*, 5443-5448.

19. Wani, M.C.; Taylor, H.L.; Wall, M.E.; Coggon, P.; McPhail, A.T. Plant Antitumor Agents. VI. The Isolation and Structure of Taxol, a Novel Antileukemic and Antitumor Agent from *Taxus brevifolia*. *J. Am. Chem. Soc.* **1971**, *93*, 2325-2327.

20. Ojima, I.; Chakravarty, S.; Inoue, T.; Lin, S.; He, L.; Horwitz, S.B.; Kuduk, S.D.; Danishefsky, S.J. A Common Pharmacophore for Cytotoxic Natural Products that Stabilize Microtubules. *Proc. Natl. Acad. Sci. U.S.A.* **1999**, *96*, 4256-4261.

21. Noble, R.L. The Discovery of the Vinca Alkaloids—Chemotherapeutic Agents Against Cancer. *Biochem. Cell Biol.* **1990**, *68*, 1344-1351.

22. Neuss, N.; Neuss, M.N. Therapeutic Use of Bisindole Alkaloids from *Catharanthus*. In *The Alkaloids*, vol 73. Brossi, A.; Suffness, M., Eds. Academic Press Inc.: San Diego, CA, 1990. pp 229-240.

23. Szantay, Csaba, Jr.; Moldvai, I.; Tarkanyi, G.; Szantay, C. Synthesis of Vinca Alkaloids and Related Compounds. 79. An Intriguing Retro Diels-Alder Reaction. *J. Org. Chem.* **1996**, *61*, 2946-2950, as well as other papers in the series.

24. Lobert, S.; Fahy, J.; Hill, B.T.; Duflos, A.; Etievant, C.; Correia, J.J. Vinca Alkaloid-Induced Tubulin Spiral Formation Correlates with Cytotoxicity in the Leukemic L1210 Cell Line. *Biochemistry* **2000**, *39*, 12053-12062.

25. Wadkins, R.M.; Jares-Erijman, E.A.; Klement, R.; Rüdiger, A.; Jovin, T.M. Actinomycin D Binding to Single-stranded DNA: Sequence Specificity and Hemi-intercalation Model from Fluorescence and 1H-NMR Spectroscopy. *J. Mol. Biol.* **1996**, *262*, 53-68.

26. Nam, J.-Y.; Kim, H.-K.; Son, K.-H.; Kim, S.-U.; Kwon, B.-M.; Han, M.-Y.; Chung, Y.J.; Bok, S.H. Actinomycin D, C2, and VII, Inhibitors of Grb2-Shc Interaction Produced by *Streptomyces*. *Bioorg. Med. Chem. Lett.* **1998**, *8*, 2001-2002.

27. Shen, J.; Wang, J.C.; Van Dyke, M.W. Identification of Preferred Actinomycin-DNA Binding Sites by the Combinatorial Method REPSA. *Bioorg. Med. Chem. Lett.* **2001**, *9*, 2285-2293.

28. Hecht, S.M. Bleomycin: New Perspectives on the Mechanism of Action. *J. Nat. Prod.* **2000**, *63*, 158-168.

29. Fulmer, P.; Zhao, C.; Li, W.; DeRose, E.; Antholine, W.; Petering, D.H. Fe- and Co-Bleomycins Bound to Site Specific and Nonspecific DNA Decamers: Comparative Binding and Reactivity of Their Metal Centers. *Biochemistry* **1997**, *36*, 4367-4374.

30. Di Marco, A.; Gaetani, M.; Orezzi, P.; Scarpinato, B. M.; Silvestrini, R.; Soldati, M.; Dasdia, T.; Valentini, L. Daunomycin, a New Antibiotic of the Rhodomycin Group**.** *Nature* **1964**, *201*, 706-707.

31. Pratesi, G.; Capranico, G.; Binaschi, M.; De Isabella, P.; Pilotti, S.; Supino, R.; Zunino, F. Relationships Among Tumor Responsiveness Cell Sensitivity, Doxorubicin Cellular Pharmacokinetics and Drug-Induced DNA Alterations in Two Human Small-Cell Lung Cancer Xenografts. *Int. J. Cancer* **1990**, *46*, 669-674.

32. Arcamone, F.; Animati, F.; Bigioni, M.; Capranico, G.; Caserini,C.; Cipollone, A.; De Cesare, M.; Ettorre, A.; Guano, F.; Manzini, S., Monteagudo, E.; Pratesi, G.; Salvatore, C.; Supino, R.; Zunino, F. Configurational Requirements of the Sugar Moiety for the Pharmacological Activity of Anthracycline Disaccharides. *Biochem. Pharmacol.* **1999**, *57*, 1133-1139.

33. Zhou, S.; Palmeira, C.M.; Wallace, K.B. Doxorubicin-induced Persistent Oxidative Stress to Cardiac Myocytes. *Toxicol. Lett.* **2001**, *121*, 151-157.

34. Penketh, P.G.; Hodnick, W. F.; Belcourt, M.F.; Shyam, K.; Sherman, D.H.; Sartorelli, A.C. Inhibition of DNA Cross-linking by Mitomycin C by Peroxidase-mediated Oxidation of Mitomycin C Hydroquinone. *J. Biol. Chem.* **2001**, *276*, 34445-34452.

35. Powell, R. G.; Weisleder, D. ; Smith, C.R., Jr.; Rohwedder, W.K. Structures of Harringtonine, Isoharringtonine, and Homoharringtonine**.** *Tetrahedron Lett*. **1970**, 11, 815-818.

36. Lee Y.J.; Hou, Z.Z.; Erdos, G.; Cho, J.M.; Corry, P.M. Homoharringtonine Induces Heat Protection and Facilitates Dissociation of Heat Shock Transcription Factor and Heat Shock Element Complex. *Biochem. Biophys. Res. Comm.* **1993**, *197*, 1011-1018.

37. Kantarjian, H.M.; O'Brien, S.; Anderlini, P.; Talpaz, M. Treatment of Myelogenous Leukemia: Current Status and Investigational Options. *Blood* **1996**, 87, 3069-3081.

38. Kantarjian, H.M.; Moshe Talpaz, M.; Santini, V.; Murgo, A.; Cheson, B.; O'Brien, S.M. Homoharringtonine: History, current research, and future directions. *Cancer* **2001**, *92*, 1591-1605.

39. Hoefle, G.; Bedorf, N.; Steinmetz, H.; Schomburg, D.; Gerth, K.; Reichenbach, H. Antibiotics from Gliding Bacteria. 77. Epothilone A and B - Novel 16-Membered Macrolides with Cytotoxic Activity: Isolation, Crystal Structure, and Conformation in Solution. *Angew. Chem., Int. Ed. Engl.* **1996**, *35*, 1567-1569.

40. Wu, K.-D.; Cho, Y.S.; Katz, J.; Ponomarev, V.; Chen-Kiang, S.; Danishefsky, S.J.; Moore, M.A.S. Investigation of Antitumor Effects of Synthetic Epothilone Analogs in Human Myeloma Models *in vitro* and *in vivo*. *Proc. Natl. Acad. Sci. U.S.A*. **2005**, *102*, 10640-10645.

41. Rinehart, K.L., Jr.; Gloer, J.B.; Hughes, R.G.; Renis, H.E.; McGovern, J.P.; Swynenberg, E.B.; Stringfellow, D.A.; Kuentzel, S.L.; Li, L.H. Didemnins: Antiviral and Antitumor Depsipeptides from a Caribbean Tunicate. *Science* **1981**, *212*, 933-935.

42. Faulkner, D.J. Marine Pharmacology. *Antoine van Leeuwenhoek* **2000**, *77*, 135-145.

43. Da Rocha, A.B.; Lopes, R.M.; Schwartsmann, G. Natural Products in Anticancer Therapy. *Curr. Opin. Pharmacol.* **2001**, *1*, 364-369.

44 Butler, M.S. Natural Products to Drugs: Natural Product Derived Compounds in Clinical Trials. *Nat. Prod. Rep.* **2005**, *22*, 162-195.

45. Hirata, Y.; Uemura, D. Halichondrins—antitumor polyether macrolides from a marine sponge. *Pure Appl. Chem.* **1986**, *58*, 701-710.

46. Zheng, W.; Seletsky, B.M.; Palme, M.H.; Lydon, P.J.; Singer, L.A.; Chase, C.E.; Lemelin, C.A.; Shen, Y.; Davis, H.; Tremblay, L.; Towle, M.J.; Salvato, K.A.; Wels, B.F.; Aalfs, K.K.; Kishi, Y.; Littlefield, B.A.; Yu, M.J. Macrocyclic Ketone Analogues of Halichondrin B. *Bioorg. Med. Chem. Lett.* **2004**, *14*, 5551-5554.

47. Zheng, W.; Seletsky, B.M.; Palme, M.H.; Lydon, P.J.; Singer, L.A.; Chase, C.E.; Lemelin, C.A.; Shen, Y.; Davis, H.; Tremblay, L.; Towle, M.J.; Salvato, K.A.; Wels, B.; Aalfs, K.K.; Kishi, Y.; Littlefield, B.A.; Yu, M.J. *In Vitro* and *In Vivo* Anticancer Activities of Synthetic Macrocyclic Ketone Analogues of Halichondrin B. *Cancer Res.* **2001**, *61*, 1013-1021.

48. Bartik, K.; Braekman, J.C.; Daloze, D.; Stoller, C.; Huysecom, J.; Vandevyver, G.; Ottinger, R. Topsentins, new toxic bis-indole alkaloids from the marine sponge *Topsentia genitrix*. *Can. J. Chem.* **1987**, *65*, 2118-2121.

49. Burres, N.S.; Barber, D.A.; Gunasekera, S.P.; Shen, L.L.; Clement, J.J. Antitumor Activity and Biochemical Effects of Topsentin. *Biochem. Pharmacol.* **1991**, *42*, 745-751.

50. Pettit, G.R.; Kamano, Y.; Herald, C.L.; Tuinman, A.A.; Boettner, F.E.; Kizu, H.; Schmidt, J.M.; Baczynskyj, L.; Tomer, K.B.; Bontems, R.J. The Isolation and Structure of a Remarkable Marine Animal Antineoplastic Constituent: Dolastatin 10. *J. Am. Chem. Soc.* **1987**, *109*, 6883-6885.

51. Bai, R.; Pettit, G.R.; Hamel, E. Dolastatin 10, a Powerful Cytostatic Peptide Derived from a Marine Animal. Inhibition of Tubulin Polymerization Mediated Through the Vinca Alkaloid Binding Domain. *Biochem. Pharmacol.* **1990**, *39*, 1941-1949.

52. Bai, R.; Pettit, G.R.; Hamel, E. Binding of Dolastatin 10 to Tubulin at a Distinct Site for Peptide Antimitotic Agents Near the Exchangeable Nucleotide and Vinca Alkaloid Sites. *J. Biol. Chem.* **1990**, *265*, 17141-17149.

53. Luesch,H.; Moore,R.E.; Paul, V.J.; Mooberry, S.L.; Corbett, T.H. Isolation of Dolastatin 10 from the Marine Cyanobacterium *Symploca* Species VP642 and Total Stereochemistry and Biological Evaluation of Its Analogue Symplostatin 1. *J. Nat. Prod.* **2001,** *64,* 907-910.

54. Rinehart, K.L.; Holt, T.G.; Fregeau, N.L.; Stroh, J.G.; Keifer, P.A.; Sun, F.; Li, L.H.; Martin, D.G. Ecteinascidins 729, 743, 745, 759A, 759B, and 770: Potent Antitumor Agents from the Caribbean Tunicate *Ecteinascidia turbinata*. *J. Org. Chem*., **1990**, *55*, 4512-4515.

55. Zewail-Foote, M.; Hurley, L.H. Ecteinascidin 743: A Minor Groove Alkylator That Bends DNA toward the Major Groove. *J. Med. Chem.* **1999**, *42*, 2493-2497.

56. Gunasekera, S.P.; Gunasekera, M.; Longley, R.E.; Schulte, G.K. Discodermolide: A New Bioactive Polyhydroxylated Lactone from the Marine Sponge *Discodermia dissoluta*. *J. Org. Chem.* **1990**, *55*, 4912-4915.

57. Martello, L.A.; LaMarche, M.J.; He, L.; Beauchamp, T.J.; Smith, A.B., III; Horwitz, S.B. The relationship between Taxol and (+)-discodermolide: synthetic analogs and modeling studies. *Chem. Biol.* **2001**, *8*, 843-855.

58. Smith, A.B., III; LaMarche, M.J.; Falcone-Hindley, M. Solution Structure of (+)-Discodermolide. *Org. Lett.* **2001**, *3*(5), 695-698.

59. Mickel, S. J.; Niederer, D.; Daeffler, R.; Osmani, A.; Kuesters, E.; Schmid, E.; Schaer, K.; Gamboni, R.; Chen, W.; Loeser, E.; Kinder, F. R., Jr.; Konigsberger, K.; Prasad, K.; Ramsey, T. M.; Repic, O.; Wang, R.-M.; Florence, G.; Lyothier, I.; Paterson, I. Large-Scale Synthesis of the Anti-Cancer Marine Natural Product (+)-Discodermolide. Part 5: Linkage of Fragments C1-6 and C7-24 and Finale. *Org. Proc. Res. Dev.* **2004**, *8*, 122-130.

60. Kingston, D.G.I. Personal communication.

61. Tsuda, M.; Mugishima, T.; Komatsu, K.; Sone, T.; Tanaka, M.; Mikami, Y.; Shiro, M.; Hirai, M.; Ohizumi, Y.; Kobayashi, J. Speradine A, a New Pentacyclic Oxindole Alkaloid from a Marine-derived Fungus *Aspergillus tamarii*. *Tetrahedron* **2003**, *59*, 3227-3230.

62. Piña, I.C.; Gautschi, J.T.; Wang, G.-Y.-S.; Sanders, M.L.; Schmitz, F.J.; France, D.; Cornell-Kennon, S.; Sambucetti, L.C.; Remiszewski, S.W.; Perez, L.B.; Bair, K.W. ; Crews, P. Psammaplins from the Sponge Pseudoceratina purpurea: Inhibition of Both Histone Deacetylase and DNA Methyltransferase. *J. Org. Chem.* **2003**, *68*, 3866-3873.

63. Mohammed, K.A.; Hossain, C.F.; Zhang, L.; Bruick, R.K.; Zhou, Y.-D.; Nagle, D.G. Laurenditerpenol, a New Diterpene from the Tropical Marine Alga *Laurencia intricata* that Potently Inhibits HIF-1 Mediated Hypoxic Signaling in Breast Tumor Cells. *J. Nat. Prod.* **2004**, *67*, 2002-2007.

64. Stierle, D.B.; Stierle, A.A.; Hobbs, J.D.; Stokken, J; Clardy, J. Berkeleydione and Berkeleytrione, New Bioactive Metabolites from an Acid Mine Organism. *Org. Lett.* **2004**, *6*, 1049-1052.

II. Isolation and Characterization of Bioactive Isomalabaricane Triterpenoids from *Rhabdastrella globostellata*

2.1 Introduction

2.1.1 Previous Investigation of the *Rhabdastrella* Genus

The genus *Rhabdastrella* is part of the family Ancorinidae, and consists of marine sponge species that are distributed around the south Pacific region. Several chemical studies of *Rhabastrella* species have been performed. At the same time, there have been many chemical studies of sponges which were not classified as *Rhabdastrella* species initially that have been subsequently been identified as such, like *Jaspis stellifera*.[1] The difficulty appears to lie in the identification of the species; although various species like *R. globostellata* and *J. stellifera* are different species,[2] they can be easily mistaken for one another.

Most of the compounds that have been reported from the genus *Rhabdastrella* are of the isomalabaricane triterpenoid class, typified by **2.1** and **2.2**. Compound **2.1** was isolated from a sponge identified as *Stelletta globostellata*, which was later identified as *R. globostellata*. Compound **2.1** was isolated by use of the P-388 murine leukemia cell line along with other active compounds, and exhibited an IC_{50} of 0.1 μg/mL against this cell line.[3] The numbering system for this class of compounds is shown for **2.1**.

From an extract of a *R. globostellata* sponge, (-)-stellettin E (**2.2**) was isolated using an assay monitoring selective toxicity towards the HCT-116 colon cancer cell line. Along with another similar compound isolated from the sponge, **2.2** displayed good activity with an IC_{50} of 39 nM towards the $p21^{WAF1/Cip1}$-deficient HCT-116 cell line,

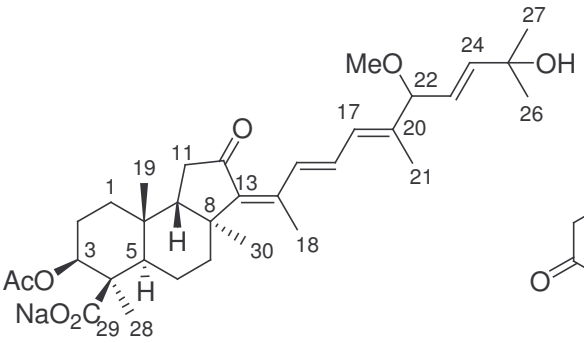

2.1

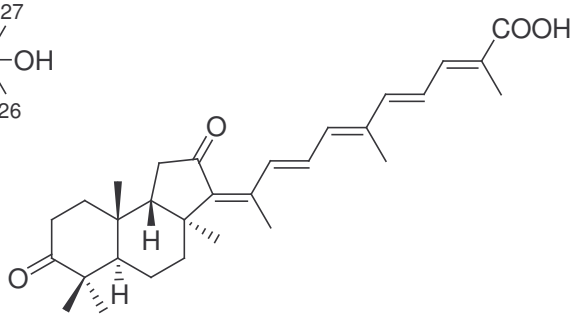

2.2

while showing less activity towards other mutant strains of the HCT-116 cells. Thus, **2.2** appears to have a specific, selective mechanism of action, although what this is has not been fully elucidated.[1]

Finally, from another collection of *R. globostellata*, aurorals 1 and 2 (**2.3a** and **2.3b)** were isolated as an isomeric mixture, along with other similar compounds. The mixture of **2.3a** and **2.3b** showed cytotoxicity towards epidermoid human carcinoma KB cells, with IC_{50} = 0.2 μg/mL. This case demonstrates one of the difficulties of working with compounds with this general structure, namely isomerization of the C13-C14 double bond; **2.2** also demonstrated this isomerism, which produces an inactive 13-*E* isomer.[4] Overall, compounds from *Rhabdastrella* species have been shown to have a variety of bioactivities with good potency.

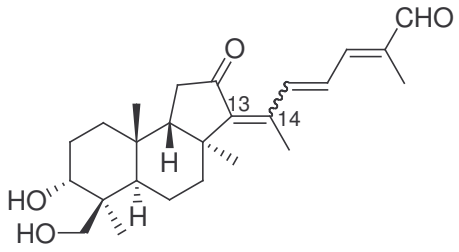

2.3a Δ^{13} = *Z*
2.3b Δ^{13} = *E*

2.1.2 The Role of DNA Polymerase β in DNA Repair and as a Drug Target

2.1.2.1 DNA Polymerase β and DNA Repair

Surprisingly, it has been estimated that the genome of every cell in the human body is damaged between 2,000 and 10,000 times every day.[5] Therefore, the repair of DNA damage in human cells, as well as other eukaryotic cells, is of the utmost importance to ensure survival. DNA is the blueprint for cellular proteins, and damaged DNA does not always allow for the synthesis of ideally functional proteins in cells. In a benign case, damaged DNA that is not repaired may cause a cell to shut down and self-destruct through the process of apoptosis. In the worst-case scenario, if DNA is damaged and the damage is passed on to daughter cells, mutations that occur over generations of cells can accumulate. Subsequent generations of cells may actually lose the ability to go through their life cycle normally. This can lead to tumorigenesis, the formation of tumors, where cells do not have checks on their proliferation. So, DNA repair in cells is important for the normal function of cells, as well as the prevention of tumorigenesis.

DNA damage can occur by several different mechanisms. These include damage from ionizing radiation, alkylation, oxidative damage, and cleavage of a base from the phosphate-sugar backbone. Because DNA repair is so important, eukaryotic cells have very complicated enzymatic machinery for maintaining the integrity of their genome. DNA polymerase β (pol β) is an enzyme that is important for the repair of DNA where a purinic or pyrimidinic base has been lost from the phosphate-sugar backbone, known as base-excision repair (BER). The formation of apurinic or apyrimidinic sites leads to single strand breaks (SSB) in DNA. Much work has focused on understanding the role of pol β in BER and other parts of DNA repair.

When a single purine or pyrimidine base in DNA has been damaged, two basic steps must occur to repair the damage. First, phosphate linkages in the DNA backbone must be broken around the damaged base so that it may be removed. Secondly, a new nucleotide must be inserted and joined to the backbone. Pol β is a 39-kDa protein that possesses two distinct domains that accomplish these two basic functions. One domain is an 8-kDa region that is able to bind to single-stranded DNA but not double-stranded DNA. The second domain is a 31-kDa region that binds to double stranded DNA, but not single-stranded DNA.[6] The 8-kDa region, the lyase domain, has been shown to be required for the removal of a single nucleotide in BER, while the 31-kDa region is able to catalyze the insertion of a new nucleotide, using the complementary strand as a template.[7] There are only two protein components required to assist pol β in BER. First, the protein AP endonuclease (APE) is required to bind to the DNA and to pol β, and then to promote the lyase activity of pol β. Secondly, DNA ligase II or III is also needed in order to reconnect phosphate linkages removed after base excision.[8] Similar steps must occur if the damaged area is larger than one nucleotide, where DNA polymerases δ and ε are needed, but damage to a single base is by far the most common form of DNA damage. The basic steps of repair for a single-strand cleavage are displayed schematically in Scheme 2.1, where the process normally proceeds in order from step A to step E.

It is known that after oxidative damage from UV-a light, pol β and its associated proteins move into action quickly in cells to carry out BER. It is believed that the cell cycle enzyme p53 is an important part of the general response to DNA damage, and p53 has been shown to directly bind to pol β and promote the repair and stabilization of DNA.[9] The enzyme p53 has been shown to be one of the most important mediators of

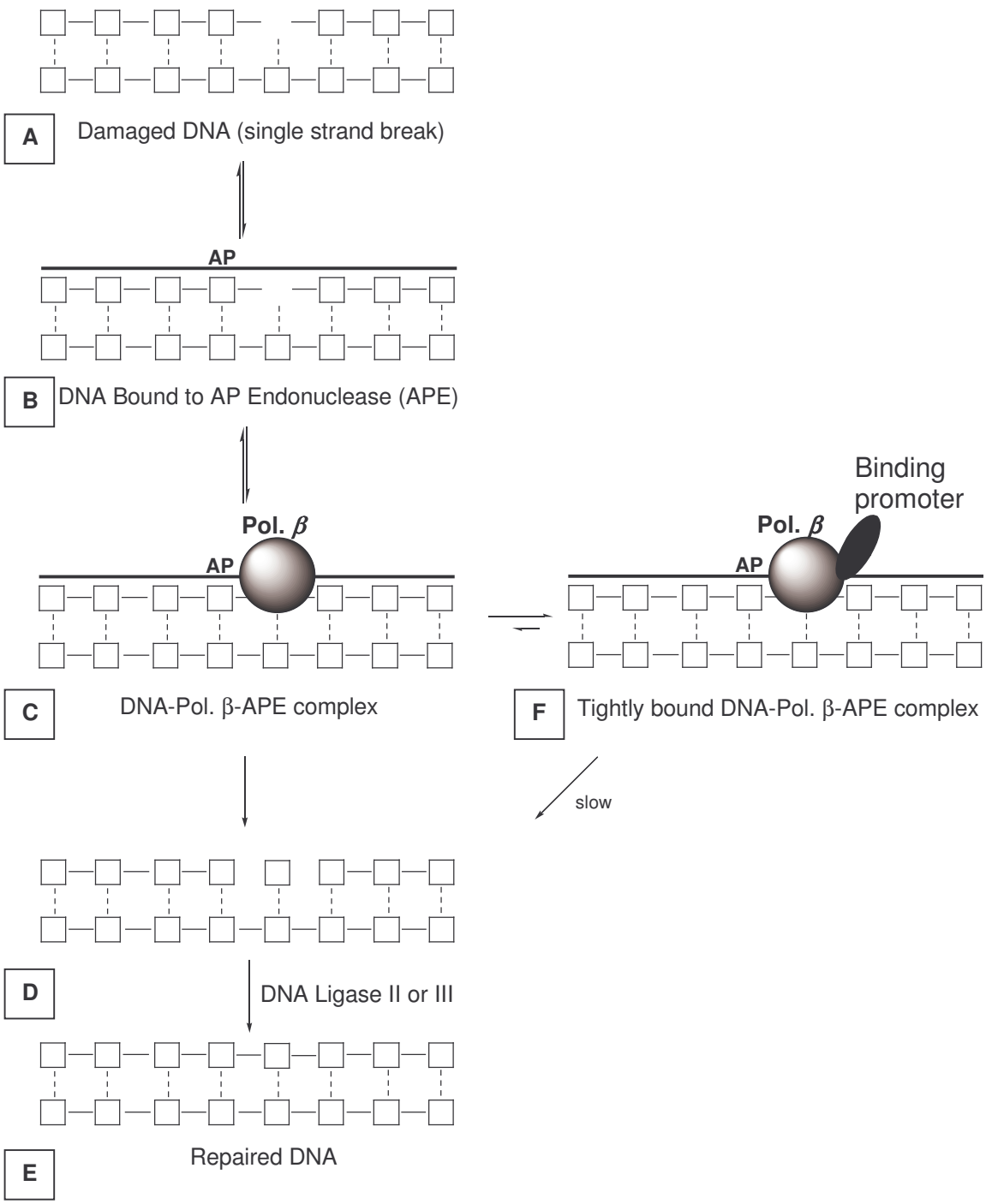

Scheme 2.1: Schematic of single strand break repair by DNA polymerase β, and effect of binding promoter on rate of DNA repair

cell cycle arrest and DNA repair. The regulation of the cellular response to DNA damage is more closely examined in Chapter 7. For now, it is clear that pol β is one of the most important enzymes for maintaining genomic integrity.

2.1.2.2 DNA Polymerase β and Antitumor Treatments

Since it has been established that pol β is important for maintaining the integrity of the genome, it is a potential target for developing combination therapies for DNA damaging agents. Ionizing radiation, cis-platin, and bleomycin treatments are all examples of DNA damaging agents that are very commonly used in cancer chemotherapy. The cell division rate for tumor cells is more rapid than for normal cells. Therefore, agents which cause damage to DNA will affect the proliferation of tumor cells more than normal cells. Two other factors are involved. First, many cancers still have a functional DNA repair system than can lessen the effects of DNA damaging agents. Second, though there may be some selectivity for killing tumor cells, DNA damaging agents are generally cytotoxic.

It has been demonstrated *in vitro* that known pol β inhibitors can potentiate the activity of bleomycins. Treating CCL46 cells with non-toxic dosages of bleomycin or

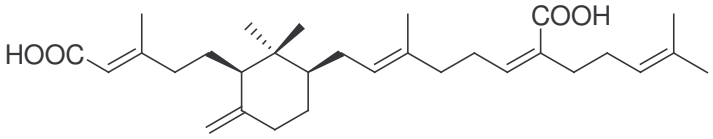

2.4

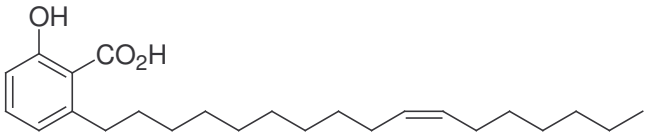

2.5

2.4 showed no effect relative to a control, but using the same dosages concurrently caused a nearly 50% decrease in cell proliferation.[10] Similarly, treatment of P388D cells with non-toxic dosages of bleomycin or **2.5** showed little effect on cell growth, but combination treatment led to a 32% decrease in cell proliferation.[11] The desired clinical consequence of the potentiation of a DNA damaging agent is that a smaller dosage of the DNA damaging agent might be used, thereby lowering the toxicity of the treatment while retaining or improving the potency. Thus, natural products that have pol β inhibitory activity might be potentially useful agents for reducing the toxicity of chemotherapy with DNA damaging agents.

A slightly different approach to pol β as a target is the use of agents which stabilize the binding of DNA with pol β. This is represented schematically in Scheme 2.1, as the alternative scheme leading to product F. When SSB repair is functioning normally, pol β is able to bind to DNA and unbind at reasonable rates. If an agent is added to the system that would cause pol β to bind to DNA more strongly than normal, this binding would disrupt the normal unbinding of DNA from pol β. Therefore, the DNA would not be repaired as quickly. The net effect is that the overall rate of DNA repair would be decreased, but the mechanism of that rate decrease would not be based on inhibition of DNA binding, but on promotion of DNA binding. As will be reported in Chapter 6, the search for enzyme inhibitors often leads to non-specific inhibitors, while promoting the binding of DNA with pol β requires a more specific interaction between the enzyme and the binding promoter. This should thus be a more selective mechanism for decreasing the rate of DNA repair. The bioactive compounds discussed in the next section are promoters of the binding of DNA with pol β.

2.2 Results and Discussion

2.2.1 Isolation of Isomalabaricane Triterpenoids from *R. globostellata*

The isolation of stelliferin riboside (**2.6**), 3-*epi*-29-acetoxy-stelliferin E (**2.7**), stellettin J (**2.8**), and stelletin K (**2.9**) is depicted in Scheme 2.2. As mentioned in section 2.1.1, many compounds isolated from the *Rhabdastrella* genus are of the isomalabaricane class. Compounds of this class typically have a bright yellow color, and are known to photoisomerize. The photoisomerism is known to affect the bioactivity of these kinds of compounds,[1] so all work was performed with covered glassware under minimal lighting conditions.

Initial fractionation by use of an amino SPE cartridge, followed by preparative reverse phase HPLC, afforded several fractions of high purity and good bioactivity. From one fraction, reverse phase HPLC was used to isolate the active compound **2.6**. Compound **2.7** was isolated by normal phase cyano HPLC of an active fraction. Compounds **2.8** and **2.9**, also isolated by HPLC, were less active and were characterized in order to obtain structure-activity relationship information for metabolites from this extract. Compounds **2.8** and **2.9** were evaluated in the A2780 ovarian cancer cell line assay, and were both found to be active. Although other fractions contained bioactive compounds, they could only be isolated in appreciable amounts from fractions A-3, A-4, A-5, and fraction B.

Positive mode FABMS analysis of **2.6** revealed a pseudomolecular ion $[M+H]^+$ at m/z = 629.4053, which implied a molecular formula of $C_{37}H_{56}O_8$. The λ_{max} in the UV spectrum was 343 nm, with log ε 4.47, which was consistent with an α,β-unsaturated ketone conjugated to two additional double bonds with several alkyl substituents, based

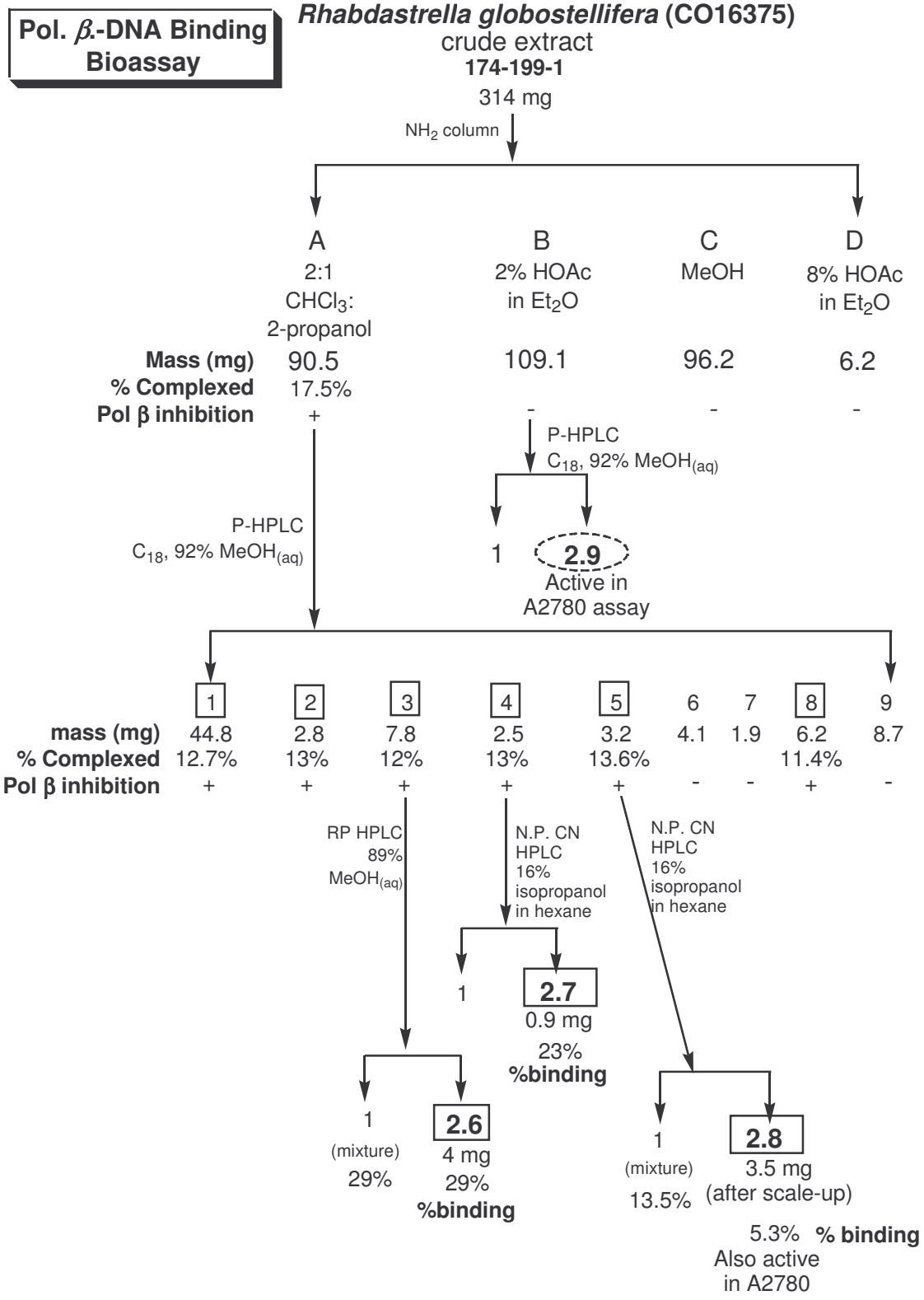

Scheme 2.2: Composite Fractionation Scheme for *Rhabastrella globostellata*

α,β unsaturated ketone		215
2 double bonds extending conjugation	2 × 30 =	60
exocyclic double bond		5
alkyl group attachments		
α		10
β		12
γ and higher	2 × 18 =	36
Calculated λ_{max}		338 nm

Table 2.1: Calculated λ_{max} for **2.6**

on Woodward's rules for α,β-unsaturated ketone UV absorbance (338 nm calculated).[12] This is summarized in Table 2.1. The formula corresponded to an unsaturation number of 10, which was consistent with the presence of several double bonds in the structure.

The ^{1}H NMR spectrum of **2.6** revealed several key signals that assisted in the determination of its structure. The ^{1}H NMR spectral data is found in Table 2.1. Nine methyl singlets (δ_H 0.88, 0.93, 1.01, 1.41, 1.61, 1.69, 1.76, 2.03, and 2.06), and four vinylic proton signals were visible (δ_H 8.00, 6.81, 6.24, and 5.04), while several signals ascribed to protons attached to oxygenated carbons were observed. The ^{13}C NMR spectrum of **2.6** consisted of thirty-seven signals. ^{13}C NMR spectral data is reported in Table 2.1. A ketone signal (δ_C 207.1) and a carboxyl carbon signal (δ_C 170.5) were observed in the low-field region, while eight sp^2 carbon signals were seen (δ_C 146.9, 142.2, 138.0, 134.5, 133.3, 130.8, 129.4, and 119.5). Seven oxygenated carbon signals were detected (δ_C 97.9, 82.0, 78.1, 72.6, 71.2, 69.8, and 62.9), and twenty aliphatic carbon signals rounded out the spectrum.

From the ^{1}H NMR spectrum, **2.6** appeared to contain a sugar moiety, and the ^{13}C NMR spectrum suggested the presence of an ester group (δ_C 170.5). The presence of an ester was supported by the presence of a methyl singlet (δ_H 2.06) in the ^{1}H NMR

Table 2.2: ^{1}H and ^{13}C NMR data (collected in $CDCl_3$) for **2.6**

Position	δ_C	δ_H	
1	29.5	1.20	m
		1.75	m
2	24.4	1.73	m
		1.98	m
3	78.1	4.76	br s
4	37.4		
5	41.6	2.28	br d, 12.3
6	18.2	1.46	m
7	38.6	2.11	m
8	44.8		
9	50.5	1.83	m
10	35.6		
11	36.8	2.20	m
12	207.1		
13	146.9		
14	142.2		
15	133.3	8.01	d, 15.6
16	129.4	6.81	dd, 11.2, 15.5
17	130.8	6.24	d, 10.8
18	16.1	2.03	
19	22.4	1.02	s
20	138.0		
21	11.8	1.76	s
22	82.1	4.19	t, 7.2
23	32.5	2.25	m
		2.42	m
24	119.5	5.04	t, 6.4
25	134.5		
26	25.8	1.69	s
27	18.0	1.61	s
28	27.9	0.89	s
29	21.6	0.93	s
30	24.2	1.41	s
3-*C*H_3CO	21.3	2.06	s
3-CH_3*C*O	170.6		
1'	97.9	4.41	d, 4.6
2'	71.2	3.51	t, 5.5
3'	72.6	3.63	t, 6.2
4'	69.8	3.75	m
5'	62.9	3.40	dd, 12.2, 6.2
		4.05	dd, 12.2, 3.5

spectrum, of which the shape and chemical shift were characteristic of an acetate methyl group. The carbon of the aglycone where the sugar was attached accounted for one oxygenated carbon, while the esterified carbon of the aglycone would account for a second oxygenated carbon. Hence, the ^{1}H and ^{13}C NMR data implied that the proposed sugar moiety would contain five carbons.

From the COSY spectrum of **2.6**, proton signals at δ_H 4.42, 4.06, 3.75, 3.63, 3.50, and 3.40 were observed as comprising a single spin system, presumably a pentose moiety. The pentose could have been either a pentofuranose or a pentopyranose, consisting of either a five or six-member ring, respectively. Neither case could be ruled out based on the COSY spectrum. The coupling constants were measured from the ^{1}H NMR spectrum, but HMBC data was needed to determine the identity of the sugar moiety.

From the COSY spectrum, the correlations of the four vinylic proton signals were informative as well. The three lower-field vinylic proton signals were shown to form an allylic system; one proton of this allylic system was also coupled to a methyl signal (δ_H 1.76) by allylic coupling. The fourth vinylic proton signal (δ_H 5.04) was correlated to two methyl signals (δ_H 1.61, 1.69), as well as two aliphatic protons (δ_H 2.40, 2.27). The structural fragments deduced by COSY are shown in Figure 2.1.

A fragment structure was deduced from all of this information. The UV data implied that three double bonds were conjugated with a ketone, and the carbon signal at δ_C 207.1 was consistent with the presence of an α,β-unsaturated ketone. So, in the skeleton, the α,β-unsaturated ketone was attached to the allylic moiety found from COSY to account for the observed conjugation to form Fragment A, shown in Figure 2.2. The

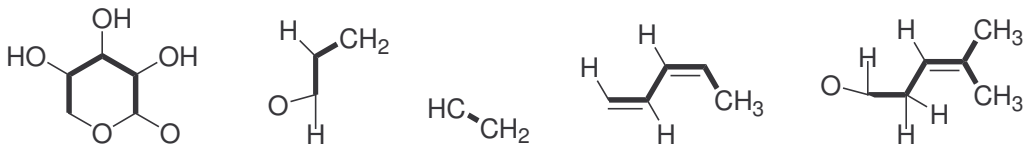

Figure 2.1: Fragments of **2.6** from COSY analysis

proposed sidechain bore resemblance to sidechains found in isomalabaricane triterpenoids discovered in other *Rhabdastrella* species (Fragment B, cf. **2.1**). Therefore, an isomalabaricane-type skeleton with a sugar substitution on the sidechain was proposed (Fragment C). HSQC data were obtained to determine C-H connectivity, and HMBC data were then used to evaluate the proposed structure and establish the full skeleton for **2.6**. The carbon-proton assignments based on the HSQC data are shown in Table 2.1.

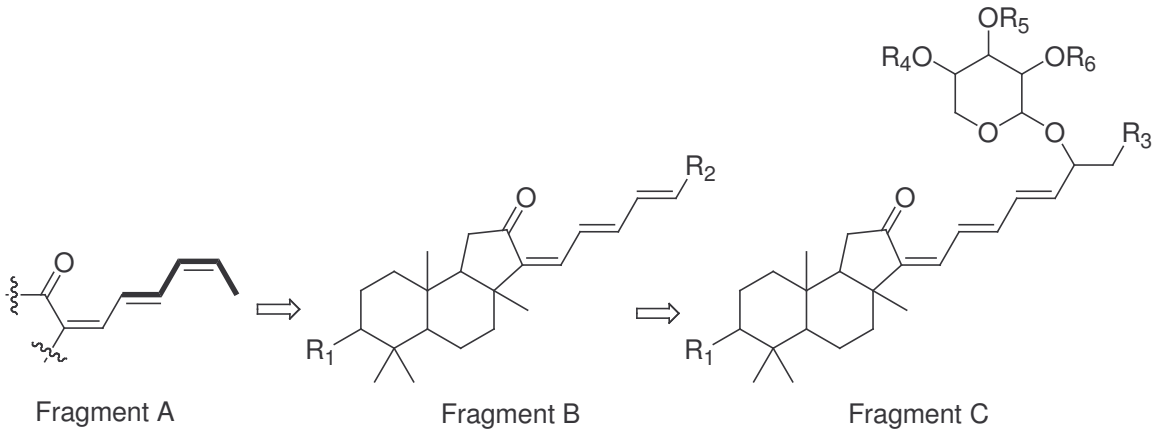

Figure 2.2: Fragment structures for **2.6**

From the HMBC data, the signal for the anomeric proton (δ_H 4.41) of the sugar unit was correlated to a methine carbon signal (δ_C 82.1). A proton connected with this methine carbon (δ_H 4.19) showed a correlation with the methyl carbon from the allylic moiety, a methylene carbon, and a quaternary carbon (δ_C 11.8, 32.5, and 138.0, respectively). This established that the sugar unit was attached to the sidechain of Fragment C. The anomeric proton signal was also correlated to a methylene carbon

signal at δ_C 62.9. This demonstrated that the sugar unit was a six-member ring, since a furanose would have yielded a correlation between the anomeric proton and a methine carbon. Because of the absence of HMBC correlations from the sugar proton signals to any other carbon signals other than those attributed to the sidechain, the groups R_4-R_6 in Fragment C were tentatively assigned as hydroxyl groups. The vinylic proton at δ_H 5.04 showed correlation with the methylene carbon at δ_C 32.5. This allowed the dimethyl moiety to be connected with the ribosyl sidechain. A correlation between the methine proton signal at δ_H 8.01 and the quaternary carbon signal at δ_C 146.9 confirmed the presence of the proposed trienone moiety, which completed the assignment of the entire sidechain. Key HMBC correlations are depicted in Figure 2.3

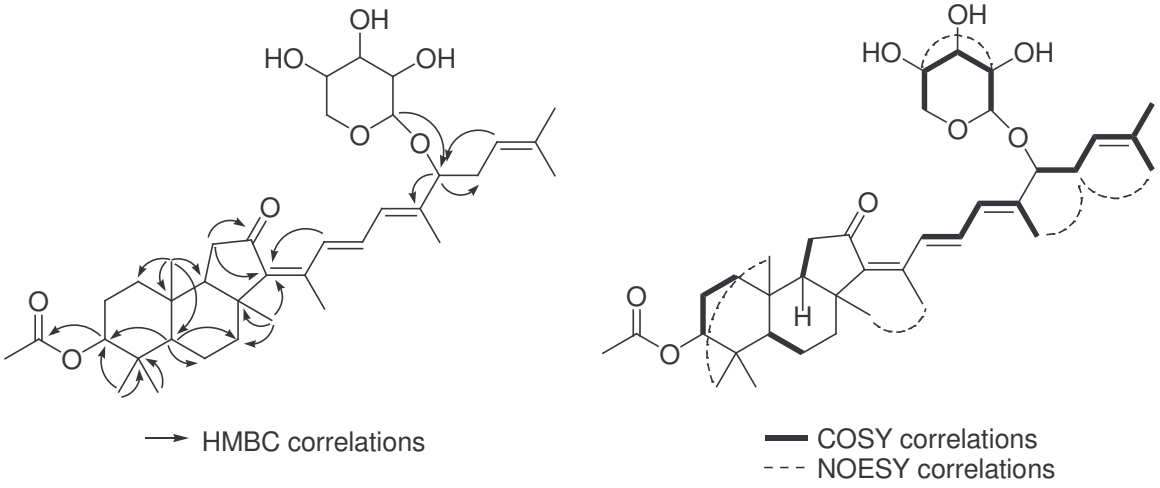

Figure 2.3: Key 2D NMR correlations for **2.6**

Staying with the proposed isomalabaricane-type skeleton, the rest of the structure was elucidated by interpretation of the HMBC spectrum. As shown in Figure 2.3, observed HMBC correlations were consistent with a tricyclic core, and the fragments deduced by COSY were shown to be connected in the tricyclic framework. Correlations between from both the methyl protons at δ_H 2.06 and the methine proton at δ_H 4.76 to the

carbonyl at δ_C 170.6 strongly implied the presence of an acetate ester group at C-3 of the ring. With a thirty-carbon framework, five-carbon sugar moiety, and an acetate group, the skeleton structure was consistent with the molecular formula from FABMS. Thus, the hypothesis that the ribosyl unit contained three hydroxyl groups was supported.

NOESY correlations allowed the C-25 and C-26 methyls to be distinguished, since a correlation was detected between the proton signal at δ_H 1.02 (C-26) and δ_H 2.25 (H-23). Based on the relatively small magnitude of the coupling constants determined for the pyranose protons H-2´, H-3´, and H-4´, these protons appeared to be in a *syn* relative configuration. A key NOESY correlation detected between H-2´ and H-4´ supported this observation. Thus, it was proposed that the pyranose moiety was a ribosyl unit. Key COSY and NOESY correlations are depicted in Figure 2.5.

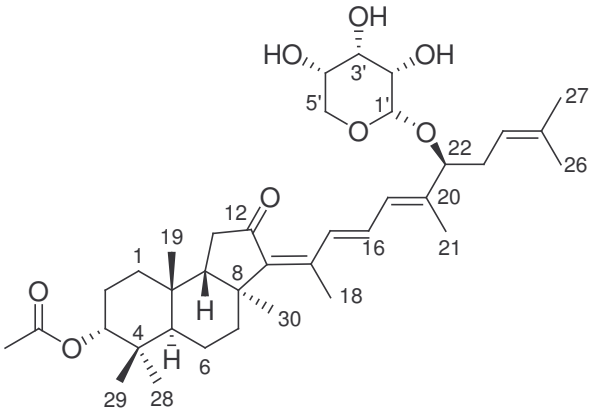

2.6

With two carbonyls, four double bonds, and four rings, the constraint of the unsaturation number was also met. Thus, the structural skeleton was determined to be that of the known compound stelliferin riboside (**2.6**), and the experimental data agree very well with data from the literature.[13] The relative stereochemistry was assigned as that previously reported, while the absolute stereochemistry of **2.6** was not determined

due to a lack of material for chemical degradation studies. Data for another compound isolated from this extract helped to resolve the stereochemistry issue, as described below.

Compound **2.7** was isolated as a yellow amorphous solid by repeated HPLC. From 2.3 g of crude extract, 0.9 mg of **2.7** was isolated; thus, **2.7** was a very minor component of the crude extract. Positive ion FABMS analysis showed a pseudomolecular ion at m/z = 597.3791, implying a molecular formula of $C_{36}H_{52}O_7$ for **2.7**. From UV spectrophotometry, **2.7** displayed a λ_{max} value of 342 nm (log ε 4.34), which was similar to the value for **2.6**. The unsaturation number for **2.7** was calculated to be eleven, which again suggested the presence of several double bonds and rings in **2.7**.

The ^{1}H NMR spectrum of **2.7** strongly suggested that the compound was very similar to **2.6**. The ^{1}H NMR spectral data is shown in Table 2.2. Four olefinic proton signals were observed at δ_H 4.98, 6.25, 6.81, and 7.99. Ten methyl singlets were observed at δ_H 1.00, 1.02, 1.41, 1.61, 1.68, 1.82, 2.01, 2.05, 2.06, and 2.08. Two oxygenated methine proton signals were observed at δ_H 5.00 and 5.15, while two proton signals from an oxygenated methylene appeared at δ_H 4.01 and 4.17. The chemical shift values for the two oxygenated methines and the oxygenated methylene suggested the presence of three ester groups. Further analysis was necessary to fully construct the structure of **2.7**.

The ^{13}C NMR spectrum did not have a good signal-to-noise ratio due to the small amount of material (0.9 mg), but several important signals could be picked out. The ^{13}C NMR spectral data is reported in Table 2.2. Eight signals arising from sp^2 carbons were observed at δ_C 118.9, 127.9, 130.1, 132.9, 134.8, 139.2, 142.6, and 146.3, implying the presence of four double bonds. Three signals for oxygenated carbons were found at δ_C

Table 2.3: ^{1}H and ^{13}C NMR data (collected in $CDCl_3$) for **2.7**

Position	δ_C	δ_H	
1	29.3	1.21	m
		1.54	m
2	24.5	1.78	m
		1.99	m
3	73.7	5.00	t, 6.8
4	41.5		
5	42.3	2.39	m
6	19.0	1.52	m
		1.70	m
7	38.9	2.10	m
8	44.7		
9	50.4	1.85	m
10	35.5		
11	36.8	2.21	m
12	206.4		
13	146.3		
14	142.6		
15	132.9	7.99	d, 15.2
16	127.9	6.81	dd, 11.2, 15.6
17	130.1	6.25	d, 10.8, 1H
18	16.2	2.01	s
19	22.5†	1.02	s
20	139.2		
21	13.7	1.82	s
22	78.6	5.15	t, 6.6
23	32.0	2.30	m
		2.37	m
24	118.9	4.98	bs
25	134.8		
26	26.0	1.68	s
27	18.1	1.61	s
28	22.4†	1.00	s
29	67.3	4.01	d, 11.2
		4.17	d, 11.6
30	24.5	1.41	s
3-$\underline{C}H_3CO$	21.5+	2.08	s
3-$CH_3\underline{C}O$	171.5*		
22-$\underline{C}H_3CO$	21.4+	2.06	s
22-$CH_3\underline{C}O$	170.4*		
29-$\underline{C}H_3CO$	21.4+	2.05	s
29-$CH_3\underline{C}O$	170.4*		

*, +, †: may be interchanged

67.3, 73.7, and 78.6. Overall, thirty-two signals were observed. Based on the molecular formula from FABMS data, it appeared there were low-intensity signals not observed in the ^{13}C NMR spectrum. Two-dimensional NMR techniques were used to solve this problem.

Based on the strong similarity of the data of **2.7** with that of **2.6**, as well as COSY analysis, fragment B from Figure 2.4 was also proposed as the skeleton for **2.7**. Proton-carbon connectivity was determined by HSQC analysis, which was used to interpret the HMBC data and establish the structure of **2.7**. The proton-carbon assignments depicted in Table 2.2 are based on HSQC analysis.

From HMBC analysis, two additional carbon signals were detected at δ_C 206.4 and 170.4; the broad signal at δ_C 170.4 consisted of three overlapped signals, based on observed correlations from three different methyl signals (δ_H 2.08, 2.06, and 2.05). Based on these correlations and the chemical shifts of the methyl signals, **2.7** appeared to contain three acetate ester groups. Correlations between the methine proton signal at δ_H 5.15 and the carbonyl signal at δ_C 170.4, as well as the sp^2 carbon signals at δ_C 139.2,

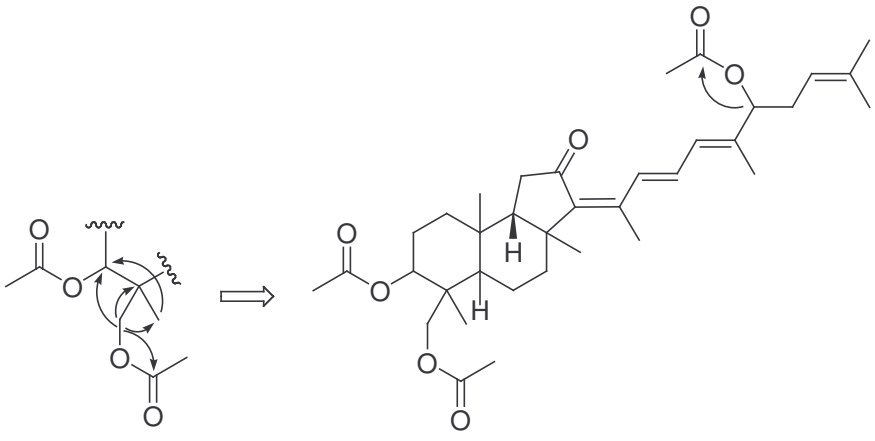

Fragment D Fragment E

Figure 2.4: Key HMBC correlations of **2.7**

127.9, and 118.9, demonstrated that one acetate group was attached to the sidechain of Fragment E. Correlations were found from the two oxygenated methylene proton signals at δ_H 4.01 and 4.17 to the carbonyl peak at δ_C 171.5 (part of the broad overlapped carbonyl signal), the methyl signal at δ_C 22.4, a quaternary carbonyl signal at δ_C 44.7, and an oxygenated carbon signal at δ_C 73.7. These data reveal that two of the ester linkages are in close proximity to each other. Correlations with the methyl and quaternary carbons strongly implied that the acetate esters were attached to positions 3 and 29 on the isomalabaricane skeleton as shown in Figure 2.4.

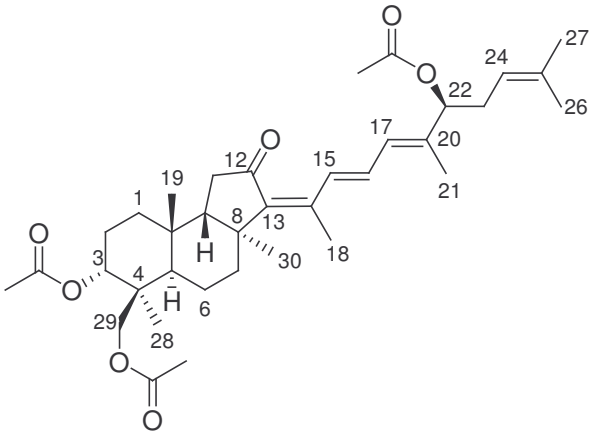

2.7

Given that the third acetate ester detected was shown to be attached to the sidechain based on HMBC correlations, and given the characteristic olefinic proton signals and the UV data suggesting the presence of a triene system conjugated to a ketone, the structure was tentatively assigned that shown for **2.7**. This structure has an unsaturation number of eleven, fulfilling the requirement based on the molecular formula deduced from FABMS. Further, the splitting pattern of H-3 suggested that the acetoxy group was in an axial position at C-3.

A search of the literature revealed that **2.7** was previously prepared as a semisynthetic derivative of a natural product, but it has not been isolated as a natural product. ^{1}H NMR data for the semisynthetic compound from the literature were compared with data for **2.7** and were found to be in very good agreement. A comparison of selected NMR signals are shown in Table 2.3. The absolute stereochemistry of the semisynthetic compound was determined by Oku *et al*.[2] Measurement of the optical rotation of **2.7** shows that the optical rotation of the natural product and the semisynthetic compound agree in sign (experimental: $[\alpha]_D^{22}$ = -45°, *c* 0.08, MeOH; literature: $[\alpha]_D^{24}$ = -50°, *c* 0.05, MeOH). So, the absolute stereochemistry for **2.7** is be assigned as shown, in accordance with the stereochemistry determined by Oku *et al.* for the semisynthetic compound. The name has been assigned as 3-*epi*-29-acetoxy-stelliferin E, in keeping with the convention for naming this class of compounds. Biosynthetically, the oxidation of C-22 in **2.6** is likely performed by the same enzyme that oxidizes C-22 in **2.7**. Because such transformations in biosynthesis are stereospecific, C-22 in both **2.6** and **2.7** probably have the same absolute stereochemistry at C-22. Therefore, **2.6** was assigned the indicated stereochemistry by analogy to **2.7**.

Compound **2.8** was isolated as a bright yellow amorphous solid from an active fraction, and was found to be weakly active in the DNA-Pol β binding assay. Positive ion FABMS analysis revealed a pseudomolecular ion $[M+H]^+$ at m/z = 453.3368, suggesting a molecular formula of $C_{30}H_{44}O_3$. The unsaturation number of nine again suggested the presence of several double bonds and rings in **2.8**. From UV analysis, **2.8** showed a λ_{max} of 396 nm (log ε = 4.46) in MeOH, which again was consistent with the presence of several conjugated double bonds.

Table 2.4: Selected ^{1}H NMR data (collected in C_6D_6) for **2.7**

Position	Experimental δ_H Values		Literature δ_H Values[2]
3	5.14	br s	5.13
15	8.76	d, 15.4	8.75
16	6.90	dd, 11.0, 15.4	6.89
17	6.53	d, 11.0	6.52
18	1.77	s	1.80
19	0.63	s	0.64
21	1.77	s	1.80
22	5.39	t, 6.7	5.38
23	2.31	m	2.30
	2.46	m	2.45
24	5.15	br s	5.14
26	1.51	s	1.52
27	1.59	s	1.60
28	0.99	s	1.00
29	4.22	d, 11.5	4.21
	3.92	d, 11.5	3.91
30	1.17	s	1.17
3-CH_3COO	1.71	s	1.72
22-CH_3COO	1.69	s	1.70
29-CH_3COO	1.66	s	1.67

The ^{1}H NMR spectrum yielded key information, and bore similarities to the spectra of **2.6** and **2.7**. Six olefinic signals were detected (δ_H 5.94, 6.23, 6.28, 6.52, 6.98, and 8.05), along with two oxygenated methylene protons (δ_H 3.57 and 3.79), an oxygenated methine proton (δ_H 4.09), and seven methyl singlets (δ_H 1.02, 1.10, 1.36, 1.82, 1.83,1.96, 2.02). ^{1}H NMR spectral data for **2.8** is found in Table 2.4.

^{13}C NMR analysis of **2.8** also revealed key information. Nine sp^2 carbon signals were detected (δ_C 126.2, 126.2, 131.4, 131.7, 132.3, 135.0, 137.1, 139.3, 143.1, 145.8), one of which was apparently two overlapped signals based on its intensity. A carbonyl signal (δ_C 206.7), and two oxygenated carbon signals, both of which appeared to be hydroxylated (δ_C 68.2 and 71.8) were also observed. Eighteen other signals rounded out the spectrum.

From COSY analysis, five different spin systems could be observed. Structural fragments for **2.8** based on COSY analysis are shown in Figure 2.5. Once again, three olefinic proton signals were correlated together with two methyl signals through allylic coupling. However, an additional spin system of olefinic protons was detected. The oxygenated methine proton at δ_H 4.09 was coupled to proton signals at δ_H 1.71 and 1.86.

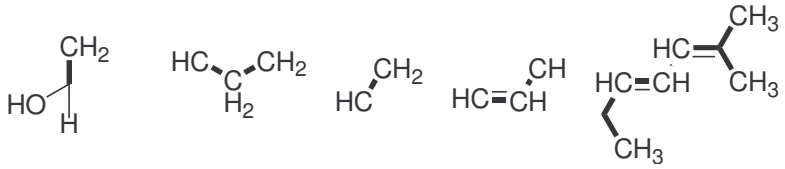

Figure 2.5: Structural fragments for **2.8** from COSY

HSQC analysis was utilized to determine the proton-carbon connectivity for **2.8**. The proton-carbon assignments based on HSQC are shown in Table 2.4. Based on the great similarity between the data for **2.8** and **2.7**, it was proposed that **2.8** was another isomalabaricane triterpenoid. Data from HMBC analysis was used to test this hypothesis.

Key HMBC correlations depicted for Fragment F in Figure 2.7 demonstrated how the hydroxylated carbons were near each other in **2.8**. Also, correlations from one olefinic proton signal (δ_H 6.28) to a carbon in a different spin system (δ_C 131.4) allowed for the two allylic spin systems from the COSY analysis to be connected. Based on the great similarity of the data for **2.8** with that of **2.6** and **2.7**, it was now proposed that **2.8** consisted of an isomalabaricane skeleton with two hydroxyl groups at the C-3 and C-29 positions, as seen for Fragment H in Figure 2.6. Further examination of the HMBC spectrum demonstrated that the proposed skeleton was completely consistent with the observed HMBC correlations. Additional key observed correlations are presented in

Table 2.5: ^{1}H and ^{13}C NMR data for **2.8**

Position	δ_C	δ_H	
1	29.1	1.23	m
		1.85	m
2	26.4	1.71	m
		1.86	m
3	71.8	4.09	dd, 2.4, 7.8
4	43.3		
5	42.4	2.23	m
6	19.4	1.42	m
		1.66	m
7	38.8	2.07	m
8	44.8		
9	50.3	1.75	m
10	34.9		
11	37.1	2.19	m
12	206.7		
13	145.8		
14	143.1		
15	132.3	8.05	d, 15.3
16	131.4	6.98	dd, 11.5, 15.3
17	131.7	6.28	d, 11.5
18	16.2	2.02	s
19	25.3	1.02	s
20	139.3		
21	13.2	1.96	s
22	135.0	6.23	d, 15.2
23	126.2	6.52	dd, 11.1, 15.2
24	126.2	5.94	d, 11.0
25	137.1		
26	18.8	1.82	s
27	26.5	1.83	s
28	19.9	1.10	s
29	68.2	3.57	d, 10.4
		3.79	d, 10.4
30	24.6	1.36	s

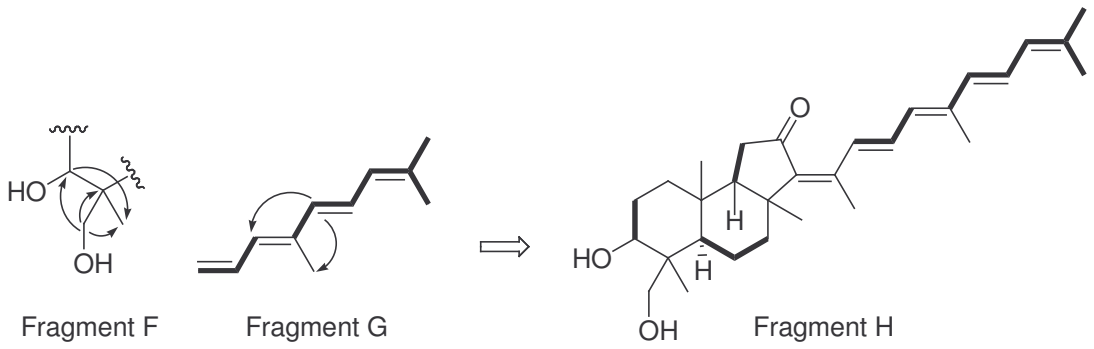

Figure 2.6: Proposed skeleton of **2.8** based on COSY and HMBC

Figure 2.7. The methyl groups from the sidechain were distinguished based on observed HMBC correlations. As in **2.6**, the HMBC correlations confirmed the connection of the sidechain to the tricyclic core.

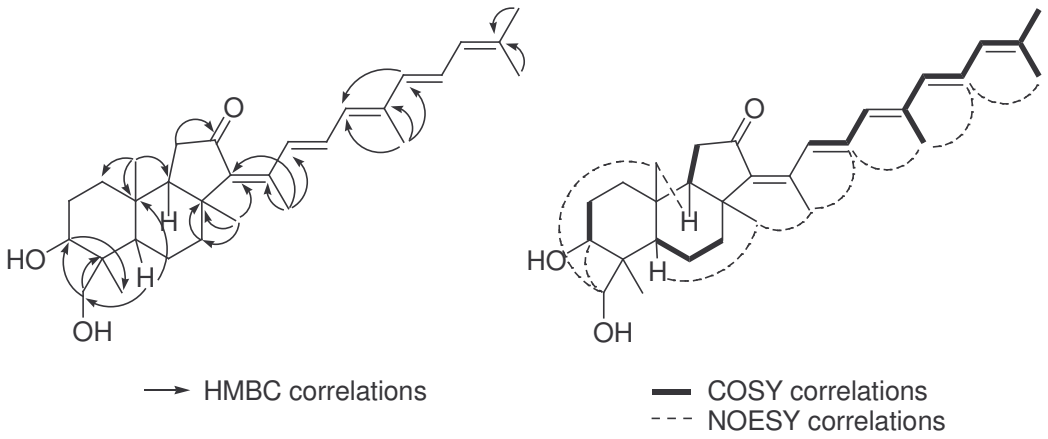

Figure 2.7: Key 2D correlations observed for **2.8**

NOESY analysis allowed for the assignment of the relative stereochemistry for **2.8**. Key NOESY correlations are shown in Figure 2.7, along with the previously described COSY correlations. NOESY correlations confirmed the assignment of the double bond configurations as shown. Correlations between the proton signal at δ_H 6.98 and the signals at δ_H 2.02 and 1.96, as well as correlations from δ_H 6.52 to the signals at δ_H 1.96 and 1.82, demonstrated the close proximity of the sidechain methyl groups to the

protons not displaying allylic coupling to any methyl signals. From the tricyclic core, strong NOESY correlations from the methyl signal at δ_H 1.02 to the methine signal at δ_H 1.75, and to the oxygenated methylene protons at δ_H 3.57 and 3.79, strongly suggested that the methine proton at H-9, the methyl protons at H-19, and the methylene protons H-29 were all on the same side of the tricyclic skeleton. A correlation from the methine at δ_H 2.23 to the methyl signal at δ_H 1.36 implied that the methyl protons H-30 were on the same face of the tricyclic skeleton as the methine proton at H-5. These correlations were fully consistent with the isomalabaricane triterpenoid skeleton discussed previously.

Based on the NOESY data mentioned, the hydroxylated methylene was assigned to C-29. The oxygenated methine proton signal at δ_H 4.09 showed a NOESY correlation to the proton at H-29b, while a strong correlation from H-3 to H-5 was not observed. Thus, the C-3 hydroxyl group was assigned an axial position. Thus, the structure of **2.8** was determined to be that shown below. The absolute stereochemistry was assumed to be that determined for **2.7**, based on the fact that the two molecules likely arise from a common biosynthetic precursor. This is the first reported isolation, characterization, and biological evaluation for this compound. We have assigned **2.8** the name stellettin J.

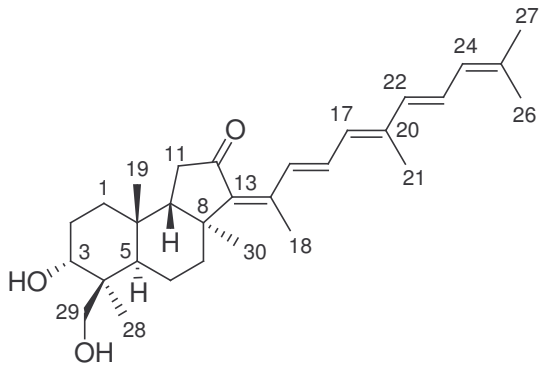

2.8

Compound **2.9** was isolated by preparative reverse phase HPLC purification of the 2% HOAc-ether fraction from the aminopropyl SPE separation, and was the most abundant compound in the extract. Compound **2.9** showed a λ_{max} of 401 nm (log ε = 4.59) in MeOH, suggesting that it might have a structure similar to known isomalabaricane triterpenoids that displayed similar UV absorption behavior. Positive ion FABMS analysis found a pseudomolecular ion at m/z = 467.3126, suggesting a molecular formula of $C_{30}H_{42}O_4$. This formula suggested an unsaturation number of ten, also consistent with the presence of several double bonds and rings.

The ^{1}H and C NMR spectral data is shown in Table 2.5. The ^{1}H NMR spectrum for **2.9** also revealed several characteristic features. Seven methyl singlets (δ_H 0.91, 1.33, 1.40, 1.82, 1.83, 1.96, and 2.04), and six olefinic proton signals (δ_H 5.94, 6.24, 6.29, 6.52, 6.98, and 8.05) were observed. Based on the splitting pattern, coupling constants, and integration for the olefinic proton signals, the olefinic proton signals were shown to arise from two separate spin systems. A proton signal arising from an oxygenated methine was observed at δ_H 4.16, suggesting the presence of a hydroxyl group. The ^{13}C NMR spectrum of **2.9** also yielded significant information. Two carbonyl peaks were found (δ_C 183.3 and 206.9), implying that **2.9** contained a ketone as well as an ester, lactone, or carboxylic acid. The signal at δ_C 183.3 was assigned to a carboxylic acid moiety, since **2.9** was isolated in a fraction by aminopropyl chromatography putatively containing carboxylic acids. Ten signals were observed in the sp^2 region of the ^{13}C NMR spectrum, two of which were overlapped, which indicated that **2.9** had five carbon-carbon double bonds. One oxygenated sp^3 carbon signal was found at δ_C 70.8, also consistent with the presence of a hydroxyl group. Twenty-nine peaks in all were detected in the ^{13}C NMR

spectrum. Because the 1D NMR data for **2.9** bore a striking similarity to that of **2.8** it seemed that **2.9** was an analog of **2.8**.

^{1}H-^{1}H COSY analysis revealed much about the connectivity of the olefinic protons. Two proton signals (δ_H 6.29 and 6.24) in two different spin systems from the ^{1}H

Table 2.6: ^{1}H and ^{13}C NMR data for **2.9**

Position	δ_C	δ_H	
1	28.8	1.14	m
		1.86	m
2	27.9	1.69	m
		2.20	bd,
3	70.8	4.16	br s
4	47.9		
5	40.6	2.46	br d, 11.2
6	20.3	1.87	m
7	38.9	2.12	m
8	45.0		
9	49.7	1.84	m
10	36.2		
11	37.2	2.24	m
12	206.9		
13	145.9		
14	143.1		
15	132.4	8.05	d, 15.2
16	131.4	6.98	dd, 11.2, 15.2
17	131.8	6.29	d, 11.6
18	16.2	2.04	s
19	19.9	0.91	s
20	139.3	1.96	s
21	13.2	6.24	d, 15.2
22	135.0	6.52	dd, 11.2, 15.2
23	126.2		
24	126.2	5.94	d, 11.2
25	137.0		
26	18.8	1.82	s
27	26.5	1.83	s
28	23.8	1.33	s
29	183.3		
30	24.9	1.40	s

NMR spectrum were shown to have COSY correlations with the same methyl signal (δ_H 1.96), suggesting that the two spin systems were actually connected through a quaternary carbon, giving rise to allylic coupling between the olefinic protons and the methyl protons. Additional correlations were observed between signals at δ_H 2.04 and 8.05, δ_H 1.82 and 5.94, and δ_H 1.83 and 5.94. These correlations strongly suggested the presence of four methyl groups attached to an conjugated alkene sidechain, like Fragment I shown in Figure 2.9. COSY correlations were also observed between the one-proton signal at δ_H 2.20 and signals at δ_H 1.14, 1.69, and 1.86. Additionally, COSY correlations were observed between the one-proton signal at δ_H 4.16 and the signals at δ_H 1.83 1.69 and 2.20. All of these correlations defined a spin system from a -CH_2CH_2-OH- moiety, depicted as Fragment J in Figure 2.9.

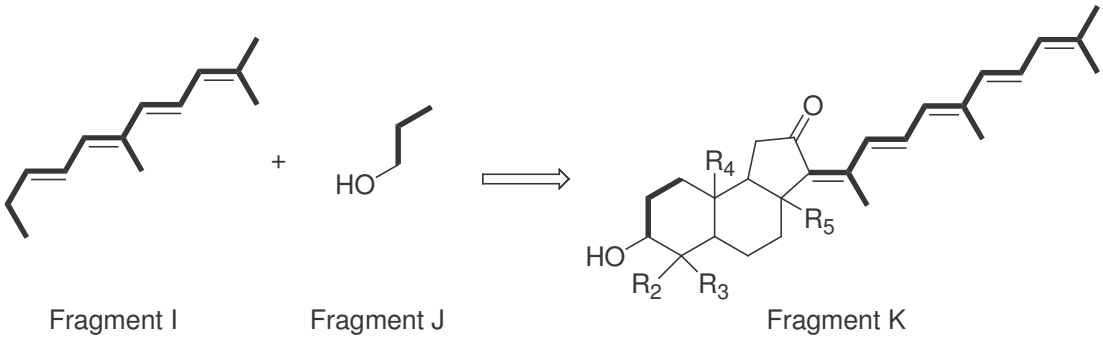

Figure 2.8: Structural fragments for **2.9**

The deduced sidechain was identical to that found for **2.8**. Along with this, based on the observation of seven methyl signals and two oxygenated sp^3 carbon signals, **2.9** was proposed to have a skeleton structure such as Fragment K, found in Figure 2.8, where R_1-R_5 represent unknown functional groups. Further analysis using 2D NMR was needed to elucidate the complete structure of **2.9**.

HSQC analysis allowed for the assignment of carbon-proton single bond connectivity. The assignments in Table 2.4 are based on the HSQC analysis. The data from the HSQC analysis was used to interpret the HMBC data, which allowed for the determination of the skeleton structure for **2.9**. The sidechain inferred from COSY analysis was confirmed by the observation of correlations between several methyl signals and signals for neighboring quaternary carbons. Key correlations between the methyl singlet at δ_H 1.33 and carbon signals at δ_C 70.8, 48.0, and 183.3 demonstrated how the proposed carboxylic acid moiety and the oxygenated carbon were in close proximity to each other, similar to the relative positions of the hydroxylated carbons in **2.8**. Correlations between the methine proton signal at δ_H 2.46 and carbon signals at δ_C 36.2 and 183.3, along with a correlation between the methyl signal at δ_H 0.91 and signals at δ_C 28.8, 36.2, and 49.7, helped to define a ring, when considered along with observed COSY correlations. These correlations are depicted for Fragment L in Figure 2.9.

The ring system of determined for **2.9** is completely consistent with the proposed isomalabaricane skeleton of Fragment K. When we consider the formula of $C_{30}H_{42}O_4$, and remember that **2.9** has seven methyls, one hydroxylated carbon, one carboxylic acid moiety, and an unsaturation number of ten, we can put Fragments K and L together and deduce that R_4 and R_5 represent methyl groups. Hence, we arrive at the skeleton structure shown in Figure 2.9. The relative stereochemistry was then determined.

Since the hydroxylated methine proton at δ_H 4.16 was a broad singlet, rather than a doublet of doublets, then the hydroxyl group was assigned an axial orientation. NOESY analysis was also employed to resolve stereochemical questions. NOESY correlations between the methine proton signals at δ_H 2.46 and 1.84 with the methyl

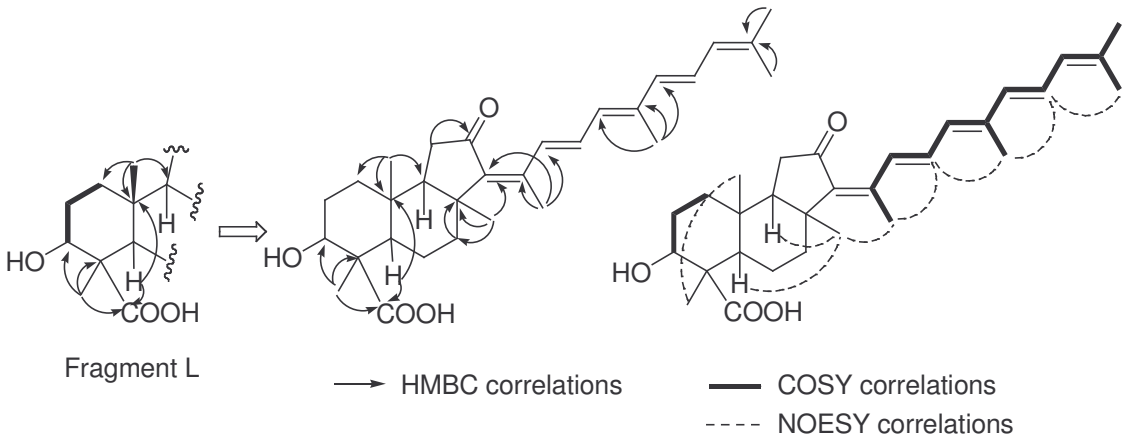

Figure 2.9: Key 2D NMR correlations for **2.9**

signal at δ_H 1.40 showed that these methines and the methyl were all on the same face of the tricyclic core of **2.9**. NOESY correlations between both the oxygenated methine proton at δ_H 4.16 and the methylene signal at δ_H 1.87 with the methyl signal at δ_H 1.33 showed that these proton sets had to be in close proximity. This suggested that both H-3 and the methyl attached at C-4 were in equatorial configurations, while at the same time the methyl at C-4 was in close proximity to a neighboring methylene. The lack of a NOESY correlation between the methyl at δ_H 1.33 and any other methyl signals further suggested that this methyl was in an equatorial position. Because of a lack of direct evidence for the stereochemistry at C-4, ^{13}C NMR data was compared with literature data for compounds with similar functional groups.

Only two relevant examples were found in the literature in which the spectra were obtained in $CDCl_3$; these were boswellic acids α and β (**2.10** and **2.11**).[14] As shown in Table 2.5, the data for the A-ring of **2.9** corresponds well with those for **2.10** and **2.11**. The deviation for C-5 may arise from the fact that the B-ring of **2.9** might adopt a twist-boat configuration, based on X-ray crystallography for similar isomalabaricane

triterpenoids,[17] which is unlikely for **2.10** and **2.11**. Otherwise, the data are consistent with the assignment of the methyl group at C-4 an equatorial configuration.

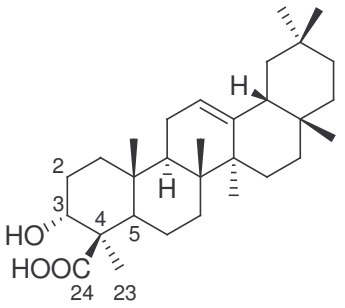

2.10

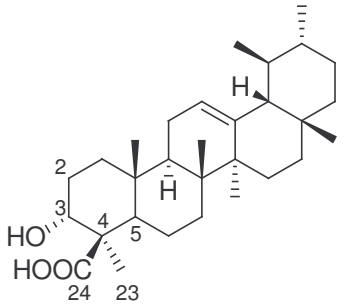

2.11

	δ_C		δ_C	
C #	**2.9**	C #	**2.10**	**2.11**
2	27.9	2	26.2	26.2
3	70.8	3	70.8	70.8
4	47.9	4	47.4	47.4
5	40.6	5	49.1	49.1
28	23.8	23	24.2	24.2
29	183.3	24	183.2	183.1

Table 2.7: ^{13}C NMR data comparison for **2.9** with compounds with similar functionality

Finally, NOESY correlations along the sidechain proves the *Z*,*E*,*E*,*E* stereochemistry for the pentaene moiety deduced by COSY. The observed NOESY correlations are depicted in Figure 2.9. The absolute stereochemistry was assigned by analogy to **2.7**, and the final structure of **2.9** is as shown below. The assignment of the

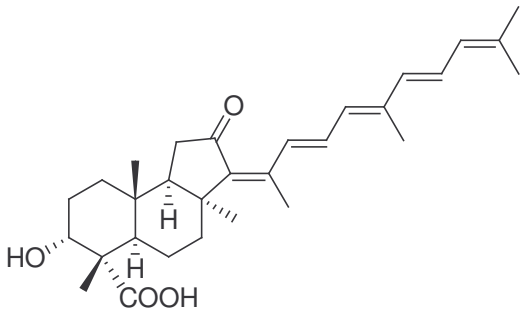

2.9

carboxylic acid to C-29 of **2.9** is analogous to the assignment of the hydroxyl group to C-29 in **2.8**. It is quite possible that either **2.8** or **2.9** is a biosynthetic precursor for the other compound. Thus, it is reasonable that the C-29 hydroxyl group in **2.8** and the C-29 acid group in **2.9** would be in analogous positions.

This is the first isolation and direct characterization of **2.9**. Following methylation of a crude sponge extract with diazomethane, the methyl ester of **2.9** was previously isolated[15] by SiO_2 chromatography, and the existence of the parent natural product was inferred. Here, we have isolated and directly characterized the natural product. The carbon data for the methylated natural product match well with the data for **2.9**, though the ^{1}H and ^{13}C assignments in the literature for the semisynthetic compound were incorrect. We have assigned **2.9** the name stellettin K.

2.2.2 Biological Evaluation of Stelliferin Riboside, 3-*epi*-29-Acetoxy-stelliferin E, Stellettin J, and Stellettin K

Compound **2.6** induces 29% binding at 28 μg/mL in the DNA-DNA polymerase β binding bioassay, while compound **2.7** induces 23% binding at that same concentration. Compound **2.8** is less active, and induces 5% binding, and **2.9** is not active in the assay. To our knowledge, **2.6** and **2.7** are first natural products shown to stabilize the interaction of DNA and pol β.

Because isomalabaricane triterpenoids have been previously reported as cytotoxic agents, **2.6**-**2.9** were tested in the A2780 ovarian cancer cell line, with IC_{50} values of 7.3, 27, 1.2, and 0.28 μM, respectively. The A2780 assay is discussed in detail in Chapter 3. This is the first report of the cytotoxicity of **2.7**-**2.9**. Some observations may be made

regarding the structure-activity relationship for these compounds. Compounds **2.6** and **2.7**, which both possess oxygenated sidechains, are active in the pol β binding assay, but they are not very active in the A2780 assay. On the other hand, **2.8** and **2.9**, which have fully conjugated sidechains, have good activity in the A2780 assay but little activity in the pol β binding assay. It appears that for pol β binding promoting activity, the flexibility of the oxygenated sidechains in **2.6** and **2.7** may allow for better binding to the enzyme-DNA complex, while the rigid polyene sidehain in **2.8** and **2.9** may not allow for this binding. At the same time, the fully conjugated sidechain in **2.8** and **2.9** appears to improve the cytotoxicity relative to **2.6** and **2.7**. As noted previously, the cytotoxicity profile of isomalabaricane triterpenoids has been shown to be very similar to that of the schweinfurthins, although the mechanism of action for neither compound class has been characterized.

2.2.3 Previous Investigation of Isomalabaricane Triterpenoids

Malabaricane and isomalabaricane triterpenoids like those isolated from *Rhabdastrella globostellata* have been previously reported to display interesting potential antitumor bioactivity. Malabaricane triterpenoids, typified by malabaricol (**2.12**) were originally isolated from the wood of the tree *Ailanthus malabarica*.[16] Later, as the study of marine natural products grew, compounds with a similar triterpenoid skeleton were isolated from various sponge species. This class of compounds, typified by **2.13**, were called the isomalabaricanes, since the new skeletons differed from the malabaricane skeleton in the stereochemistry at C-9 and C-10.[17] McCabe and co-workers elucidated the *trans-syn-trans* stereochemistry of the tricyclic core of **2.13** by X-ray crystallography,

and further work with NOESY spectroscopy has confirmed this stereochemistry for this skeleton.[3]

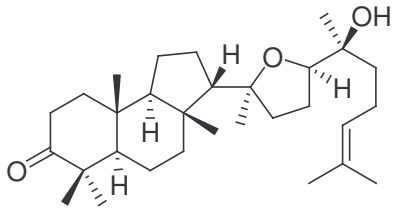

2.12

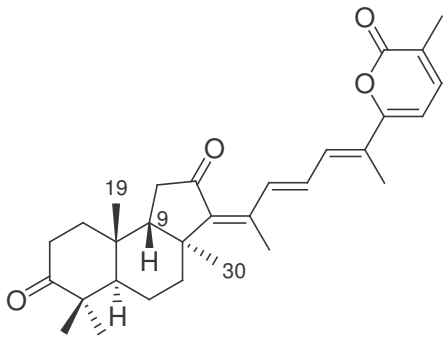

2.13

Using an assay that monitored changes in rat fibroblasts to find compounds with unique cytotoxic effects on cells, the isomalabaricane triterpene **2.14** was isolated from the sponge *Stelleta globostellata*, along with other similar compounds.[2] The assay measured vacuole size changes and persisting spindle fibers in rat fibroblasts. Observation of such morphological changes in the cell was used as a way of assaying agents which might inhibit actin polymerization or arrest cell division, among other effects. The IC_{50} of **2.14** in the 3Y1 rat fibroblast assay was 60 nM. Like other isomalabaricane triterpenes, **2.14** and compounds isolated along with it were subject to photoisomerization.

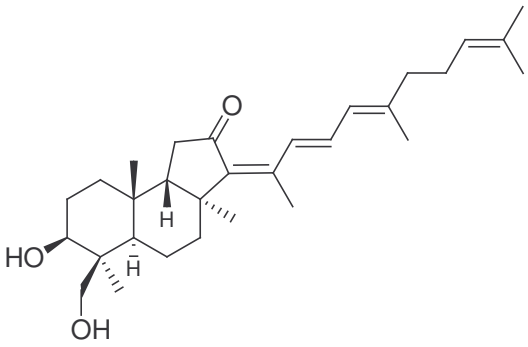

2.14

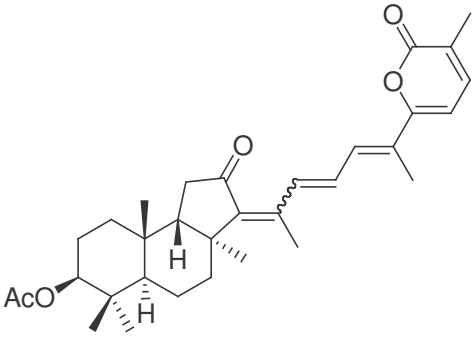

2.15a $\Delta^{13} = Z$
2.15b $\Delta^{13} = E$

From an extract of a sponge of *Stelletta* sp., compounds **2.15a** and **2.15b** were isolated as an isomeric mixture, along with other similar compounds. The compounds were all tested in the NCI's 60-cell line panel of assays, and the mixture of **2.15a** and **2.15b** was found to be the most potent, with a mean GI_{50} of 90 nM.[18] The cytotoxicity profile determined by COMPARE analysis for **2.15a** and **2.15b**, as well as the other active compounds isolated from the same extract, did not match any profiles in the NCI database, suggesting that these compounds may operate by a mechanism different from other known antitumor agents.[19] In summary, isomalabaricane triterpenoids have been shown to have good activity, and the study of these compounds may yield insights into new mechanisms of antitumor activity.

2.3 Experimental Section

General Experimental Procedures. IR spectra were recorded for neat samples with a MIDAC M-series FTIR spectrophotometer. UV spectra were recorded with a Shimadzu UV-1201 spectrophotometer. Molar absorptivities were determined at one concentration for each compound. HRFAB mass spectra were collected with a JEOL HX-110 spectrometer. NMR spectra were collected on either a Varian Inova 400 spectrometer operating at 399.9 MHz for ^{1}H and 100.6 MHz for ^{13}C, or a JEOL Eclipse+ 500 spectrometer operating at 500.2 MHz for ^{1}H and 125.8 MHz for ^{13}C.

Marine Sample Extraction. The sponge sample used in this work was collected for the National Cancer Institute by Pat Colin of the Coral Reef Research Foundation in Fiji on October 30, 1996, at 12 meters depth. The taxonomist was Michele Kelly (National Institute of Water & Atmospheric Research, Auckland, NZ) and a voucher is at the

Smithsonian Department of Worms under the collector number 0CDN4278. The deep frozen sample was pulverized at the National Cancer Institute in dry ice by use of a worm-fed grinder (hamburger mill), the powder produced was allowed to stand at -30 °C until the CO_2 sublimed, and the mass was then extracted at 4°C with de-ionized water (1 L) by stirring (30 rpm) for 30 min. The mixture was centrifuged at room temperature and the supernatant lyophilized to give the aqueous extract. The insoluble portion from the centrifugation was lyophilized and then statically extracted overnight at room temperature with 1 L of 1:1 MeOH–CH_2Cl_2. The organic phase was filtered, the pellet was washed with a 10% volume of fresh MeOH, and the combined organic phase was concentrated dryness at < 35°C by rotary evaporation and then finally dried under vacuum at room temperature to give the organic extract as a gum. An extract of this sponge was received from the National Cancer Institute as sample number C016375 (3.0 g).

DNA-DNA polymerase β binding bioassay (DNA binding mobility shift assay).
The bioassay was performed by Dr. Mei Li in the laboratory of Prof. Sidney Hecht at the University of Virginia, Charlottesville, VA, and this procedure was provided by them. The affinity of Pol β for a DNA substrate containing an apurinic site at position 20 was studied using a gel mobility assay in the presence and absence of the natural product samples. Pol β protein (30 nM) was incubated with 200 nM radiolabeled DNA substrate, and natural product samples (28 μg/mL) in buffer containing 10 mM HEPES-KOH, 50 mM KCl, 5 mM $MgCl_2$, 10 mg/mL bovine serum albumin (BSA) (10 μL total volume) at 37^{o}C for 2 hrs. Samples were loaded and separated by electrophoresis on a 12% non-

denaturing polyacrylamide gel, and the resulting bands were visualized by autoradiography. Bound protein was quantified using ImageQuant software, after scanning the gel using a Molecular Dynamics Phosphorimager.

3´-End Radiolabeling. A 36-base pair oligodeoxyribonucleotide containing a uridine at position 20 was radiolabeled at its 3´-end with terminal deoxynucleotidyltransferase using [α-^{32}P]2´,3´-dideoxyadenosine triphosphate (ddATP) as a substrate. The product was then purified using a 20% denaturing polyacrylamide gel. The band of interest was visualized by autoradiography and excised from the gel. After removal by the "crush and soak" method, these oligodeoxyribonucleotides were then annealed to their complementary strands by heating the solution at 70 °C for 3 min, followed by slow cooling to 25 °C.

Apurinic Site Preparation. A nicked apurinic (AP) site site was created in a reaction mixture (200 μL total volume) that contained 354 nM [α-^{32}P]-labeled double-stranded oligodeoxynucleotide having a uridine at position 20, 10 mM HEPES-KOH (pH 7.4), 50 mM KCl, 5 mM $MgCl_2$, 10 mg/mL BSA, 3 units AP endonuclease, and 2.4 units uracil-DNA glycosylase. After incubation at 37 °C for 20 min, the [α-^{32}P]-labeled double-stranded oligodeoxynucleotide containing an AP site at position 20 was ready for the assay.

Isolation of stelliferin riboside, 3-*epi*-29-acetoxy-stelliferin E, stellettin J, and stellettin K.

The crude extract of *Rhabdastrella globostellata* induced 0.3% binding of pol β with DNA in an initial screening and was selected for bioassay-guided fractionation. The crude extract (314 mg) was subjected to aminopropyl SPE chromatography (5 g stationary phase), to afford four fractions: a 2:1 $CHCl_3$:2-propanol wash (fraction A, 91 mg), a 2% acetic acid-ethyl ether wash (fraction B, 109 mg), a methanol wash (fraction C, 96 mg), and an 8% acetic acid-ethyl ether wash (fraction D, 6 mg). Fraction A was active in the polymerase β binding assay (18% binding), while fraction B was active in the A2780 cytotoxicity assay. Fraction A was further fractionated by use of preparative C_{18} reversed phase HPLC (25 cm × 2.1 cm, isocratic, 92% aq MeOH) to afford nine fractions, six of which were active. The most active fraction (fraction A-3, 11.5 min., 8 mg) was purified further by C_{18} reversed phase HPLC (25 cm × 1 cm, isocratic, 89% aq. MeOH), to afford **2.6** (4 mg, 29% binding). From another active fraction (fraction A-4, 13.5 min, 2.5 mg), repeated cyano normal phase (25 cm × 1 cm, isocratic, 84:16 hexane:2-propanol) and C_{18} reversed phase (25 cm × 1 cm, isocratic, 92% aq. MeOH) HPLC afforded **2.7** (0.4 mg, 23% binding; separation later scaled up to afford 0.9 mg). A third active fraction (fraction A-5) was unstable, so after scaling up and repeating the separation, compound **2.8** (3.5 mg, 5.3% binding) was isolated from fraction A-5 after repeated cyano normal phase and C_{18} reversed phase HPLC (same conditions as above). From fraction B of the aminopropyl separation, **2.9** was isolated by reversed phase HPLC (25 cm × 1 cm, isocratic, 92% aq MeOH) in high yield (25 mg) following a scaled up separation.

Stelliferin riboside (**2.6**): Light yellow powder; UV (MeOH) λ_{max} 343 (log ε 4.47); $[\alpha]_D^{22}$ = -60° (*c* 0.6, MeOH); IR (neat film) 3415, 2931, 1732, 1689, 1560, 1373, 1243, 1162, 1028, 970 cm^{-1}; ^1H NMR ($CDCl_3$) see Table 2.1; ^{13}C NMR ($CDCl_3$) see table 2.1; HRFABMS (positive ion) 629.4011 ($[M+H]^+$, calc. for $C_{37}H_{57}O_8$: 629.4053, Δ = 6.7 ppm).

3-*epi*-29-acetoxy-stelliferin E (**2.7**): Light yellow powder; UV (MeOH) λ_{max} 342 (log ε 4.34); $[\alpha]_D^{22}$ = -45° (*c* 0.08, MeOH); IR (neat film) 2915, 2849, 1732, 1693, 1373, 1234, 1018, 798 cm^{-1}; ^1H NMR ($CDCl_3$) see Table 2.2; ^{13}C NMR ($CDCl_3$) see Table 2.2; HRFABMS (positive ion) 596.3748 ($[M]^+$, calc. for $C_{36}H_{52}O_7$: 596.3714, Δ = 5.9 ppm).

Stellettin J (**2.8**): Bright yellow powder; UV (MeOH) λ_{max} 396 (log ε 4.46); $[\alpha]_D^{22}$ = -13° (*c* 0.3, $CHCl_3$); IR (neat film) 3432, 2917, 2849, 1674, 1555, 1536, 1449, 1378, 1205, 1028, 970 cm^{-1}; ^1H NMR ($CDCl_3$) see Table 2.4; ^{13}C NMR ($CDCl_3$) see Table 2.4; HRFABMS (positive ion) 453.3368 ($[M+H]^+$, calc. for $C_{30}H_{44}O_3$: 453.3369, Δ = 0.1 ppm).

Stellettin K (**2.12**) Bright yellow powder; UV (MeOH) λ_{max} 401 (log ε 4.59); $[\alpha]_D^{25}$ +56° (*c* 0.1, $CHCl_3$); IR (neat film) 3453, 2926, 1688, 1559, 1536, 1449, 1209, 1163, 974 cm^{-1}; ^1H NMR ($CDCl_3$) see Table 2.4; ^{13}C NMR ($CDCl_3$) see Table 2.4; HRFABMS (positive ion) 467.3174 ($[M+H]^+$, calc. for $C_{30}H_{43}O_4$: 467.3161 , Δ = 6.7 ppm).

References for Chapter 2

1. Tasdemir, D.; Mangalindan, G.C; Concepción, G.P.; Verbitski, S.M.; Rabindran, S.; Miranda, M.; Greenstein, M.; Hooper, J.N.A.; Harper, M.K.; Ireland, C.M. Bioactive Isomalabaricane Triterpenes from the Marine Sponge *Rhabdastrella globostellata.* *J. Nat. Prod.* **2002**, *65*, 210-214.

2. Oku, N.; Matsunaga, S.; Wada, S.; Watabe, S.; Fusetani, N. New Isomalabaricane Triterpenes from the Marine Sponge *Stelletta globostellata* that Induce Morphological Changes in Rat Fibroblasts. *J. Nat. Prod.* **2000**, *63*, 205-209.

3. Ryu, G.; Matsunaga, S.; Fusetani, N. Globostellatic Acids A-D, New Cytotoxic Isomalabaricane Triterpenes from the Marine Sponge *Stelletta globostellata.* *J. Nat. Prod.* **1996**, *59*, 512-514.

4. Bourguet-Kondracki, M.-L.; Longeon, A.; Debitus, C.; Guyot, M. New cytotoxic isomalabaricane-type sesterterpenes from the New Caledonian marine sponge *Rhabdastrella globostellata*. *Tetrahedron Lett.* **2000**, *41*, 3087-3090.

5. Lindahl, T. Instability and decay of the primary structure of DNA. *Nature* **1993**, *362*, 709-715.

6. Casas-Finet, J.R.; Kumar, A.; Karpel, R.L.; Wilson, S.H. Mammalian DNA Polymerase β: Characterization of a 16-kDa Transdomain Fragment Containing the Nucleic Acid-Binding Activities of the Native Enzyme. *Biochemistry* **1992,***31,* 10272-10280.

7. Lan, L.; Nakajima, S.; Oohata, Y.; Takao, M.; Okano, S.; Masutani, M.; Wilson S.H.; Yasui, A. *In situ* analysis of repair processes for oxidative DNA damage in mammalian cells. *PNAS* **2004**, *101*, 13738–13743.

8. Nicholl, I.D. Nealon, K.; Kenny, M.K. Reconstitution of human base excision repair with purified proteins. *Biochemistry* **1997**, *36*, 1557-1566.

9. Zhou, J.; Ahn, J.; Wilson, S.H.; Prives, C. A role for p53 in base excision repair. *EMBO J.* **2001**, *20*, 914-923.

10. Sun, D.-A.; Deng, J.-Z.; Starck, S.R.; Hecht, S.M. Mispyric Acid, a New Monocyclic Triterpenoid with a Novel Skeleton from *Mischocarpus pyriformis* that Inhibits DNA Polymerase β. *J. Am. Chem. Soc.* **1999**, *121*, 6120-6124.

11. Chen, J.; Zhang, Y.-H.; Wang, L.-K.; Sucheck, S.J.; Snow, A.M.; Hecht, S. M. Inhibitors of DNA polymerase β from *Schoepfia californica*. *J. Chem. Soc., Chem. Commun.*, **1998**, 2769–2770.

12. Silverstein, R.M.; Bassler, G.C.; Morrill, T.C. *Spectrometric Identification of Organic Compounds*, 5th Edition.; Wiley and Sons: New York. p 302.

13. Tabudravu, J.N.; Jaspars, M. Stelliferin Riboside, a Triterpene Monosaccharide Isolated from the Fijian Sponge *Geodia globostellifera*. *J. Nat. Prod.* **2001,** *64,* 813-815.

14. Culioli, G.; Mathe, C.; Archier, P.; Vieillescazes, C. A Lupane Triterpene from Frankincense (*Boswellia* sp., Burseraceae). *Phytochemistry* **2003**, *62*, 537-541.

15. Ravi, B. N.; Wells, R. J. Malabaricane Triterpenes from a Great Barrier Reef Collection of the Sponge *Jaspis Stellifera*. *Aust. J. Chem*. **1982**, *35*, 39-50.

16. Ravi, B. N.; Wells, R. R.; Croft, K. D. Malabaricane Triterpenes from a Fijian Collection of the Sponge *Jaspis stellifera*. *J. Org. Chem.* **1981**, *46*, 1998-2001.

17. McCabe, T.; Clardy, J.; Minale, L.; Pizza, C.; Zollo, F.; Riccio, R. A Triterpenoid Pigment with the Isomalabaricane Skeleton from the Marine Sponge *Stelletta* sp. *Tetrahedron Lett*. **1982**, *23*, 3307-3310.

18. McCormick, J.L.; McKee, T.C.; Cardellina, J.H.; Leid, M.; Boyd, MR. *J. Nat. Prod.*, **1996**, *59*, 1047-1050.

19. McKee, T.C.; Bokesch, H.R.; McCormick, J.L.; Rashid, M.A.; Spielvogel, D.; Gustafson, K.R.; Alavanja, M.M.; Cardellina, J.H.; Boyd, MR. *J. Nat. Prod.*, **1997**, *60*, 431-438.

III. Heteronemin, a Cytotoxic Sesterterpenoid from a Sponge of Genus *Dysidea*: Isolation, Characterization, and Semisynthetic Modification

3.1 Introduction

Using an assay measuring cytotoxicity towards the A2780 ovarian cancer cell line, bioassay-guided fractionation of an extract of a sponge of species *Dysidea* yielded the known scalarane sesterterpenoid heteronemin in good yield. Four derivatives of heteronemin were prepared semisynthetically from the natural product, and were tested for their bioactivity. We present results for the isolation and characterization of heteronemin, and synthesis and biological characterization of derivatives of the natural product.

3.1.1 Previous Investigation of *Dysidea* Species

As discussed in Chapter 1, marine natural products have generated enormous interest in the past 25 years, and sponges have been a major source of interesting bioactive compounds. The genus *Dysidea* has afforded several interesting compounds with activities ranging from anti-HIV activity to cytotoxicity. The diversity of bioactive structures available from the *Dysidea* genus makes it an attractive source of extracts for natural products drug discovery.

Many different sesquiterpenoids have been isolated from various *Dysidea* species. One important set are the avarols, which possess a rearranged drimane skeleton coupled to an aromatic moiety. Several avarol derivatives,[1] represented by avarol (**3.1**), have been isolated from various *Dysidea* species, and these compounds have generated some interest for their potential antileukemic and anti-HIV activity.[2] Compound **3.1** has also

been shown to be an inhibitor of tubulin polymerization. A similar compound from a *Dysidea* sponge, popolohuanone E (**3.2**), has been shown to be an effective inhibitor of

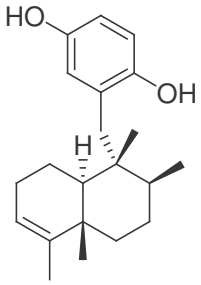

3.1

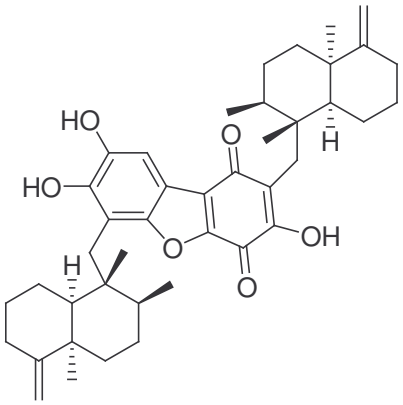

3.2

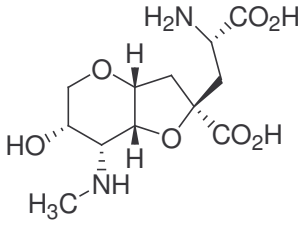

3.3

topoisomerase II, and it has even shown selective toxicity to a non-small cell human lung cancer cell line.[3] Other avarols have also shown activity as antioxidants and antimutagenic agents.[4]

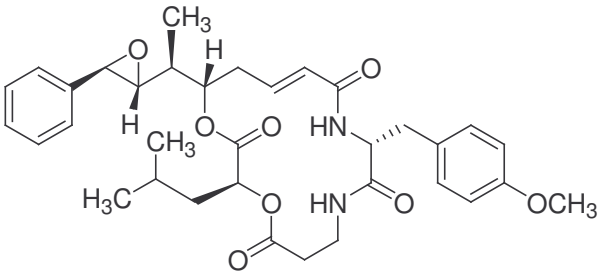

3.4

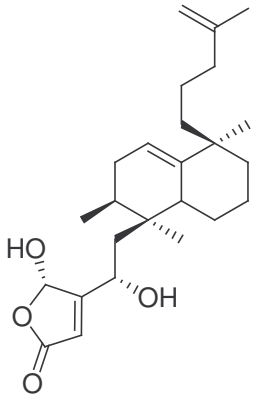

3.5

Dysiherbaine (**3.3**) is an amino acid from *Dysidea herbacea* that is a glutamic acid (Glu) agonist at kainate receptors in mouse brain tissue. Though its neuroexcitatory activity causes it to be a neurotoxin, such compounds are of interest as structural probes of the Glu receptor, for the development of potential neuroprotective agents.[5]

Arenastatin A (**3.4**) is a depsipeptide (a peptide-like compound that contains both amide linkages as well as ester bonds) that was originally isolated from an extract of *Dysidea arenaria*.[6] The compound has also been isolated from blue-green algae, suggesting a possible microbial origin.[7] Like the epothilones, **3.4** is a macrocyclic lactone with tubulin-binding ability, and it possesses picomolar *in vitro* activity against KB leukemia cells. Much work has focused on the total synthesis of **3.4**[8] and the synthesis of analogues.[9]

The sesterterpenoid dysidiolide (**3.5**) was isolated from the sponge *Dysidea etheria*, and showed micromolar inhibition of the phosphatase activity of Cdc25a.[10] Compound **3.5** also showed micromolar IC_{50} values in the A-549 human lung carcinoma and P388 murine leukemia cell lines. Several total syntheses have been published for **3.5**,[11,12] and a solid phase synthetic approach to the synthesis of **3.5** has led to derivatives with improved activity.

3.1.2 Background of the A2780 Assay

In order to guide the search for bioactive natural products, a bioassay that serves as an *in vitro* model of biological conditions is important for the identification of interesting drug-like compounds from natural sources. Most *in vitro* assays used in drug discovery are either mechanism-based or cell-based assays. Cell-based assays used in the search for potential antitumor agents usually involve measuring the toxicity of chemical agents towards a cell line culture. The A2780 cell line cytotoxicity assay measures the ability of chemical agents to inhibit the proliferation of A2780 ovarian tumor cells. A2780 cells are epithelial-type adenocarcinoma cells that are derived from tumor cells

collected from a patient who was not treated by chemotherapy.[13] Assays measuring toxicity to A2780 cells have been implemented as methods for finding new antitumor agents.

Tumors develop as a result of a sequence of mutations that lead to uncontrolled cell growth, but the biochemical factors leading to the formation of ovarian tumors have not been fully elucidated. A2780 cells have been widely studied as a model for ovarian tumors. As part of understanding ovarian tumorigenesis (the formation of new tumors), it has been found that a loss of a region of human chromosome 17 is very commonly observed in ovarian and breast tumor cells. A2780 cells have a mutation on chromosome 17 in the region 17p13.3 that codes for a protein named OVCA1. When the mutated *OVCA1* gene is replaced by the wild-type gene, the growth of the transfected A2780 cells is reduced as much as 60%. Thus, *OVCA1* has been identified as a potential ovarian tumor suppression gene, much as *BRCA1* was identified as a breast tumor suppression gene.[14]

Additionally, loss of expression of the gene pRb2/p130, which maps to human chromosome 16 at region 16q12.2, has been observed in 40% of ovarian carcinoma samples in one study, and this loss of expression was also found in A2780 cells. Transfection of a repaired pRb2/p130 gene into A2780 cells led to a 20% increase in the number of cells arrested in the G_1 phase of the cell cycle, which suggests that pRb2/p130 might also serve as a tumor suppression gene.[15] At the same time, it is known that the parent strain of A2780 cells has the wild-type, unmutated *p53* gene,[16] mutations of which occur in about 50% of ovarian tumors. The role of the p53 protein in cell cycle regulation is discussed further in Chapter 7. Several drug-resistant A2780-derived cell

lines have been developed and analyzed to aid in understanding the relationship between drug resistance in tumors and gene expression.[17] Because the A2780 cell line displays key mutations that are commonly found in ovarian tumors, it is a good cell-based target for antitumor drug discovery efforts.

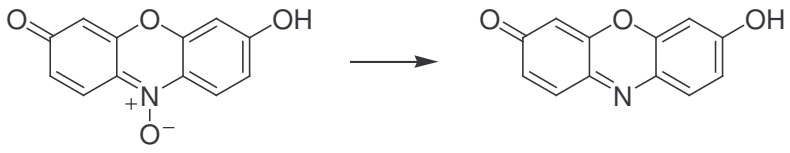

3.6 **3.7**

Blue, non-fluorescent Pink, highly fluorescent

Scheme 3.1: Reduction of resazurin (**3.6**) to resorufin (**3.7**).

The A2780 bioassay used in the Kingston laboratory is a microtiter plate-based method which uses resazurin (**3.6**, sold as a saline solution under the name Alamar blue) as a dye for the purpose of detecting live cells in culture. The tumor cells are treated with a potential cytotoxic agent, and are then incubated for two days. The cells are then stained with **3.6**. Compound **3.6** is the *N*-oxide of the hydroxyphenoxazone resorufin (**3.7**). When the cells in the growth medium are stained with **3.6**, living cells take in the dye. While **3.6** is blue and non-fluorescent, **3.7** is pink and highly fluorescent, and thus fluorescence can be used as a measure of cell viability. It has been shown that living cells reduce the dye internally and excrete **3.7**, since minimal fluorescence is observed from stained cells that have been separated from stained growth medium. The actual mechanism of this reduction is not known.[18] It has been shown that cytotoxicity measurements performed using Alamar blue with a fluorescent plate reader for live cell

detection compare very well with other methods in terms of accuracy,[19] and the sensitivity of Alamar blue-based assays is comparable to radioactivity-based assays.[18]

3.2 Results and Discussion

3.2.1 Isolation of Heteronemin

The isolation of **3.8** is depicted in Schemes 3.2 and 3.3. The crude extract showed activity in the A2780 ovarian cancer cell line assay, with IC_{50} = 1.2 μg/mL. The crude extract was subjected to liquid partitioning, affording three active fractions. After bioassay guided fractionation using Sephadex® LH-20 purification and reverse phase C_{18} column chromatography on each active fraction, **3.8** was isolated as the most active compound (IC_{50} = 0.9 μg/mL), and was detected in each fraction with significant activity (IC_{50}<10 μg/mL).

A pseudomolecular ion at m/z = 495.3292 ($[M+Li]^+$) was observed by high resolution positive ion FABMS analysis of compound **3.8**. This corresponded to a formula of $C_{27}H_{40}O_4$. ^1H and ^{13}C NMR spectral data are reported in Table 3.1. The data presently discussed were collected using *d*-pyridine (C_5D_5N) as a solvent for NMR spectroscopic analysis. ^1H NMR spectroscopy revealed several key signals. These included seven methyl singlets, two of which appeared to be sharp acetate singlets (δ_H 0.86, 0.76, 0.79, 0.74, 1.13, 1.97, and 2.15), a signal arising from a proton attached to a hydroxylated carbon (δ_H 3.65), and a singlet due to a proton attached to a sp^2 hybridized carbon (δ_H 6.58). Twenty-nine signals were observed by ^{13}C NMR spectroscopic analysis. These signals included two signals ascribed to carbonyl carbons from either a carboxylic acid or an ester functional group (δ_C 169.8, 170.0). Also, two other signals for

sp^2 carbons were detected (δ_C 135.6, 114.5), and a signal characteristic of a carbon attached to two oxygens was observed (δ_C 100.5). DEPT spectral analysis aided in the interpretation of the carbon spectrum, and revealed that compound **3.8** contained seven methyls, seven methylenes, and eight methines, and, therefore, seven quaternary carbons.

Scheme 3.2: The isolation of **3.8**

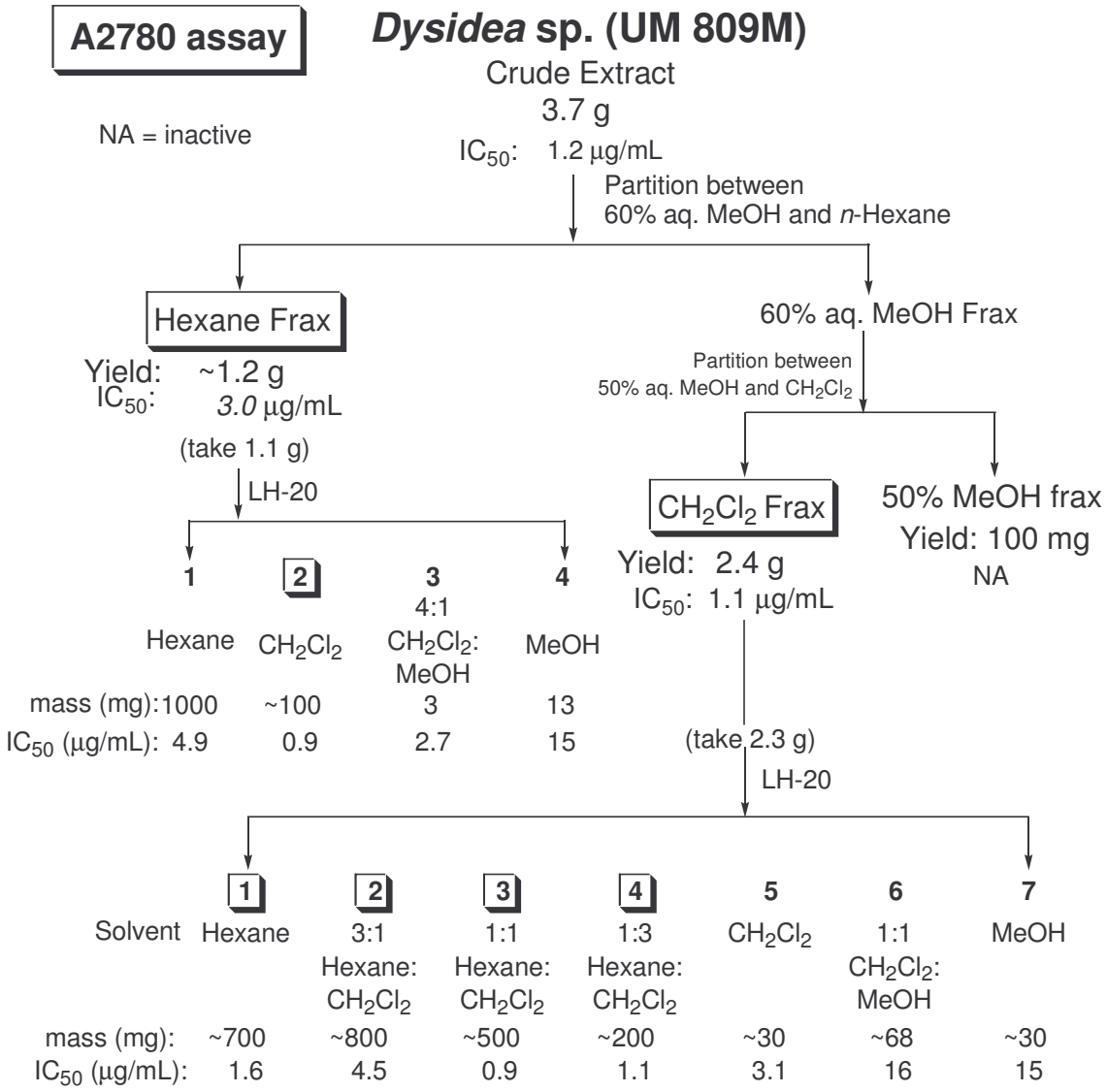

Scheme 3.3: The final purification of **3.8**

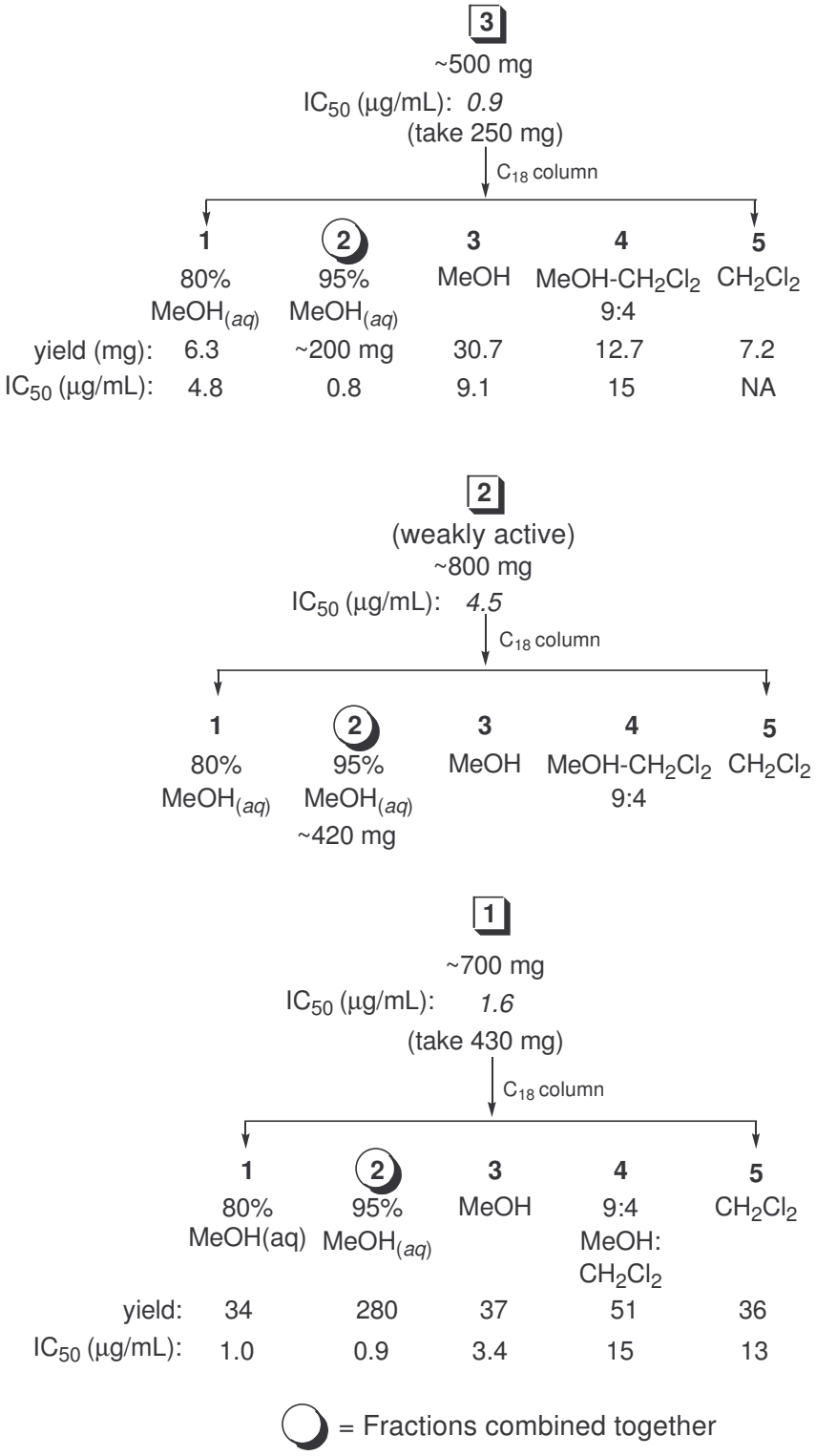

Table 3.1: ^{13}C and ^{1}H NMR data for **3.8**

Position	δ_C [a]	δ_H [a]		δ_C [b]	δ_H [b]	
1	40.3	0.72	m	39.8	0.72	m
		1.58	m		1.58	m
2	18.8	1.33	m	18.1	1.37	m
		1.52	m		1.52	m
3	42.6	1.11	m	42.0	1.02	td, 3.6, 13.2
		1.33	m		1.27	m
4	33.7	-	-	33.1	-	
5	56.8	0.70	m	56.4	0.73	m
6	19.2	1.38	m	18.5	1.28	m
		1.59	m		1.44	m
7	42.1	0.69	m	41.7	0.75	m
		1.61	m		1.63	m
8	37.9	-	-	37.3	-	
9	59.0	0.79	m	58.6	0.75	m
10	38.5	-	-	37.9	-	
11	28.6	1.54	m	27.1	1.37	m
		2.14	m		1.59	m
12	81.1	3.69	dd, 3.9, 11.2	80.4	3.34	dd, 3.9, 11.4
13	42.8	-	-	42.4	-	
14	55.3	1.02	dd, 1.8, 12.8	54.5	0.81	m
15	28.8	1.57	m	27.8	1.29	m
		1.83	m		1.94	m
16	70.3	5.73	m	69.3	5.25	m
17	115.1	-	-	114.2	-	
18	63.6	2.90	s	63.7	2.35	bs
19	33.7	0.89	s	33.2	0.74	s
20	21.7	0.79	s	21.2	0.70	s
21	17.9	0.82	s	17.3	0.74	s
22	16.9	0.89	s	16.3	0.72	s
23	9.8	1.16	s	8.7	0.79	s
24	136.2	6.61	bs	135.2	6.05	t, 1.8
25	101.0	7.71	d, 2	101.2	6.68	d, 1.2
16-$\underline{C}H_3CO$	170.6	-	-	171.0	-	
16-$CH_3\underline{C}O$	21.4	2.00	s	21.2	2.00	s
25-$\underline{C}H_3CO$	170.4	-	-	170.0	-	
25-$CH_3\underline{C}O$	21.3	2.10	s	20.9	1.98	s

[a] Collected in C_5D_5N
[b] Collected in $CDCl_3$

With twenty-nine total carbons, and two acetates detected from ^{1}H NMR spectroscopy, **3.8** appeared to have a C_{25} skeleton. With this skeleton, two acetates, and five other methyls, our initial hypothesis was that **3.8** was a sesterterpenoid, a class of compounds which are found in marine sponges.

^{1}H-^{1}H COSY analysis of **3.8** suggested the presence of several structural fragments, as shown in Figure 3.1. The proton signal at δ_H 3.66 was coupled to signals at δ_H 1.61 and 1.83, indicating the presence of a CH_2 group. The signal at δ_H 1.61 displayed a correlation with the proton signal at δ_H 0.79, establishing fragment A. The

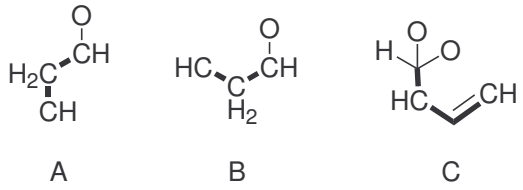

Figure 3.1: Structural fragments for **3.8** deduced from COSY

signal at δ_H 3.66 most likely arose from the presence of a hydroxyl group attached to fragment A. The signal at δ_H 5.73 showed a correlation with the proton signal at δ_H 1.57. This signal at δ_H 1.57 showed a correlation to the proton signal at δ_H 1.02 (dd, J = 1.8, 12.8). Because of the multiplicity of the signal at δ_H 1.02, the signal at δ_H 1.57 was determined to be part of a CH_2 group, thereby establishing fragment B. For fragment C, the proton signal at δ_H 7.71 was correlated to the signal at δ_H 2.90, which was correlated to the proton signal at δ_H 6.61. This correlation appeared to arise from long-range proton coupling such as allylic coupling, since the signal at δ_H 2.90 was a broad singlet. Therefore, fragment C was constructed as indicated. Other correlations were visible in

the aliphatic region of the COSY spectrum, which were clarified by use of additional 2D NMR data.

HSQC analysis of **3.8** allowed for the determination of carbon-proton one-bond coupling. The assignments in Table 3.1 are based on the HSQC data. It should be noted that spectral data were initially recorded in $CDCl_3$, but poor resolution of methyl signals in the ^1H NMR spectrum led to the use of d_5-pyridine as the solvent for full characterization of **3.8**.

The assignment of carbon-proton one-bond coupling permitted the interpretation of the HMBC spectrum of **3.8**. The HMBC spectrum allowed for the determination of the connectivity between these structural fragments. Correlations between the proton signal at δ_H 5.73 and the carbon signals at δ_C 115.1 and 136.2, as well as a correlation between the proton signal at δ_H 6.61 and the carbon signal at δ_C 70.3, showed that fragments B and C were connected through the quaternary carbon of fragment C. A correlation between the proton signal at δ_H 6.61 and δ_C 101.0 revealed that fragments B and C were also connected through an oxygen to form a dihydrofuran moiety. The proton signal at δ_H 5.73 showed a correlation with the carbonyl signal at δ_C 170.6, while the proton signal at δ_H 7.71 showed a correlation with the carbonyl signal at δ_C 170.4. The methyl singlet at δ_H 2.15 showed a correlation to the carbonyl signal at δ_C 170.6, while the methyl singlet at δ_H 1.96 showed a correlation to the carbonyl signal at 170.4. These correlations demonstrated that the acetate esters were attached to fragments B and C.

From fragment B, the proton signal at δ_H 1.02 showed a correlation to the carbon signal at δ_C 81.1, establishing that B and C were connected indirectly, likely through a

quaternary carbon. Correlations from the methyl singlet at δ_H 1.16 to carbon signals at δ_C 81.1, 55.3, 63.6, and the quaternary carbon signal at 42.8 revealed the linkage between fragments B and C. Similarly, correlations from the methyl singlet at δ_H 0.82 to the carbon signals at δ_C 59.0, 42.1, and 55.3 establish how fragments B and C, along with two quaternary carbons, form a six-membered ring. All of these correlations establish the structure of a larger fragment, fragment D, as shown in Figure 3.3. Further, the oxygenated methine signal at δ_H 3.66 was a doublet of doublets, strongly suggesting that the relative stereochemistry at the hydroxylated carbon was *β*.

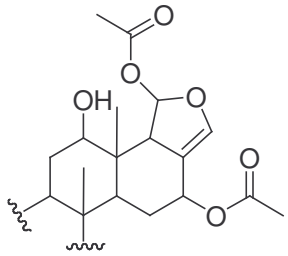

Figure 3.2: Fragment D of **3.8**

To check and see if **3.8** was a known compound, a literature search was performed for compounds with a molecular formula of $C_{29}H_{44}O_6$ containing a

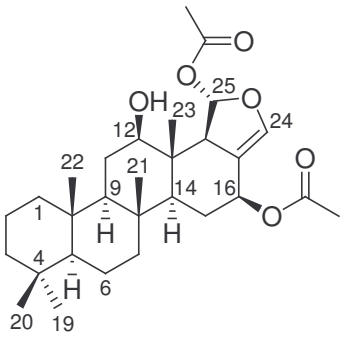

3.8 heteronemin

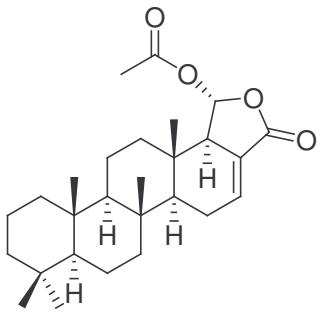

3.9

substructure like that of fragment D, with an hydroxyl group in a *β* configuration. A

search of the literature yielded one possibility. The preliminary data matched the structure of heteronemin (**3.8**), a known sesterterpenoid found in several sponge species. Additional key HMBC correlations as well as COSY correlations are shown in Figure 3.3, showing how the data match very well with the heteronemin skeleton. The final step was the determination of absolute stereochemistry for **3.8**.

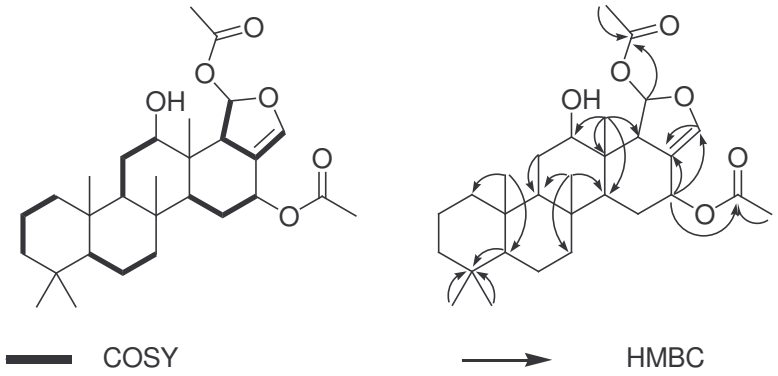

Figure 3.3: Key 2D NMR correlations for 3.8

The absolute optical rotation for heteronemin has been reported, as well as the X-ray crystal structure,[20] but no data has directly connected the absolute stereochemistry of heteronemin with its optical rotation. A recent reference reported the isolation, identification, and the absolute sterochemical determination of **3.9**, which was isolated along with heteronemin from a sponge of genus *Brachiaster*.[21] Based on the stereospecificity of biosynthetic pathways, it can be argued that **3.9** and heteronemin from the *Brachiaster* sp. both possess the same absolute stereochemistry. The absolute stereochemistry for **3.9** was determined to be that shown. The reported optical rotation for heteronemin isolated with **3.9** was $[\alpha]_D$ = -71.4° (*c* 0.055, CH_2Cl_2). Our experimentally determined rotation for **3.8** was $[\alpha]_D^{22}$ = -59.7° (*c* 0.009, $CHCl_3$). Because the values are similar and are of the same sign, we can conclude that heteronemin from

Brachiaster sp. and **3.8** possess the same absolute stereochemistry, which is the same as that of **3.9**. So, **3.8** is assigned the structure shown previously, in accordance with the stereochemistry determined for **3.9**.

This is the first report of the activity (IC_{50} = 1.7 μM) of **3.8** in the A2780 bioassay. Heteronemin has been previously isolated and shown to have antituberculosis activity (13 μM minimum inhibitory concentration against *M. tuberculosis* $H_{37}Rv$), as well as activity against KB cells (human oral epidermoid carcinoma, IC_{50} = 0.37 μM),[21] and human thyroid carcinoma cells (IC_{50} = 0.39 μM).[22] Heteronemin has also shown inhibitory action (IC_{50} = 3μM) against protein farnesyl transferase (PFTase); PFTase plays a role in activating the Ras protein, which is mutated in many forms of cancer.[23] Thus, heteronemin might provide an interesting scaffold for investigation of potential antitumor agents.

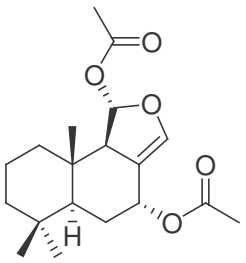

3.10

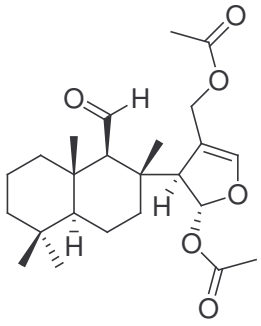

3.11

3.2.2 Preparation of Derivatives of Heteronemin

The diacetylated dihydrofuran moiety found in **3.8** is a unique functional group that, aside from sesquiterpenoid heteronemin derivatives, has only been reported in two other examples from natural products, the sesquiterpenoid **3.10** and its derivatives, and the rearranged diterpenoid **3.11**. Since little systematic study had been done regarding

the cytotoxic effects of derivatives of **3.8**, **3.10**, and **3.11** as related to their structure, it was interesting to know more about the structure-activity relationship for **3.8**. We therefore undertook the semisynthetic preparation of derivatives of **3.8** and tested them in the A2780 assay.

Scheme 3.4: Preparation of derivatives of **3.8**

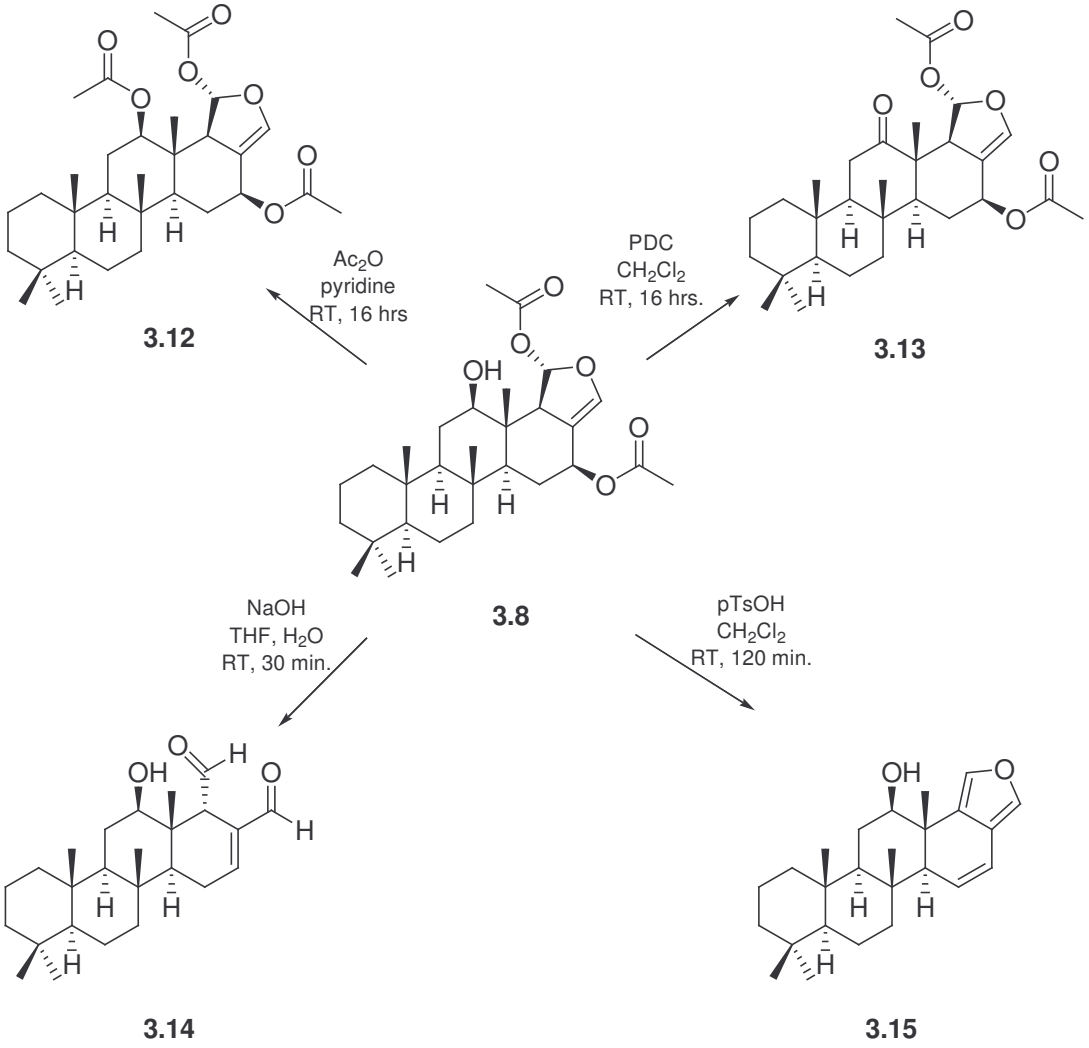

Acetylation of **3.8** using acetic anhydride and pyridine afforded heteronemin acetate (**3.12**) in fair yield after purification. Oxidation of **3.8** using pyridinium dichromate gave heteronemin ketone (**3.13**) in high yield. Base hydrolysis of **3.8** with 5% NaOH in THF for 15 minutes afforded 12-deacetyl-12,18-diepiscalaradial (**3.14**) as

the major product in 18% yield after SiO_2 chromatography. Treatment of **3.8** with *para*-toluylsulfonic acid (pTsOH) gave the vinyl furan **3.15** as the major product in 35% yield after SiO_2 PTLC. These reactions are summarized in Scheme 3.4. The structures of **3.12** and **3.13** were confirmed by comparison of ^{1}H NMR, IR, and FABMS data with literature values, while the structures for **3.14** and **3.15** were determined by full 1D and 2D NMR analysis. The ^{13}C NMR data for **3.12** and **3.13** are found in Table 3.2, while the ^{13}C and ^{1}H NMR data for **3.14** and **3.15** are shown in Table 3.3. This is the first report of the full NMR assignment for **3.14** and **3.15**.

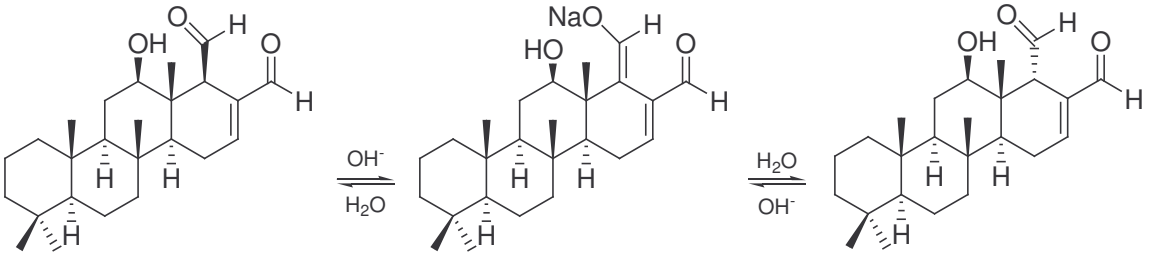

3.16 **3.17** **3.14**

Scheme 3.5: Pathway for the epimerization of C-18 to form **3.14**

Because of the epimerization of C-18 in the formation of **3.14**, this hydrolysis reaction deserves further examination. Base hydrolysis of **3.8** causes the acetylated hemiacetal to fall apart, forming the dialdehyde **3.16**. Compound **3.16** is then deprotonated, forming the enolate **3.14**. Scheme 3.5 depicts how the initial product from hydrolysis of **3.8** epimerizes to form **3.14**. Intermediate **3.17** can tautomerize to either **3.16** or **3.14**. The final product is **3.14**, which is obtained by protonation of the enolate from the β face. This leaves the formyl substituent at C-18 in a pseudoaxial conformation, which at first glance appears to be a thermodynamically unfavored product. However, if we consider that the hydrolysis and epimerization proceeded

Table 3.2: ^{13}C NMR data for derivatives of **3.8**

Position	**3.12**[a]	**3.13**[b]
1	40.1	38.2
2	18.6	18.1
3	41.9	41.7
4	33.6	33.4
5	56.5	56.6
6	19.0	18.5
7	41.3	39.5
8	37.8	35.6
9	58.2	56.6
10	38.3	38.2
11	24.3	27.7
12	83.0	215.1
13	42.4	41.9
14	55.1	50.1
15	28.1	29.9
16	69.8	69.1
17	114.3	112.7
18	62.5	60.2
19	33.6	33.5
20	21.6	21.5
21	17.7	17.0
22	16.7	15.8
23	10.4	13.6
24	136.7	136.7
25	99.4	99.2
12-*C*H$_3$CO	21.6[1]	
12-CH$_3$*C*O	170.6[2]	
16-*C*H$_3$CO	21.20[1]	21.3[3]
16-CH$_3$*C*O	170.6[2]	170.2[4]
25-*C*H$_3$CO	21.23[1]	21.2[3]
25-CH$_3$*C*O	170.4[2]	170.1[4]

[a] Recorded in C_5D_5N
[b] Recorded in $CDCl_3$
[1,2,3,4] May be interchanged

Table 3.3: ^{1}H and ^{13}C NMR data for **3.8** and derivatives (in $CDCl_3$)

Position	**3.14**			**3.15**		
1	40.0	0.79	m	40.0	0.84	m
		1.69	m		1.71	m
2	18.2	1.36	m	18.1	1.42	m
		1.59	m		1.60	m
3	42.2	1.12	td, 3.6, 13.4	42.2	1.15	m
		1.39	m		1.39	m
4	33.4	-		33.5	-	
5	58.4	0.79	m	56.9	0.81	m
6	18.7	0.77	m	18.8	1.45	m
		1.54	m		1.64	m
7	41.4	0.95	m	41.2	0.92	m
		1.70	m		1.91	m
8	37.5	-		37.0	-	
9	56.5	0.83	m	58.4	0.98	m
10	37.8	-		37.6	-	
11	27.1	1.48	m	28.1	1.54	m
		1.70	m		1.83	ddd, 12.6, 4.2, 2.2
12	76.1	3.61	m	78.9	3.88	dd, 4.0, 11.3
13	43.7	-		40.7	-	
14	48.3	1.42	m	57.0	1.93	t, 2.9
15	24.4	2.30	dt, 5.2, 20.8	127.7	5.79	dd, 2.9, 9.8
		2.50	ddt, 2.3, 11.5, 20.7			
16	153.1	7.09	dd, 2.8, 4.9	119.2	6.49	dd, 2.7, 9.6
17	137.3	-		121.2	-	
18	55.3	3.68	t, 2.1	132.7	-	
19	33.5	0.84	s	33.5	0.84	s
20	21.5	0.80	s	21.5	0.82	s
21	17.2	0.92	s	18.8	1.01	s
22	16.9	0.84	s	16.4	0.87	s
23	16.0	0.91	s	16.2	1.04	s
24	192.9	9.43	s	136.3	7.23	bs
25	203.1	9.88	d, 2.6	135.6	7.41	bs

through an enolate intermediate, and we remember the principle of least motion that suggests that a kinetic product will involve the least amount of movement of atoms from reactant to product, then it is apparent that **3.14** is a thermodynamically favored product. To explain the thermodynamic preference for this epimer, we must examine the ring system of **3.14** and its role in governing the steric preferences of the enolate intermediate.

Computational studies using the Spartan '04 Molecular Modeling package support the notion that **3.14** is thermodynamically favored compared to **3.16**. Conformational searches were performed for both **3.14** and **3.16** using MMFF molecular mechanics calculations to probe for low-energy conformations for each compound. These calculations returned conformers having ΔH_f values of 114 kcal/mol for **3.14** (shown in Figure 3.4), and 117 kcal/mol for **3.16**. This demonstrated that at a low level of theory, **3.14** was the thermodynamically favored product. This type of epimerization has been observed before for the analogous sesquiterpenoids polygodial and epipolygodial (**3.18** and **3.19**), where treatment of **3.18** with dilute acid affords **3.19**.[24]

If we examine the optimized geometries for **3.14** and **3.16**, we can see key differences in these epimers that suggest that the energetic differences may emerge from allylic strain. Allylic strain in a six-membered ring arises from steric interactions from groups brought in close proximity by an endocyclic double bond relative to a ring which has no double bond. In the case of **3.14**, the two formyl carbons are 3.09 Å apart, while the two formyl carbons are 2.95 Å apart in **3.16.** The closeness of the formyl groups in **3.16** leads to steric repulsion between the groups that is not as great as the repulsion found between the formyl groups in **3.14**. So, both molecular modeling and structural considerations suggest that **3.14** is the thermodynamically favored epimer

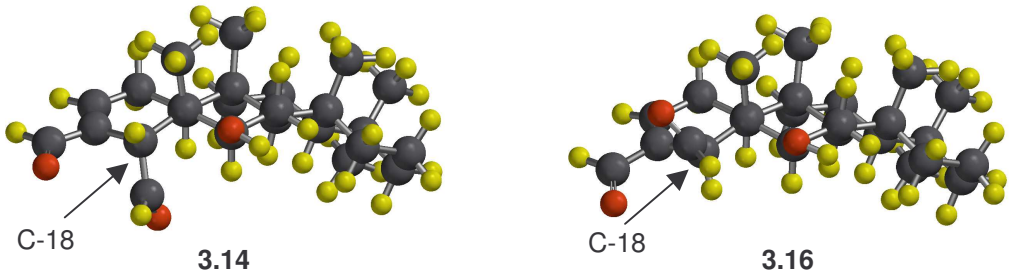

Figure 3.4: Optimized geometry of **3.14** and **3.16** by MMFF calculations
The perspective is looking down the C-13 – C-14 axis.

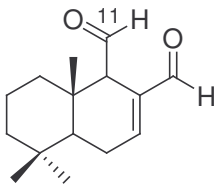

3.18 β-C-11
3.19 α-C-11

in the tautomerization between **3.14** and **3.16**, and so it is clear that this hydrolysis and tautomerism are under thermodynamic control.

From the literature, it was known that hydrolysis of **3.10** by treatment with a very small amount of *para*-toluene sulfonic acid (pTsOH) for 1 hr. in CH_2Cl_2 affords **3.18** in good yield.[25] So, hydrolysis of **3.8** with pTsOH was attempted in hopes of obtaining a dialdehyde sesterterpenoid analogue of **3.18**. Surprisingly, although the procedure was

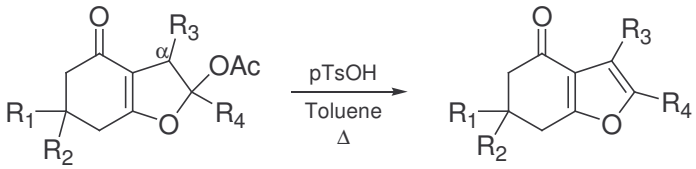

3.20 **3.21**

Scheme 3.6: Acid catalyzed elimination to form substituted furan

followed carefully, the major product of the reaction was the double elimination product **3.15**. This reaction proceeded through an E1-type mechanism, which accounts for the *syn* elimination at C-25. From a model system in the literature, we found that treatment of **3.20** with pTsOH affords the elimination product **3.21** (Scheme 3.6), the yield apparently being unaffected by the orientation of the hydrogen at the α position relative to the acetoxy substituent.[26] This result was comparable to the formation of **3.15**. The common theme between the model reaction forming **3.21** and that forming **3.15** was that the products formed were not hydrolysis products, but appeared to be formed without the

participation of water. In our case, since the CH_2Cl_2 used for the reaction was not dry, water was present in the reaction mixture in very low amounts; also, the pTsOH was in the form of a hydrate. For the hydrolysis of **3.10**, the literature procedure did not specify the amount of pTsOH used or whether the pTsOH was in the form of a hydrate or not. If excessive pTsOH were added, even if it were a hydrate, the amount of water in the reaction mixture might have been insufficient for carrying out the hydrolysis, since you would expect to need a 1:1 molar ratio of **3.8** and water to form a dialdehyde product. Yet, the pTsOH present might have been able to effect the elimination reaction to form **3.15**. So, **3.15** was likely formed as a result of an insufficient amount of water in the reaction mixture, leading to an elimination product rather than a hydrolysis product.

Attempted hydrolysis by HCl afforded complex mixtures of products, while an attempted hydrolysis with oxalic acid gave no observable reaction. Reduction with H_2 using a palladium/carbon catalyst also gave a complex mixture of products. In an attempt to functionalize the C-12 position under mild conditions, bromination with *N*-bromosuccinimide and triphenylphosphine also produced no observable reaction. In an effort to make a water-soluble succinate ester analogue of **3.8**, an esterification was attempted with succinic anhydride and a pyridine catalyst which did not give any observable reaction. These results show how the functionality of **3.8**, though apparently simple, is fairly challenging to modify.

3.2.3 Biological Evaluation of Heteronemin and Semisynthetic Derivatives

Heteronemin (**3.8**), which was isolated by bioassay-guided fractionation from a crude extract from a sponge of genus *Dysidea*, displayed good cytotoxicity in the A2780

assay, with an IC_{50} of 1.7 μM. The scalarane derivatives prepared by semisynthetic derivatization of **3.8** (**3.12**-**3.15**) were all submitted for testing in the A2780 assay. Compounds **3.12**-**3.14** all had activity similar to that of **3.8**. The furan derivative **3.15** was only weakly active. The cytotoxicity data are displayed in Table 3.4. These bioactivity data suggest that the oxygenated functionality of C-24 and C-25 in the structure of **3.8** is required for good bioactivity. When it is removed to form the furan **3.15**, the activity is largely lost. At the same time, it appears that the hydroxyl group at C-12 is less important for good activity. Oxidation at this position does not change the activity much, though acetylation makes the activity slightly worse.

Compound	IC50 (μM)
3.8	1.7
3.12	3.2
3.13	1.4
3.14	2.4
3.15	30

Table 3.4: A2780 cytotoxicity data for **3.8** and semisynthetic derivatives

Though many papers have reported the isolation of **3.8** from natural sources along with other scalarane sesterterpenoids, this is the first systematic study of the structure-activity relationship for **3.8**-based compounds. One issue that might be worth further investigation is whether **3.8** is an active principle, or if it is metabolized in the cell to form some other compound. If **3.8** were deacetylated in the cell, it would likely form a mixture of dialdehydes. Though **3.14** is cytotoxic, the C-18 epimer may also be active or even more active. Similar dialdehyde compounds have a hot taste to humans, and the stereochemistry at C-18 of similar dialdehydes has been shown to play a critical role in

maintaining the hot taste.[27] Perhaps the stereochemistry at C-18 is also important for the cytotoxicity of these compounds, since the aldehyde groups allow for covalent interactions with free amines on proteins. This is explored further in the next section. Only the preparation and testing of the C-18 epimer of the dialdehyde **3.14** would help to answer that question.

This is the first reported study of the structure-activity dependence for **3.8**-based compounds, and the first full NMR assignment for **3.14** and **3.15**. Overall, we have shown that **3.8** is cytotoxic to the A2780 ovarian cancer cell line, and its derivatives **3.12**-**3.14** all possess activity similar to that of **3.8**, while **3.15** is essentially inactive. These results suggest that the C-24 and C-25 oxygenation is critical for activity, while the functionality of C-12 and C-16 – C-18 is not as important for activity.

3.2.4 Previous Investigation of Scalarane Sesterterpenoids

From the literature, scalarane sesterterpenoids like **3.8** and **3.12**-**3.14** have been isolated from several sponge and nudibranch species, and many scalarane sesterterpenoids have been shown to possess interesting biological activity. Sesterterpenoids are one of the least common groups of terpenoids. Sesterterpenoids arise biosynthetically from the head-to-tail connection of five isoprene units, often cyclized to form a ring system. Though rare, sesterterpenoids have been discovered from a number of sources, both terrestrial and marine. Scalarane sesterterpenoids are characterized by the tetracyclic ring system shown in Figure 3.4. Since the 1970's, when the study of the secondary metabolites of sponges became very prominent, many bioactive scalarane sesterterpenoids have been isolated,[28] and several compounds have

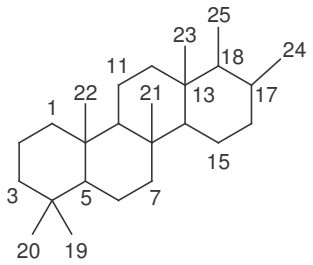

Figure 3.5: Scalarane sesterterpenoid skeleton

been shown to be cytotoxic. Not surprisingly, scalaranes have been shown to serve as antifeedant agents in sponges.[29] Scalarane derivatives have been isolated from nudibranchs as well, which are marine mollusks that often feed on sponges.[30]

From the sponge *Hyrtios erecta*, **3.17** was isolated using a P388 murine lymphatic leukemia cell line assay, with IC_{50} = 38 nM. Compound **3.17** also possessed nanomolar cytotoxicity towards three human gastric tumor cell lines. Compound **3.17** was also shown to have a dose-dependent effect on increasing the mean survival times of P388-

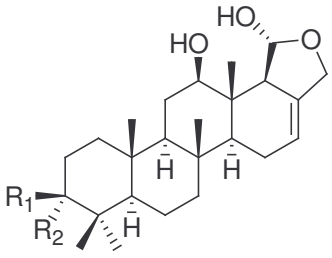

3.17 R_1, R_2 = O
3.18 R_1 = H; R_2 = OH

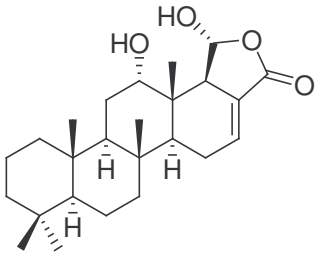

3.19

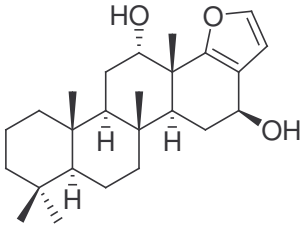

3.20

implanted mice. It was believed that the oxygenation of carbons 11-18 and 23-25 was required for the cytotoxicity of scalarane sesterterpenoids; however, the alcohol **3.18** was seventeen times less potent than the ketone **3.17**, suggesting that the structure of the A-ring of these compounds may play a less obvious but significant role their mechanism of

action.[31] Based on this information, attempts to functionalize the A ring of the **3.8** scaffold might prove profitable in improving the potency of new derivatives.

From another sponge of genus *Hyrtios*, the compounds **3.19** and **3.20** (a modified scalarane) were isolated and were shown to stimulate nerve growth factor (NGF) synthesis in mouse astroglial cells, while possessing little cytotoxicity.[32] NGF has been shown to prevent cholinergic neuronal loss like that associated with Alzheimer's disease, and compounds which promote the activity of NGF might have potential as neuroprotective agents.[33]

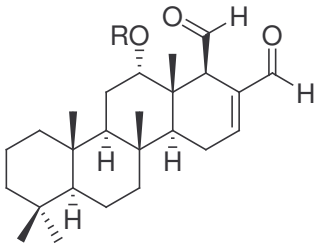

3.21 R = Ac
3.22 R = H

The sclaranes scalaradial (**3.21**) and deacetylscalaradial (**3.22**) have both received much attention for their anti-inflammatory activity, in addition to their toxicity.[34,35] Both **3.21** and **3.22** have been shown to be inhibitors of phospholipase A_2 (PLA_2) enzymes.[36,37] PLA_2 enzymes are important for the biosynthesis of leukotrienes and prostaglandins, lipids which are important in signaling pathways for inflammation in mammals. Compound **3.21** has served as a model compound for study of the inhibition of PLA_2 enzymes. It is believed that the inhibition of PLA_2 enzymes by **3.21** occurs when the compound covalently binds to the protein. The close proximity and reactivity of the dialdehyde groups allow for a nucleophilic attack on one of the aldehydes by a basic

amino acid residue in the enzyme to form imide **3.24**. An acid catalyzed cyclization, followed by addition of an additional nucleophile yields **3.26**. The loss of a second water molecule yields the pyrrole **3.27**.[36] Compound **3.21** has also been shown to act as a feeding deterrent in an assay using the freshwater fish *Curussius rurussirrs*.[35]

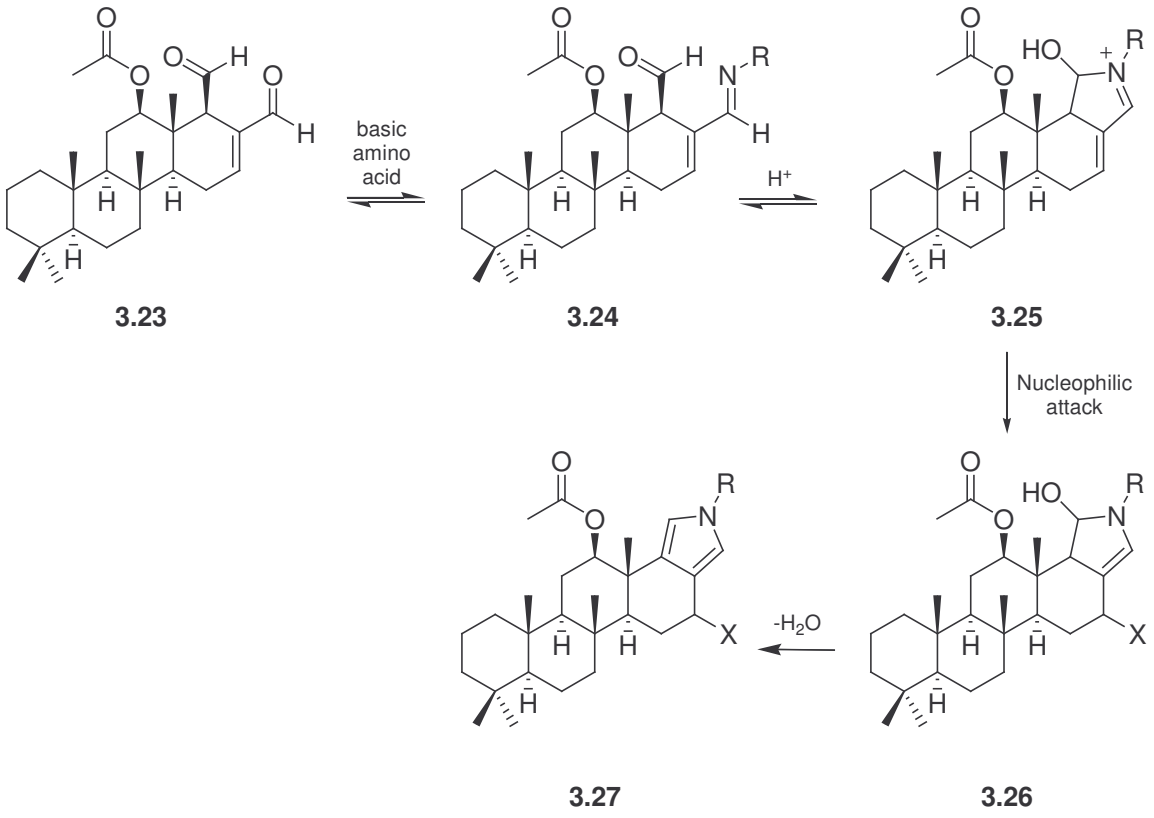

3.23 **3.24** **3.25**

3.27 **3.26**

Scheme 3.7: Covalent interactions between **3.23** and amino acids with amine residues

3.3 Experimental Section

General Experimental Procedures. IR spectra were recorded for neat samples with a MIDAC M-series FTIR spectrophotometer. HRFAB mass spectra were collected with a JEOL HX-110 spectrometer. NMR spectra were collected on either a Varian Inova 400 spectrometer operating at 399.9 MHz for ^{1}H and 100.6 MHz for ^{13}C, or a JEOL Eclipse+ 500 spectrometer operating at 500.2 MHz for ^{1}H and 125.8 MHz for ^{13}C.

Animal material and sample preparation

The deep frozen sample was pulverized at the National Cancer Institute in dry ice by use of a worm-fed grinder (hamburger mill), the powder produced was allowed to stand at –30 °C until the CO_2 sublimed, and the mass was then extracted at 4 °C with de-ionized water (1 L) by stirring (30 rpm) for 30 min. The mixture was centrifuged at room temperature and the supernatant lyophilized to give the aqueous extract. The insoluble portion from the centrifugation was lyophilized and then statically extracted overnight at room temperature with 1 L of a 1:1 ratio of MeOH:CH_2Cl_2. The organic phase was filtered off, the pellet washed with a 10% volume of fresh MeOH, and the combined organic phases reduced to dryness at <35 °C by rotary evaporation and then finally dried under high vacuum at RT to give the organic extract as a gum. An extract of this sponge was received from the National Cancer Institute as sample number UM 809M (4.3 g).

A2780 Bioassay. The A2780 bioassay was performed by Mrs. Jennifer Schilling and Mr. Andrew Norris, and is described here for completeness. The cell growth medium was prepared by the addition of 55.5 mL of fetal bovine serum (Gibco), 2 mL of 10 mg/mL gentamicin (Sigma), and 5.6 mL of amphotericin B (Sigma) to 500 mL of RPMI medium (Gibco). The reaction medium was prepared by adding Alamar Blue (Biosource) to growth medium to give a final concentration of 1% of the dye. The 10% trypsin/EDTA solution (Sigma) was prepared in pH 7.4 phosphate buffered saline solution (PBS) (Sigma).

Methods *Preparation of drug plate*: Potentially cytotoxic agents ("drugs") were prepared at a concentration of 1000 μg/mL in 50% $DMSO_{(aq)}$. To a 96-well microtiter plate, 200 μL was added to each well in columns 1-11, and 50 μL of drug solution was added to row A (or rows A and E), columns 1-10 to give an initial concentration of 20 μg/mL in row A (or rows A and E). Serial dilutions were performed down each column to give either 4 or 8 final drug concentrations. Typically, drugs were tested with four doses from 0.160 to 20 μg/mL or eight doses from 0.00640 to 50 μg/mL. The drug concentrations after the serial dilutions are indicated in Scheme 3.8. A solution of actinomycin D was prepared and diluted to the concentrations indicated for column 11, rows A-H in Scheme 3.8.

	1	2	3	4	5	6	7	8	9	10	11	12
A	20.0	50.0									0.0320*	M
B	4.00	10.0									0.00640*	M
C	0.800	2.00									0.00128*	M
D	0.160	0.400									0.000256*	M
E	20.0	0.0800									N	M
F	4.00	0.0160									N	M
G	0.800	0.00320									N	M
H	0.160	0.000640									N	M

Numbers in columns 1-2 indicate drug concentrations (μg/mL) commonly used for testing. * = concentrations (μg/mL) of actinomycin D, used as positive control; N = negative controls, cells + medium; M = medium alone.

Scheme 3.8: Drug plate for A2780 assay

Preparation of test plate: Initially, A2780 cells were grown to 95% confluency in a cell growth flask. After addition of 10% trypsin/EDTA to the growth flask and a 5 minute incubation at room temperature, the cells were transferred to a 50 mL centrifuge tube. The harvested cells were centrifuged at 1000 rpm for 5 minutes, the supernatant

was removed, and the cells were resuspended in 20 mL of growth medium. The cells were counted under a microscope using a hemacytometer, and the culture was diluted with growth medium to achieve a cell count of 2.7×10^5 cells/mL. From this solution, 180 μL were added to the wells of a 96-well plate in columns 1-11. Column 12 received 200 μL growth media with no cells. The test plate was incubated for 4 hours to allow the cells to adhere to the plate.

Once the drug plate was prepared and the test plate was incubated, 20 μL was transferred from each well of the drug plate to the corresponding well of the test plate using a multipipettor. After mixing, the test plate was incubated for 44 hours at 37^{o}C under a 5% CO_2 atmosphere. At the end of this incubation period, the test plate was inverted and the growth medium was gently shaken out. The reaction medium was added to each well, and the test plate was incubated an additional 4 hours.

After this final incubation, the fluorescence of each well was measured using a Cytofluor fluorescence plate reader (PerCeptive Biosystems). Since column 12 contained no cells, these wells functioned as positive controls, and gave a zero point for cell detection (100% inhibition). Rows E-H of column 11, which contained cells with no added drug, gave a zero inhibition point for cell detection. The fluorescence values for these wells were measured and used to calculate a scale of fluorescence as a function of cell growth. The fluorescence of each well on the test plate was compared with this scale, and a percent growth inhibition was calculated for each well. These were tabulated in an Excel spreadsheet. Linear regression analysis of the data corresponding to percent inhibition above and below 50% was performed, and the IC_{50} value was interpolated.

Isolation and characterization of heteronemin:

The crude extract (3.2 g) was subjected to liquid partitioning, which yielded three fractions, two of which were active: the hexane and dichloromethane fractions (1.2 g and 2.4 g, respectively). The hexane fraction was further fractionated by use of Sephadex® LH-20, using a step gradient with various concentrations of hexane, dichloromethane, and methanol. This separation afforded one fraction with improved activity, the dichloromethane wash of the LH-20 column (0.1 g). ^{1}H NMR analysis revealed that this fraction consisted of compound **3.8** in very high purity, with IC_{50} = 0.9 μg/mL. Thin-layer chromatography (TLC) analysis of **3.8** and the initial fractions from liquid partitioning, using vanillin-sulfuric acid for visualization, suggested that **3.8** was also present in the dichloromethane fraction from liquid partitioning. Additional amounts of **3.8** were obtained from the dichloromethane fraction by LH-20 purification, followed by reverse phase C_{18} column chromatography, to afford an additional 900 mg in high purity. Based on the intensity of spots visualized by TLC analysis, **3.8** was found to be the major compound in the extract and therefore accounted for the great majority of the activity of the crude extract. Additional fractionations did not yield any compound with activity comparable to that of **3.8**.

Heteronemin (**3.8**) white crystalline solid; $[\alpha]_D^{22}$ = -59^{o} (*c* 0.9, $CHCl_3$); IR (neat powder) 3545, 2924, 1734, 1696, 1369, 1266, 1236, 1100, 1022, 918 cm^{-1}; ^{1}H NMR ($CDCl_3$ and C_5D_5N) see Table 3.1; ^{13}C NMR ($CDCl_3$ and C_5D_5N) see Table 3.1; HRFABMS (positive ion) 495.3292 ($[M+Li]^+$, calc. for $C_{29}H_{44}O_6Li$: 495.3299 , Δ = 1.2 ppm); 428.2940 ($[M-C_2H_4O_2]^+$, calc. for $C_{27}H_{40}O_4$, 428.2927, Δ = 3.2 ppm).

Semisynthetic preparation of derivatives of 3.8

Heteronemin acetate (3.12): To a vial was added 8.1 mg (17 μmol) of **3.8**, 0.5 mL Ac_2O (3 mmol), and 5 drops pyridine (≈ 1.5 mmol), and the mixture was stirred overnight. The excess Ac_2O was quenched with MeOH, and the crude product was concentrated under nitrogen and by evaporation under vacuum. The crude product was subjected to normal phase PTLC to afford 4.6 mg (8.7 μmol, 52% yield) of **3.12**: white crystalline solid; $[\alpha]_D^{28}$ = -63° (*c* 0.5, $CHCl_3$); IR (neat thin film) 2928, 1737, 1463, 1366, 1229, 1019, 735 cm^{-1}; ^1H NMR (C_5D_5N): 7.08 (d, 2.2, H-25), 6.57 (t, 2.1, H-24), 5.65 (m, H-16), 4.88 (dd, 4.2, 11.4, H-12), 2.86 (bs, H-18), 2.20 (s, OAc), 2.16 (s, OAc), 2.04 (s, OAc), 1.82 (dd, 3.5, 12.4), 1.57 (dt, 2.9, 12.6), 1.03 (s, CH_3), 0.86 (s, CH_3) 0.77 (s, CH_3), 0.76 (s, CH_3), 0.72 (s, CH_3); ^{13}C NMR (C_5D_5N) see Table 3.2.

Heteronemin ketone (3.13): To a 25 mL round bottom flask was added 9.6 mg **3.8** (20 μmol), 140 mg of pyridinium dichromate (120 μmol), and 3 mL CH_2Cl_2. This mixture was stirred overnight at room temperature. The reaction mixture was then washed with 5% NaOH, 5% HCl, sat. $NaHCO_{3(aq)}$, and brine, and then dried over Na_2SO_4. The product was a white crystalline solid that produced one spot on SiO_2 TLC (65:35 hexane:acetone, R_f = 0.4) The reaction afforded 8.1 mg (17 μmol, 85% yield) of **3.13**: white crystalline solid; $[\alpha]_D^{22}$ = -25° (*c* 0.5, $CHCl_3$); IR (neat thin film) 2925, 2852, 1741, 1702, 1458, 1363, 1225, 1022, 924, cm^{-1}; ^1H NMR ($CDCl_3$): 6.52 (bs, H-25), 6.16 (bs, H-24), 5.34 (bs, H-16), 2.89 (bs, H-18), 2.55 (t, 14.0), 2.30 (d, 13.3), 2.13 (s, OAc), 2.10 (s, OAc), 1.84 (d, 12.8), 1.10 (s, CH_3), 1.05 (s, CH_3), 0.85 (s, CH_3), 0.81 (s, CH_3); ^{13}C NMR

($CDCl_3$): see Table 3.2; LRFABMS (positive ion) 509.31 ($[M+Na]^+$, calc. for $C_{29}H_{42}O_6Na$: 509.29); HRFABMS (positive ion) 426.2776 ($[M-C_2H_4O_2]^+$, calc. for $C_{27}H_{38}O_4$: 426.2770 , Δ = 1.4 ppm).

12-Deacetyl-12,18-diepiscalaradial (3.14): In a 25 mL round bottom flask, 10 mg **3.8** (20 μmol) was dissolved in 6 mL THF. To this was added 2 mL of 1.75 M NaOH (3.5 mmol), and the biphasic mixture was stirred vigorously for 30 minutes until a slight brownish yellow color change was observed. TLC analysis indicated the reaction mixture contained starting material (invisible under UV light) plus a UV-absorbing spot with R_f nearly equal to that of **3.8**. CH_2Cl_2 was added to the mixture, and the organic layer was washed with water and brine solution. The organic layer was dried and concentrated under vacuum. The crude product was purified by SiO_2 HPLC, which afforded 1.4 mg (3.5 μmol, 18% yield) of **3.14**: white amorphous solid; $[\alpha]_D^{22}$ = -49° (*c* 0.2, $CHCl_3$); IR (neat thin film) 3450, 2923, 2848, 1717, 1681, 1481, 1388, 1035 cm^{-1}; ^1H NMR ($CDCl_3$) see Table 3.3; ^{13}C NMR ($CDCl_3$) see Table 3.3; HRFABMS (positive ion) 369.2815 ($[M-OH]^+$, calc. for $C_{25}H_{37}O_2$: 369.2794 , Δ = 5.8 ppm); 385.2734 ($[M-H]^+$, calc. for $C_{25}H_{37}O_3$: 385.2734 , Δ = 2.2 ppm).

15,16-Dehydrosesterstatin 3 (3.15): To 25 mL round bottom flask was added 11.7 mg **3.8** (23.9 μmol), which was dissolved in 12 mL CH_2Cl_2. To this mixture was added 3 small crystals of *p*TsOH (≈1mg, 5.8 μmol), and the mixture was stirred at room temperature overnight. TLC analysis indicated that the mixture contained several components, with one major spot with R_f = 0.7. The acid was extracted from the organic

layer by liquid partitioning. The organic layer was concentrated and separated by SiO_2 PTLC. The major spot from TLC was isolated to afford 3.1 mg (8.41 μmol, 35% yield) of **3.15**: white film; $[\alpha]_D^{22}$ = -47° (*c* 0.1, $CHCl_3$); IR (neat thin film) 3419, 2922, 2849, 1740, 1463, 1387, 1263, 1066, 978, 799, 736 cm^{-1}; ^1H NMR ($CDCl_3$) see Table 3.3; ^{13}C NMR ($CDCl_3$) see Table 3.3; HRFABMS (positive ion) 368.2730 ($[M]^+$, calc. for $C_{25}H_{36}O_2$: 368.2715, Δ = 3.7 ppm).

References for Chapter 3

1. Stewart, M.; Fell, P.M.; Blunt, J.W.; Munro, M.H.G. Avarol and Related Compounds from the New Zealand Marine Sponge *Dysidea* sp. *Aust. J. Chem*. **1997**, *50*, 341-347.

2. Loya, S.; Hizi, A. The Inhibition of Human Immunodeficiency Virus type 1 Reverse Transcriptase by Avarol and Avarone Derivatives. *FEBS Lett.*, **1990**, *269*, 131-134.

3. Carney, J.R., and Scheuer, P.J. Popolohuanone E, a Topoisomerase-II Inhibitor with Selective Lung Tumor Cytotoxicity from the Pohnpei Sponge *Dysidea* sp. *Tetrahedron Lett*., **1993**, *34*, 3727.

4. Minale, L.; Riccio, R.; Sodano, G. Avarol, a Novel Sesquiterpenoid Hydroquinone with a Rearranged Drimane Skeleton from the Sponge *Disidea avara*. *Tetrahedron Lett.* **1974**, *38*, 3401-3404.

5. Sakai, R.; Kamiya, H.; Murata, M.; Shimamoto, K. Dysiherbaine: A New Neurotoxic Amino Acid from the Micronesian Marine Sponge *Dysidea herbacea. J. Am. Chem. Soc.* **1997,** *119*, 4112-4116.

6. Kobayashi, M.; Aoki, S.; Ohyabu, N.; Kurosu, M.; Wang, W.; Kitagawa, I. Arenastatin A, a Potent Cytotoxic Depsipeptide from the Okinawan Marine Sponge *Dysidea arenaria*. *Tetrahedron Lett.* **1994**, *35*, 7969-7972.

7. Chaganty, S.; Golakoti, T.; Heltzel, C.; Moore, R.E.; Yoshida, W.Y. Isolation and Structure Determination of Cryptophycins 38, 326, and 327 from the Terrestrial Cyanobacterium *Nostoc* sp. GSV 224. *J. Nat. Prod.* **2004,** *67,* 1403-1406.

8. Kobayashi, M.; Kurosu, M.; Wang, W.; Kitagawa, I.. A Total Synthesis of Arenastatin A, an Extremely Potent Cytotoxic Depsipeptide, from the Okinawan Marine Sponge *Dysidea arenaria*. *Chem. Pharm. Bull*. **1994**, *42*, 2394-2396.

9. Murakami, N.; Tamura, S.; Koyama, K.; Sugimoto, M.; Maekawa, R.; Kobayashi, M. New Analog of Arenastatin A, a Potent Cytotoxic Spongean Depsipeptide, with Anti-tumor Activity. *Bioorg. Med. Chem. Lett.* **2004**, *14*, 2597-2601.

10. Gunasekera, S.P.; McCarthy, P.J.; Kelly-Borges, M.; Lobkovsky, E; Clardy, J. Dysidiolide: a Novel Protein Phosphatase Inhibitor from the Caribbean Sponge *Dysidea etheria* de Laubenfels. *J. Am. Chem. Soc*. **1996**, *118*, 8759-8760.

11 Corey, E.J.; Roberts, B.E. Total Synthesis of Dysidiolide**.** *J. Am. Chem. Soc*. **1997**, *119*, 12425-12431.

12. Kaliappan, K.P.; Gowrisankar, P. An Expedient Enyne Metathesis Approach to Dysidiolide. *Tetrahedron Lett.* **2004**, *45*, 8207-8209.

13. HyperCLDB Database. http://www.biotech.ist.unige.it/cldb/cl194.html (accessed June 14, 2005).

14. Bruening, W.; Prowse, A.H.; Schultz, D.C.; Holgado-Madruga, M.; Wong, A. Godwin, A.K. Expression of OVCA1, a Candidate Tumor Suppressor, Is Reduced in Tumors and Inhibits Growth of Ovarian Cancer Cells. *Cancer Res*. **1999**, *59*, 4973–4983.

15. D'Andrilli, G.; Masciullo, V.; Bagella, L.;Tonini, T.; Minimo, C.; Zannoni, G.F.; Giuntoli, R.L., II; Carlson, J.A., Jr.; Soprano, D.R.; Soprano, K.J.; Scambia, G.; Giordano, A. Frequent Loss of pRb2/p130 in Human Ovarian Carcinoma. *Clin. Cancer Res.* **2004**, *10*, 3098–3103.

16. Salvatorea, C.; Binaschia, M.; Bigionia, M.; Camardaa, G.; Maggia C.A.; Gosoa, C. MEN15658: a New Promising Anti-tumoral Drug Active on Resistant Tumor Cells. *Anti-Cancer Drugs* **2004**, *15*, 151-156.

17. Vikhanskaya, F.; Colella, G.; Valenti, M.; Parodi, S.; D'Incalci, M.; Broggini, M. Cooperation between p53 and hMLH1 in a Human Colocarcinoma Cell Line in Response to DNA Damage. *Clin. Can. Res.* **1999**, *5*, 937-941.

18. O'Brien, J.; Wilson, I.; Orton, T.; Pognan, F. Investigation of the Alamar Blue (Resazurin) Fluorescent Dye for the Assessment of Mammalian Cell Cytotoxicity. *Eur. J. Biochem.* **2000**, *267*, 5421-5426.

19. Page, B.; Page, M.; Noel, C. A New Fluorometric Assay for Cytotoxicity Measurements *in Vitro*. *Int. J. Oncol.* **1993**, *3*, 473-476.

20. Patil, A.D.; Westley, J.W.; Baures, P.W.; Eggleston, D.S. Structure of Heteronemin. *Acta Crystallographica, Section C: Crystal Structure Communications* **1991**, *C47*, 1250-1253.

21. Wonganuchitmeta, S.-N.; Yuenyongsawad, S.; Keawpradub, N.; Plubrukarn, A. Antitubercular Sesterterpenes from the Thai Sponge *Brachiaster* sp. *J. Nat. Prod.* **2004**, *67*, 1767-1770.

22. Fontana, A; Cavaliere, P.; Ungur, N.; D'Souza, L.; Parameswaram, P.S.; Cimino, G.; New Scalaranes from the Nudibranch *Glossodoris atromarginata* and Its Sponge Prey. *J. Nat. Prod.* **1999,** *62,* 1367-1370.

23. Ledroit, V.; Debitus, C.; Ausseil, F.; Raux, R.; Menou, J.L.; Hill, B.T.; Heteronemin as a Protein Farnesyl Transferase Inhibitor. *Pharm. Biol*. **2004**, *42*, 454-456.

24. Kubo, I.; Ganjian, I. Insect Antifeedant Terpenes, Hot-tasting to Humans. *Experientia* **1981**, *37*, 1063-1064.

25. Okuda, R.K.; Scheuer, P.J.; Hochlowski, J.E.; Walker, R.P.; Faulkner, D.J. Sesquiterpenoid Constituents of Eight Porostome Nudibranchs. *J. Org. Chem.* **1983**, *48*, 1866-1869.

26. Lee, Y.R.; Morehead, A.T., Jr. A New Route for the Synthesis of Furanoflavone and Furanochalcone Natural Products. *Tetrahedron* **1995**, *51*, 4909-4922.

27. Caprioli, V.; Cimino, G.; Colle; Gavagnin, M.; Sodano, G.; Spinella, A. Insect Antifeedant Activity and Hot Taste for Humans of Selected Natural and Synthetic 1,4-Dialdehydes. *J. Nat. Prod.* **1987**, *50*, 146-151.

28. Hanson, J.R. The Sesterterpenoids. *Nat. Prod. Rep.* **1996**, *13*, 529-535, and previous references in the series.

29. Cimino, G.; De Rosa, S.; De Stefano, S.; Sodano, G. The Chemical Defense of Four Mediterranean Nudibranchs. *Comp. Biochem. Phys., Part B: Biochem. Mol. Biol.* **1982**, *73*, 471-474.

30. Terem, B.; Scheuer, P.J. Scalaradial Derivatives from the Nudibranch *Chromodoris youngbleuthi* and the Sponge *Spongia oceania*. *Tetrahedron* **1986**, *42*, 4409-4412.

31. Tsuchiya, N.; Sato, A.; Hata, T.; Sato, N.; Sasagawa, K.; Kobayashi, T. Cytotoxic Scalarane Sesterterpenes from a Sponge, *Hyrtios* erecta. *J. Nat. Prod.* **1998,** *61,* 468-473.

32. Doi, Y.; Shigemori, H.; Ishibashi, M.; Mizobe, F.; Kawashima, A.; Nakaike, S.; Kobayashi, J. New Sesterterpenes with Nerve Growth Factor Synthesis-stimulating Activity from the Okinawan Marine Sponge *Hyrtios* sp. *Chem. Pharm. Bull.* **1993**, *41*, 2190-2191.

33. Clement, J.A.; Yoder, B.J.; Kingston, D.G.I. Natural Products as a Source of CNS-active Agents. *Mini-Rev. Org. Chem.* **2004**, *1*, 183-208.

34. Yasuda, F.; Tada, H. Deacetylscalaradial, a Cytotoxic Metabolite from the Sponge *Cacospongia scalaris*. *Experientia* **1981**, *37*, 110-111.

35. De Rosa, S.; Puliti, R.; Crispino, A.; De Giulio, A. A New Scalarane Sesterterpenoid from the Marine Sponge *Cacospongia mollior J. Nat. Prod.* **1994**, *57*, 256-262.

36. Monti, M.C.; Casapullo, A.; Riccio, R.; Gomez-Paloma, L. The Inactivation of Phospholipase A2 by Scalaradial: a Biomimetic Study by Electrospray Mass Spectrometry. *Rapid Commun. Mass Spectrom*. **2005**, *19*, 303–308.

37. Potts, B.C.M.; Faukner, D.J.; de Carvalho, M.S.; Jacobs, R.S. Chemical Mechanism of Inactivation of Bee Venom Phospholipase A2 by the Marine Natural Products Manoalide, Luffariellolide, and Scalaradial. *J. Am. Chem. Soc.* **1992**, *114,* 5093-5100.

IV. Isolation and Characterization of a Tie2 Kinase Inhibitory Sulfated Triterpenoid from a Green Alga of the *Tuemoya* Genus

4.1 Introduction

The tyrosine kinase Tie2 has been implicated as in important mediator of mammalian angiogenesis, or the growth of new vascular tissue. Angiogenesis is an important part of the development of tumors, and so Tie2 is an interesting target for natural products drug discovery. Bioassay guided-fractionation of an extract of a *Tuemoya* sp. green alga, using an assay for inhibitors of the enzyme Tie2 kinase, afforded two sulfated cycloartanol triterpenoids. Both the major and minor compounds were identified by spectroscopic methods.

4.1.1 Previous Investigations of Genus *Tuemoya*

Only one report was found in the literature for chemical study of the alga of genus *Tuemoya*. The sulfated cycloartanol derivative **4.1** was isolated from an extract of this green alga, and was shown to inhibit the activity of VZV and CMV proteases.[1] Because this species had not been studied extensively, and because few inhibitors of Tie2 had been discovered, this extract had potential as a source of interesting drug leads.

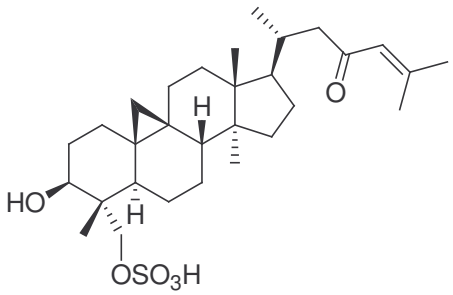

4.1

4.1.2 Role of Tie2 in Angiogenesis and Tumor Growth

Angiogenesis is the growth of new capillary blood vessel tissue that leads to neovascularization, the expansion of blood vessels into surrounding tissue. Angiogenesis is required for the survival of most tumors, as was established by Folkman *et al.* in the 1960's and 1970's.[2] Angiogenesis is a complex process that involves many different cellular signals. The tyrosine kinase Tie2 (also referred to as Tek) is a cellular receptor that plays a role in mediating angiogenesis. Below is a brief description of the role of Tie2 in angiogenesis, the relationship between tumor growth and angiogenesis, and studies of Tie2 as an antitumor drug target.

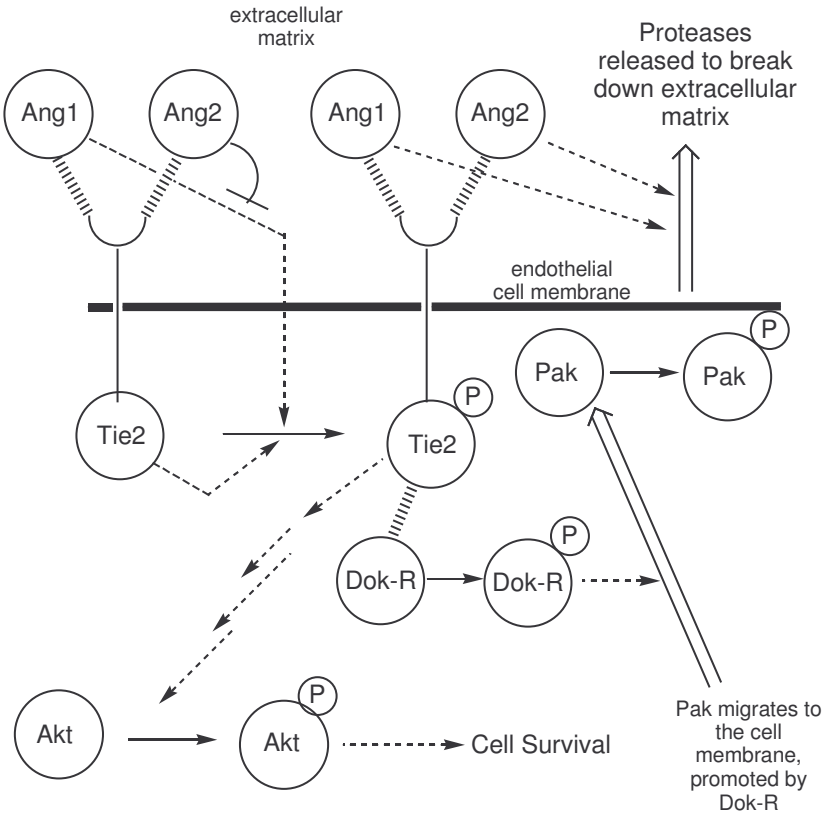

Scheme 4.1: Overview of Tie2-mediated endothelial cell growth
Dotted arrows indicate activation; wedged lines indicate enzyme binding; broad arrows indicate enzyme migration; blunt headed lines indicate antagonism.

Because blood vessels are composed of endothelial tissue, the development of the vascular system in developing mammals requires the growth and spread of new endothelial cells (EC). Partly through the study of tumors, the existence of growth factors produced by tumors to stimulate the formation of new blood vessels was proposed. By the 1990's, members of the vascular endothelial growth factor (VEGF) family of proteins were discovered. These were shown to have a stimulatory effect on the growth of vascular tissue, and receptors for VEGF proteins were found. Further, it was also found that mice that had even one allele of the VEGF-A gene knocked out died as embryos.[3] Thus, VEGF is vitally important for the proper growth of endothelial tissue.

It is also known that the phosphorylation of tyrosine is common in proteins from ECs, and that this is characteristically found more frequently in embryonic cells than in adult cells. Because of this phenomenon, it is apparent that tyrosine phosphorylation of cellular proteins might play an important role in the control of EC growth. Hence, several tyrosine kinases that are important to the proliferation of ECs have been characterized. Among these, Tie2 appears to be the most critical for the proper growth of new endothelial tissue. Tie2 is a kinase that is found in the cell membrane of ECs and hemopoietic cells (cells of sprouting blood vessels).[4] Mouse embryos that have the *tie2* gene removed do not survive the second week of embryonic life. These embryos suffer from poor heart development, decreased sprouting of new endothelial tissue, and decreased EC survival times.[5] Mice which have overexpressed Tie2 show signs of skin distress similar to human psoriasis.[6] Scheme 4.1 provides an overview of the key enzymatic relationships that govern Tie2-mediated EC proliferation.

Activated Tie2 has been shown to be play an important role in several events related to EC proliferation. Tie2 plays a role in promoting the survival of ECs through the activation of the cell survival promoter Akt,[7] but other mechanisms govern its role in EC growth. Once Tie2 is phosphorylated at tyrosine 1106, it is able to bind to the docking molecule Dok-R. Dok-R is phosphorylated by Tie2, which then promotes the movement of Nck-p21 activated kinase (Pak) to the cell membrane. The gathering of Pak to the cell membrane causes Pak to be activated, which leads to changes in the cytoskeleton and cell migration, an important part of angiogenesis.[8]

Tie2 has known ligands that have been shown to play crucial roles in controlling vascularization. Angiopoietin 1 (Ang1) is a protein that was shown to be critically important in the proper development of embryonic vascular tissue, but Ang1 does not have the same kind of direct stimulatory effect on EC growth as the VEGF proteins. It is known that Ang1 plays its role mainly in promoting the sprouting of new EC tubules.[9] Ang1 is detectable mainly around sites where cell migration and tubule formation is occurring.[10] Mice embryos deficient in Ang1 display symptoms similar to those of Tie2-deficient mice.[11] Ang1 has been shown to promote the autophosphorylation of Tie2, which activates the kinase.

Another protein that binds to the Tie2 receptor is angiopoietin 2 (Ang2). The role of Ang2 is complex, and is context-specific. Embryos that lack the *Ang2* gene die between the ninth and eleventh day of gestation, demonstrating the critical role of Ang2 in normal development.[12] In the presence of VEGF, Ang2 appears to cooperate with VEGF at the edge of growing vascular sprouts, perhaps to sensitize these cells to VEGF stimulation and promoting vascularization. In the absence of VEGF, Ang2 appears to

inhibit the activation of Tie2 induced by Ang1. So, in the case of ECs, the activation of Tie2 apparently depends on VEGF, and is highly regulated by both Ang1 and Ang2. It has been found that Ang2 can in certain circumstances promote Tie2 activation, which leads to Akt activation and cell survival.[13]

Ang1 and Ang2 can both activate matrix metalloproteinase-2 (MMP-2), a protease that participates in the breakdown of the proteins of the extracellular matrix around endothelial cells.[14,15] The breakdown of the extracellular matrix allows for open zones for new vascular sprouts to form. This is also an important part of the entire angiogenesis process. Overall, angiogenesis is a very complex process with many factors governing the process, among which Tie2 plays an important role. Since it is clear that angiogenesis not only involves the growth of new vascular tissue but also the destruction of protein structures in surrounding areas around endothelial cells, it should come as no surprise that angiogenesis is an important factor in the development of tumors.

From the work of Folkman, it was shown that tumors organs isolated in glass chambers with nutrients supplied by perfusion did not advance beyond a small size. Yet, if the same tumor cells were implanted into a host mouse, the tumor eventually killed the host. Since it was known that one of the problems of isolated perfused organs was the breakdown of ECs, which was not a problem in a living mouse, the connection between the growth of tumors and the proliferation of endothelial cells was strongly implied. Initial results like these generated much interest in studying angiogenesis, which led to much of the work that was discussed regarding Ang1, Ang2, and Tie2.

The roles of VEGF, Tie2, Ang1, and Ang2 in angiogenesis and tumor growth have been extensively studied, and these studies have yielded conflicting findings. The

only consistent observation is that these four factors are typically overexpressed in malignant tumors.[6] Overexpression of Ang1 has been shown to play a critical role in the angiogenesis-dependent growth of myeloma cells (tumor cells in bone marrow) through the upregulation of Tie2.[16] Also, in one glioma model, Ang2 plays a critical role at the boundary of the tumor, apparently acting in concert with VEGF to promote the regression of tissue surrounding the tumor. It should be noted that one of the major modes of tumor angiogenesis is the cooption of pre-existing blood vessels in surrounding tissue.[17]

VEGF also has key relationships to tumor cell proliferation. It has also been shown in a glioblastoma model that inducing an antisense expression of the *VEGF* gene causes tumor growth to be significantly diminished, while the reduction of blood vessel growth is proportional to the decrease in amount of VEGF production.[18] Murine mutated p53 has even been shown to promote the expression of VEGF mRNA,[19] suggesting that part of the tumor-promoting effects of mutated p53 may be angiogenesis-related. VEGF receptors have been studied as drug targets, and synthetic inhibitors of these receptors have shown *in vivo* antiproliferative effects against tumors in mice.[20]

As expected, it has also been shown that Tie2 can play a critical role in the growth of tumors. In a key experiment, a protein mimic of the extracellular domain of Tie2 was produced and tested as an inhibitor of angiogenesis. In an *in vivo* murine tumor model, mammary tumors treated with this protein showed a 75% reduction in tumor growth.[21] Presumably, the presence of the Tie2 mimic inhibits Ang1 and Ang2 binding to Tie2, resulting in reduced angiogenic potential. Not only does this once again establish a role for Tie2 in the angiogenesis of tumors, but it also suggests that Tie2 inhibitors might also serve as antitumor agents. This has been an active area of research in the past decade. A

few classes of synthetic Tie2 inhibitors have been patented or published.[22,23] Few natural products have been reported as having Tie2 inhibitory activity.[24,25]

Targeting angiogenesis has produced some drug candidates, with several polypeptide-based antitumor drugs that target angiogenesis entering clinical trials. These include endostatin, a polypeptide derived from collagen that has completed Phase I and II clinical trials;[26] Vitaxin®, which has completed Phase I and II clinical trials and produces few harmful side effects;[27] and bevacizumab, which is an antibody for VEGF and has received FDA approval for the treatment of colorectal cancer.[28] It has been suggested that, unexpectedly, anti-angiogenic agents may actually cause blood flow to tumors to become more efficient because of the removal of excess ECs. This could cause improved blood flow to tumors, opening them up to drug treatment with cytotoxic agents or making them more sensitive to ionizing radiation. This might explain how angiogenesis inhibitors act synergistically with chemotherapeutic agents and ionizing radiation.[29] The quest for antiangiogenic agents continues, fueled by the understanding that tumors have to tap into the blood supply of their host to survive. In this chapter we report the isolation and characterization of sulfated cycloartanol triterpenoids that inhibit Tie2 kinase.

4.2 Results and Discussion

4.2.1 Isolation of Tie2 Inhibitory Sulfated Cycloartane Derivatives

The isolation of **4.2** is depicted in scheme 4.2. A methanol extract of an algal *Tuemoya* sp. showed good activity in a bioassay for inhibition of Tie2 kinase, with an IC_{50} of 4.4 μg/mL. Bioassay-guided fractionation of the crude extract was performed using polyamide chromatography, followed by separation on CHP20P resin and on a C_{18}

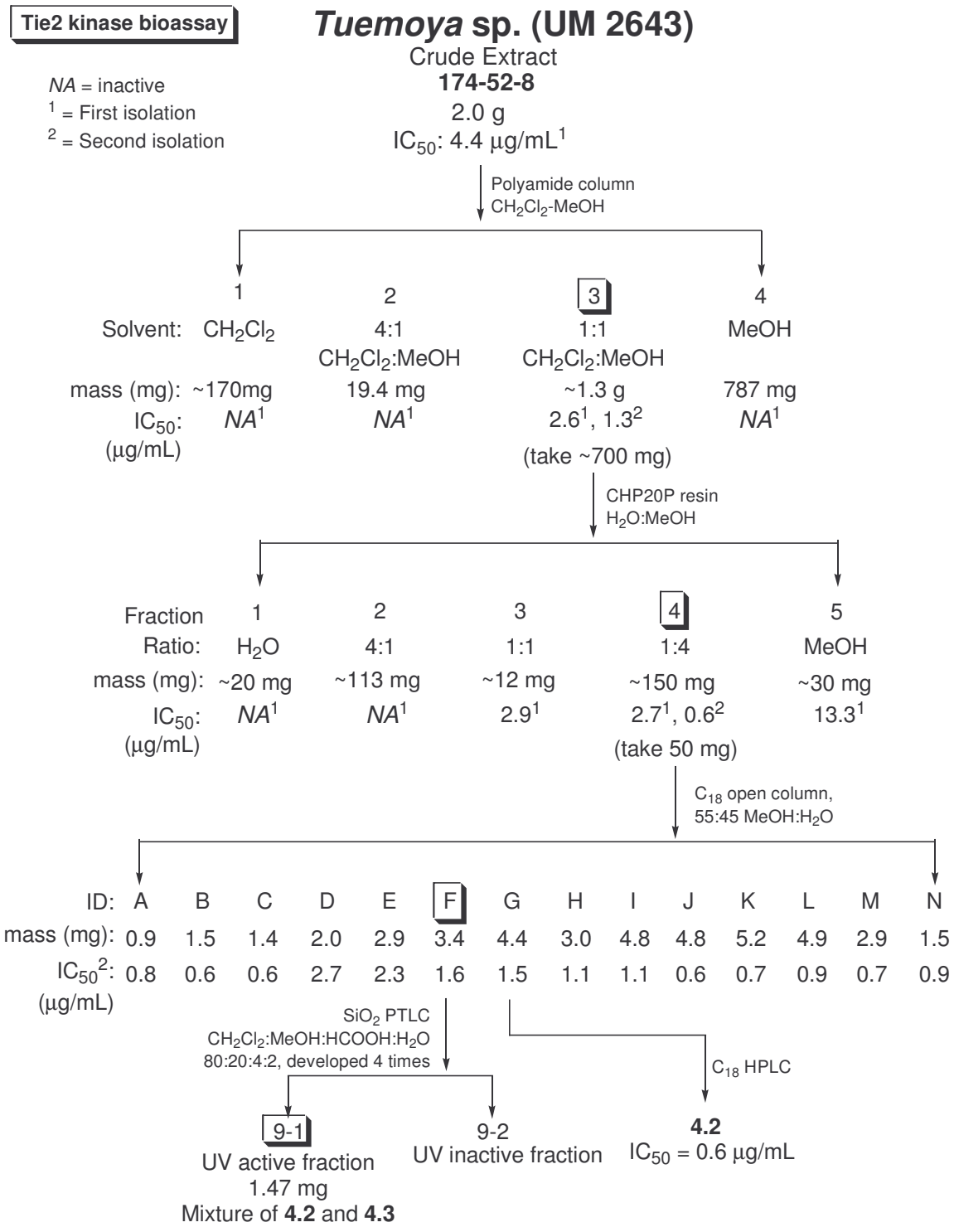

Scheme 4.2: Isolation of **4.2** and **4.3**

reversed-phase column. Several active fractions were obtained from reversed-phase chromatography, and analysis of these fractions by NMR spectroscopy indicated that they all contained closely related triterpenoids, most probably of the cycloartanol type, based on ^{1}H NMR analysis of these fractions. C_{18} HPLC analysis indicated that fractions A-N from the C_{18} open column separation contained mixtures of compounds that were difficult to separate. So, because fractions A-N contained mixtures of similar compounds, one active fraction (fraction G) was selected for detailed investigation, since it contained one major component and possessed good activity. Reverse phase HPLC of fraction F yielded **4.2**, the major compound from fraction G, in very low yield.

Fractionation of fraction F by normal phase TLC afforded a fraction (fraction F-1) that was identified as a 2:1 mixture of two triterpenoids, based on integration of its ^{1}H NMR spectrum. Despite repeated attempts to separate the mixture by TLC (normal and reverse phase) and HPLC, it did not prove possible to separate the two components in fraction F. The major compound from the mixture was identified as **4.2**. Because the two compounds differed in their relative abundance, it was possible to identify the major compound **4.2** and assign its NMR spectra using 1D and 2D NMR techniques without significant interference from the minor compound **4.3**, as discussed below. Thus, **4.3** was also identified based on analysis of fraction F-1.

Negative ion HRFABMS analysis of **4.2** indicated a formula of $C_{30}H_{48}O_9S_2$. The presence of a sulfate group in the major compound was strongly suggested by a peak at *m/z* = 535.3137 $[M\text{-}SO_3H]^-$. UV analysis of the **4.2** showed absorption maxima at 203 and 239 nm, consistent with the presence of an α,β-unsaturated carbonyl group.

The ^{1}H NMR data for **4.2** is reported in Table 4.1. The ^{1}H NMR spectrum of **4.2** was complex, with overlapping signals consistent with the presence of a mixture of two similar compounds. Clear signals at δ_H 0.44 and 0.61, characteristic of methylene protons in a three-member ring, could be identified, and signals at δ_H 4.49, 3.75, and 4.07 could be assigned to methine and methylene protons attached to oxygenated carbons. Signals for six methyl groups could also be identified. Two of the methyl signals appeared at δ_H 2.11 and 1.90 ppm, and were assigned to vinyl methyls, and a multiplet at δ_H 6.17 was assigned to an α proton of an α,β-unsaturated ketone; these signals suggested the presence of the $R^1COCH{=}CMe_2$ structural subunit for **4.2**. Overall, based on the formula determined by FABMS and the number of methyl signals detected in the ^{1}H NMR spectrum, it appeared likely that **4.2** was a sulfated triterpenoid containing a three-member ring. Because of the three-member ring detected by ^{1}H NMR analysis, it was proposed that **4.2** was a cycloartane triterpenoid derivative. The cycloartane skeleton, typified by a three-member ring at C-19, is shown in Figure 4.1.

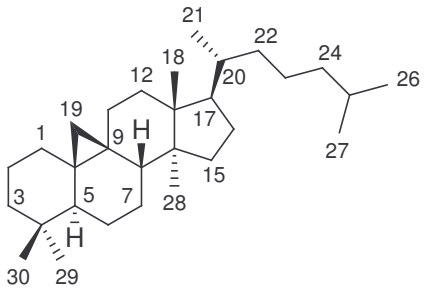

Figure 4.1: The cycloartane skeleton and numbering

The ^{13}C NMR data for **4.2** is reported in Table 4.1.From ^{13}C NMR analysis, thirty signals were detected for **4.2.** The ^{13}C data for **4.2** included a signal for one carbonyl

Table 4.1: ^{1}H and ^{13}C NMR **4.2**, and ^{13}C NMR assignments for **4.3**

	4.2			**4.3**
Position	δ_C[a]	δ_H[a]		δ_C[a]
1	32.6	1.31	m	32.6
		1.56	m	
2	28.3	1.79	m	28.3
		2.25	m	
3	81.2	4.49	dd, 4.8, 12	81.2
4	44.5	-		44.5
5	41.7	1.85	dd, 4.2, 12	41.7
6	21.5	0.86	m	21.5
		1.67	m	
7	26.8	1.16	m	29.3 [a]
		1.34	m	
8	49.7	1.55	m	49.7
9	21.1	-		21.1
10	26.5	-		26.5
11	27.4	1.17	m	27.4
		2.05	m	
12	34.0	1.67	m	36.7 [a]
13	46.6	-		46.6
14	50.1	-		50.1
15	36.7	1.35	m	36.7
16	29.4	1.35	m	29.4
		1.90	m	
17	53.9	1.65	m	53.6 [a]
18	18.7	1.06	s	18.7
19	30.8	0.44	d, 4.4	30.8
		0.60	d, 4.1	
20	34.9	1.98	m	34.9
21	19.7	0.86	d, 6.2	19.7
22	52.7	2.10	m	51.5 [a]
		2.53	dd, 3.0, 15	
23	204.2	-		214[b]
24	125.3	6.17	m	53.3 [a]
25	156.9	-		25.6 [a]
26	20.8	2.11	d, 0.95	22.9 [a]
27	27.7	1.90	d, 0.90	22.8 [a]
28	19.8	0.95	s	19.8
29	69.7	3.75	d, 9.4	69.7
		4.07	d, 9.4	
30	11.7	0.85	s	11.7

[a]Non-overlapped peaks for **4.3**. [b]Observed from HMBC spectrum

carbon at δ_C 204.2 as well as two other sp^2 carbon signals at δ_C 125.3 and 156.9 and two oxygenated carbons at δ_C 69.7 and 81.2. The chemical shifts of these carbons were consistent with the attachment of sulfate groups at those positions. DEPT analysis detected six methyl, eleven methylene, and six methine carbon signals for **4.2,** implying seven quaternary carbons for **4.2** to account for all thirty carbons detected by FABMS analysis.

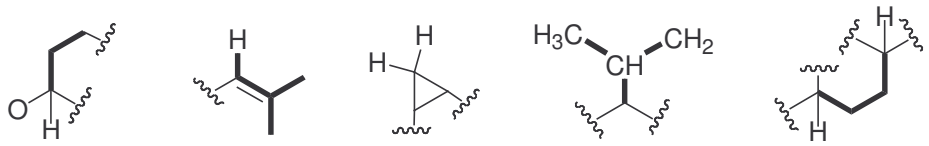

Figure 4.2: Spin systems for **4.2** determined by COSY analysis

HSQC analysis allowed for the correlation of the proton signals of **4.2**, which were badly overlapped in places, with their corresponding carbon signals, and thus allowed a full assignment of the ^{1}H NMR spectrum of **4.2**. The assignments shown in Table 4.1 are based on the HSQC spectrum. HSQC analysis of **4.2** then permitted the interpretation of the COSY and HMBC spectra for **4.2**. Spin systems suggested by COSY analysis are shown in Figure 4.2. The HMBC correlations that allowed for the spin systems to be connected are depicted in Figure 4.3 and Figure 4.4.

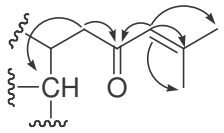

Figure 4.3: Spin system elucidated for **4.2** by HMBC

HMBC analysis permitted the determination of the entire skeleton of **4.2**. Observed HMBC correlations for **4.2** are tabulated in Table 4.1. As shown in Figure 4.4, correlations between the proton signal at δ_H 6.17 and the carbon signals at δ_C 204.2,

156.9, 27.7, and 20.8, along with the observed COSY correlations, defined an α,β-unsaturated ketone moiety. Correlations between the proton signal at δ_H 2.10 and the carbon signals at δ_C 204.2 and 19.7, when taken along with the observed COSY correlations, fully defined an eight-carbon sidechain. A correlation between the proton signal at δ_H 4.49 and the carbon signal at δ_C 69.7 strongly suggested that the two proposed sulfated carbons were in close proximity to each other. This was further suggested by a correlation between the proton signals at δ_H 3.75 and 4.07 and the carbon signal at δ_C 81.2. Correlations between the proton signals at δ_H 3.75, 4.07, and 0.85 and the carbon signal at δ_C 44.5 showed how one methyl and the oxygenated methylene were both connected to a common quaternary carbon. Finally, along with the COSY data, correlations between the methylene proton at δ_H 0.60 and the carbon signals at δ_C 41.7 and 32.6, as well as correlations between the methylene proton at δ_H 0.44 and the carbon signal at δ_C 49.7, fully established both the A and B rings of a cycloartane triterpene

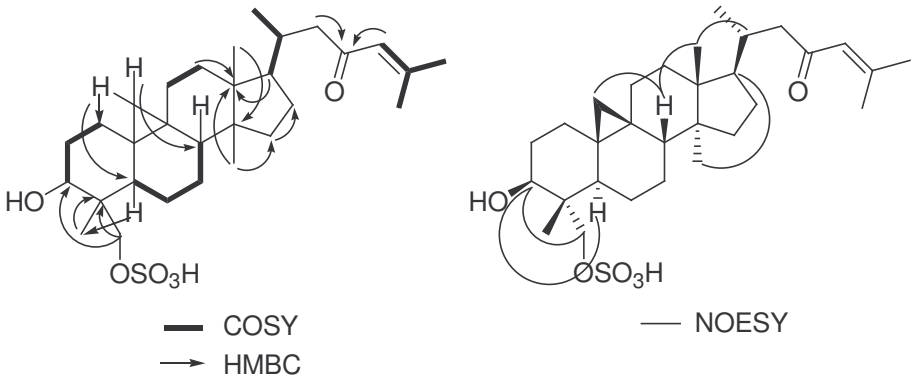

Figure 4.4: Observed 2D NMR correlations for **4.2**

skeleton. The observed HMBC correlations are completely consistent with the proposed cycloartane skeleton for **4.2**, as shown in Figure 4.4.

NOESY analysis assisted in the determination of the relative stereochemistry for **4.2.** H-3, which gave rise to a doublet of doublets, was assumed to be in an axial position. So, the observation of NOESY correlations between the proton signal at δ_H 4.49 and the signals at δ_H 3.75, 4.07, and 1.85 demonstrated how H-3 and H-5 were on the same face of the molecule and that C-28 was in an equatorial position on the ring. Other observed NOESY correlations were consistent with the assignment of the relative stereochemistry as shown. Therefore, the structure of **4.2** was determined to be that shown below. The absolute stereochemistry assigned is arbitrary, but is consistent with the structures of similar cycloartanols isolated from green algae.[30]

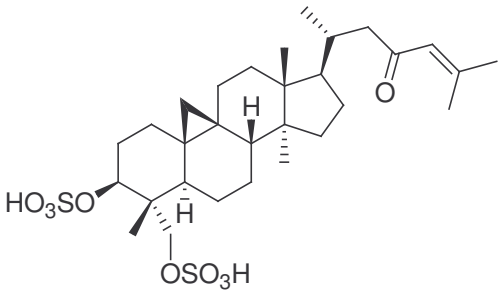

4.2

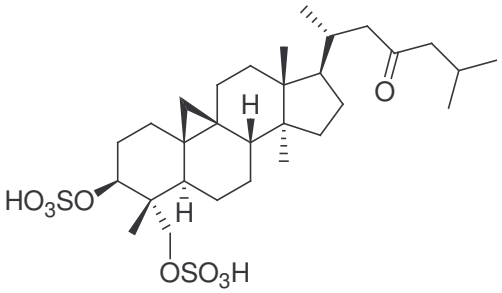

4.3

Once **4.2** was characterized, the minor compound **4.3** could be characterized from fraction F-1. From low resolution FABMS for fraction F-1, ions at *m/z* = 617.28 ($[M-H]^-$) and *m/z* = 537.27 ($[M-SO_3H]^-$) were detected for **4.3**, implying a formula of $C_{30}H_{50}O_9S_2$ for this compound. The ^1H NMR spectrum of **4.3** was badly overlapped with signals for **4.2**, but signals in a 2:1 ratio were clearly observed at δ_H 2.30 and 2.48. The ^{13}C NMR spectrum of **4.3**, coupled with DEPT analysis, revealed the presence of six methyls, twelve methylenes, six methines, and five quaternary carbons, and the HMBC spectrum also revealed a carbonyl signal at δ_C 214. The three-membered ring and the six

methyl groups for **4.3**, together with the overlap of many of its ^{13}C-NMR signals with those of **4.2** in fraction F-1, confirmed that it also possessed a cycloartane triterpenoid skeleton. Because of the weakness of the gHSQC signals for **4.3**, its ^{1}H NMR assignments could not be fully determined. However, weak correlations for **4.3** were observable from the HMBC spectrum of fraction F-1, which supported the assignment of **4.3** as a hydrogenated analogue of **4.2**. The structure was deduced as that shown for **4.3** from its ^{13}C NMR data and the limited ^{1}H NMR data that could be assigned. This structure is fully consistent with all the available data, since the FABMS and NMR data also suggested that **4.3** was a hydrogenated analogue of **4.2**. The ^{13}C NMR assignments of **4.3** are included in Table 4.1.

The sodium salts of **4.2** and **4.3** were previously isolated from the green alga *Tydemania expeditionis,* and were shown to be an inhibitors of the tyrosine kinase pp60$^{v\text{-}src}$. The data for **4.2** and **4.3** compare well with the available data in the literature.[30] Other sulfated cycloartanols have been reported from the *Tuemoya* species.[1] However, this is the first time that the Tie2 kinase inhibitory activity of these compounds has been reported, and it is the first time that the ^{1}H and ^{13}C NMR spectra have been completely assigned for **4.2**.

4.2.2 Biological Evaluation of Sulfated Cycloartane Derivatives

Changes in research emphasis at GlaxoSmithKline Pharmaceuticals (GSK) resulted in the discontinuance of access to the Tie2 kinase bioassay before samples of both **4.2** and **4.3** could be tested, so it was not possible to be sure of the activity of compound **4.3**. The purified sample of **4.2** had an IC_{50} of 0.7 μg/mL in the Tie2 kinase

assay, indicating that compound **4.2** was responsible for at least a part of the activity of the crude extract. However, since compounds **4.2** and **4.3** were the major constituents of the active fraction F-1, and since these or other closely related compounds were present in all the active fractions of the reverse phase column, it is most probable that compound **4.3** also has significant activity as an inhibitor of Tie2 kinase. Regrettably, even though fractions A-N contained additional active components, the activity of other purified compounds from these fractions could not be determined due to the discontinuation of our collaboration with GSK. Because **4.2** had good bioactivity towards an interesting target and the full ^{1}H and ^{13}C NMR assignment of **4.2** had not been previously reported, this work has been published.[31]

4.2.3 Previous Discoveries of Bioactive Sulfated Triterpenoids

The vast majority of triterpenoids containing sulfate groups are triterpenoid glycosides with sulfated sugar residues. This class of compounds, which are structurally dissimilar to **4.2** and **4.3**, is beyond the scope of this survey of the literature. Several bioactive sulfated triterpenoids, including sulfated cycloartanol derivatives, have been isolated previously. As mentioned in the introduction, **4.1** was isolated from a *Tuemoya* sp. green alga and shown to have inhibitory activity towards VZV (varicella-zoster virus, which causes chickenpox) protease and CMV (cytomegalovirus) proteases. The compounds isolated in this current study, **4.2** and **4.3**, were previously shown to be inhibitors of the tyrosine kinase $pp60^{v\text{-}src}$. $pp60^{v\text{-}src}$ is a kinase derived from the Rous sarcoma virus, an oncogenic virus capable of causing cancer in chickens.[32]

Capisterone A (**4.4**) was isolated along with its deacetoxy derivative from the green alga *Penicillus capitatus* and found to have antifungal activity against the marine organism *Lindra thallasiae*.[33] Compound **4.5** was isolated from the red alga *Tricleocarpa*

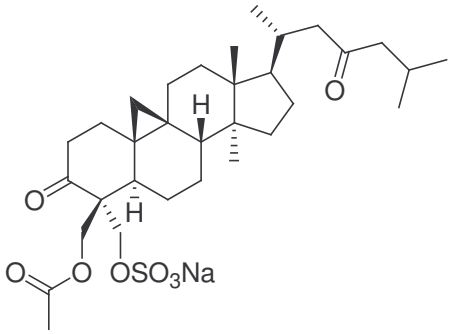

4.4

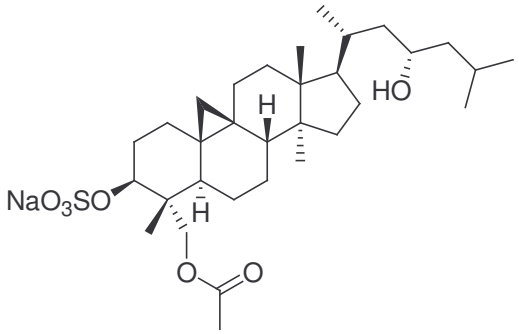

4.5

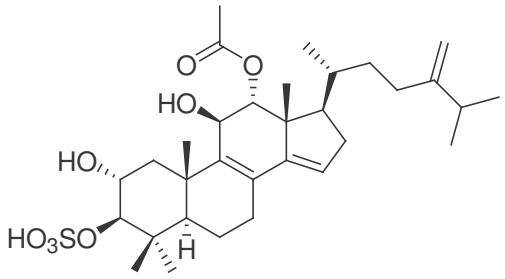

4.6

fragilis and found to have potent toxicity towards brine shrimp at 17 μg/mL.[34] A sulfated terpenoid that is not a cycloartane derivative, **4.6** was originally isolated from the fungus *Fusarium compactum* and was shown to have anti-HIV activity.[35] Compound **4.6** also inhibited the activity of rhinovirus 3C protease.[36]

4.2.4 Proposed Mechanism of Action of 4.2 and 4.3

Both Patil *et al.* and Govindan *et al.* reported that hydrolysis of **4.1** and **4.2**-**4.3** yielded alcohol derivatives without activity in their respective assays. Therefore, the sulfate groups appear to be critical for their tyrosine kinase inhibitory activity. Sulfated compounds with hydrophobic backbones are not the only kinds of compounds that were

bioactive in the Tie2 assay. Several long-chain fatty acids were also found to be active.[37] Also, the triterpenoid acid **4.7** was active in the Tie2 assay.[24] Having shown all of this,

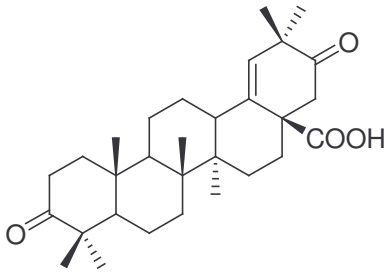

4.7

there appears to be a trend that molecules with hydrophobic structures and polar headgroups can act as inhibitors of tyrosine kinases. It has been reported by our collaborators at the University of Virginia that the steroid derivative halistanol sulfate G (**4.8**) is also active in the Tie2 bioassay. A very similar compound, halistanol trisulfate (**4.9**) is an inhibitor of the pp60$^{v\text{-}src}$ tyrosine kinase mentioned before.[38] Because the catalytic domains of tyrosine kinases are all so similar,[39] these halistanols can be viewed as prototypes for tyrosine kinase inhibitors that possess hydrophobic backbones and sulfate polar headgroups, like **4.1**-**4.3**.

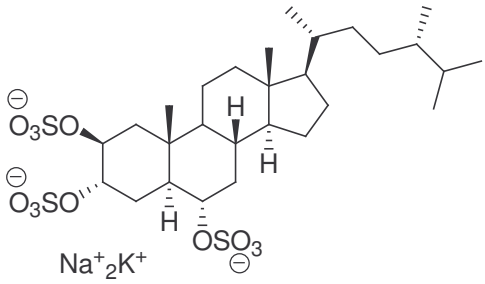

4.8

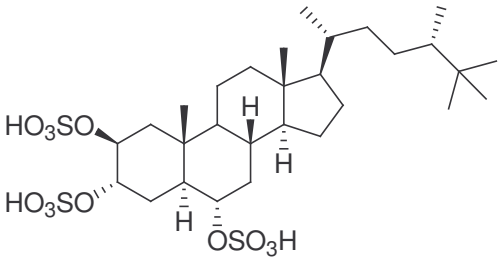

4.9

Kinetic studies performed by Slate *et al.*[38] suggested that **4.9** is a competitive inhibitor of pp60$^{v\text{-}src}$ with respective to the typical peptide substrate, but it is a mixed

A)

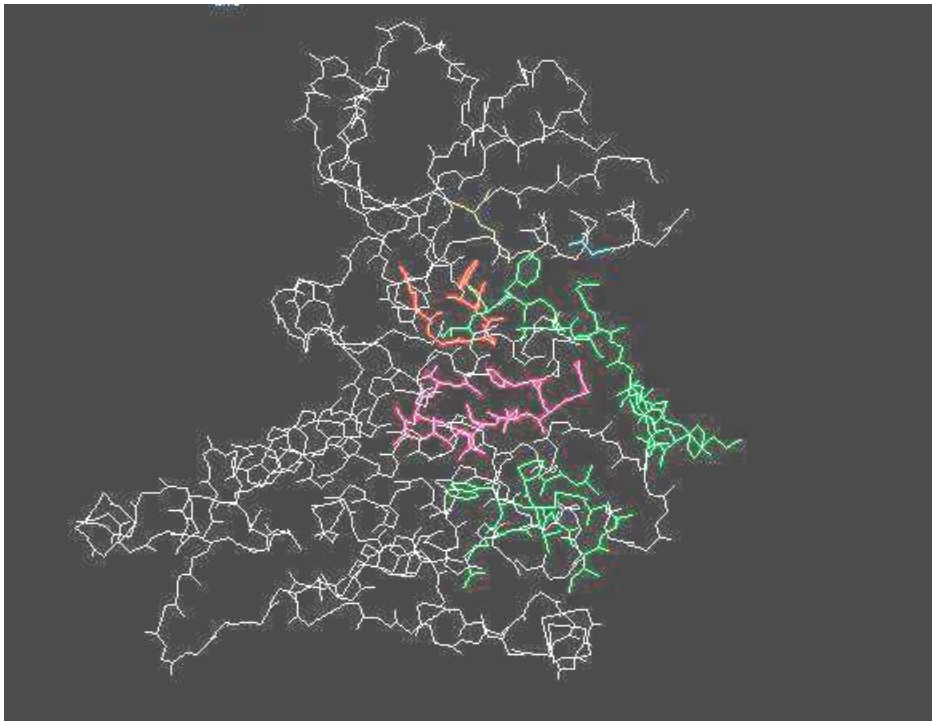

B)

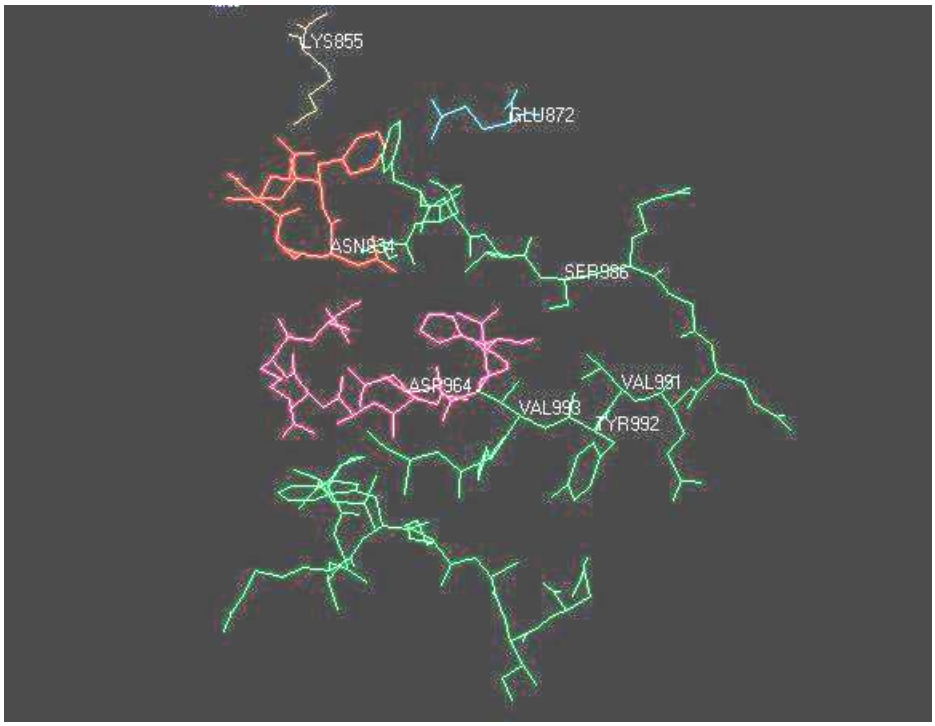

Figure 4.5: Two views of the kinase domain of Tie2

A) Catalytic site of within the kinase domain of Tie2 B) Catalytic site of Tie2. Green: activation loop. Magenta: Catalytic loop. Red: Nucleoside binding loop. Yellow and blue: salt bridge for binding to ATP. Note positions of Tyr992, Val992, and Val993, the proposed binding site of **4.2**. Drawings generated in Swiss Pdb Viewer v.3.7, based on the crystal structure published by Shewchuk *et al.*[39]

inhibitor with respect to ATP. That is, in terms of Michaelis-Menten enzyme kinetics, addition of **4.9** as an inhibitor would cause K_m to increase, while v_{max} would decrease with respect to ATP. The implication is that an inhibitor like **4.9** would not affect the affinity of $pp60^{v\text{-}src}$ for its peptide substrate, but that the affinity of the kinase for ATP would be changed. This seems to suggest that **4.9** probably does not bind in the catalytic site, but it might be binding at another site that somehow changes the ability of $pp60^{v\text{-}src}$ to bind to ATP. Again, this is a prototypical example based on $pp60^{v\text{-}src}$, but since tyrosine kinases are all similar, these same facts may hold true for Tie2.

The crystal structure of the kinase domain of Tie2 shows some unique features that may explain why Tie2 is sensitive to molecules like **4.2**, **4.3**, and **4.7** (See Figure 4.5). This exploration of the structure of the kinase domain of Tie2 is based on the work of Shewchuk *et al.*[39] Like other kinases, Tie2 possesses an activation loop that controls kinase activity, a nucleotide binding domain that binds ATP and positions it for phosphate transfer, and a catalytic domain that performs the phosphate transfer (see Figure 4.5). There are also two residues, lysine 855 and glutamic acid 872 (Lys855 and Glu872) which form a so-called salt bridge to position the α and β phosphates of ATP into position so that the γ phosphate can be transferred. In the published crystal structure, this salt bridge (without ATP co-crystallized) in Tie2 is 7.2 Å wide, while in normal kinases it is 3-4 Å. This suggests that some additional conformational change must occur after Tie2 is activated in order for the enzyme to have catalytic activity.

The activation loop of Tie2 is also unusual. The activation loop must be phosphorylated before the kinase is activated, and a portion of the activation loop (Phe983, as shown in Figure 4.5) actually passes between Lys855 and Glu872, the salt

bridge needed to position ATP properly. Again, special conformation changes are required after activation in order to open up the salt bridge to ATP. Finally, the nucleoside binding domain (residues 832-836) is self-inhibitory. Residues 832-836 are also needed to bind to the phosphate groups of ATP, and in the crystal structure there is evidence that glutamic acid 832 can form a hydrogen bond to glutamic acid 903, which appears to bind to the adenosine portion of ATP. Additionally, there are other hydrogen bonding interactions that stabilize this nucleoside binding site conformation. Thus, the structure of pre-activated Tie2 actually precludes ATP binding in the ATP binding site. These conformational requirements are not well understood, but they suggest that the mechanism of activating Tie2 is very complex. Again, we can compare Tie2 with other tyrosine kinases. The tyrosine kinase $pp60^{c\text{-}src}$ (also referred to as c-Src) is the human tyrosine kinase that is thought to be the genetic precursor to $pp60^{v\text{-}src}$. This tyrosine kinase also possesses special conformational features that make it autoinhibitory like Tie2.[40]

Because the activity of Tie2 is highly sensitive to changes in pre-activated conformation, we propose that **4.2**, **4.3**, and **4.7** act as inhibitors of Tie2 by preventing conformational changes needed for Tie2 activity. Compounds **4.2**, **4.3**, and **4.7** may act like surfactants, and they may interfere with the overall secondary structure of the kinase domain of Tie2. As an example, we will examine binding of **4.2** to the activation loop of Tie2. The peptide sequence of the activation loop is ANFGLSRGQEVYVKKLPVRWMAIE, where the underlined residue is the tyrosine that must be phosphorylated to activate Tie2. This is shown in green in Figure 4.5(B). In the published crystal structure, the tyrosine residue points slightly out towards the solvent,

while the sidechains of the two valines (991 and 993) flanking the tyrosine point slightly inward. The sidechain of serine 986 points down toward the two valines. We can envision **4.2** having weak interactions with valines 991 and 993. This might disrupt the activation loop just enough to cause inhibition of the ATP-dependent kinase activity of Tie2. Because this would involve conformational effects, the affinity of Tie2 for ATP might be decreased. At the same time, these surfactant-type interactions would be expected to interfere with the peptide binding ability of Tie2, but the effects on the peptide substrate may not be as pronounced since the peptide binding domain of Tie2 is found on a different subunit. Thus, if we assume that the kinetic behavior of **4.9** towards the tyrosine kinase $pp60^{v\text{-}src}$ is similar to that of **4.2** towards Tie2, then our explanation involving surfactant-type interactions between Tie2 and **4.2** would account for a decreased affinity for ATP and an unchanged affinity for the peptide substrate.

To summarize, Tie2 has shown sensitivity to fatty acids, triterpenoid carboxylic acids, and triterpenoid sulfonic acids. Because the effects of **4.2-4.3**, **4.7** and long-chain fatty acids appear to arise from non-specific surfactant-type interactions with a conformationally sensitive tyrosine kinase, and the tyrosine kinase inhibitory effects of **4.1**-**4.3** are eliminated after sulfate cleavage, these sulfated triterpenoids do not represent potential drug candidates.

4.3 Experimental Section

General Experimental Procedures

Mass spectra were obtained on a JEOL HX-110 instrument. NMR spectra were collected on either a Varian Inova 400 spectrometer operating at 399.9 MHz for ^{1}H and 100.6 MHz

for ^{13}C, or a JEOL Eclipse+ 500 spectrometer operating at 500.2 MHz for ^{1}H and 125.8 MHz for ^{13}C. Polyamide was obtained from MP Biomedicals (formerly ICN Biomedicals, Inc.). Dianion CHP20P MCI gel was obtained from the Mitsubishi Chemical Corporation. Normal phase preparative TLC was carried out on SiO_2 plates. HPLC was performed on a Shimadzu LC-10AT instrument with an ODS A323 column (250 × 10 mm).

Tyrosine Kinase Bioassay

The bioassay for Tie2 kinase inhibitory activity was performed by Dr. Paul Fisher at GlaxoSmithKline Pharmaceuticals (GSK). The Tie2 assay procedure used by GSK was confidential, so a typical procedure for measuring Tie2 inhibition is included for completeness, from the work of Kissau *et al*.[25]

Tie2 was expressed as a glutathione fusion protein. The assay was performed in white 96-well microtiter plates which had been coated with the polypeptide used as a Tie2 substrate, poly(Glu-Tyr) 125 μL of phosphate buffered saline (PBS) per well at 4°C. The coating solution was shaken out by hand, and the wells were washed with a mixture of PBS and detergent. Tie2 was diluted to a concentration of 20 ng protein in 50 μL of solution by addition of a buffer containing 100 mM HEPES (pH 7.4) and 100 mM NaCl. Stock solutions of potential Tie2 inhibitors ("drugs") were prepared in DMSO, and 1:2 serial dilutions were prepared from the stock solutions. The final drug concentrations were over a range from 0.013 to 13 μg/mL. The kinase reaction was initiated by the addition of 25 μL of 100 μM ATP solution containing 40 mM $MnCl_2$. Negative control wells received 40 mM $MnCl_2$ solution with no ATP. The plates were incubated for thirty

minutes at room temperature, then washed with a mixture of PBS and detergent to remove the reaction mixture components, leaving the phosphorylated polypeptide in the wells of the plate. A solution of an anti-phosphotyrosine antibody (typically conjugated to horseradish peroxidase) was added and incubated for one hour at room temperature. The plates were then washed five times with PBS and detergent, leaving the phosphorylated peptide with the antibody attached. Finally, to detect the presence of the antibody, a chemiluminescence substrate was added that emits light when bound to the anti-phosphotyrosine antibody. The resulting light emission was detected with a luminescence reader. Percent inhibition of samples was calculated based on the luminescence values for the positive control (reaction well without ATP) and the negative control (reaction with no drug). From the dose response curves for each drug, the concentration that achieved 50% enzyme inhibition was estimated to give the IC_{50} value.

Isolation and Characterization of 4.2 and 4.3

The crude extract (2.0 g) was chromatographed on a polyamide column with elution with CH_2Cl_2-MeOH, increasing to MeOH. The bioactive fraction eluted with 1:1 CH_2Cl_2:MeOH (1.3 g) was further purified by chromatography on CHP20P MCI gel, with elution with a step gradient of MeOH and H_2O, beginning with pure H_2O and increasing to pure MeOH. The fraction eluted with MeOH:H_2O, 4:1 (150 mg) was the most active, with IC_{50} = 0.6 μg/mL. A portion of this fraction (50 mg) was further purified by chromatography on a reversed phase column (C_{18} open column, 25 × 1 cm; 55:45 MeOH:H_2O, 17 fractions) to yield several active fractions with similar activity (IC_{50} = 0.6-1.6 μg/mL). Based on ^{1}H-NMR and HPLC-UV analysis, these fractions all

contained similar compounds. After examining all active fractions by HPLC-UV, fractions F and G (IC_{50} = 1.6 and 1.5 μg/mL, respectively) seemed to be a less complex mixtures than the other fractions, so these fractions were purified further.

Compound **4.2** was isolated in low yield (0.3 mg) from fraction G by C_{18} reverse phase HPLC (25 cm x 1 cm, isocratic, 55% aq. MeOH), and was shown to be active in the Tie2 inhibition assay (IC_{50} = 0.7 μg/mL). Separation of fraction F by normal phase SiO_2 TLC (CH_2Cl_2:MeOH:HCOOH:H_2O, 80:20:4:2), produced two bands visualized by vanillin-H_2SO_4 treatment. The major band was visible under UV light at 256 nm, and was determined to be a 2:1 mixture of **4.2** and **4.3** (1.5 mg), based on NMR analysis. Attempts to further separate the mixture by normal phase and reversed phase TLC were unsuccessful. It is likely that both **4.2** and **4.3** possess Tie2 inhibitory activity, but the activity of **4.3** was not confirmed due to the discontinuation of the Tie2 assay at GSK.

Cycloart-24-en-3,29-diol-23-one 3,29-disulfate (4.2): Colorless needles; UV (MeOH) λ_{max} = 249 nm; ^{1}H NMR (CD_3OD) see Table 4.1; ^{13}C NMR (CD_3OD) see Table 4.1; HRFABMS (negative ion) 615.2592 ($[M-H]^-$, calc. for $C_{30}H_{48}O_9S_2$: 615.2661, Δ = 11 ppm).

Cycloartan-3,29-diol-23-one 3,29-disulfate (4.3): Colorless needles; ^{13}C NMR (CD_3OD) see Table 4.1; LRFABMS (negative ion) 617.28 ($[M-H]^-$, calc. for $C_{30}H_{50}O_9S_2$), 537.27 ($[M-SO_3H]^-$, calc. for $C_{30}H_{49}O_6S$).

References for Chapter 4

1. Patil, A.D.; Freyer, A.J.; Killmer, L.; Breen, A.; Johnson, R.K. A New Cycloartanol Sulfate from the Green Alga *Tuemoya* Sp.: An Inhibitor of VZV Protease. *Nat. Prod. Lett.* **1997**, *9*, 209-215.

2. Folkman, J. "Tumor Angiogenesis." In *Advances in Cancer Research*. Academic Press: New York, 1985. Vol. 43, pp 175-203.

3. Carmeliet, P.; Ferreira, V.; Breier, G.; Pollefeyt, S.; Kieckens, L.; Gertenstein, M.; Fahrig, M.; Vandenhoeck, A.; Harpal, K.; Eberhardt, C.; Declercq, C.; Pawling, J.; Moons, L.; Collen, D.; Risau, W.; Nagy, A. Abnormal Blood Vessel Development and Lethality in Embryos Lacking a Single VEGF Allele. *Nature* **1996**, *380*, 435-439.

4. Schnürch, H.; Risau, W. Expression of Tie-2, a Member of a Novel Family of Receptor Tyrosine Kinases, in the Endothelial Cell Lineage. *Development*, **1993**, *119*, 957-968.

5. Puri, M.C.; Partanen, J.; Rossant, J.; Bernstein, A. Interaction of the TEK and TIE receptor tyrosine kinases during cardiovascular development. *Development* **1999**, *126*, 4569-4580.

6. Ward, N.L.; Dumont, D.J. The Angiopoietins and Tie2/Tek: Adding to the Complexity of Cardiovascular Development. *Cell Devel. Biol.* **2002**, *13*, 19-27.

7. Kontos, C.D.; Stauffer, T.P.; Yang, W.-P.; York, J.D.; Huang, L.; Blanar, M.A.; Meyer, T.; Peters, K.G. Tyrosine 1101 of Tie2 Is the Major Site of Association of p85 and Is Required for Activation of Phosphatidylinositol 3-Kinase and Akt. *Mol. Cell. Biol.* **1998**, *18*, 4131-4140.

8. Master, Z.; Jones, N.; Tran, J.; Jones, J.; Kerbel, R.S.; Dumont, D.J. Dok-R Plays a Pivotal Role in Angiopoietin-1-Dependent Cell Migration Through Recruitment and Activation of Pak. *EMBO J.* **2001**, *20*, 5919-5928.

9. Koblizek, T.I.; Weiss, C.; Yancopoulos, G.D.; Deutsch, U.; Risau, W. Angiopoietin-1 Induces Sprouting Angiogenesis *in Vitro*. *Curr. Biol.* **1998**, *8*, 529-532.

10. Davis, S.; Aldrich, T.H.; Jones, P.F.; Acheson, A.; Compton, D.L.; Jain, V.; Ryan, T.E.; Bruno, J; Radziejewski, C.; Maisonpierre, P.C.; Yancopoulos, G.D. Isolation of Angiopoietin-1, a Ligand for the TIE2 Receptor, by Secretion-Trap Expression Cloning. *Cell* **1996**, *87*, 1161-1169.

11. Suri, C.; Jones, P.F.; Patan, S.; Bartunkova, S.; Maisonpierre, P.C.; Davis, S.; Sato, T.N.; Yancopoulos, G.D. Requisite Role of Angiopoietin-1, a Ligand for the TIE2 Receptor, during Embryonic Angiogenesis. *Cell*, **1996**, *87*, 1171-1180.

12. Maisonpierre, P.C.; Suri, C., Jones, P.F., Bartunkova, S.; Wiegand, S.J., Radziejewski, C.; Compton, D.; McClain, J.; Aldrich, T.H.; Papadopoulos, N.; Daly, T.J.; Davis, S.; Sato, T.N.; Yancopoulos, G.D. Angiopoietin-2, a Natural Antagonist for Tie2 That Disrupts in vivo Angiogenesis. *Science* **1997**, *277*, 55-60.

13. Kim, I.; Kim, J.-H.; Moon, S.-O.; Kwak, H.J.; Kim, N.-G.; Koh, G.Y. Angiopoietin-2 at High Concentration Can Enhance Endothelial Cell Survival Through the Phosphatidylinositol 3'-kinase/Akt Signal Transduction Pathway. *Oncogene* **2000**, *19*, 4549-4552.

14. Kim, I.; Kim, H.G.; Moon, S.-O.; Chae, S.W.; So, J.-N.; Koh, K.N.; Ahn, B.C.; Koh, G.Y. Angiopoietin-1 Induces Endothelial Cell Sprouting Through the Activation of Focal Adhesion Kinase and Plasmin Secretion. *Circulation. Res.* **2000**, *86*, 952-959.

15. Hu, B.; Guo, P.; Fang, Q.; Tao, H.-Q.; Wang, D.; Nagane, M.; Huang, H.-J.S.; Gunji, Y.; Nishikawa, R.; Alitalo, K.; Cavenee, W.K.; Cheng, S.-Y. Angiopoietin-2 induces human glioma invasion through the activation of matrix metalloprotease-2. *Proc. Natl. Acad. Sci. U.S.A.* **2003**, *100*, 8904-8909.

16. Giuliani, N.; Colla, S.; Morandi, F.; Rizzoli, V. Angiopoietin-1 and Meloma-induced Agiogenesis. *Leukemia and Lymphoma*, **2005**, *46*, 29-33.

17. Holash, J.; Maisonpierre, P.C.; Compton, D.; Boland, P.; Alexander, C.R.; Zagzag, D.; Yancopoulos, G.D.; Wiegand, S.J. Vessel Cooption, Regression, and Growth in Tumors Mediated by Angiopoietins and VEGF. *Science*, **1999**, *284*, 1994-1998.

18. Cheng, S.-Y.; Huang, H.-J.S.; Nagane, M.; Ji, X.-D.; Wang, D; Shih, C.C.-Y.; Arap, W.; Huang, C.-M.; Cavenee, W.K. Suppression of Glioblastoma Angiogenicity and Tumorigenicity by Inhibition of Endogenous Expression of Vascular Endothelial Growth Factor. *Proc. Natl. Acad. Sci. U.S.A.* **1996**, *93*, 8502-8507.

19. Kieser A.; Weich, H.A.; Brandner, G.; Marme, D.; Kolch, W. Mutant p53 Potentiates Protein Kinase C Induction of Vascular Endothelial Growth Factor Expression. *Oncogene* **1994**, *9*, 963-969.

20. Hennequin, L.F.; Stokes, E.S.E.; Thomas, A.P.; Johnstone, C.; Ple, P.A.; Ogilvie, D.J.; Dukes, M.; Wedge, S.R.; Kendrew, J.; Curwen, J.O. Novel 4-Anilinoquinazolines with C-7 Basic Side Chains: Design and Structure Activity Relationship of a Series of Potent, Orally Active, VEGF Receptor Tyrosine Kinase Inhibitors. *J. Med. Chem.* **2002**, *45*, 1300-1312.

21. Lin, P.; Polverini, P.; Dewhirst, M.; Shan, S.; Rao, P.S.; Peters, K. Inhibition of Tumor Angiogenesis Using a Soluble Receptor Establishes a Role for Tie2 in Pathologic Vascular Growth. *J. Clin. Invest.* **1997**, *100*, 2072-2078.

22. Miyazaki, Y.; Matsunaga, S.; Tang, J.; Yutaka, M.; Nakano, M.; Philippe, R.J.; Shibahara, M.; Liu, W.; Sato, H.; Wang, L.; Nolte, R.T. Novel 4-amino-furo[2,3-*d*]pyrimidines as Tie-2 and VEGFR2 dual inhibitors. *Bioorg. Med. Chem. Lett.* **2005**, *15*, 2203-2207.

23. Staehle, W.; Buchstaller, H.-P.; Jonczyk, A.; Rautenberg, W. Preparation of Benzimidazolyls as TIE-2 Tyrosine Kinase Inhibitors for the Treatment of Tumors. German Patent DE 10349587, May 12, 2005.

24. Zhou, B.-N.; Johnson, R.K.; Mattern, M.R.; Fisher, P.W.; Kingston, D.G.I. The First Naturally Occurring Tie2 Kinase Inhibitor *Org. Lett.* **2001**, *3*, 4047-4049.

25. Kissau, L.; Stahl, P.; Mazitschek, R.; Giannis, A.; Waldmann, H. Development of Natural Product-Derived Receptor Tyrosine Kinase Inhibitors Based on Conservation of Protein Domain Fold. *J. Med. Chem.* **2003**, *46*, 2917-2931.

26. Thomas, J.P.; Arzoomanian, R.Z.; Alberti, D.; Marnocha, R.; Lee, F.; Friedl, A.; Tutsch, K.; Dresen, A.; Geiger, P.; Pluda, J.; Fogler, W.; Schiller, J.H.; Wilding, G. Phase I Pharmacokinetic and Pharmacodynamic Study of Recombinant Human Endostatin in Patients with Advanced Solid Tumors. *J. Clin. Oncol.* **2003,** *21*, 223-231.

27. Kimball, J. Fighting Cancer with Angiogenesis Inhibitors. http://users.rcn.com/jkimball.ma.ultranet/BiologyPages/A/Angiogenesis.html (accessed August 19, 2005).

28. Ferrara, N.; Hillan, K. J.; Novotny, W. Bevacizumab (Avastin), a Humanized Anti-VEGF Monoclonal Antibody for Cancer Therapy. *Biochem. Biophys. Res. Comm.* **2005**, *333*, 328-335.

29. Mazitschek, R.; Giannis, A. Inhibitors of Angiogenesis and Cancer-related Receptor Tyrosine Kinases. *Curr. Opin. Chem. Biol.* **2004**, *8*, 432-441.

30. Govindan M.; Abbas, S.A.; Schmitz, F.J.; Lee, R.H.; Papkoff, J.S.; Slate, D.L. New Cycloartanol Sulfates from the Alga *Tydemania expeditionis*: Inhibitors of the Protein Tyrosine Kinase $pp60^{v\text{-}src}$. *J. Nat. Prod.* **1994**, *57*, 74-78.

31. Clement, J.A.; Zhou, B.-N.; Johnson, R.K.; Kingston, D.G.I. Isolation and Characterization of a Tie-2 Inhibitory Sulfated Triterpenoid from a Green Alga of the *Tuemoya* Genus: Complete Assignment of the ^{1}H and ^{13}C Spectra of a Sulfated Triterpenoid Tie-2 Inhibitor. *Mag. Reson. Chem.* **2003**, *41*, 644-646.

32. Kimball, J. The Rous Sarcoma Virus (RSV) http://users.rcn.com/jkimball.ma.ultranet/BiologyPages/R/RSV.html (accessed August 19, 2005).

33. Puglisi, M.P.; Tan, L.T.; Jensen, P.R.; Fenical, W. Capisterones A and B from the Tropical Green Alga *Penicillus capitatus*: Unexpected Anti-fungal Defenses Targeting the Marine Pathogen *Lindra thallasiae*. *Tetrahedron* **2004**, *60*, 7035-7039.

34. Horgen, F.D.; Sakamoto, B.; and Scheuer, P.J. New Triterpenoid Sulfates from the Red Alga *Tricleocarpa fragilis*. *J. Nat. Prod.* **2000**, *63*, 210-216.

35. Singh, S.B.; Ondeyka, J.G.; Schleif, W.A.; Felock, P.; Hazuda, D.J. Chemistry and Structure-Activity Relationship of HIV-1 Integrase Inhibitor Integracide B and Related Natural Products. *J. Nat. Prod.* **2003**, *66*, 1338-1344.

36. Brill, G..; Kati, W.M.; Montgomery, D.; Karwowski, J.P.; Humphrey, P.E.; Jackson, M.; Clement, J.J.; Kadam, S.; Chen, R.H.; McAlpine, J.B. Novel Triterpene Sulfates from *Fusarium compactum* Using a Rhinovirus 3C Protease Inhibitor Screen. *J. Antibiot.* **1996**, *49*, 541-546.

37. Zhou, B.-N. Personal communication.

38. Slate, D.L.; Lee, R.H.; Rodriguez, J.; Crews, P.. The Marine Natural Product, Halistanol Trisulfate, Inhibits pp60v-src Protein Tyrosine Kinase Activity. *Biochem. Biophys. Res. Comm.* **1994**, *203*, 260-264.

39. Shewchuk, L.M.; Hassell, A.M.; Ellis, B.; Holmes, W.D.; Davis, R.; Horne, E.L.; Kadwell, S.H.; McKee, D.D.; Moore, J.T. Structure of the Tie2 RTK Domain: Self-Inhibition by the Nucleotide Binding Loop, Activation Loop, and C-Terminal Tail. *Structure* **2000**, *8*, 1105-1113.

40. Wenqing Xu, Amish Doshi, Ming Lei, Michael J. Eck, and Stephen C. Harrison. Crystal Structures of c-Src Reveal Features of Its Autoinhibitory Mechanism. *Molec. Cell*, **1999**, *3*, 629-638.

V. Isolation and Characterization of Triterpenoids from *Petalonyx parryi* that Inhibit the Lyase Domain of DNA Polymerase β

5.1 Introduction

The enzyme DNA polymerase β has been shown to play an important role in mediating DNA repair. It has also been shown that in combination treatments, known inhibitors of polymerase β can potentiate the action of DNA damaging agents such as bleomycins *in vitro*. We present the isolation and characterization of three oleanane triterpenoids from *Petalonyx parryi*. This is the first reported study of the chemical components of *Petalonyx parryi*.

5.1.1 Previous Study of the *Petalonyx* Genus

Petalonyx parryi is a flowering shrub of the family Loasaceae that grows in arid regions of Arizona, Utah, and New Mexico.[1] There have been no published chemical studies of compounds from the species *P. parryi*. There is only one published report of chemical study of the genus *Petalonyx*. In that paper, it is reported that two members of the genus *Petalonyx* contain iridoid glycosides similar to loganin (**5.1**).[2] Iridoid

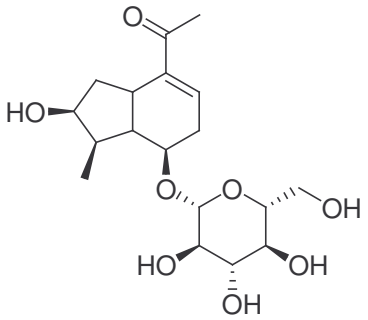

5.1

glycosides are a common plant metabolite with several reported bioactivities. Compound **5.1**, for example, has been reported as having contraceptive,[3] hepatoprotective (liver-protective) and immunostimulating[4] activities. The family Loasaceae is a little-studied family of plants that occurs throughout North and South America, and there have been several chemical studies of Loasaceae genera. Again, these papers report the presence of iridoid glycosides in members of the Loasaceae family.[5-7] Overall, the family Loasaceae and the genus *Petalonyx* have received little attention. Hence, *P. parryi* represents a possible source of bioactive compounds, since no studies of its possible medicinal value have been reported up to this point.

5.1.2 Background of the DNA Polymerase β Lyase Assay

The role of DNA polymerase β (pol β) in DNA repair and its potential as an antitumor drug target was reviewed in Chapter 2. As previously discussed, pol β possesses two distinct catalytic domains: an 8 kDa lyase domain that catalyzes the removal of a damaged deoxyribosyl unit from DNA, and a 31 kDa domain which catalyzes the insertion of a nucleotide into damaged double-stranded DNA using the complementary strand as a template. Pol β is part of the cellular response to DNA damage caused by UV light, ionizing radiation, or chemicals like bleomycins. It has been shown that inhibitors of pol β can potentiate the activity of bleomycins *in vitro*. Because DNA damaging agents are toxic, improving their potency towards tumors is desirable so that smaller dosages could be used while maintaining the efficacy of the treatment. Pol β inhibitors might one day serve to improve the efficacy of currently used anticancer drugs.

5.2 Results and Discussion

5.2.1 Isolation of Oleanane Triterpenoids from *Petalonyx parryi*

The crude extract of *Petalonyx parryi* showed moderate pol β lyase inhibitory activity, with about 50% inhibition at 16.2 μg/mL. The isolation of **5.2**, **5.3**, and **5.4** is depicted in the fractionation scheme in Schemes 5.1 and 5.2. In an initial separation, the crude extract was fractionated by liquid partitioning, which afforded three fractions, all of which retained the activity of the crude extract. Bioassay-guided fractionation by an aminopropyl SPE separation, followed by CHP20P MCI gel fractionation, reverse phase chromatography, and normal phase SiO_2 and reverse phase phenyl HPLC, afforded compounds **5.2**, **5.3**, and **5.4**, which were active in the pol β lyase assay. Because the active compounds originated from 2% HOAc-ether washes from the aminopropyl SPE columns, the active components were likely to contain carboxylic acid functionality.[8] Further fractionation of the 2:1 $CHCl_3$:2-propanol fractions from the aminopropyl separations did not afford fractions with reproducible activity. Fractions A and B from fraction 174-125-11 contained mixtures of several putative triterpenoids that were difficult to separate; thus, isolation of appreciable amounts of active components from these fractions was not successful.

It should be noted that when a particular sample is tested in the Pol β lyase assay, results from week to week for that sample can show significant variability. This was not only the case for *Petalonyx parryi*, but also for an extract of *Planchonella papyracea*. Therefore, the assay results were interpreted in terms of a control sample, which was a sample of the crude extract that was analyzed each time the assay was performed.

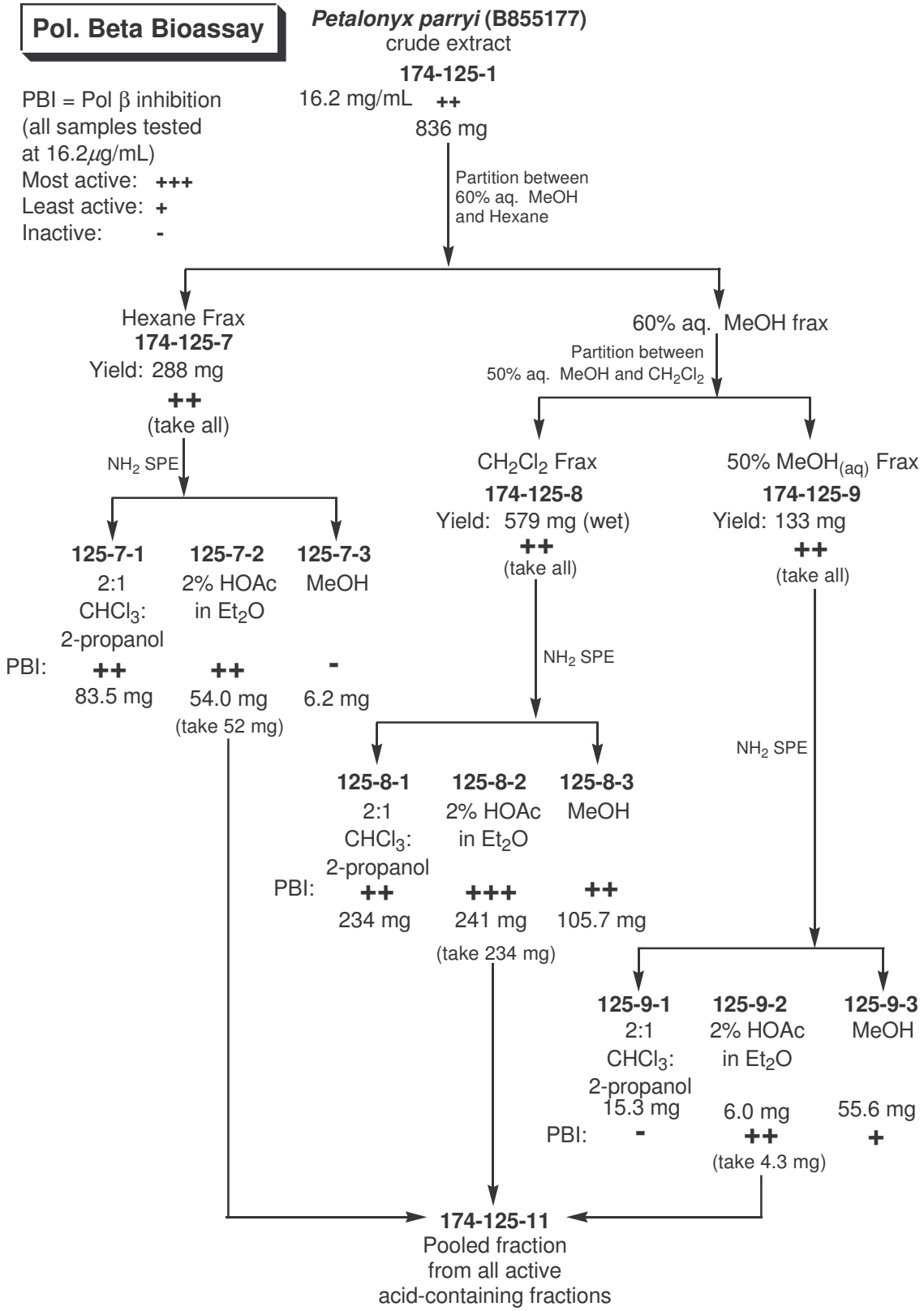

Scheme 5.1: Initial fractionation of the extract of *Petalonyx parryi*

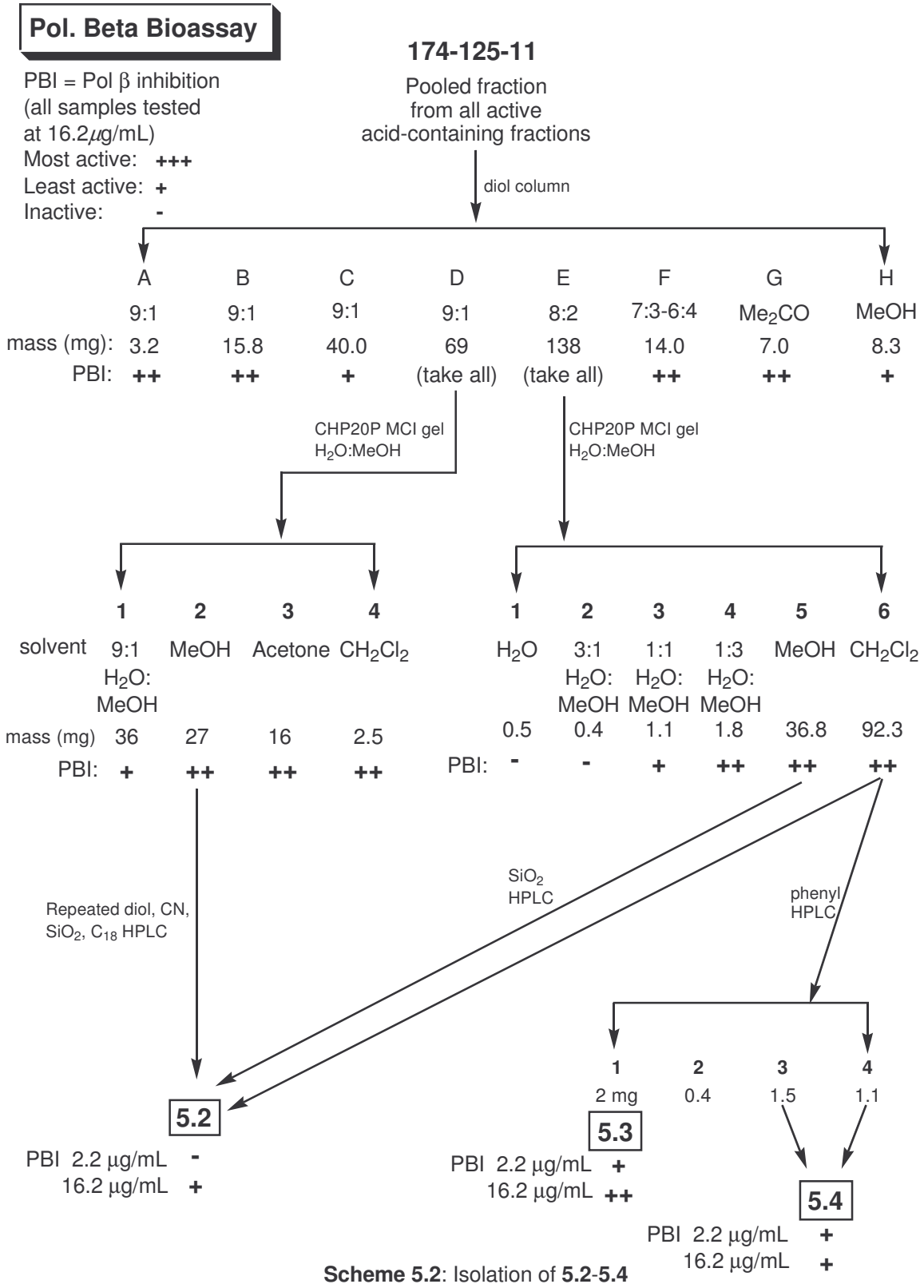

Scheme 5.2: Isolation of **5.2**-**5.4**

Because of this approach, we are convinced that we have isolated the most active components from the extract, even though the assay data appear to fluctuate and decrease over the course of the isolation.

Compound **5.2** was isolated as an amorphous white solid, and was the major component of fractions C-H from 174-125-11. Positive ion FABMS analysis showed that **5.2** possessed a formula of $C_{30}H_{48}O_3$. The ^{1}H NMR spectrum (CD_3OD) revealed several distinctive signals. Six signals corresponding to seven methyl groups were observed at δ_H 0.73, 0.77, 0.855, 0.861, 0.899 (6H), and 1.15. A proton signal corresponding to a hydroxylated methine was found at δ_H 3.14, and a triplet ascribed to a vinylic proton neighboring a methylene group was detected at δ_H 5.24.

The ^{13}C NMR spectrum ($CDCl_3$) for **5.2** consisted of thirty signals, which was consistent with the FABMS data. These data are presented in Table 5.1. A carbonyl signal was detected at δ_C 182.8, suggesting the presence of an ester or carboxylic acid in **5.2**. Two sp^2 carbon signals were observed at δ_C 143.7 and 122.7, and an oxygenated carbon signal was found at δ_C 79.1. All of this preliminary data, including the presence of seven methyls and the molecular formula determined by FABMS, suggested that **5.2** was a triterpenoid. Triterpenoids are natural products which typically possess multiple rings and multiple methyl groups, examples of which were discussed in Chapters 2 and 4.

In order to check to see if **5.2** was a known compound, a search of the literature using SciFinder was performed for compounds with formula $C_{30}H_{48}O_3$ with the following constraints, based on the preliminary data: compounds containing an oxygenated methine adjacent to a methylene, a carboxylic acid moiety, a double bond with a single proton

attached, and seven methyl groups. This search yielded 49 hits, all of which were triterpenoid acids. To account for the fact that all of the methyl signals from the ^{1}H NMR

Table 5.1: ^{13}C NMR data for **5.2** and **5.3** (in $CDCl_3$ and C_5D_5N, respectively)

Position	**5.2**	**5.3**
1	38.5	38.1
2	27.3	23.8
3	79.1	80.5
4	38.8	37.2
5	55.3	55.6
6	18.4	18.5
7	32.7	33.2
8	39.4	39.7
9	47.7	47.9
10	37.2	38.2
11	23.0	24.1
12	122.7	122.4
13	143.7	145.0
14	41.7	42.0
15	27.8	28.3
16	23.5	23.7
17	46.6	46.7
18	41.1	42.2
19	45.9	46.4
20	30.8	31.0
21	33.9	34.2
22	32.5	33.0
23	28.2	28.3
24	15.6	15.4
25	15.4	17.1
26	17.2	17.4
27	26.0	26.2
28	182.8	180.2
29	33.1	33.3
30	23.7	23.8
1’		167.3
2’		115.8
3’		144.9
4’		126.2
5’		130.7
6’		116.9
7’		161.5
8’		116.9
9’		130.7

spectrum of **5.2** were singlets, this set of 49 hits was refined by selecting compounds where all seven methyl groups were attached to quaternary carbons. This gave a set of 25 compounds, all of which were pentacyclic triterpenoids. A compilation of the ^{13}C NMR data of several pentacyclic triterpenoids was published by Mahato and Kundu,[9] and the ^{13}C NMR data for **5.2** was compared with values within the compilation. The ^{13}C NMR

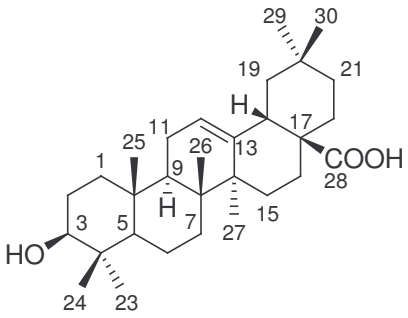

5.2: Oleanolic acid

data for **5.2** matched very well with the data published for oleanolic acid. The optical rotation measured for **5.2** did not agree well with the value reported in the literature (experimental: +37.9° (*c* 0.1, $CHCl_3$); literature: +79.5° (*c* 0.6, $CHCl_3$), reported values range from +60 ° to +80 °),[10] suggesting an experimental error in sample preparation. However, since the signs of these rotations were the same, and all the other available data was self-consistent, **5.2** was identified as oleanolic acid as shown above. As mentioned, **5.2** was the major component of fractions C-H from fraction 174-125-11. Thus, the bioactivity of fractions C, F, G, and H, as well as fractions 1, 3, and 4 from fraction 174-125-11-D was ascribed to **5.2**, the major component of all these fractions.

Compound **5.3** was also isolated as an amorphous white solid, and was the second-most abundant component of 174-125-11 after **5.2**. Negative ion FABMS analysis indicated that **5.3** had a formula of $C_{39}H_{54}O_5$, which indicated that **5.3** had an

unsaturation index of 13. The ^{1}H NMR spectrum (C_5D_5N) of **5.3** revealed several key signals. Six methyl singlets were observed representing seven methyl groups at δ_H 0.89, 0.99, 1.00 (6H), 1.03, 1.04, and 1.32. A signal arising from an oxygenated methine proton was observed at δ_H 4.90, with the chemical shift suggesting the presence of an ester. Five proton signals arising from seven olefinic protons were found at δ_H 5.51, 6.74, 7.21 (2H, partially obscured by solvent signal), 7.69 (2H), and 8.06. The splitting pattern and integration of the lower field signals suggested that **5.3** possessed a 1,4-disubstituted phenyl ring. The appearance of the higher field region of the ^{1}H NMR spectrum of **5.3** was very similar to that of **5.2**, which suggested that **5.3** was a derivative of **5.2**.

The ^{13}C NMR spectrum (C_5D_5N) also revealed several features of **5.3**. These data are tabulated in Table 5.1. Eight signals corresponding to 10 sp^2 carbons were observed at δ_C 115.8, 116.9 (2C), 122.4, 126.2, 130.7 (2C), 144.9, 145.0, 161.5, and 167.3. Two carbon signals characteristic of either ester or carboxylic acid carbonyls were detected at δ_C 180.2 and 167.3. Again, the overall appearance of the higher-field region of the ^{13}C NMR spectrum of **5.3** was very similar to that of **5.2**, which also hinted that **5.3** was an analogue of **5.2**.

As mentioned, the unsaturation index for **5.3** (rings + double bonds) was 13. If **5.3** was an analogue of **5.2**, then the oleanane skeleton would contribute a value of 7 to the total of 13. If **5.3** also possessed a disubstituted phenyl ring, the phenyl ring would contribute a value of 4 to the total of 13, which leaves a remainder of 2 for which to account. From the ^{13}C NMR spectrum, two carboxyl carbonyl signals were observed; one was ascribed to the acid carbon from the presumed oleanane skeleton, while the other

evidently arose from another carboxyl carbon. This second carbonyl contributed a value of 1 to the total of 13 for the unsaturation index, leaving a remainder of 1 for which to account. From the ^{13}C NMR spectrum, 10 sp^2 carbons were detected. If two of these carbons were part of the oleanane skeleton and six other sp^2 carbons were part of the phenyl ring, then another double bond had to be present. Thus, **5.3** appeared to be composed of the following fragments, as shown in Figure 5.1: an oleanane skeleton with undetermined attachments (Fragment A); a carboxylic acid group (Fragment B); an ester group (Fragment C); a disubstituted phenyl ring (Fragment D) and another double bond

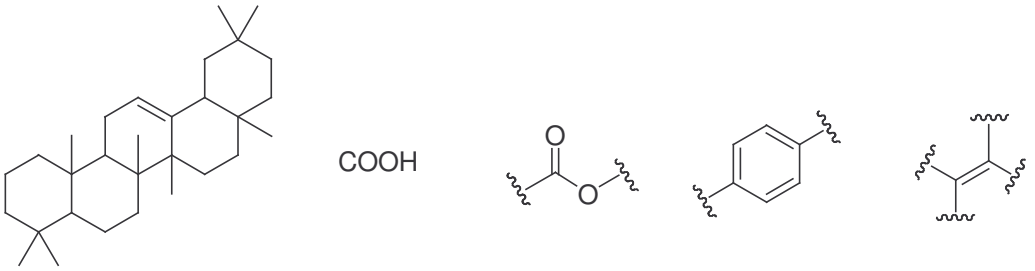

Figure 5.1: Proposed fragments of **5.3**

(Fragment E). Assuming that the carboxylic acid group was actually part of the oleanane skeleton as in **5.2**, these fragments accounted for all 39 carbons in the molecular formula. Therefore, 2D NMR techniques were needed to conclusively piece together the structure of **5.3** to prove whether it was an oleanane derivative or not.

HSQC analysis was used to fully assign the proton and carbon one-bond connectivity for **5.3**. The assignments presented in Table 5.1 are based on data from the HSQC spectrum of **5.3**. These assignments were used to interpret the HMBC and COSY spectra of **5.3**. From the COSY spectrum for **5.3**, correlations were observed between the proton signals at δ_H 6.70 and 8.04, and between the two-proton signals at δ_H 7.18 and

7.66. These correlations were consistent with the presence of a disubstitued double bond and a disubstituted phenyl ring, respectively. COSY correlations are depicted in Figure 5.2.

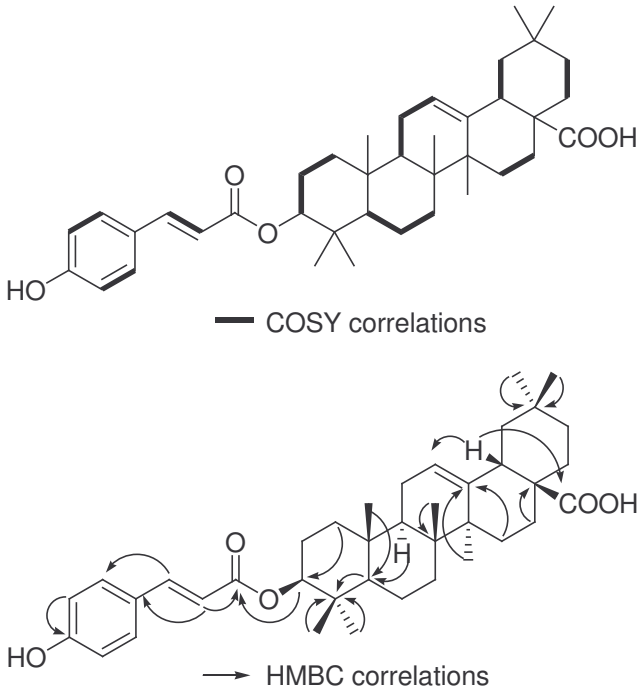

Figure 5.2: 2D correlations for **5.3**

HMBC correlations were observed between the proton signal at δ_H 6.74 and the carbon signals at δ_C 167.3 and 126.2. An additional correlation was observed between the proton signal at δ_H 8.06 and the carbon signal at δ_C 130.7. A correlation between the two-proton signal at δ_H 7.18 and the carbon signal at δ_C 161.5 was also observed; these together data suggested the presence of a phenyl ring attached to an α,β-unsaturated ketone. Thus, fragments C, D, and E from Figure 5.1 could be connected. Finally, a correlation from the proton signal at δ_H 4.90 to both the carbonyl signal at δ_C 167.3, as well as to the quaternary carbon signal at δ_C 38.1, showed how the esterified carbon was in close proximity to a dimethylated carbon. This was consistent with the ester being

connected to the C-3 position of an oleanane skeleton. When the remaining HMBC correlations are superimposed onto an oleanane skeleton, the data match completely with

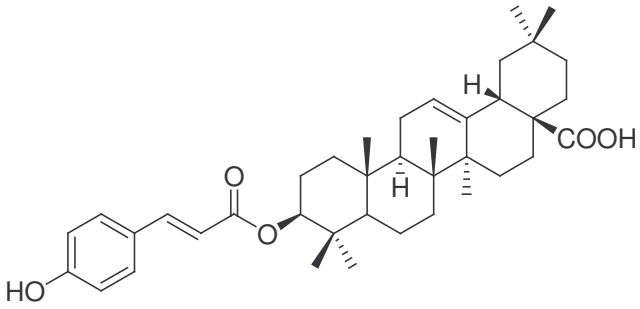

5.3

the proposed structure with an ester attachment at C-3, as shown in Figure 5.2. Since the esterified oleanane skeleton accounted for all carbons detected by FABMS analysis, it was left to determine where the remaining oxygen was attached. Because the data for **5.3** matched so well with that of **5.2**, it appeared that the final oxygenated carbon would be attached to the phenyl ring sidechain. Closer examination of the quaternary carbon signals from the phenyl ring showed that the quaternary carbon signal at δ_C 161.5 possessed a higher chemical shift than any of the other phenyl ring carbons. Thus, it was logical to assign an oxygen attachment to the 4-position of the phenyl ring. Having accounted for 47 hydrogens in the oleanane skeleton, 4 hydrogens on the phenyl ring, and 2 hydrogens on the sidechain double bond, and since no additional oxygenated functionality like a methoxy group was observed, the oxygenation was determined to be a hydroxyl group. This accounted for all 54 hydrogens found by FABMS analysis. The assigned 1,4-disubstitution pattern was consistent with ^{1}H NMR and HMBC data. The deduced sidechain is trivially referred to as a *p*-coumaroyl group, or a *p*-hydroxycinnamoyl group. Thus, the structure of **5.3** was determined to be

3-*O*-*p*-(*E*)-coumaroyloleanolic acid, as shown above. Compound **5.3** was first reported by Takahashi *et al*., and our data agree very well with that previously published.[11]

Compound **5.4** was isolated in low yield as a white amorphous solid. From the same phenyl HPLC separation that afforded **5.3**, compound **5.4** was isolated as a major component of two fractions (shown in Scheme 5.2), one of which was active in the pol β assay (≈25% pol β lyase inhibition at 2.2 and 16.2 μg/mL). Because of this activity, **5.4** was chosen for characterization. Negative ion FABMS analysis showed that **5.4** possessed a molecular formula of $C_{40}H_{56}O_6$. The ^{1}H NMR spectrum of **5.4** was very similar to that of **5.3**, except for two important differences. In the olefinic and aromatic region of the ^{1}H NMR spectrum for **5.3**, four signals in a 1:2:2:1 ratio were observed corresponding to two vinylic protons and two sets of two protons attached to an aromatic ring. For **5.4**, five signals in a 1:1:1:1:1 ratio were observed in the olefinic-aromatic region of the ^{1}H NMR spectrum (CD_3OD): δ_H 7.59 (d, J = 16 Hz), 7.20 (d, J = 1.8), 7.07 (dd, J_1 = 1.8, J_2 = 8.2), 6.81 (d, J = 8.3), and 6.35 (d, J = 15.9). The vinylic proton signals (δ_H 7.59 and 6.35) were nearly identical to those of **5.3**, while the splitting pattern for the other three aromatic signals of **5.4** was typical of an ABX-type spin system. This splitting pattern for an aromatic ring suggested the presence of a trisubstituted aromatic

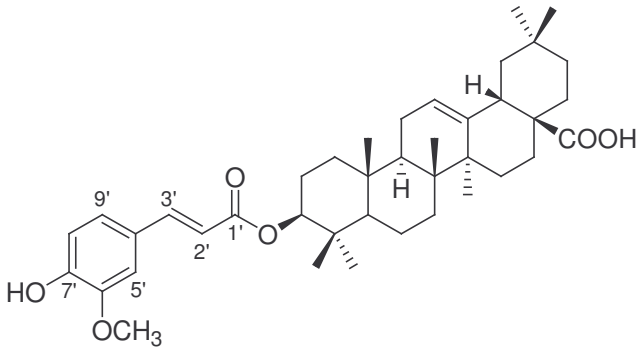

5.4

ring in **5.4**, specifically a 1,2,4-trisubstituted aromatic derivative. A second key difference in the ^{1}H NMR spectrum of **5.4** was a sharp methyl singlet at δ_H 3.90, which was indicative of the presence of a methoxy group in **5.4**. Thus, it initially appeared that **5.4** was an analog of **5.3** with a methoxy group and a different substitution pattern on the aromatic ring.

Thus, based on the preliminary analysis, the structure shown below for **5.4** was proposed. This structure possessed the same oleanane skeleton as **5.3**, but it was proposed that **5.4** also possessed a *m*-methoxy-*p*-coumaroyl sidechain (also trivially known as a feruloyl sidechain), rather than a *p*-coumaroyl sidechain. This proposed structure was previously published, so the experimental data for **5.4** was compared with literature data[12] to determine if the proposed structure was correct. The initial ^{1}H NMR analysis of **5.4** was performed using CD_3OD as an NMR solvent, so a second analysis was performed using $CDCl_3$ as an NMR solvent. The experimental data matched well with that reported for 3-*O*-feruloyloleanolic acid. Because of the small amount of material isolated for **5.4**, and due to some sample decomposition, a ^{13}C NMR spectrum was not obtained for **5.4**. So, based on the available data, the structure of **5.4** was assigned as 3-*O*-(*E*)-feruloyloleanolic acid. Because of the limited amount of **5.4** that could be isolated, a full spectroscopic determination was not feasible. Thus, the stereochemistry of **5.4** is assigned by analogy to that of **5.2** and **5.3**.

5.2.2 Biological Evaluation of Oleanane Triterpenoids from *Petalonyx parryi*

After the bioassay guided isolation of **5.2**, **5.3**, these compounds were submitted for testing in the pol β lyase inhibition assay. Compound **5.2** was found to have low inhibitory activity at 2.2 μg/mL and moderate inhibitory activity at 16.2 μg/mL. Compound **5.2** was also isolated at around the same time by our group from another extract, and its IC_{50} was reported as 8.8 μg/mL (19 μM). The lyase inhibition assay was performed at multiple concentrations of **5.3**, and its IC_{50} was determined to be 1.3 μg/mL (2.2 μM). Although the activity of **5.4** was demonstrated in a two-dose assay, its IC_{50} was not determined due to apparent decomposition of the originally isolated sample.

This is the first report of the isolation of secondary metabolites with interesting biological activity from *Petalonyx parryi*. This is also the first report of the pol β lyase inhibitory activity of **5.3** and **5.4**. As discussed in Chapter 4 and in Chapter 6, it is possible for compounds with surfactant-like properties to show activity in enzyme-based assays, where the inhibition is not based on useful ligand-enzyme interactions but on surfactant-type disruption of an enzyme's tertiary structure. The structures of **5.2**-**5.4** all contain polar carboxylate headgroups and nonpolar oleanane backbones. Fatty acids are also known to be active in the pol β assay, as will be discussed in Chapter 6. Therefore, we believe that both the oleanane triterpenoid-type molecules and fatty acids might act to disrupt the secondary structure of pol β, resulting in apparent inhibition. Hence, we do not consider these compounds as potential drug candidates.

5.3 Experimental Section

General Experimental Procedures. IR spectra were recorded for neat samples with a MIDAC M-series FTIR spectrophotometer. HRFAB mass spectra were collected with a JEOL HX-110 spectrometer. NMR spectra were collected on either a Varian Inova 400 spectrometer operating at 399.9 MHz for ^{1}H and 100.6 MHz for ^{13}C, or a JEOL Eclipse+ 500 spectrometer operating at 500.2 MHz for ^{1}H and 125.8 MHz for ^{13}C.

DNA Polymerase β Inhibition Bioassay. The pol β lyase inhibition assay was performed by Dr. Mei Li in the laboratory of Dr. Sidney Hecht at the University of Virginia, as described below. The pol β substrate used for the inhibition assay was prepared in a manner identical to that used for the binding assay described in Chapter 2. The deoxyribose (dRP) excision activity of pol β was determined using a reaction mixture (5 μL) containing 354 nM [α-^{32}P]-labeled DNA substrate containing an apurinic site at position 21, 0.172 units pol β , and various concentrations of test samples (typically 2.2 or 16.2 μg/mL for single-dose measurements). After incubating the sample mixtures at room temperature for 30 min, the reactions were terminated, and the products was stabilized by the addition of 0.5 M $NaBH_4$ to a final concentration of 50 mM. The reaction mixtures were then incubated at room temperature for 10 min, followed by an additional incubation at 75 °C for 20 min. The reaction products were finally separated on a 20% denaturing polyacrylamide gel and visualized by autoradiography.[13] A typical gel plate is shown in Figure 5.3.

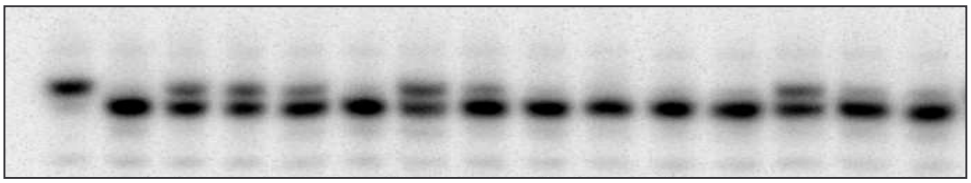

Figure 5.3: Typical gel plate for pol β assay

Inhibitory activities are reported semiquantitatively on a scale of 0 to 3, examples of which are shown in Figure 5.3: a value of 0 is assigned to samples yielding no measurable pol β inhibition (column B); 1 indicates a low level of inhibition (column C); 2 indicates about 50% inhibition (column D); 3 is assigned to samples with significant pol β inhibition, about 50-100% (column A). Once an active compound is isolated and identified, the compound is tested at multiple concentrations and an IC_{50} value is determined for the active compound towards pol β.

Isolation of Oleanolic Acid (5.2), 3-*O*-*p*-(*E*)-Coumaroyloleanolic Acid (5.3), and 3-*O*-(*E*)-Feruloyloleanolic Acid (5.4). The crude extract (836 mg) was subjected to an initial liquid partition, affording three fractions: a hexane fraction (288 mg), a CH_2Cl_2 fraction (579 mg), and a MeOH fraction (133 mg). Each of these fractions was further separated by aminopropyl (NH_2) SPE columns (5g bonded phase) with three 50 mL washes for each column: 2:1 $CHCl_3$:2-propanol, 2% HOAc/Ether, and MeOH washes. These separations yielded nine fractions, six of which retained good activity. Based on comparison of TLC and NMR analyses, active fractions containing similar compounds were recombined. The 2% HOAc/Ether washes from each amino column separation were combined. Hence, fraction 174-125-11 (290 mg) was the combination of fractions 174-125-7-2, 174-125-8-2, and 174-125-9-2. ^{1}H NMR data suggested that the major

components of all active fractions were triterpenoids. From the 2:1 $CHCl_3$:2-propanol washes of each amino column, no reproducibly active components could be isolated. Thus, fraction efforts focused on 174-125-11.

Fraction 174-125-11 was further chromatographed by use of a diol open column (21 cm × 1.8 cm column, 28 g bonded phase; step gradient, 9:1-6:4 hexane:acetone, followed by acetone and MeOH flushes) which afforded several active fractions. About 72% of the mass of 174-125-11 eluted in two of the eight fractions, fractions 174-125-11-D (final 9:1 hexane:acetone flush, 69 mg) and 174-125-11-E (8:2 hexane:acetone flush, 138 mg). TLC analysis revealed that fractions C through E contained mixtures of the similar components in varying concentrations. Fractions A and B (3 and 16 mg, respectively), though active, contained mixtures of compounds which were not readily separated by efforts using HPLC. Fractions F-H contained mixtures of triterpenoids and compounds strongly retained on SiO_2 and diol TLC plates. Because the majority of the activity was concentrated in fractions D and E, efforts were focused on these fractions.

Fraction D was subjected to CHP20P MCI gel separation (7 g stationary phase, 5 cm × 1.8 cm column; four washes, 50 mL each: 9:1 MeOH:H_2O, MeOH, acetone, and CH_2Cl_2), which afforded three active fractions. By TLC analysis, the three active fractions all appeared to contain identical components: a major spot, and very faint spots. The largest fraction, 174-125-11-D-2 (20 mg), was further fractionated by medium pressure reverse phase chromatography (10 cm × 1 cm prepacked column, Biotage). This separation accomplished little, with only 9 of 48 fractions containing a measurable amount of material. Finally, fractions 40-48 were combined and various methods were applied to analyze the sample. Based on HPLC analysis by cyano (CN), diol, and silica

(SiO_2) stationary phases (all columns: 25 cm × 1 cm, 1-2% hexane-2-propanol, 2 mL/min) fractions 40-48 were shown to contain one major compound and a very minor impurity which could not be submitted for assay due to lack of material. The major compound, **5.2** (2 mg), was isolated by SiO_2 HPLC (as described above), characterized, and tested. Compound **5.2** was estimated to compose 90% of 174-125-11-D, and most of 174-125-11.

Fraction 174-125-11-E was shown to contain several compounds by SiO_2 TLC analysis, and this fraction was fractionated by use of CHP20P MCI gel (7 g stationary phase, 5 cm × 1.8 cm column; four washes, 50 mL each: H_2O, 1:3, 1:1, 3:1 MeOH:H_2O, MeOH, and CH_2Cl_2). This yielded three active fractions. Two of these fractions, 174-125-11-E-4 (2 mg) and 174-125-11-E-5 (37 mg), were analyzed by HPLC using methods mentioned above and were shown to contain mixtures of two compounds, **5.2** and a component which was inactive and thus not characterized.

Fraction 174-125-11-E-6 (92 mg) was fractionated by use of HPLC using a phenyl stationary phase (25 cm × 1 cm, 87:11:2 MeOH:H_2O:HOAc) to afford four fractions containing strongly UV-absorbing compounds. Compound **5.2** was also the major component of 174-125-11-E-6, but was not re-isolated. One of these fractions was a pure compound, **5.3** (2 mg), while fractions 174-125-195-2 (0.4 mg), 174-125-195-3 1.5 mg), and 174-125-195-4 (1.1 mg) were mixtures of similar compounds. While **5.2** and **5.3** were the most abundant compounds from 174-125-11-E-6, fractions 174-125-195-3 and 174-125-195-4 contained the third most abundant compound, **5.4**. Fractions 174-125-195-1 and 174-125-195-4 were tested and were active. However, a lack of material for the four fractions necessitated a scaled-up separation in order to purify and

fully characterize the active components. The separation was simplified and scaled-up, and the major component of 174-125-195-3 and 174-125-195-4, **5.4**, was isolated and found to be active.

Oleanolic acid (5.2): colorless amorphous solid; UV (MeOH) λ_{max} 204 (log ε 4.14); $[\alpha]_D^{22}$ = +37.9° (*c* 0.1, $CHCl_3$); IR (neat film) 3416, 2926, 2864, 1686, 1457,1270, 1027, 996, 750 cm^{-1}; ^1H NMR ($CDCl_3$) δ_H 0.76, 0.77, 0.90, 0.91, 0.93, 0.99, 1.13 (s, 3H each, 7 CH_3), 2.81 (dd, 4.5, 13.9), 3.22 (dd, 4.5, 10.8), 5.29 (t, 3.5); ^{13}C NMR ($CDCl_3$) see Table 5.1; HRFABMS (positive ion) 456.3610 ($[M]^+$, calc. for $C_{30}H_{48}O_3$: 456.3603, Δ = 1.5 ppm).

3-*O*-*p*-(*E*)-Coumaroyloleanolic acid (5.3): colorless amorphous solid; IR (neat film) 3309, 2928, 1686, 1634, 1604, 1515, 1457, 1272, 1202, 1166, 1146, 1010, 965, 822, 751, cm^{-1}; ^1H NMR (C_5D_5N, 500 MHz) δ_H 0.96 (m, H-1a), 1.47 (m, H-1b), 1.69 (m, H-2a), 1.82 (m, H-2b), 4.90 (dd, 4.6, 11.7, H-3), 0.92 (m, H-5), 1.27 (m, H-6a), 1.41 (m, H-6b), 1.83 (m, H-7a), 2.06 (td, 4.2, 13.8, H-7b), 1.68 (t, 8.7, H-9), 1.66 (m, H-11a), 1.81 (m, H-11b), 5.51 (t, 3.3, H-12), 1.20 (m, H-15a), 2.16 (m, H-15b), 1.99 (m, H-16a), 1.93 (m, H-16b), 3.34 (dd, 3.5, 13.5, H-18), 1.31 (m, H-19a), 1.85 (m, H-19b), 1.20 (m, H-21a), 1.43 (m, H-21b), 1.27 (m, H-22a), 1.45 (m, H-22b), 1.00 (s, H-23), 0.89 (s, H-24), 1.00 (s, H-25), 1.03 (s, H-26), 1.32 (s, H-27), 0.99 (s, H-29), 1.04 (s, H-30), 6.74 (d, 16.0, H-2') 8.06 (d, 15.9, H-3'), 7.69 (d, 8.6, H-5' and H-9'), 7.18 (d, overlapped with solvent, H-6' and H-8'); ^{13}C NMR (C_5D_5N) see Table 5.1; HRFABMS (negative ion) 601.3906 ($[M-H]^-$, calc. for $C_{39}H_{53}O_5$: 601.3893, Δ = 2.2 ppm).

3-*O*-(*E*)-Feruloyloleanolic acid (5.3): white amorphous solid; ^{1}H NMR ($CDCl_3$, 500 MHz) 0.88, 0.91, 0.94, 0.96, 0.98, 1.10 (each 3H, 7 CH_3), 3.93 (s, 3H, OMe-6'), 4.63 (t, 7.8, 1H, H-3), 5.27 (bs, H-12), 6.29 (d, 15.8, H2'), 6.91 (d, 8.0, H-8'), 7.04 (bs, H-5'), 7.07 (d, 8.2, H-9'), 7.59 (d, 16.0, H-3'); HRFABMS (positive ion) 632.4085 ($[M]^+$, calc. for $C_{40}H_{56}O_6$: 632.4077, Δ = 1.3 ppm).

References for Chapter 5

1. Weigend, M.; The Loasaceae web page. http://www.nybg.org/bsci/res/loas/webspecies.htm (accessed July 13, 2005).

2. Weigend, M.; Kufer, J.; Muller, A.A. Phytochemistry and the Systematics and Ecology of Loasaceae and Gronoviaceae (Loasales). *Am. J. Bot.* **2000**, *87*, 1202-1210.

3. Misra, A.P.; Mathad, V.T.; Raj, K.; Bhaduri, A.P.; Tiwari, R.; Srivastava, A.; Mehrotra, P.K. Modified Iridoid Glycosides as Anti-implantation Agents: Inhibition of Cell Adhesion as an Approach for Developing Pregnancy Interceptive Agents. *Bioorg. Med. Chem.* **2001**, *9*, 2763-2772.

4. Mathad, V.T.; Raj, K.; Bhaduri, A.P.; Sahai, R.; Puri, A.; Tripathi, L.M.; Srivastava, V.M.L. Studies on the Profile of Immunostimulant Activities of Modified Iridoid Glycosides. *Bioorg. Med. Chem.* **1998**, *6*, 605-611.

5. Zidorn, C.; Ellmerer, E.P.; Ziller, A.; Stuppner, H. Occurrence of (E)-aldosecologanin in *Kissenia capensis* (Loasaceae). *Biochem. Syst. Ecol.* **2004**, *32*, 761-763.

6. Rodriguez, V.; Schripsema, J.; Jensen, R.S. An Iridoid Glucoside from *Gronovia scandens* (Loasaceae). *Biochem. Syst. Ecol.* **2002**, *30*, 243-247.

7. Muller, A.A.; Kufer, J.K.; Dietl, K.G.; Reiter, S.A.; Grau, J.; Weigend, M. Iridoid Glucosides-chemotaxonomic Markers in Loasoideae. *Phytochemistry* **1999**, *52*, 67-78.

8. Blevins, D.D.; Burke, M.F.; Good, T.J.; Harris, P.A.; Van Horne, K.C.; Simpson, N., and Yago, L.S., eds. *Varian Sorbent Extraction Technology Handbook.* Harbor City, CA: Varian Sample Preparation Products, 1993, 82–84.

9. Mahato, S.B.; Kundu, A.P. Review Article Number 98: 13C NMR Spectra of Pentacyclic Triterpenoids - a Compilation and Some Salient Features. *Phytochemistry* **1994**, *37*, 1517-1575.

10. Lee, M.H.; Han, Y.N. A New I*n Vitro* Tissue Factor Inhibitory Triterpene from the Fruits of *Chaenomeles sinensis*. *Planta Med.* **2003**, *69*, 327-331.

11. Takahashi, H; Iuchi, M.; Fujita, Y.; Minami, H.; Fukuyama, Y. Coumaroyl Triterpenes from *Casuarina equisetifolia*. *Phytochemistry* **1999**, *51*, 543-550.

12. Vardamides, J.C.; Azebaze, A.G.B.; Nkengfack, A.E.; Van Heerden, F.R.; Fomum, Z.T.; Ngando, T.M.; Conrad, J.; Vogler, B.; Kraus, W. Scaphopetalone and Scaphopetalumate, a Lignan and a Triterpene Ester from *Scaphopetalum thonneri*. *Phytochemistry* **2003**, *62*, 647-650.

13. Chaturvedula, V.S.P.; Gao, Z.; Hecht, S.M.; Jones, S.H.; Kingston, D.G.I. A New Acylated Oleanane Triterpenoid from *Couepia polyandra* that Inhibits the Lyase Activity of DNA Polymerase β. *J. Nat. Prod.* **2003**, *66,* 1463-1465.

VI. Aminopropyl Bonded Silica for Removal of Long-Chain Fatty Acids in Natural Products Drug Discovery

6.1 Introduction

6.1.1 The Importance of Dereplication in Natural Products Drug Discovery

Many interesting bioactive compounds have been previously isolated from natural sources. At the same time, many known compounds and compound classes have been shown to interfere with *in vitro* assays, sometimes providing "false-positive" results in bioassays. In order to focus research efforts on more interesting samples and avoid known or interfering compounds, various dereplication methods may be applied to identify known compounds within bioactive samples. Dereplication is defined as the rapid identification of known compounds within a sample.

Pharmaceutically interesting natural products must be purified from crude natural extracts in order to fully characterize the compounds chemically and biologically. Though natural products can be randomly isolated and tested, a more productive approach is that of bioassay-guided fractionation. Bioassay-guided fractionation of a natural extract is the process by which a bioactive natural product is purified by iterative separation methods, with each separation step focusing on the most active fractions from the previous fractionation. As the active principle(s) from the extract are further concentrated by fractionation, the bioactivity of fractions containing those principle(s) should increase. Many important anticancer compounds have been discovered through this basic procedure. Overall, the isolation of bioactive natural products from crude extracts is labor-intensive, and streamlining the process is very desirable.

As reported in Chapter 1, natural products chemistry has afforded many interesting compounds already. Many of these compounds have toxicity towards a whole range of tumor cell lines, and therefore some compounds are likely to be encountered frequently during investigations using cytotoxicity-based assays. Camptothecin and deoxypodophyllotoxin are examples of cytotoxic compounds that our group has encountered that have been previously investigated for use as drugs. Also, as mechanism-based assays become more common, there are also compounds that have been discovered that have a wide range of activities towards targeted enzymes. For example, staurosporine is a potent inhibitor of several different cell cycle enzymes. One of the chief applications for dereplication methods is in rapidly identifying known bioactive components from an extract. Though the compound may have good activity and an interesting structure, if the compound has been thoroughly investigated previously, further investigation may not be profitable.

On the other hand, some components that show activity in a particular bioassay may not actually have a desirable pharmacological effect. As an example, tannins, biopolymers that are ubiquitous in the plant kingdom, have high potency in several mechanism-based bioassays. However, it is believed that their inhibitory activity is due to a disruption of the structure of enzymes through non-specific interactions on the enzyme surface. Tannins also have poor cell permeability and have little potential as drugs for specifically targeting enzymes in cells. Long-chain fatty acids (LCFAs), which are also very common in plants, have a similar profile in mechanism-based assays and often appear to be very active. Also, it has been found that polysulfonates found in natural marine extracts are active in anti-HIV assays,[1] but the polysulfonates face the

same problems as tannins as far as usefulness is concerned. In addition to dereplicating known compounds, it is also desirable to dereplicate and remove nuisance compounds like tannins, LCFAs, and polysulfonates, since the isolation of such compounds is not productive.

6.1.2 Established Dereplication Methods

Compared to the number of papers published in the area of natural products drug discovery, the number of papers dealing with dereplication methods is relatively very small. While most dereplication methods use several different techniques concurrently, the methods currently used most by natural products chemists may be grouped into five general categories: mass spectrometry (MS)-based methods, NMR-based methods, chromatographic methods, and activity profiling. These methods will be briefly discussed below.

MS-based methods include liquid chromatography-MS (LC-MS), LC-UV-MS, and LC-MS-NMR methods. The unifying feature of these methods is that MS-based methods allow for the rapid determination of the molecular weights of compounds in either a purified or crude sample. LC-MS methods utilizing an electrospray ionization (ESI) source with a triple quadrupole filter allow for the selective monitoring of fragment ions produced from the molecular ion, as well as the monitoring of further fragmentation of the initial fragment ions.[2] In some MS-based methods, the LC-MS, UV, and bioactivity profiles of a particular crude extract can be compared with a library of data, and a particular known active compound can be rapidly identified.[3,4] An MS-based method for whole-cell analysis has also been reported to be useful in the discrimination of various actinomycete strains for use in production of bacterial natural products, so that

redundant strains can be eliminated.[5] The bulk of published dereplication methods involve MS-based methods.

NMR methods rely on the ability of NMR-based techniques to resolve signals produced by a variety of functional groups within a molecule, separate signals from different molecules in a mixture, and aid in the rapid identification of functional groups and structural motifs. One NMR-based method involves using diffusion-edited TOCSY experiments (DECODES experiments) or diffusion-edited HSQC (HETDECODES) to resolve the TOCSY or HSQC spectra of two molecules in a bioactive mixture of marine natural products. When used in conjunction with LC-MS, these NMR methods allow for the identification of spin systems and functional groups and, if the compound is known, aids in the comparison of the sample with known structures. If the compound is unstable or difficult to isolate, this can save many steps needed to reisolate a known compound.[6] Another reported NMR based method involves the rapid identification of isolated compounds using a search algorithm for commercially available compound databases. NMR methods (i.e. DEPT, gHSQC) were applied to an unknown compound to classify protonated carbons as methines, methylenes, or methyls, while the molecular weight was determined by MS. The search algorithm was designed to search the databases for compounds that matched these variables for the unknown. This method was shown to aid in the rapid identification of an alkaloid and a sesquiterpenoid.[7]

Chromatographic prefractionation methods rest on the ability to selectively remove certain undesirable classes of compounds, so that the activity of any remaining bioactive compounds can be assessed. These methods thus combine dereplication of known compounds or compound classes with prefractionation of the sample, and are

therefore most appropriately termed prefractionation-dereplication methods. One of the most widely used prefractionation-dereplication methods is the selective removal of tannins by use of polyamide chromatography. Sephadex LH-20[8] and HP20 MCI gel[9] have also been reported as being useful for selectively removing tannins from plant extracts. The remaining extract after removal of the tannins can then be evaluated for bioactivity in the assay system of interest, and can be subjected to fractionation if it proves to contain non-tannin active components.

Activity profiling is method of dereplication where the bioactivity of an extract or a semipure sample is profiled in several different assays. The COMPARE algorithm used with the NCI's sixty-cell line panel is the most well-known of these methods. A particular compound with a known mechanism of action (a "seed" compound) may be tested in the panel, and the activities in all sixty cell lines statistically analyzed. Subsequently, other compounds may be tested in the sixty-cell line panel. COMPARE considers IC_{50} values, which represent the concentration of a compound that inhibits cell growth by 50%. COMPARE uses statistical methods to correlate the activities of the test compounds to the original "seed" compound. When there is a high degree of correlation, this indicates that the test compound has a profile of cytotoxicity similar to that of the seed compound. In turn, if the toxicities are similar in selectivity, then the mechanisms of action might be similar. COMPARE is an important part of NCI's decision as to whether a new antitumor agent is worth moving into preclinical trials. COMPARE analysis has been used to identify an extract of *Pyrenacantha klaineana* as having a mechanism of action similar to that of camptothecin; upon fractionation, camptothecin was isolated from the crude extract.[10]

6.2 Results and Discussion

6.2.1 Initial Tests of Aminopropyl SPE Prefractionation-dereplication Method

While performing bioassay-guided fractionation on crude extracts using liquid partioning and reverse phase C_{18}, normal phase SiO_2, and gel filtration chromatography methods, it became apparent in our group that the enzyme-based bioassays were sensitive to the presence of both tannins and fatty acids. Weeks of the iterative process of fractionation, sample preparation, biological testing of fractions, and further fractionation would sometimes afford a purified fatty acid such as oleic acid (**6.1**). Thus, it became

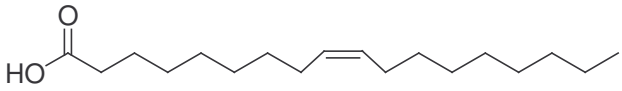

6.1

desirable to find ways to quickly dereplicate LCFAs so that time could be focused on potentially more profitable extracts.

A review of the literature revealed that many dereplication methods have been developed for LCFAs involving chemical derivatization of extracts, followed by gas chromatography (GC) or gas chromatography-mass spectrometry (GC-MS).[11] For natural products drug discovery, the problem with these methods is that they do not quickly allow for the direct identification of active principles within the extracts. We did not wish to spend resources in characterizing the activity of all LCFAs found in nature, and then use GC to identify the LCFAs found in a particular extract. Also, the identification a particular active LCFA in an extract did not mean that it would be the only active principle in the extract. So, we wished to have a dereplication method by

which we could efficiently isolate LCFAs, test the resulting fractions in our bioassays, and deduce whether the LCFAs were responsible for the activity of the crude extract. A liquid chromatography-based methods seemed to be the most likely candidate to fit these requirements.

From the literature, it was found that aminopropyl-bonded silica gel had been used to efficiently fractionate chloroform extracts of human adipose tissue.[12] In the reported method, an aminopropyl SPE was used to separate different compounds including fatty acids, phospholipids, cholesterol esters, triglycerides, cholesterol, diglycerides, and triglycerides. All compounds other than fatty acids and phospholipids were flushed out with an initial wash with 2:1 $CHCl_3$:2-propanol. These compounds were reconcentrated and further fractionated by use of additional aminopropyl SPEs to obtain the purified compounds. Fatty acids were flushed out with 2% HOAc in ethyl ether, while the phospholipids were finally flushed out with methanol.

It seemed that this method could be adapted to natural products research for the dereplication of LCFAs. Since the aminopropyl SPE could reportedly isolate LCFAs into one fraction, our proposed application of this method was to collect only three fractions from the column, without additional fractionation of the first fraction before bioassay testing of the initial three fractions. After conditioning the SPE cartridge with hexane, the sample dissolved in 2:1 $CHCl_3$:2-propanol (solvent **A**) would be applied to the cartridge, and the cartridge would be washed with solvent **A**, 2% HOAc in ether (solvent **B**), and finally MeOH (solvent **C**).

A simple experiment was devised to test the usefulness of this method, as depicted in Scheme 6.1. A test mixture was prepared by combining pure samples of the

LCFAs oleic acid, linoleic acid, and palmitic acid with the sesterterpenoid heteronemin (see Chapter 3, compound **3.8**). These LCFAs were typical of what had been previously isolated in our group, while heteronemin served as a representative natural product. After conditioning the cartridge with hexane, the sample was dissolved in solvent **A** and loaded

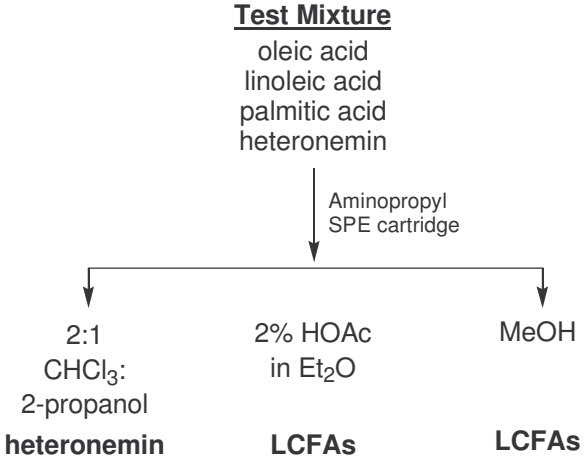

Scheme 6.1: Fractionation of LCFA test mixture

onto the cartridge. The column was washed with solvents **A**,**B**, and **C**, and fractions were collected from each wash. Each of these fractions was concentrated, dried, and analyzed by ^{1}H NMR.

As shown in Figure 6.1 A-D, the ^{1}H NMR spectra reveal how well the SPE separation works. Figure 6.1A shows the ^{1}H NMR spectrum for the LCFA test mixture, without added heteronemin. Figure 6.1B shows the ^{1}H NMR spectrum for heteronemin alone. Figure 6.1C-D are the ^{1}H NMR spectra for fractions 1-3 from the SPE cartridge. Clearly, fraction 1 contains heteronemin with no trace of LCFAs. The signal at δ_H 1.24 is apparently due to grease contamination from the isolation procedure; the absence of vinylic methine proton multiplets at δ_H 5.35 and the presence of an oxygenated methine proton signal at δ_H 5.36 from heteronemin demonstrate that the LCFAs are not present in

fraction 1. Fraction 2 contains LCFAs as well as grease, but it does not contain detectable amounts of heteronemin. Finally, fraction 3 also contains LCFAs, though this fraction is small. From this experiment, it appears that LCFAs can be separated away from a typical natural product by use of an aminopropyl SPE cartridge.

6.2.2 Application of the Aminopropyl SPE Prefractionation-dereplication Method

The next step was to see if the aminopropyl SPE separation could be applied to natural extracts in order to isolate LCFAs and measure their bioactivity. We needed a detection method that would be efficient for routine use to confirm the presence of LCFAs. ^{1}H NMR analysis was chosen for this purpose, since LCFAs produce characteristic signals in ^{1}H NMR analysis, and their spectra are fairly uncomplicated. Also, with a large enough sample, grease eluting from the column would not interfere significantly, and any large signal at about δ_H 1.24 could safely be ascribed to LCFAs. For the purposes of dereplication, since the solvent **C** wash of the column apparently contained the same components as the solvent **B** wash, our attention focused mainly on the solvent **A** and **B** washes (fractions 1 and 2, respectively) from the aminopropyl SPE cartridge.

Figure 6.1: ^{1}H NMR spectra of test mixtures from LCFA purification (impurities labeled)

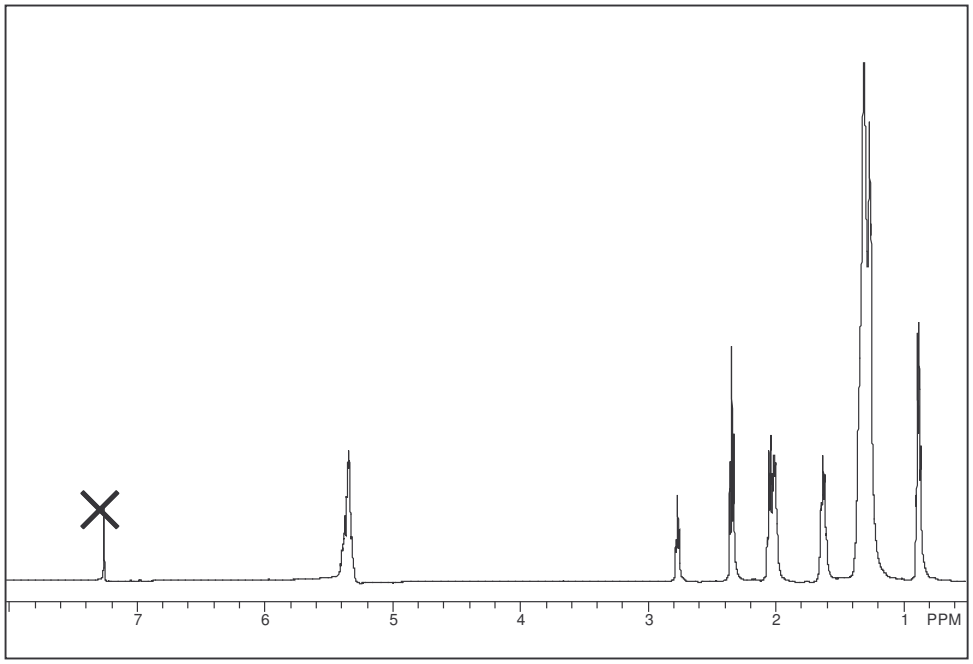

A) ^{1}H NMR spectrum of mixture of fatty acids (δ_H 7.26: $CHCl_3$)

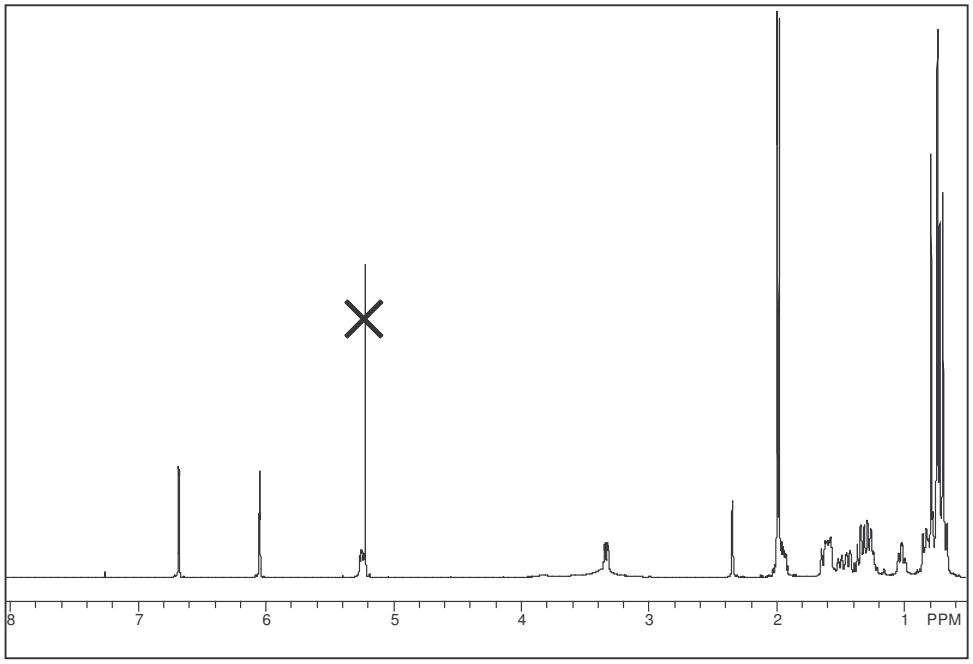

B) ^{1}H NMR spectrum of heteronemin (δ_H 5.22: CH_2Cl_2)

Figure 6.1 (continued)

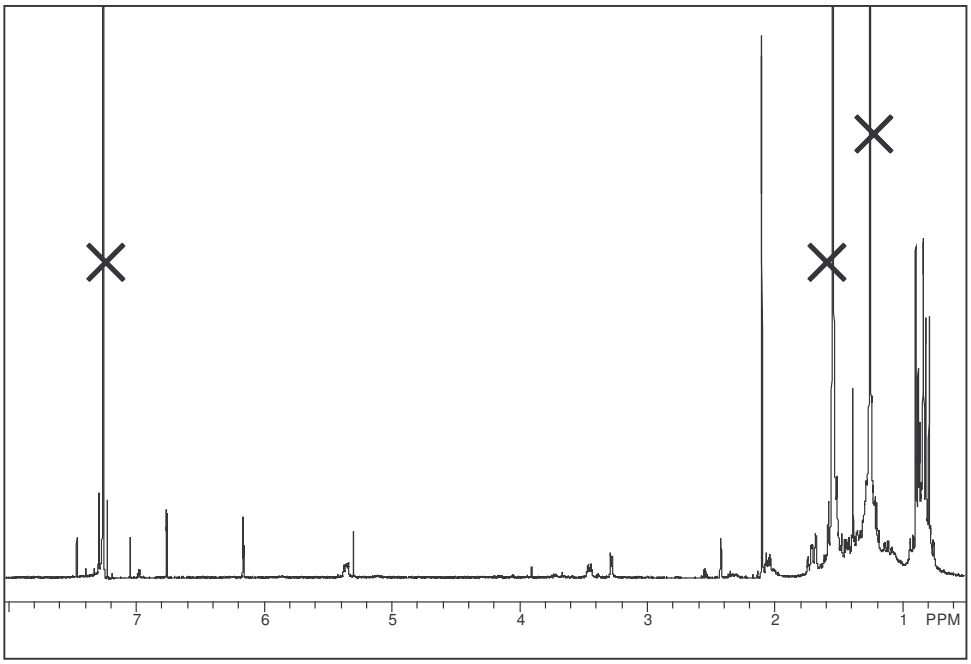

C) ^{1}H NMR spectrum of fraction 1 (solvent **A**) (δ_H 1.55: H_2O; δ_H 1.24: grease)

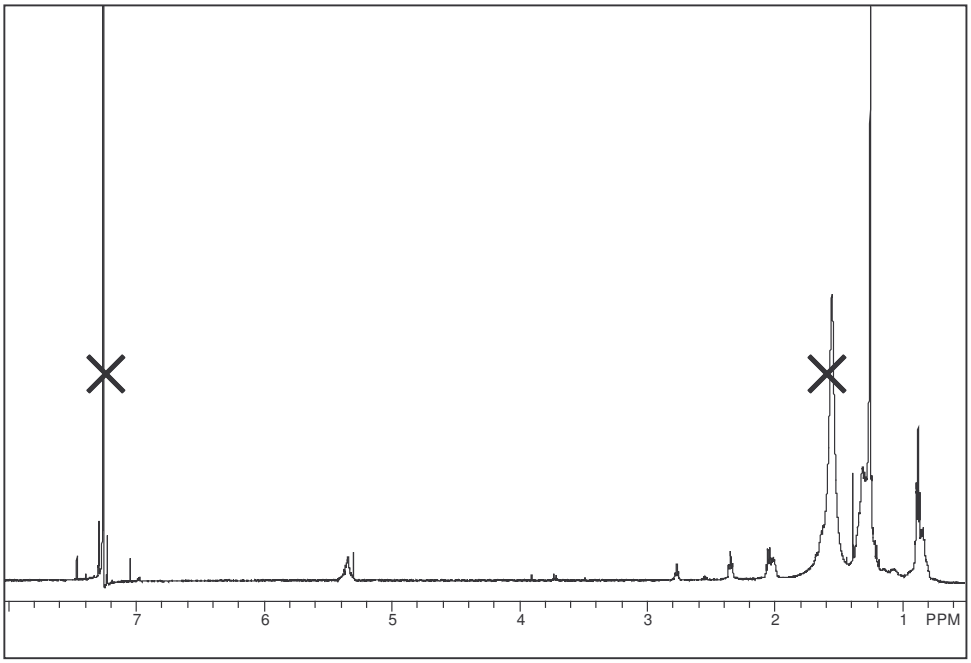

D) ^{1}H NMR spectrum of fraction 2 (solvent **B**)

Figure 6.1 (continued)

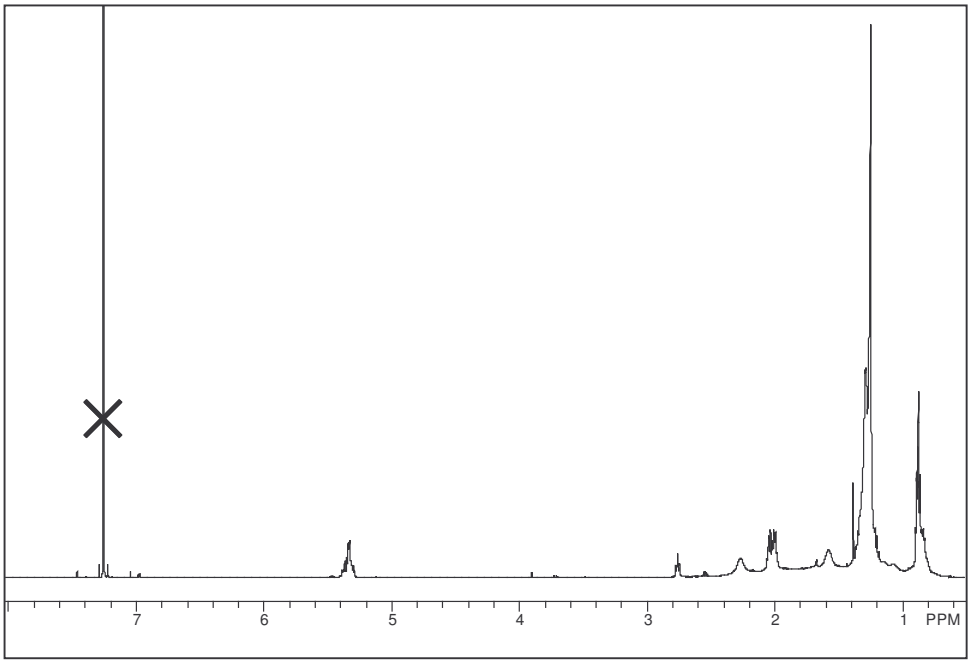

E) ^{1}H NMR spectrum of fraction 3 (solvent **C**)

Assuming that by this method we could isolate LCFAs from a crude extract into one fraction, we envision that in practice there would be at least six possible scenarios that could result. Scheme 6.2 is a flowchart that illustrates the possible outcomes after the aminopropyl SPE separation. In summary, in cases where fraction 1 is active, and fraction 2 either contains LCFAs (based on ^{1}H NMR analysis) or is inactive, fraction 2 is dropped while work proceeds on fraction 1. If fraction 1 is inactive, work proceeds with fraction 2 only if it does not contain LCFAs, based on ^{1}H NMR analysis. If neither fraction is active, it is assumed that the method is not compatible with the active principles of the extract, so another fractionation procedure is employed. Also, if fraction 2 is active and does not appear to contain LCFAs, while fraction 1 is inactive, work proceeds with fraction 2.

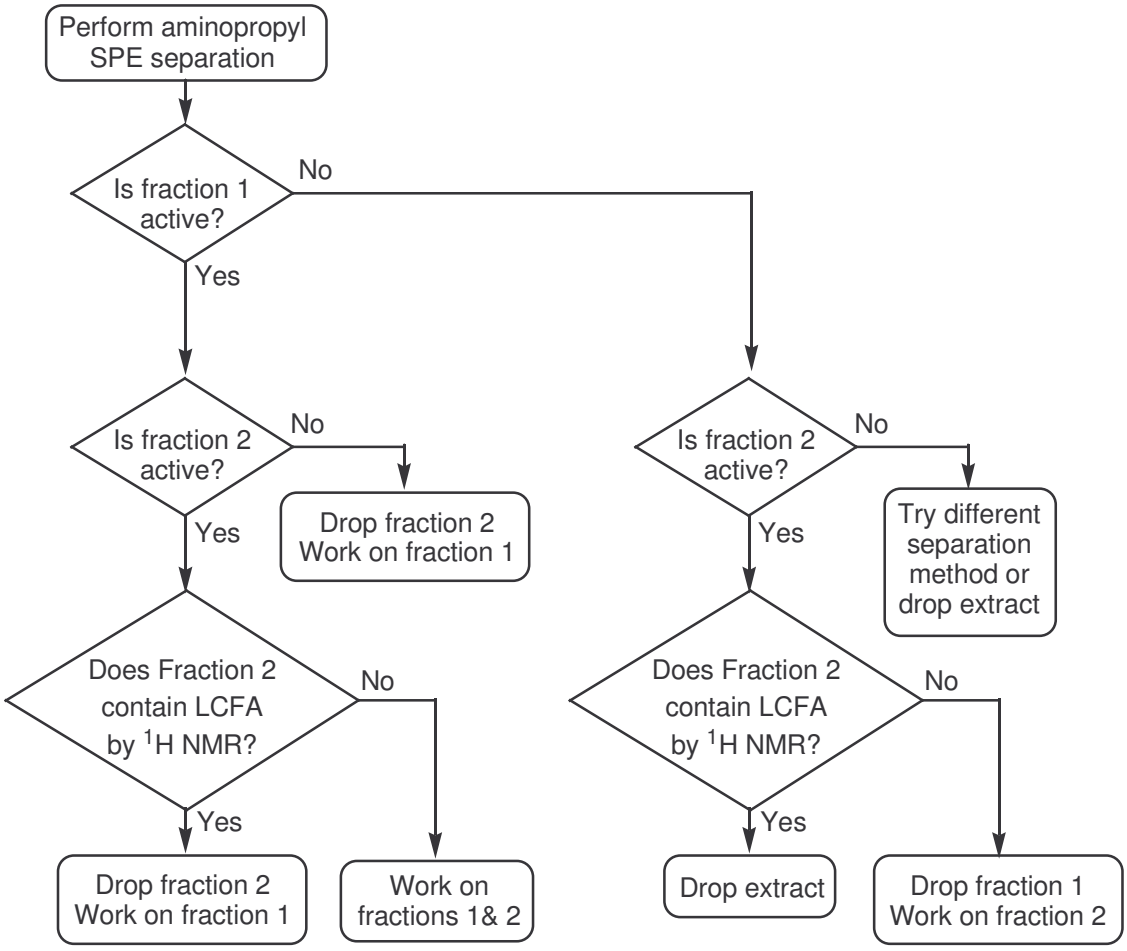

Scheme 6.2: Decision making for LCFA dereplication

At this point, we proceeded to apply the aminopropyl SPE separation method and compare it to results from typical purification methods. An initial screen of extracts from a collection at the University of Virginia indicated that a hexane extract of the Australian tree *Planchonella papyracea* was active in the pol β bioassay, with weak inhibition of the lyase domain of pol β at 2.2 μg/mL. As summarized in Scheme 6.3, fractionation of the crude extract by use of liquid partitioning followed by reverse phase C_{18} chromatography, LH-20 gel filtration, and an additional reverse phase C_{18} chromatography step afforded two fractions that had the best activity of all fractions collected. ^{1}H NMR analysis of

these two fractions suggested that fraction 2 from the final C_{18} column contained long-chain compounds (Figure 6.2A), while fraction 24 contained an apparent mixture of long-chain compounds and triterpenoids. Based on ^{1}H NMR analysis of other weakly active fractions collected, these were shown to contain long-chain compounds and triterpenoids. This extract was considered to be a good candidate for the aminopropyl SPE fractionation method.

The second fractionation of the crude *P. papyracea* extract is shown in Scheme 6.4. Based on the previous separation, the 60% MeOH fraction from the liquid partition was shown to be inactive. Therefore, the crude extract was initially partitioned between hexane and 60% MeOH to remove inactive, polar compounds. The hexane fraction was then dried and redissolved in solvent **A** for the SPE separation. This afforded three fractions. The most active fraction was fraction 2, while fraction 1 was also active and contained the majority of the mass of the extract. ^{1}H NMR analysis of fraction 2 showed that it contained long-chain compounds (Figure 6.2B). Further fractionation of fraction 1 afforded active fractions that appeared to contain triterpenoids based on ^{1}H NMR analysis, but the activity of these fractions was not reproducible enough to allow for the isolation of any active compounds. Therefore, since the most intensely and reproducibly active compounds in this extract were shown to be long-chain compounds,

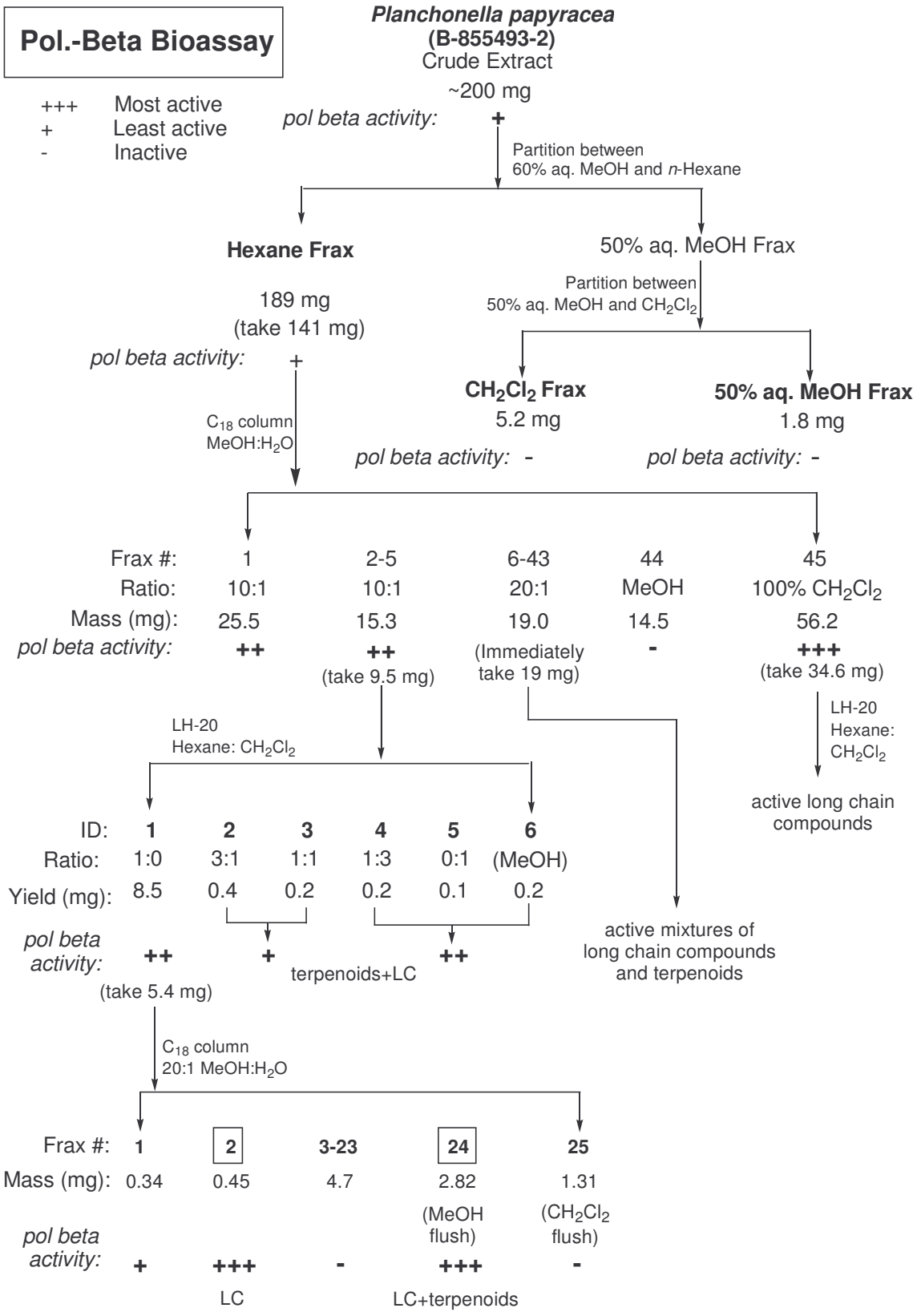

Scheme 6.3: Initial fractionation scheme for *P. papyracea* extract

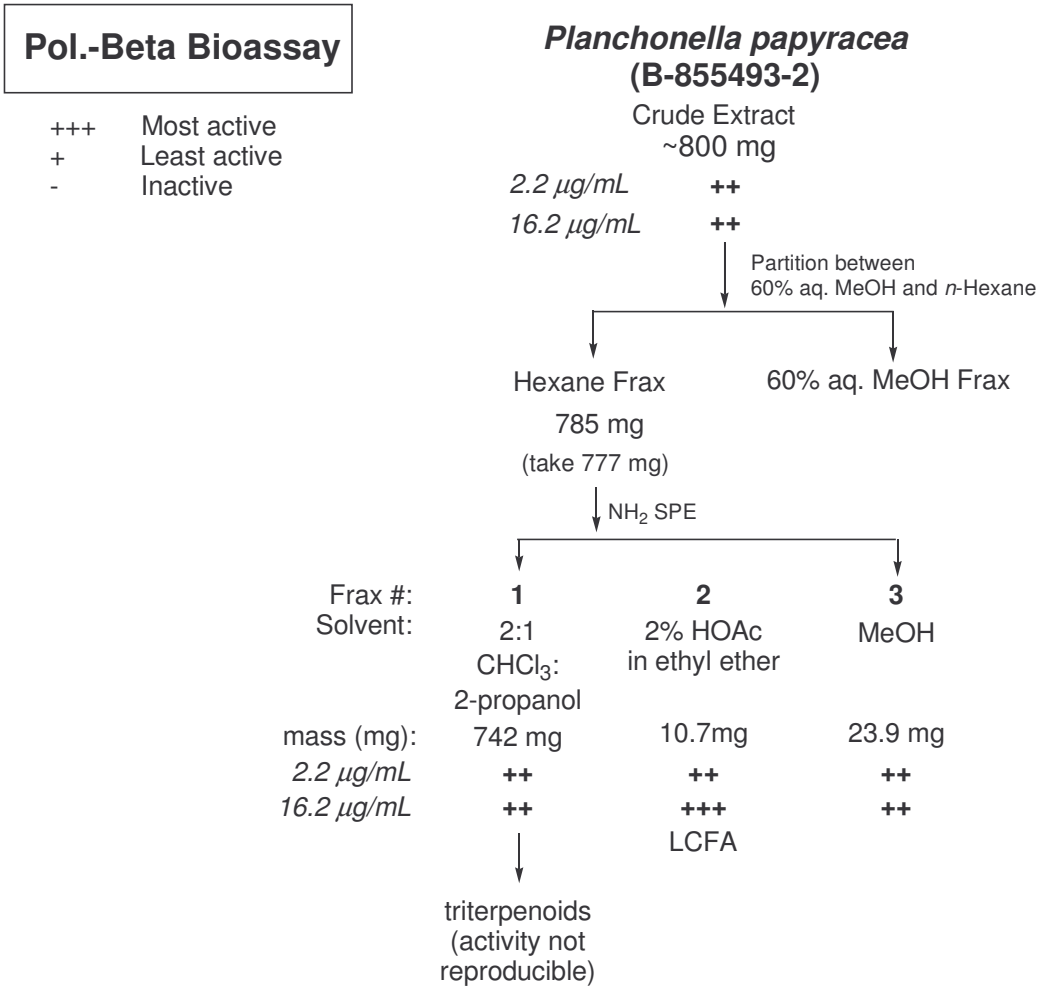

Scheme 6.4: Aminopropyl separation of *P. papyracea* extract

and they were selectively isolatable using an aminopropyl SPE, we concluded that LCFAs were responsible for the majority of the activity of this extract. We therefore dropped the extract.

We proceeded to try the aminopropyl column on another extract that had been found to contain putative LCFAs. An extract of *Magnolia virginiana* was shown to be active in the pol β assay, with moderate inhibition at 2.2 µg/mL and strong inhibition at 16.2 µg/mL. The initial fractionation scheme is summarized in Scheme 6.5. This extract

Figure 6.2: ^{1}H NMR spectra of LCFA-containing fractions from *P. papyracea* (impurities labeled)

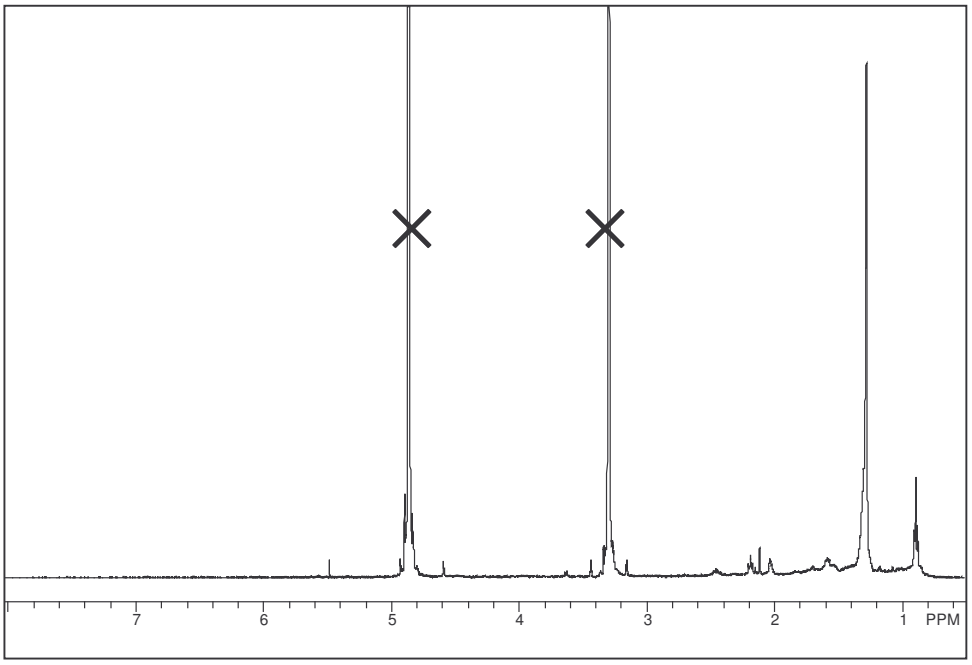

A) Fraction 2 from the final C_{18} column

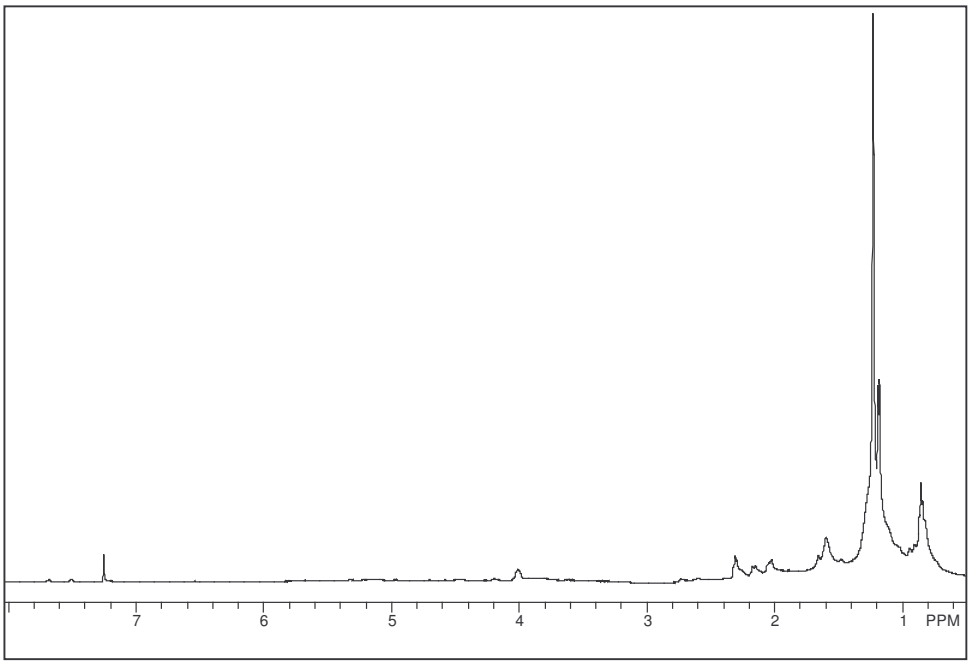

B) Fraction 2 from the aminopropyl SPE

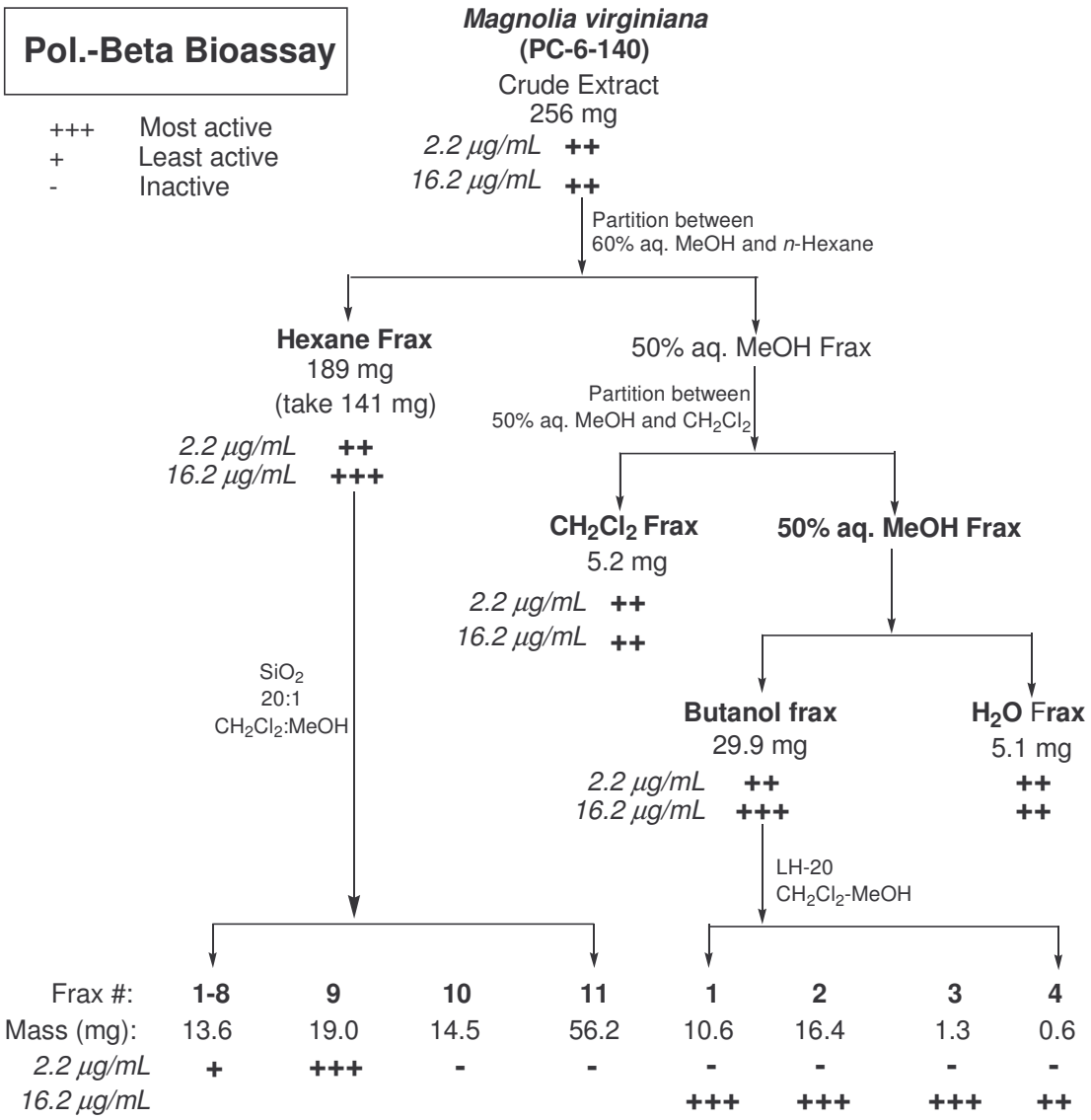

Scheme 6.5: Initial fractionation scheme for *M. virginiana* extract

was initially studied by Dr. Bing-Nan Zhou in our lab, but this work ended when Dr. Zhou left our group. An initial liquid partitioning step afforded four active fractions. Two of these fractions, the hexane fraction and the butanol fraction, were further fractionated. The hexane fraction was chromatographed over SiO_2 to afford eleven fractions, one of which was strongly active at 2.2 µg/mL. Fractionation of the butanol fraction by Sephadex LH-20 filtration afforded four fractions, all of which were strongly

active at 16.2 μg/mL. ^{1}H NMR analysis of fraction 9 from the hexane fraction suggested that it was a long-chain compound (Figure 6.3A). The fractions from the LH-20 column appeared to contain tannins, based on their polarity, color, poor solubility, and positive test in a reagent test for phenols. This extract was judged to be a good candidate for the aminopropyl SPE dereplication procedure.

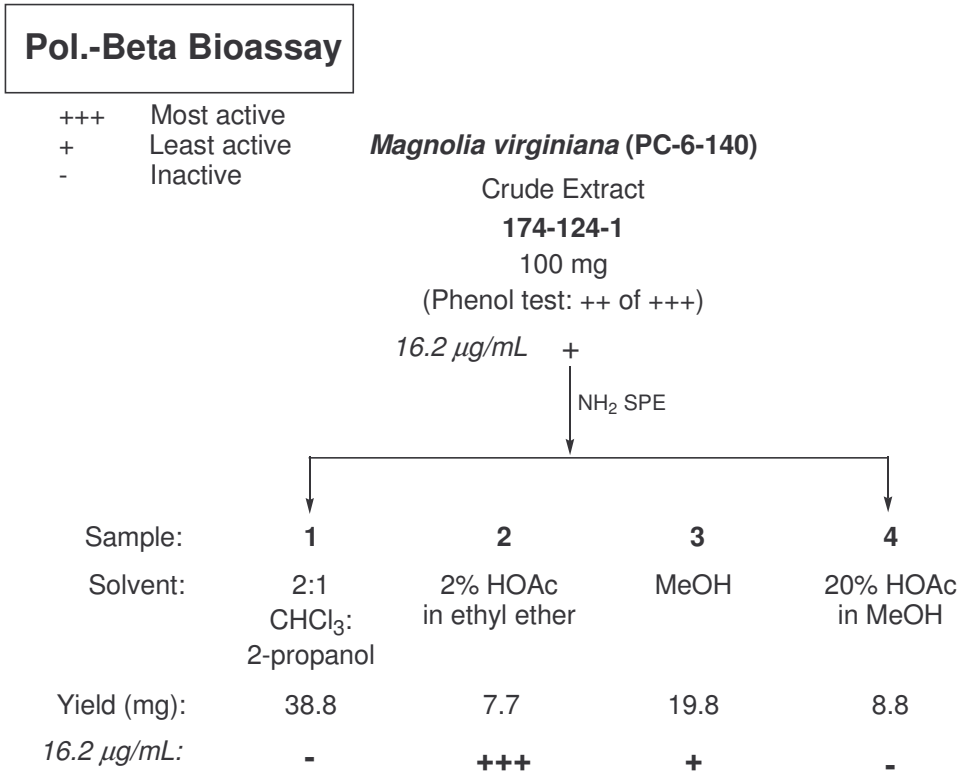

Scheme 6.6: Aminopropyl separation of *M. virginiana* extract

The second fractionation of the crude extract of *M. virginiana* is shown in Scheme 6.6. The typical three fractions were initially collected, but an additional fraction with more concentrated acid was collected in order to flush more strongly-bound compounds off the column. Fraction 1 was inactive, while fraction 2 was strongly active. ^{1}H NMR analysis of fraction 2 showed that it apparently contained long-chain compounds (Figure

6.3B). Based on the isolation procedure and the ^{1}H NMR analysis, we concluded that the majority of the activity of the extract was due to the presence of LCFAs.

Figure 6.3: ^{1}H NMR spectra of LCFA-containing fractions from *M. virginiana*

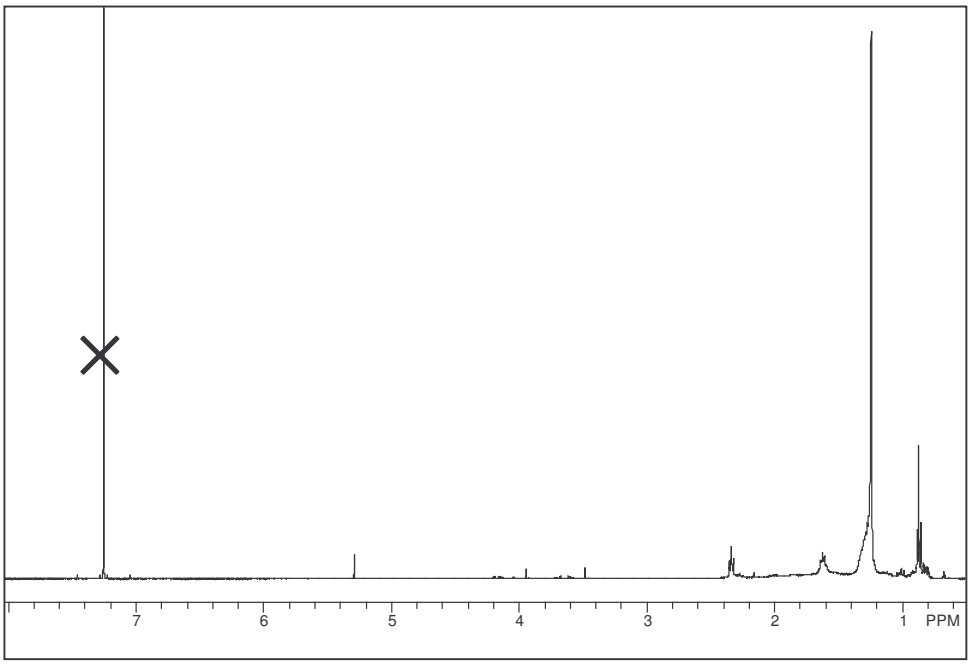

A) LCFA-containing fraction from Dr. Zhou's work

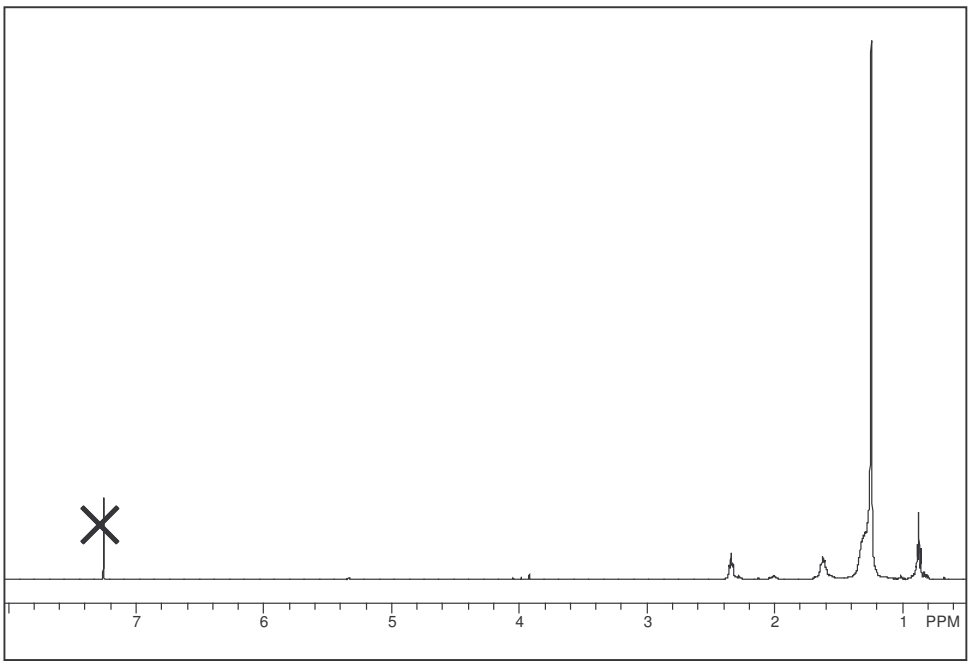

B) Fraction 2 from the aminopropyl SPE separation of the crude extract of *M. virginiana*

The fractionation of the extract of *M. virginiana* only afforded a 75% recovery by mass of the crude extract. It appeared that the material lost on the column was likely to be something polar that might bind irreversibly with the aminopropyl stationary phase. The material was also strongly colored, like the color of tea. Tannins, with their phenolic functionality, large molecular weight, and reddish color seemed to fit this description. As mentioned, the crude extract was believed to contain tannins based on our previous studies of the extract. Thus, we concluded that the lost material was likely to be irreversibly bound tannins. So, it appeared that dereplication of LCFAs by use of an aminopropyl SPE was possible, but with some limitation based on the presence of strongly polar compounds.

At this point, we applied the aminopropyl SPE dereplication method to several extracts in the course of our bioassay-guided fractionation of crude extracts using the pol β assay. An extract of *Juniperus chinensis* was selected for fractionation after it produced weak inhibition of pol β at 2.2 μg/mL and moderate inhibition at 16.2 μg/mL . The fractionation of the extract of *J. chinensis* is shown in Scheme 6.7. An initial liquid partitioning afforded four fractions, all of which were active. The major component of the hexane fraction was a compound which was insoluble at higher concentrations in all solvents tested. The compound was tested and shown to be moderately active. ^{1}H NMR analysis of the compound showed that was most likely some sort of long-chain compound. We therefore did not examine the hexane fraction further and focused our efforts on the butanol and CH_2Cl_2 fractions. Because the reagent test for phenols was positive for the crude extract, we suspected that the extract contained tannins. So, the butanol and CH_2Cl_2 fractions were subjected to polyamide

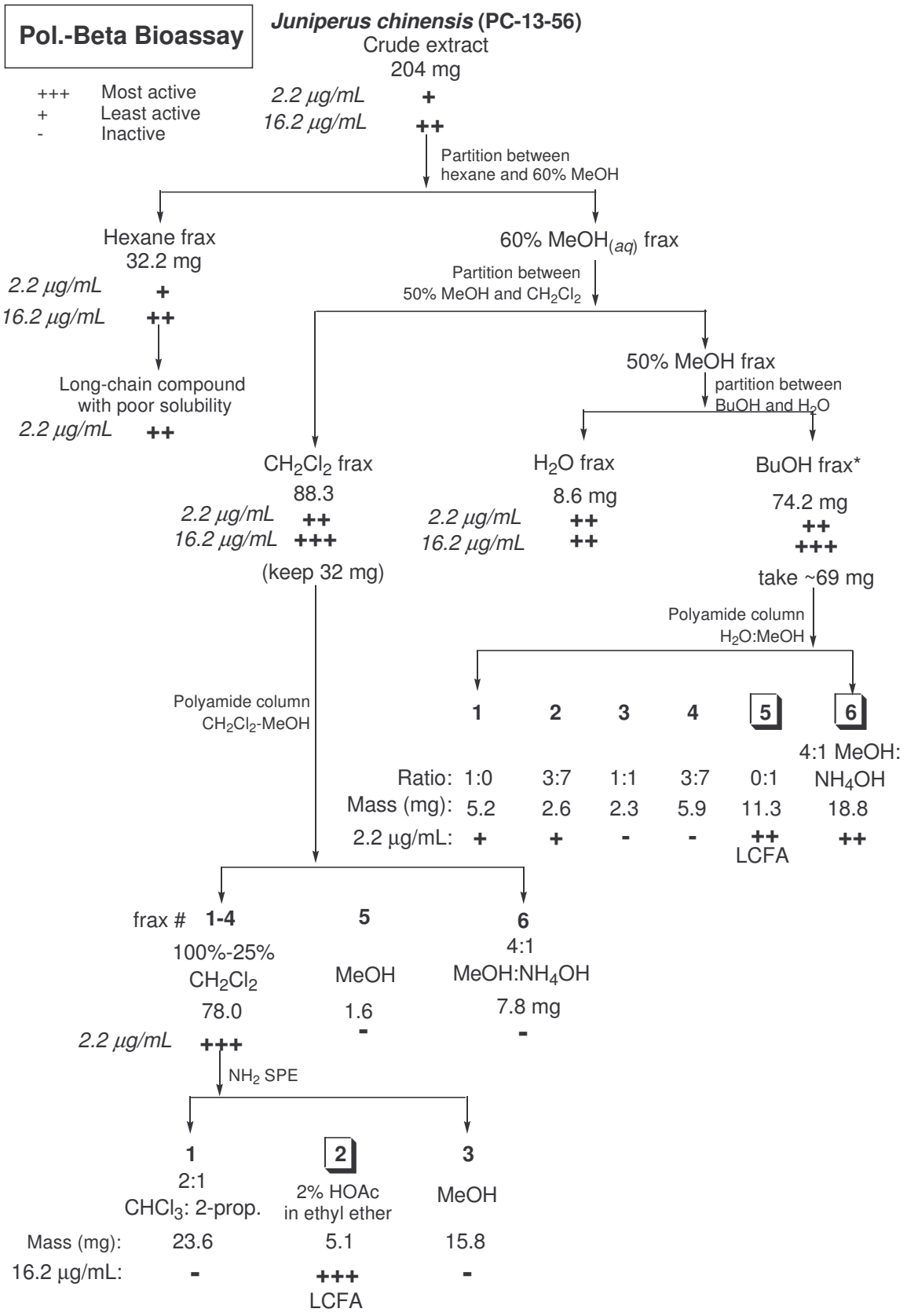

Scheme 6.7: Fractionation scheme for extract of *J. chinensis* extract

chromatography. Polyamide is routinely used for the removal of tannins from natural product samples. Polyamide chromatography of the butanol fraction afforded two fractions with significant activity. The 4:1 MeOH:NH_4OH fraction was the tannin-containing fraction. ^1H NMR analysis of the MeOH wash indicated the presence of a long-chain compound, most likely a LCFA (Figure 6.4A).

Polyamide chromatography of the CH_2Cl_2 fraction afforded six fractions, four of which were active. These fractions were combined, and this pooled fraction was fractionated by use of the aminopropyl SPE. Fraction 2 from this separation was strongly active at 16.2 μg/mL. ^1H NMR analysis of this fraction indicated the presence of a long-chain compound (Figure 6.4B). Based on the NMR evidence, and since the most active components of this extract were selectively isolated by use of polyamide and the aminopropyl SPE, the activity of the extract was ascribed to the presence of tannins and LCFAs, and the extract was dropped.

Finally, an extract of *Stigmaphyllon convolvulifolium* was selected for it *in vitro* activity in the pol β assay, where it had moderate activity at both 2.2 and 16.2 μg/mL. An initial detanninization using Sephadex LH-20 afforded three fractions, two of which were strongly active at 16.2 μg/mL and one of which was weakly active at 16.2 μg/mL (see Scheme 6.8). Reverse phase C_{18} chromatography of the weakly active fraction yielded six fractions, one of which was more active than the parent fraction. This fraction was further fractionated by use of the aminopropyl SPE method. ^1H NMR analysis of fraction 2 indicated that it contained LCFAs (Figure 6.5). Because the vast majority of the bioactivity of the crude was due to tannins, and because LCFAs were isolatable from the most active non-tannin fraction, this extract was dropped.

Figure 6.4: ^{1}H NMR spectra of LCFA-containing fractions from *J. chinensis*

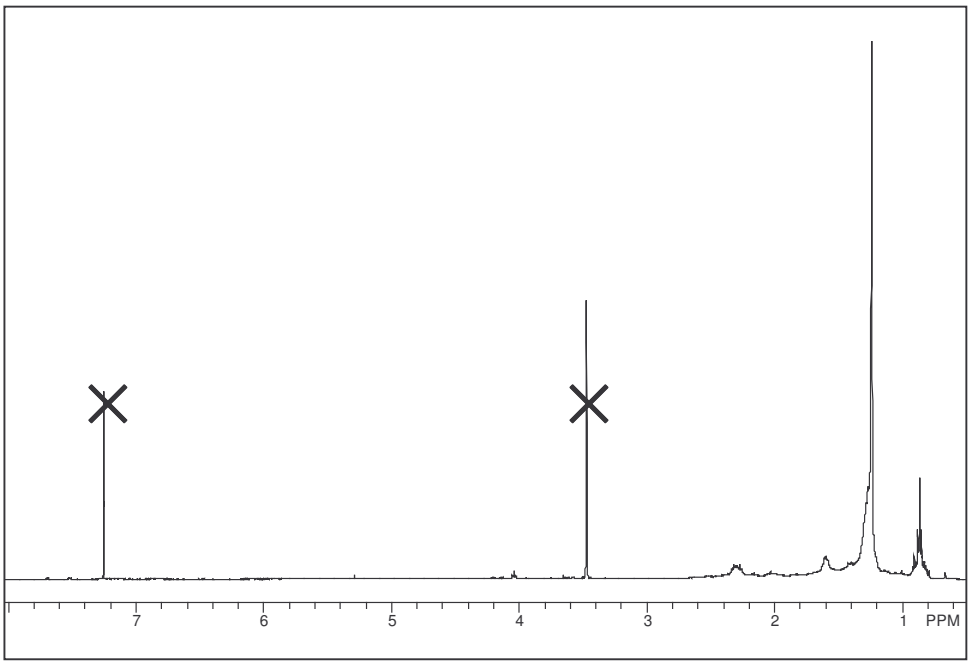

A) Fraction 2 from the aminopropyl SPE separation following polyamide chromatography of the CH_2Cl_2 fraction from liquid partitioning of the crude extract of *J. chinensis.*

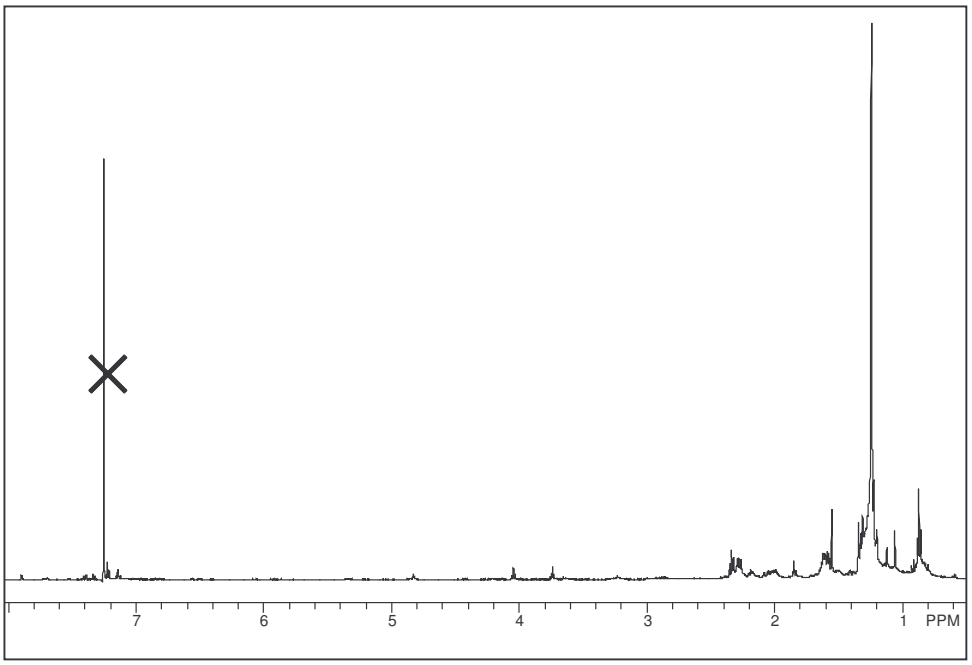

B) MeOH wash from the polyamide separation of the butanol fraction of the crude *J. chinensis* extract.

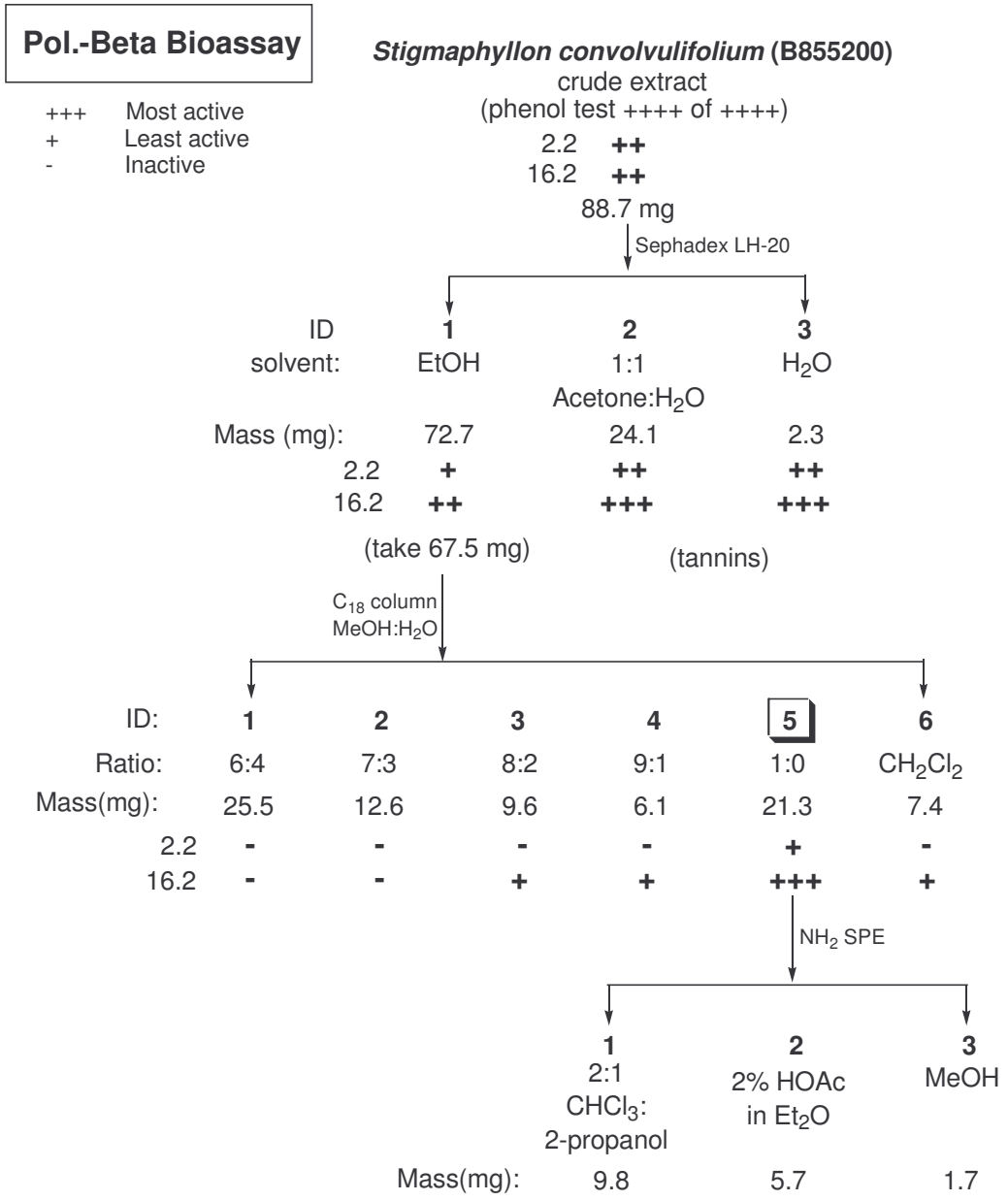

Scheme 6.8: Fractionation scheme for extract of *S. convolvulifolium* extract

Through the course of our research, it became apparent that the aminopropyl SPE LCFA dereplication method was not a perfect solution for LCFA dereplication and removal. The dereplication method was applied to the extracts of *R. globostellata* and *P. parryi* (see Chapters 2 and 5). As reported for these extracts, fraction 2 contained little or

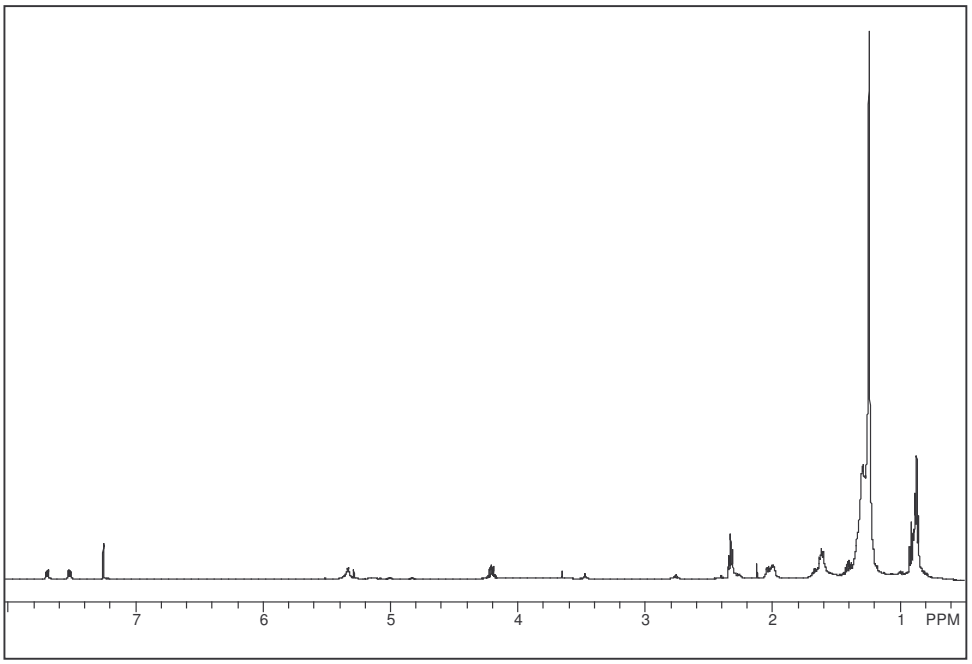

Figure 6.5: ^{1}H NMR spectra of the LCFA-containing fraction from *S. convolvulifolium* Fraction 2 from the aminopropyl SPE separation following C_{18} and LH-20 chromatography of the crude extract of *S. convolvulifolium.*

no LCFAs, but fraction 2 did contain terpenoids with carboxylic acid functionality.

Since the pKa of a carboxylic acid is around 4-5, while the pKa of the aminopropyl sorbent in the SPE is reported to be 9.8,[12] the aminopropyl sorbent is not selective for LCFAs alone, but it can selectively retain any carboxylic acid-containing compounds. A proposed mechanism for the selective isolation of carboxylic acids is shown in Scheme 6.9. When carboxylic acid-containing compounds are loaded into the SPE, the aminopropyl sorbent deprotonates the acids. The carboxylate ions form an ion pair with the sorbent, since the negatively charged carboxylate is attracted to the positively charged aminopropyl sorbent. After solvent **A** is flushed through, which elutes compounds without the carboxylic acid functionality, and solvent **B** with acetic acid is flushed through the sorbent, the acetic acid can also protonate the sorbent. This allows

for the resulting acetates to compete with the carboxylates from the sample for the protonated amines on the sorbent. If the concentration of the acetic acid and the amount

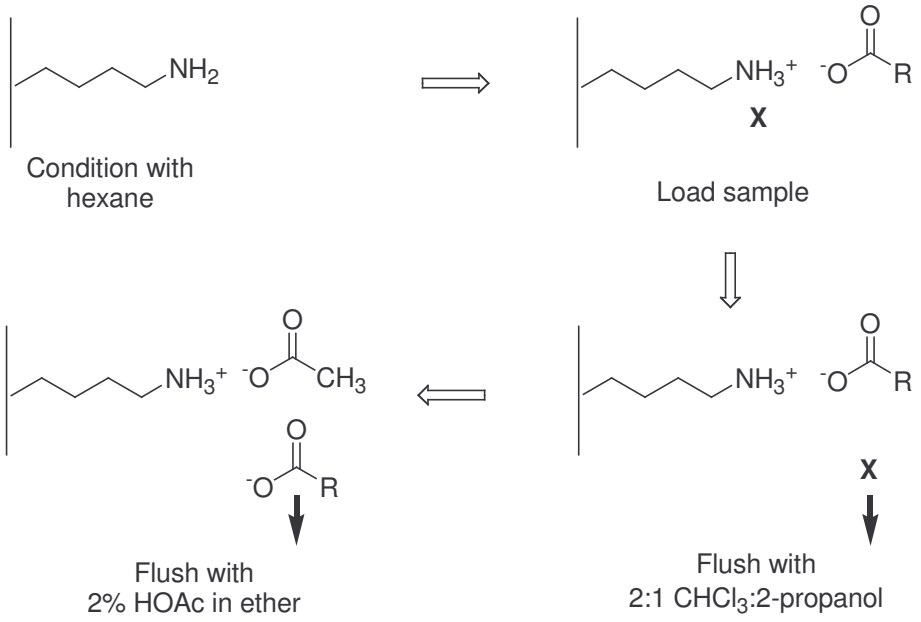

Scheme 6.9: Mechanism of the isolation of carboxylic acids by aminopropyl SPE
X = non-carboxylic acid compounds in the sample

flushed through are sufficient, the acetates will eventually displace the acids from the sample for the binding sites at the protonated amines, and the sample will be washed out of the SPE. When the SPE is flushed with methanol at the end, the methanol likely mixes with some of the residual acetic acid in the column to produce an acidic mobile phase that is also more polar than the ethereal acetic acid solution. This would explain how phospholipids may be flushed out with methanol. From our experiments, the presence of LCFAs in the methanol wash may indicate that the acetic acid concentration in the eluent, the volume of eluent, or the flow rate are inadequate for complete elution of carboxylic acids within fraction 2. This work is really a proof of principle along with some applications, and further experimentation is necessary to optimize this technology for routine use in natural products work.

In applying this technology to the removal and dereplication of LCFAs, it must be kept in mind that a secondary method of LCFA detection such as ^{1}H NMR or GC-MS must be employed in order to confirm the presence of LCFAs. Overall, these results show that the aminopropyl SPE method can be used for the selective removal of carboxylic acids, and this can allow for the evaluation of the bioactivity of any LCFAs present in a sample. The ability to rapidly remove LCFAs and other carboxylic acids from a crude extract, evaluate their biological activity, and perform rough identifications by ^{1}H NMR can help save time that might otherwise be spent on the labor-intensive, iterative process of bioassay-guided isolation of LCFAs.

6.3 Experimental Section

NMR spectra were collected on a JEOL Eclipse+ 500 spectrometer operating at 500.2 MHz for 1H. Aminopropyl SPE cartridges were obtained from both Varian Sample Preparation Products (5 g cartridges) and Supelco (1 g cartridges and smaller).

DNA Polymerase β Lyase Inhibition Bioassay

The pol β bioassay was performed by our collaborators at the University of Virginia as described in the experimental section of Chapter 5.

General experimental procedure for aminopropyl SPE fractionation

The size of the SPE used for the fractionation depended on the amount of sample or crude extract to be loaded. Aminopropyl SPE cartridges are available in sizes of 5 g, 1 g, 500 mg, 250 mg, and 100 mg. The ratio of sorbent mass to sample mass was kept to at

least a ratio of 40 to 1. Larger samples (>500 g) were fractionated using multiple SPE cartridges by the same procedure, and the common fractions were pooled.

The samples were dissolved in 2:1 $CHCl_3$ (solvent **A**), and the solution was added directly to the head of the SPE. A syringe was connected to a special adapter which fit in the head of the SPE, and the syringe plunger was pushed in to pressurize and elute the mobile phase. The elution rate was kept around 1 drop of eluent per second. The solvent **A** wash was collected (fraction 1), and the column was washed with 2% HOAc in ethyl ether (solvent **B**) using the same method as for solvent **A** to afford fraction 2. The solvent **B** fraction contained the LCFAs, based on the published procedure. Finally, the SPE was flushed with methanol (solvent **C**) to yield fraction 3. In some cases, the SPE retained color that ranged from pale yellow to deep reddish brown. The intensity of the retained color was proportional to the amount of material lost through the separation, although sample recoveries were typically greather than 90%.

Fractions 1-3 were concentrated under vacuum, and samples were prepared for bioassay. Samples of fractions 1 and 2 were checked by ^{1}H NMR analysis. If fraction 2 was shown to contain long-chain compounds and to be active, the fraction was dropped; in this case, if fraction 1 was also inactive, the extract was dropped. Otherwise, if the activity of an extract was shown to be due to compounds other than LCFAs, work was focused on those samples.

References for Chapter 6

1. Beutler, J.A.; McKee, T.C.; Fuller, R.W.; Tischler, M.; Cardellina, J.H.; Snader, K.M.; McCloud, T.G.; Boyd, M.R. Frequent Occurrence of HIV-inhibitory Sulphated Polysaccharides in Marine Invertebrates. *Antiviral Chem. Chemother.* **1993** *4*, 167-172.

2 Stefanowicz, P.; Prasain, J.K.; Yeboah, K.F.; Konishi, Y. Detection and Partial Structure Elucidation of Basic Taxoids from *Taxus wallichiana* by Electrospray Ionization Tandem Mass Spectrometry. *Anal. Chem.* **2001**, *73*, 3583-3589.

3. Strege, M.A. High-performance Liquid Chromatographic-electrospray Ionization Mass Spectrometric Analyses for the Integration of Natural Products with Modern High-throughput Screening. *J. Chrom. B.* **1999**, *725*, 67-78.

4. Constant, H.L.; Beecher, C.W.W. A Method for the Dereplication of Natural Product Extracts Using Electrospray HPLC/MS. *Nat. Prod. Lett.* **1995**, *6*, 193-196.

5. Colquhoun J A; Zulu J; Goodfellow M; Horikoshi K; Ward A C; Bull A T Rapid characterisation of deep-sea actinomycetes for biotechnology screening programmes. *Antonie van Leeuwenhoek* **2000**, *77*, 359-367.

6. Williamson, R.T.; Chapin, E.L.; Carr, A.W.; Gilbert, J.R.; Graupner, P.R.; Lewer, P.; McKamey, P.; Carney, J.R.; Gerwick, W.H. New Diffusion-Edited NMR Experiments to Expedite the Dereplication of Known Compounds from Natural Product Mixtures. *Org. Lett.* **2000**, *2*, 289-292.

7. Bradshaw, J.; Butina, D.; Dunn, A.J.; Green, R.H.; Hajek, M.; Jones, M.M.; Lindon, J.C.; Sidebottom, P.J. A Rapid and Facile Method for the Dereplication of Purified Natural Products. *J. Nat. Prod.* **2001**, *64*, 1541-1544.

8. Wall, M. E.; Wani, M.C.; Brown, D.M.; Fullas, F.; Olwald, J.B.; Josephson, F.F.; Thornton, N.M.; Pezzuto, J.M.; Beecher, C.W.W.; Farnsworth, N.R.; Cordell, G.A.; Kinghorn, A.D. Effect of Tannins on Screening of Plant Extracts for Enzyme Inhibitory Activity and Techniques for Their Removal. *Phytomedicine* **1996**, *3*, 281-285.

9. Tomomasa, K. Studies on Characteristics of Polyphenols in Apples. The Japan Food Chemical Research Foundation. http://www.ffcr.or.jp/zaidan/FFCRHOME.nsf/7bd44c20b0dc562649256502001b65e9/b8e815d99bcea74e49256953000bc99b/$FILE/190-3.pdf. (accessed September 6, 2005).

10. Zhou, B.-N.; Hoch, J.M.; Johnson, R.K.; Mattern, M.R.; Eng, W.-K.; Ma, J.; Hecht, S.M.; Newman, D.J.; Kingston, D.G.I. Use of COMPARE Analysis to Discover New Natural Product Drugs: Isolation of Camptothecin and 9-Methoxycamptothecin from a New Source. *J. Nat. Prod.* **2000**, *63*, 1273-1276.

11. Stavri, M.; Schneider, R.; O'Donnell, G.; Lechner, D.; Bucar, F.; Gibbons, S. The Antimycobacterial Components of Hops (*Humulus lupulus*) and Their Dereplication. *Phytother. Res.* **2004**, *18*, 774-776.

12. Blevins, D.D.; Burke, M.F.; Good, T.J.; Harris, P.A.; Van Horne, K.C.; Simpson, N., and Yago, L.S., eds. *Varian Sorbent Extraction Technology Handbook.* Harbor City, CA: Varian Sample Preparation Products, 1993, 82–84.

VII. Determination of Sequence Length Requirements and Sequence Specificity for a Directed Library of Checkpoint Kinase 1 Substrates

7.1 Introduction

The protein kinase Chk1 is an important mediator of DNA repair in both prokaryotic and eukaryotic cells. Non-toxic inhibitors of DNA repair pathways may potentiate the activity of antitumor DNA damaging agents such as doxorubicin or ionizing radiation, thus reducing the necessary dosage of these toxic treatments. For the discovery of inhibitors of Chk1 by bioassay-guided fractionation of natural extracts, efficient bioassays are necessary. Currently, bioassays typically used for Chk1 activity involve either expensive or radioactive reagents. To facilitate the development of new bioassays for Chk1, it is useful to characterize peptides of shorter length which retain all or most of the activity of the commonly-used substrates. Shorter peptides can be synthesized more rapidly and more economically than longer peptides. Herein, we

---

List of abbreviations for Chapter 7

Akt = Protein kinase B, critical for cell survival; AP endonuclease = Apurinic endonuclease; ATM = Ataxia telangiectasia mutated protein; ATP = Adenosine triphosphate; ATR = ATM and Rad3-related protein; BER = Base excision repair; BRCA1 = Breast cancer 1 protein; BSA = Bovine serum albumin; Cdc25 = Cell division cycle protein 25; Cdk kinases = Cyclin-dependent kinases; Chk1 = Checkpoint kinase 1; DIEA = Diisopropyl ethyl amine; DNA = Deoxyribonucleic acid; DTT = Dithiothreitol; EGTA = Ethylene glycol-bis(2-aminoethylether)-*N,N,N′,N′*-tetraacetic acid; HEPES = 1-[4-(2-Hydroxyethyl)-1-piperazinyl]ethane-2-sulfonic acid; ELISA = Enzyme-Linked Immunosorbent Assay ; Fmoc = Fluorenylmethoxy carbonyl; G_1 = gap 1 of cell cycle; G_2 = gap 2 of cell cycle; H2AX = member X of histone family H2A, responsible in part for organization of chromatin; HBTU = *O*-(Benzotriazol-1-yl)-*N,N,N′,N′*-tetramethyluronium hexafluorophosphate; HIV-Tat = HIV transcription activator; HOBT = 1-Hydroxybenzotriazole; MALDI-TOF = Matrix-assisted laser desorption ionization-time-of-flight mass spectrometry; MDC1 = Mediator of DNA damage checkpoint 1; MDM2 = Mouse double minute 2 protein; Mre11 = Meiotic recombination 11 protein; MRN = Complex of Mre11, Rad9, and Nbs1 enzymes; Nbs1 = Nijmegen breakage syndrome protein 1; NMP = *N*-methylpyrrolidinone; p48 = 48 kDa subunit of DNA binding protein DDB; p53 = Tumor protein 53; Rad9 = Radiation-sensitive protein 9; S = Synthesis phase of cell cycle; SPPS = Solid phase peptide synthesis; TFA = Trifluoroacetic acid; TIPS-H = Triisopropyl silane; γ-H2AX = Phosphorylated form of H2AX;

present a study of the sequence and length requirements for biological activity of synthetic peptide substrates of Chk1.

7.1.1 The Cell Cycle

Studies of cellular systems have revealed that while cells live out their lives, they proceed through several distinct steps of development. This progression is referred to as the cell cycle, which is schematically represented in Figure 7.1. Cells divide, grow, and replicate their genetic material, and then cell division occurs again. The steps of cell division occur during mitosis. In the G_1 phase, or gap 1, the cell grows and prepares for DNA replication. During the S phase, or synthesis phase, the DNA is replicated. In the

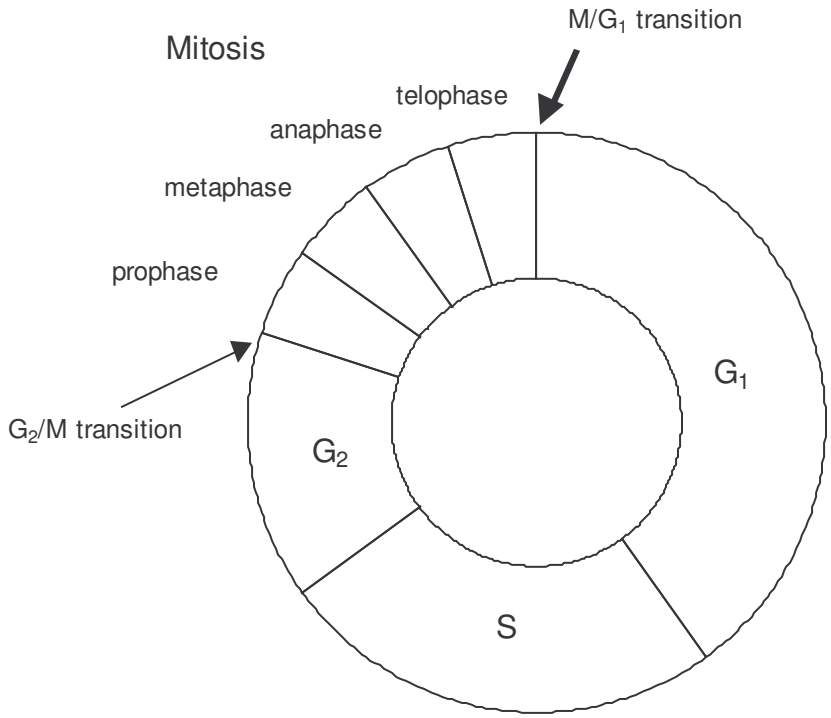

Figure 7.1: Schematic representation of the cell cycle

G_2 phase, the cell prepares for mitosis. It has been shown that the there are events in the cell cycle that, if not completed, actually cause inhibition of later cell cycle events.[1] These events have been observed at the transitions between G_1 and S, during S, and

between G_2 and M, and these transitions are therefore referred to as cell cycle checkpoints. Cell checkpoints include mechanisms for preventing DNA replication if cellular nutrition is insufficient, as well as a checkpoint for preventing cell division if the DNA is damaged.[2] The checkpoint for the S/G_1 transition is where cellular DNA is checked for errors after mitosis and repaired if necessary. The cell cycle checkpoints are highly regulated systems, and much work has focused on understanding how the various enzymes work together to allow cell division to occur or to prevent cell division until problems in the cell are solved. Checkpoint kinases 1 and 2 (Chk1 and Chk2) are key enzymes that mediate DNA repair as part of the G_2/M checkpoint, but also play other roles throughout the cell cycle. Our focus is on the role of the checkpoint kinases in promoting cell cycle arrest and DNA repair, so the following is a brief review of the roles of Chk1 and Chk2 in the cell cycle checkpoints.

7.1.2 Review of the Role of Chk1 and Chk2 in the Cell Cycle

Cells encounter many potential problems with their genomic integrity, and these problems must be fixed to ensure the proper function of the cell. These problems can include DNA damage from ionizing radiation or DNA damaging chemicals, random mutations, or even overreplicated DNA. To repair genomic problems, cells have several methods of DNA repair. Some methods require cell cycle arrest in order to prevent a cell from entering another phase of the cell cycle with a compromised genome, while other mechanisms exist for repairing DNA during the S phase. DNA damage detected in the transition between the G_2 and M phases or the S and G_1 phases can activate cellular mechanisms which arrest the cell cycle and allow for DNA repair before mitosis. The

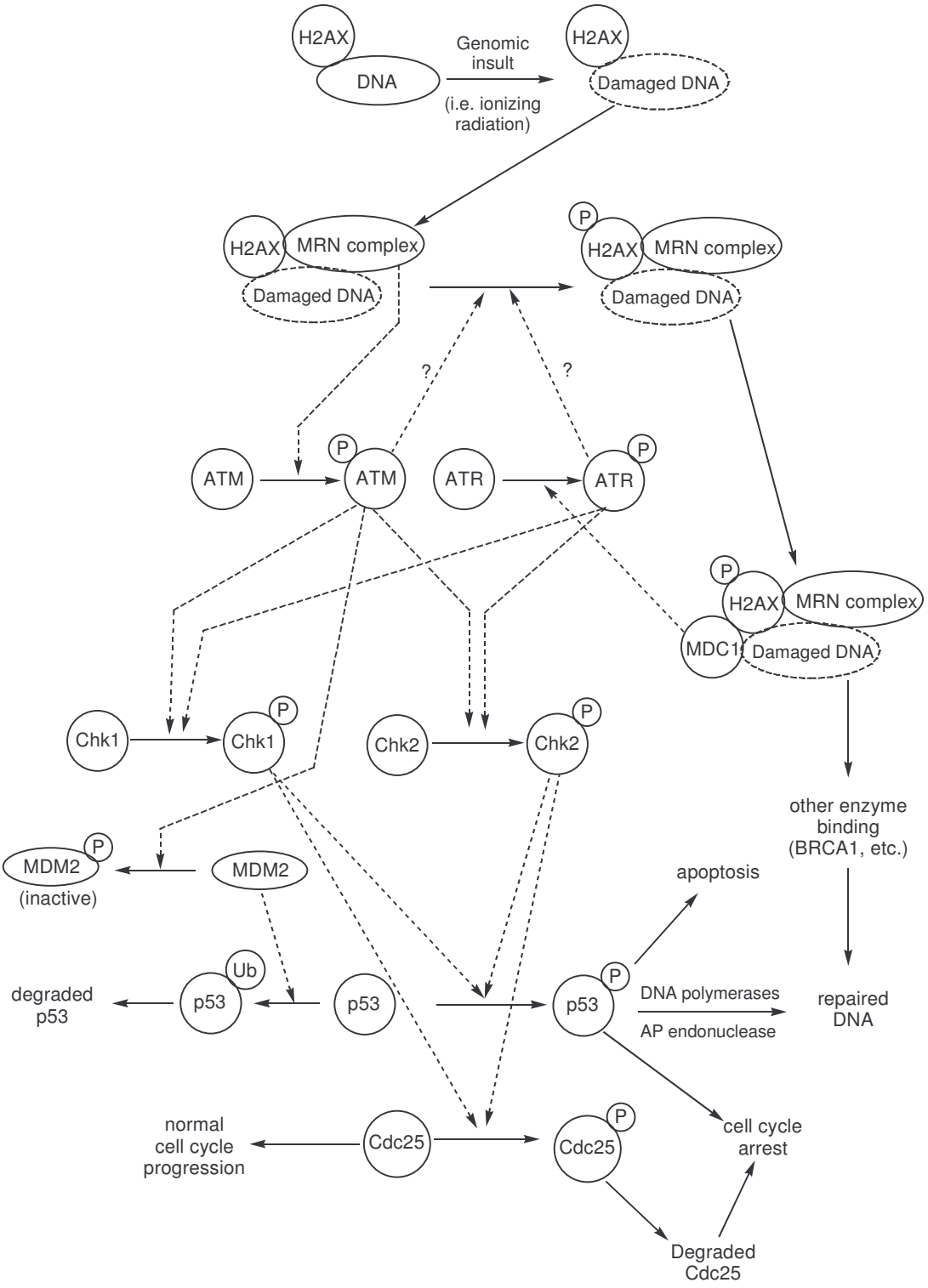

Scheme 7.1: Overview of the DNA damage cell cycle checkpoint[2]

principle enzymes in the G_2/M checkpoint are shown schematically in Scheme 7.1. The connection between DNA damage and cell cycle checkpoints is not well-understood, but it has been conceptualized as consisting of DNA damage sensors, mediators between sensors and signal transducers, signal transducers, and effectors. The roles of particular enzymes in these pathways may overlap between these classifications. For the purposes of understanding the relevance of Chk1 and Chk2 as potential anticancer drug targets, the following is a synopsis of key relationships that to explain this connection based on the current knowledge base.

It is well-known that DNA damage by ionizing radiation or DNA methylating agents activates particular enzymes in the cell nucleus, although specific DNA damage sensors and their connection to cell cycle arrest are not fully understood in mammalian cells. Through studies of both human and *Saccharomyces cerevisiae* yeast cells, progress has been made in elucidating the enzymatic pathways from DNA damage sensors to checkpoint mediators. In humans, the phosphorylated histone variant γ-H2AX, the enzyme MDC1, and the MRN complex (a complex of the enzymes Mre11, Rad9, and Nbs1) have been implicated as important sensors of double-stranded breaks of DNA. One of the first events noticeable after exposure of cells to ionizing radiation is the phosphorylation of the histone H2AX to form γ-H2AX. The MRN complex binds to H2AX , which further promotes the signal of DNA damage. MRN can participate in the activation of the ATM enzyme.[3] ATM and ATR are key mediators of the DNA damage checkpoint, and the phosphorylation of H2AX is likely carried out by enzymes in the PI-3-like family of enzymes, such as ATR or ATM.[4] Once H2AX is phosphorylated to form γ-H2AX, the signaling pathway moves from the sensors to the signal transducers.

γ-H2AX is localized around areas of DNA damage, forming foci that can be visualized *in vitro* by use of antibodies for γ-H2AX.[4] It is believed that γ-H2AX initiates the cellular response to DNA damage and recruits other enzymes to the site of DNA damage such as MDC1, which binds to γ-H2AX, and BRCA1. The role of MDC1 and γ-H2AX could be even more complex, since the exact nature of the requirement for MDC1 for the recruitment of other signal transduction proteins is not fully known.[5] MDC1 then promotes the binding of the MRN complex and plays a role in the activation of ATR, which can phosphorylate Chk1. As mentioned, the MRN complex has been shown to be important for the activation of ATM. Overall, ATM and ATR are believed to be activated by enzymes which bind to the γ-H2AX foci, like MDC1 and BRCA1, and activated ATM and ATR are important mediators of the G_2/M checkpoint response.

The BRCA1 enzyme has received much attention because of the clear link established between BRCA1 and DNA damage. In cells that have the *Brca1* gene removed, which codes for the protein BRCA1, chromosomal errors accumulate. Also, mutations of *Brca1* have been associated with an increased risk of breast cancer in women.[6] BRCA1 is believed to directly interact with DNA in the cell nucleus during S phase DNA replication, and is believed to bind to γ-H2AX foci on damaged DNA. Upon exposure to several different kinds of DNA damaging agents during S phase, BRCA1 is rapidly released from the DNA. At this point, BRCA1 moves to a different part of the nucleus where DNA polymerase δ and ε processivity factors are found. This suggests that the BRCA1 protein may disconnect from the DNA when DNA polymerases are stalled. This stalling occurs as a result of DNA damage, and it is believed that DNA polymerase stalling leads to the phosphorylation and activation of BRCA1.[7] BRCA1 is

believed to mediate the phosphorylation of p53 by ATM and ATR.[8] So, it should be noted that there may be redundancy built into the cell cycle that would allow for activation of p53 in a Chk1- or Chk2-independent manner.

Various types of DNA damage sensors and signal transducers may be in operation for different kinds of DNA damage. The overarching idea is that, whether at the G_1/S transition, the S phase, or the G_2/M transition, DNA damage signals activate ATM and ATR, which then activate Chk1 and Chk2.[9] It has been shown that after DNA damage, the phosphorylation and activation of Chk1 and Chk2 by ATM and ATR depends on the type of DNA damage. For example, ionizing radiation induces phosphorylation of Chk1 and Chk2 by both ATM and ATR. On the other hand, DNA damage by UV radiation causes ATR-dependent phosphorylation of Chk1 and ATM-dependent phosphorylation of Chk2.[10] Overall, this network of signal transduction proteins consists of feedback loops and redundancy that makes the cellular response to DNA damage quick and efficient.

Once Chk1 and Chk2 are activated as a result of DNA damage, the process toward cell cycle arrest begins. One pathway that has been studied thoroughly is p53-mediated cell cycle arrest, and activation of p53 by Chk1 and Chk2 is an important contributor to this pathway. The protein p53 has been identified as an important part of cell cycle arrest, and the mutation of the *P53* gene has been observed in many cancers.[11] The levels of p53 found in the nucleus are kept low by the presence of the protein MDM2. The production of MDM2 is activated by the presence of p53, while at the same time, MDM2 binds to p53 and blocks the domain of p53 that activates MDM2 production.[12] MDM2 also promotes the ubiquitination of p53, a process which leads to the degradation of p53.[13] So, after DNA damage occurs and ATM is activated, two

things occur: first, ATM phosphorylates MDM2, inactivating it; secondly, once Chk1 and Chk2 are activated, these two kinases phosphorylate p53.

It is known that phosphorylated p53 can lead to either cell cycle arrest, which can lead to cell survival after DNA repair, or apoptosis. The combination of the inactivation of MDM2 and the phosphorylation of p53 ensures that high levels of activated p53 are present in the nucleus, which then helps put the "brakes" on the cell cycle. It must also be mentioned that apoptosis can occur in a p53-independent manner, as will be discussed later.

Another part of the brake on the cell cycle is the phosphorylation of Cdc25 kinases by Chk1 and Chk2. The Cdc25 kinases are involved in activating cyclin-Cdk kinases. The cyclin-Cdk kinases are complexes of cyclin with cyclin dependent kinases, and they allow the cell to proceed through the cell cycle normally.[14] Chk1 phosphorylates human Cdc25a at two positions, serine 178 and threonine 507 (S178 and T507), while *Xenopus* Cdc25a is phosphorylated at T504[15] (the checkpoint enzymes of *Xenopus laevis*, the African clawed frog, are very similar to those of humans and are often used as a model system). It has been shown that *Xenopus* Chk1 phosphorylation of Cdc25a at T504 leads to the degradation of Cdc25a through binding with 14-3-3 proteins.[16] Mutation of T504 to alanine results in improved activity of Cdc25a *in vitro*, suggesting that T504 is critical for the inactivation of Cdc25a. This improved activity for mutated Cdc25a also leads to early entry into mitosis before correct DNA replication and error checking can be completed.[17] Thus, the inactivation of Cdc25 enzymes by Chk1 is very important in protecting the integrity of the genome during the cell cycle.[18]

Once cell cycle arrest has occurred because of DNA damage, the normal cell either repairs the damage or enters apoptosis. Once activated, p53 has been shown to be active in promoting DNA repair. For example, a role for p53 has been suggested in nucleotide excision repair, the repair of a damaged nucleotide, through the activation of the p48 gene. Also, there is evidence that p53 interacts directly with DNA polymerase β and AP endonuclease, two enzymes that cooperate in base excision repair (BER), the repair of a single damaged DNA base. In cells depleted of p53, BER is reduced, suggesting that p53 promotes BER. At the same time, tumor-derived mutated p53 has been shown to have no stimulatory effect on BER,[19] once again implicating p53 mutation in tumorigenesis. So, through a complex network of enzymatic pathways, various kinds of DNA damage can lead to the activation of Chk1 and Chk2, which then help initiate cell cycle arrest. This is accomplished through, but not limited to, p53 activation and Cdc25 inactivation, both of which lead to cell cycle arrest and an opportunity for either DNA repair or apoptosis.

An important point is that, although Chk1 and Chk2 have very similar substrate requirements,[20] the two proteins are structurally dissimilar and have differing functions. It has been shown that Chk1 is activated during mitotic stress, but Chk2 is not,[21] and Chk1 is required for murine embryonic viability while Chk2 is not.[22] Chk2 seems to play its critical role only when DNA damage appears.[23] Chk1 is involved in the response to DNA damage during DNA replication as well as at the G_2/M transition, while Chk2 plays a role mainly at the G_2/M transition.[24,25] This would suggest that Chk1 and Chk2 are fundamentally different kinds of drug targets. Therefore, the therapeutic usefulness of Chk1 and Chk2 inhibitors would be expected to be different. It has been shown that,

following DNA damage, Chk2 inhibition accomplished through either a Chk2-deficiency mutation or through chemical inhibition by use of debromohymenialdisine promotes a specific kind of apoptosis during mitosis in a p53-independent manner in an engineered HeLa cell line following DNA damage.[26] DNA damage followed by Chk2 inhibition could lead to apoptosis through p53, but if the tumor cells have a mutated p53 protein, they may possess resistance to apoptosis.[27] Thus, Chk2 inhbition that leads to p53-independent apoptosis could potentiate the activity of a DNA damaging agent while cancelling out the survival-promoting effects of mutated p53.

It has also been recently reported that a Chk1 inhibitor developed by Pfizer potentiates the activity of gemcitabine, irinotecan, and cis-platin in certain tumor models.[28] Also, Chk1 inhibition has been found to act synergistically with farnesyl transferase inhibitors in inducing apoptosis in human leukemia cells.[29] Together, the available studies of Chk1 and Chk2 demonstrate that both are viable targets for combination drug therapy for cancer. Because of the clear potential for Chk1inhibitors demonstrated in cell models, the Kingston group has recently set out to discover novel Chk1 inhibitors.

7.1.3 Purpose for the Study of Chk1 Substrate Length Requirements

Because Chk1 is an interesting target for antitumor drug discovery, we decided to include a Chk1 bioassay as part of our natural products isolation program. Initially, we wished to implement an assay for Chk1 that would be more cost-effective than commonly available assay methods, such as radioactive ATP methods[30] or ELISA methods. After initial work with a new method involving colorimetric detection of

phosphorylation[31] proved fruitless, a new method marketed by the Molecular Devices Corporation was picked as the primary assay method for Chk1 in our lab. We decided that there was still something to be learned regarding the substrate specificity of Chk1 from our initial work, so the project was directed more towards studying the substrate specificity of Chk1. The preparation of shorter peptide substrates is quicker, less expensive, and higher yielding than that of longer peptide substrates. Therefore, for future assays that might be developed for Chk1 that are less expensive than current methods, shorter peptide substrates are desirable. So, we set out to synthesize small libraries of peptides, and test the libraries of peptides for their usefulness as substrates for Chk1.

There has been previous study of the substrate specificity of human Chk1. Chk1 is able to phosphorylate a number of substrates *in vivo*, but one important substrate is Cdc25C. Peptides representing partial sequences of Cdc25C from both human and *Xenopus* forms of Cdc25C have been shown to be good substrates for Chk1, with the *Xenopus* peptide being a slightly better substrate for human Chk1 than the human peptide. The sequence for the *Xenopus* peptide is RLYRSP**S**MPEKLDRK, where the emboldened letter represents the phosphorylated residue. Previous work showed that the minimum sequence for substrate recognition by Chk1 consisted of a six-residue domain represented as ϕ-X-β-X-X-(**S/T**), where ϕ represents a hydrophobic residue such as Leu, Ile, or Met, β-represents a nitrogen-containing residue such as Lys or Arg, and Ser or Thr are required at the site of phosphorylation.[30]

O'Neill *et al.* followed up on the work of Hutchins and characterized the activity of synthetic peptide substrates of Chk1 and Chk2. The authors found the optimum

sequence to be that of a Cdc25A-based peptide, CSPLKRSH**S**DSLDH. This sequence, though different from the Cdc25C-based peptide, still includes the ϕ-X-β-X-X-(**S/T**) motif (underlined) shown by Hutchins to be required for peptide activity. O'Neill also showed that the substrate specificity of Chk1 and Chk2 is not the same. The "Akt-tide" AKRERAY**S**FGHHA, a peptide sequence derived from the Chk1 substrate protein Akt, was shown to be specifically phosphorylated by Chk1, but not Chk2. Interestingly, the Akt-tide does not fully match the optimum motif.[30] To our knowledge, no systematic studies of the length dependence for Chk1 substrates, or the substrate specificity of short substrates have been published.

Progress towards the development of peptide-based Chk1 inhibitors was another impetus for this study. It has been shown previously that peptide-based inhibitors based on the Cdc25C sequence can sensitize leukemia cells to the DNA damaging effects of bleomycins. The peptide sequences studied were 22-residue peptides; 11 residues consisted of a sequence derived from HIV-Tat, a transcription activator from HIV, while the other 11 residues were derived from the Cdc25C sequence. One of the peptides possessed an alanine rather than serine at the phosphorylated residue, while the other had the phosphorylated serine. Interestingly, the two peptides had similar abilities to sensitize leukemia cells to bleomycins.[32] This might suggest that these peptides do not act as transition-state mimics, but inhibit Chk1 by some other mechanism. So, further work towards understanding the interactions of substrates with Chk1 might aid in the development of novel peptide-based inhibitors.

7.2 Results and Discussion

7.2.1 Sequence Design and Synthesis

The libraries of peptides synthesized in this study were based on the sequence of the Cdc25C enzyme from *Xenopus laevis*. Cdc25C is a member of the Cdc25 family of phosphatases. Because it was previously found that Ser-285 of Cdc25C is neither phosphorylated nor required for activity, the serine two residues upstream of the phosphorylated residue was included in the sequences studied. In order to study both the substrate activity dependence on both length and sequence specificity, two libraries of peptides were designed. The first library consisted of fifteen peptides, where the sequence length was varied from six to fifteen residues while maintaining the portion of the Cdc25C sequence shown to be required for activity.[30] The second library was made up of seven- and eight-residue peptides which were also based on the minimum sequence required for activity, but the residues were varied at the positions ϕ, β, and **S/T** as discussed above. One positive and one negative control rounded out the set of peptides. The sequences of the peptides are shown in Table 7.1.

The peptides were synthesized by standard solid phase peptide synthesis (SPPS) methods,[33] and the peptides were purified by reverse phase HPLC. A typical synthesis using SPPS is shown schematically in Scheme 7.2. Initially, Rink amide resin is employed as a polymer support; this particular resin is used so that the final peptide product will possess a carbamate rather than a carboxylic acid at the C-terminus following cleavage from the resin. Fluorenyl methoxy carbonyl (Fmoc)-protected Rink amide resin (**1**) is initially deprotected to give the resin with a free amine **2**. The resin is then treated with a desired Fmoc-protected amino acid in the presence of the coupling

Table 7.1: Sequences and MALDI-TOF data for synthesized Chk1 substrate peptides

		Sequence	Expected MALDI-TOF MS [M+H]	Observed MALDI-TOF MS [M+H]
	7.1[+]	R L Y R A P G M P E K L D R K	1871.0	1871.6
	7.2[†]	R L Y R A P S M P E K L D R K	1901.1	1902.3
Library 1	**7.3**	R L Y R S P S M P E K L D R K	1917.0	1917.3
	7.4	R L Y R S P S M P E K L D R	1789.0	1789.0
	7.5	R L Y R S P S M P E K L D	1632.9	1633.8
	7.6	R L Y R S P S M P E K	1404.7	1405.1
	7.7	R L Y R S P S M P E	1276.6	1276.6
	7.8	R L Y R S P S M P	1147.6	1147.6
	7.9	R L Y R S P S M	1050.6	1050.3
	7.10	R L Y R S P S	919.5	919.4
	7.11	L Y R S P S M P E K L D R K	1760.9	1762.0
	7.12	L Y R S P S M P E K L D R	1632.9	1633.5
	7.13	L Y R S P S M P E K L D	1476.8	1477.4
	7.14	L Y R S P S M P E K L	1361.7	1362.8
	7.15	L Y R S P S M P E K	1248.6	1249.3
	7.16	L Y R S P S M P E	1120.5	1120.8
	7.17	L Y R S P S	763.4	763.2
Library 2	**7.18**	M Y R S P S M P	1009.5	1010.6
	7.19	I Y R S P S M P	991.5	991.6
	7.20	L Y R S P S M P	991.5	992.6
	7.21	M Y K S P S M P	981.5	981.6
	7.22	I Y K S P S M P	963.5	965.2
	7.23	L Y K S P S M P	963.5	964.0
	7.24	M Y R S P T M P	1023.5	1023.7
	7.25	I Y R S P T M P	1005.5	1005.7
	7.26	L Y R S P T M P	1005.5	1005.9
	7.27	M Y K S P T M P	995.5	995.6
	7.28	I Y K S P T M P	977.5	977.2
	7.29	L Y K S P T M P	977.5	977.1
	7.30	M Y R S P S M	912.4	914.3
	7.31	L Y R S P S M	894.5	894.9
	7.32	I Y R S P S M	894.5	893.7
	7.33	M Y K S P S M	907.4 *	906.9 *
	7.34	L Y K S P S M	889.4 *	890.2 *
	7.35	I Y K S P S M	866.4	865.9
	7.36	M Y R S P T M	926.4	927.3
	7.37	L Y R S P T M	908.5	909.0
	7.38	I Y R S P T M	908.5	908.5
	7.39	M Y K S P T M	898.4	899.5
	7.40	L Y K S P T M	880.5	881.7
	7.41	I Y K S P T M	880.5	880.3

+ = Negative control
† = Positive control
* = Sodium adducts observed

agent HBTU and the anti-racemizing agent HOBT, which introduces an amide bond attached to the resin as in **3**. However, the reaction does not go to 100% completion, so there is a very small amount of unreacted **2** left over. The mixture of **2** and **3** are treated with acetic anhydride to cap the unreacted amines in **2**; Fmoc-protected **3** is not acetylated, while **2** is acetylated to form **4**. This amide does not react further. Previous work from the literature has shown that impurities in crude SPPS product mixtures often include the desired peptide that has not been fully deprotected.[34] Another concern in

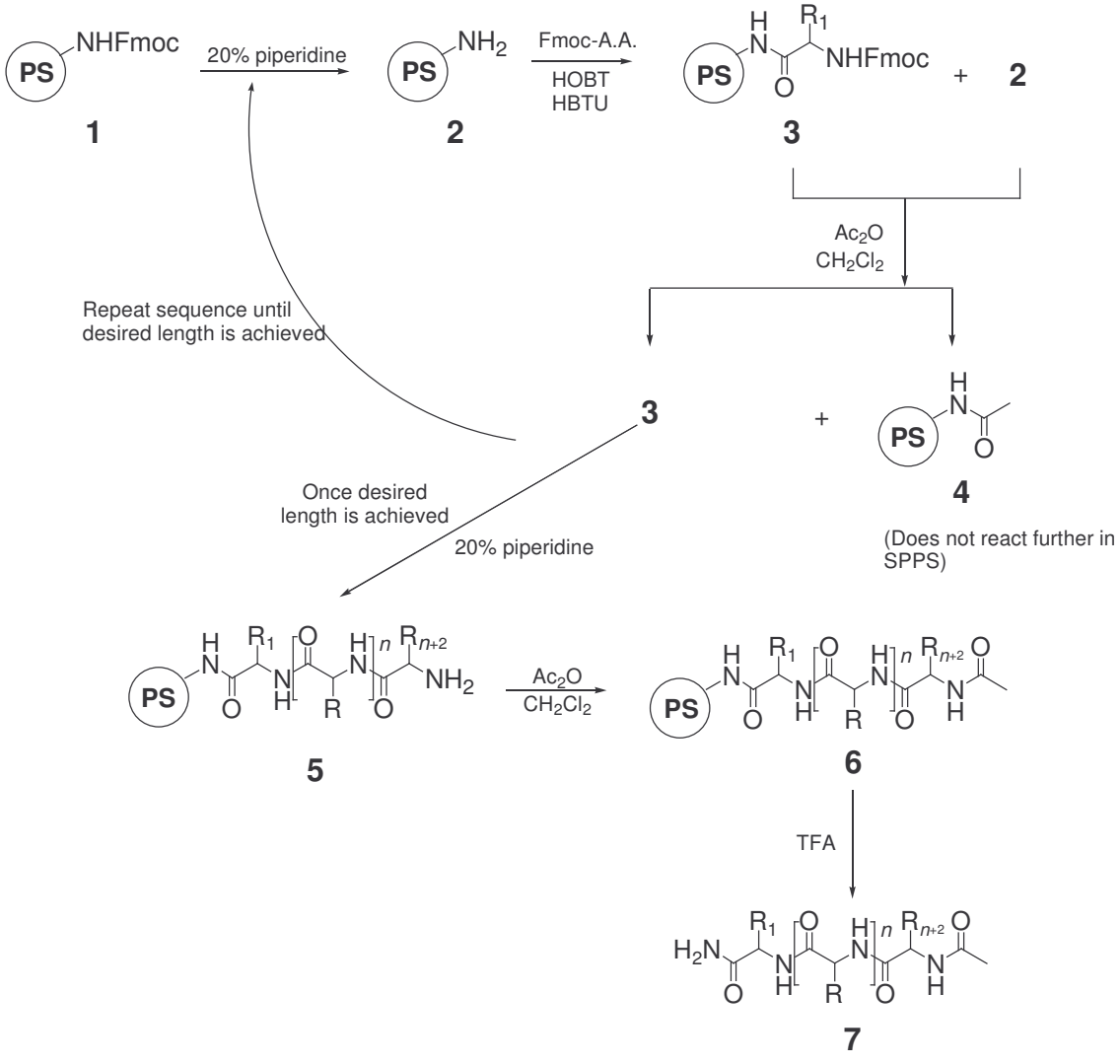

Scheme 7.2: Synthetic Scheme for Solid Phase Peptide Synthesis

SPPS is the formation of deletion sequences, where a deprotected amine fails to react in an initial coupling reaction, but reacts in a second coupling reaction with a different residue. This acetic anhydride capping is employed to overcome these problems.[35] in order to inactivate unreacted amines after each amide coupling reaction. Thus, unreacted amines do not enter into further amide coupling reactions, and the purity of the final product peptide can be increased.

This cycle of deprotection, coupling, and capping is repeated until the peptide has the desired length. At this point, the terminal amine is deprotected with piperidine to afford the resin-bound product **5**, which is followed by acetic anhydride capping of the N-terminal amine to form **6**. Cleavage of the peptide from the resin was performed using a "cocktail" consisting of trifluoroacetic acid (TFA), H_2O, and triisopropylsilane (TIPS-H). When appropriate sidechain protecting groups are chosen, use of this cocktail simultaneously cleaves the peptide from the resin while also deprotecting the sidechains of the peptides, to afford peptide product **7**.

From peptide synthesis, the crude yields of peptides were about 50% by mass, while the desired peptides typically made up about 50% of the crude products, based on integration of the chromatograms. Crude peptide mixtures were fractionated by HPLC, and the desired peptides typically were the major products in each crude mixture. The peptides were lyophilized, and the major products were characterized by matrix-assisted laser desorption ionization-time of flight (MALDI-TOF) mass spectrometry. Because of the systematic nature of SPPS and the suppression of deletion sequences by acetic anhydride capping during SPPS, the peptides synthesized had the sequences imparted by the ordered addition of reagents, which was carried out very carefully in order to achieve

specific desired sequences. Thus, if the experimentally determined mass for a peptide was identical to that expected, the sequence was assumed to be that which was desired.

After confirming the identity for each peptide, the peptides were prepared for bioassay. The peptides were diluted to produce stock solutions, the UV absorbance of the stock was checked, and a final sample was prepared at a concentration of 1 mM for each peptide based on the stock concentration calculated from UV analysis.

The activity of each peptide was measured by Mr. Ian Auckland in the laboratory of Dr. Jill Sible (Department of Biology, Virginia Tech), using an assay which measures incorporation of a radiolabelled phosphate group from [γ-^{32}P]-ATP into a substrate peptide. Kinase reactions for each peptide were allowed to incubate, quenched, and a sample of each reaction mixture was added to cation-exchange chromatography paper. Basic sidechain residues allowed peptides to bind to the cation-exchange paper, while other phosphate sources were washed off the paper. The level of [γ-^{32}P]-ATP incorporation into the bound peptides was determined by measuring the radioactivity of the cation-exchange paper by a Cerenkov counter. A blank sample, which consisted of only washed cation-exchange paper, was also included to provide a background reading. A positive control and a negative control peptide were synthesized and included for comparison, and a second positive control was used, the known Chk1 substrate RLYRAPSMPEKLDRK, where the N-terminus was not acetylated and the C-terminus was not amidated. This peptide will be referred to as "p1860," in reference to its molecular weight.

7.2.2 Assay Results

In an initial assay, the substrate activities for all 41 peptides towards Chk1 were measured in single-sample assays. Thereafter, the activities of selected peptides from Library 1, where the peptide lengths were scanned from 9 to 15 residues, were re-tested in duplicate to confirm the positive results. The average values of the activities for peptides **7.1**-**7.17** are shown in Figure 7.2, while the data for peptides **7.18**-**7.41** are shown in Figure 7.3. The dotted line on the left represents the activity of the negative control **7.1**, which corresponds to zero phosphorylation, while the dotted line on the right represents the activity of p1860. Peptides with activity over that of the negative control were considered to be active. Overall, peptide **7.2** was the most active, while peptides **7.3**, **7.6**, and **7.11** were all comparably active, retaining much of the activity of **7.2**. Both **7.2** and **7.3** had been previously shown to be active in a Chk1 assay.[30] Peptides **7.6** and **7.13** were the shortest peptide to possess activity above the negative control, both possessing 11-residue sequences. The negative control displayed apparent substrate activity in this assay for unknown reasons, so peptide activity was judged based on the threshold activity of **7.1** (indicated as the left dotted line on the graphs in Figures 7.2 and 7.3.). Perhaps this peptide is able to strongly bind through coulombic attractions to a radioactive ATP molecule while also binding to the cation exchange paper, resulting in apparent phosphorylation. The general trend for the activity of these peptides was that the shorter the peptide, the lower the level of phosphorylation. To our knowledge, this is the first time that peptides with fewer than 15 residues have shown activity as a substrate for Chk1, and we have demonstrated this activity for two separate 11-residue peptides.

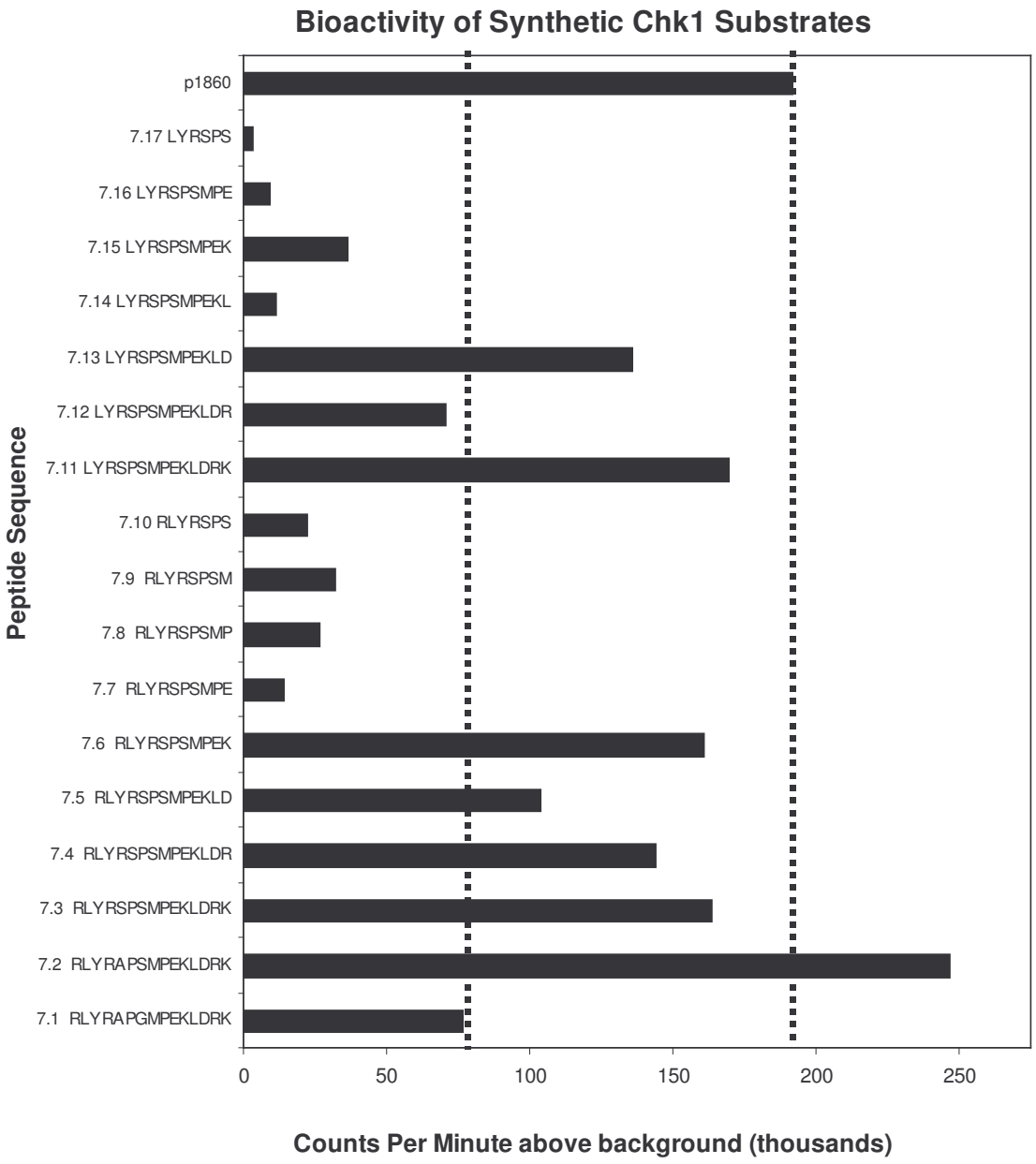

Figure 7.2: Kinase assay data for synthetic Chk1 peptide substrates from library 1 Peptides **7.1**-**7.17**, **7.19**, **7.31**, and p1860 were run three times to find an average activity, while all other peptides were tested in single runs. Peptide sample numbers are found in Table 7.1.

Disappointingly, the measured activities of peptides **7.18**-**7.41** were all below that of the negative control. There was not a discernible sequence dependence, since all the activity values were very similar. These results prompted us to wonder if the inactivity of

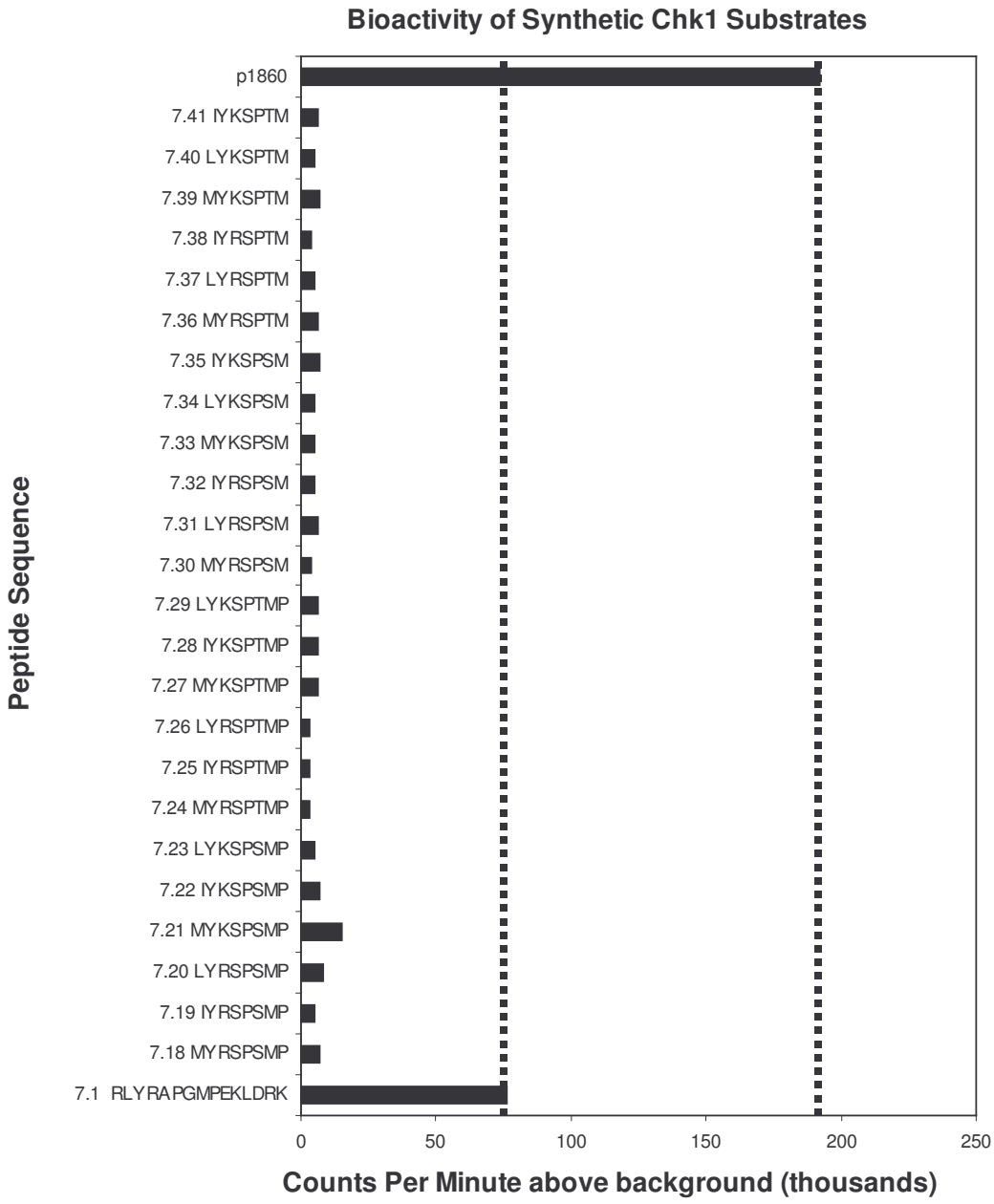

Figure 7.3: Kinase assay data for synthetic Chk1 peptide substrates from library 2 Peptides **7.1** and p1860 were run three times to find an average activity, while all other peptides were tested in single runs. Peptide sample numbers are found in Table 7.1.

the smaller peptides was truly based on their shorter structures, or if the assay detection method was somehow selecting longer peptides as having better activity by default. That

is, would longer substrates bind to the cation-exchange paper better than shorter peptides?

Upon further review of the assay method, it appeared that shorter peptides with less than three basic sidechain residues (K or R in our case) would not bind well to the cation exchange paper used to bind phosphorylated peptides for Cerenkov counting, with the exception of **7.13**, which possessed two basic sidechains. Let us consider peptide **7.18** (sequence: MYRSPSMP). In solution at pH 7, the arginine (R) sidechain is protonated, giving the peptide an overall positive charge. If the peptide is phosphorylated by Chk1, a phosphate is attached to only one of the serines. At pH 7, this phosphate is negatively charged, giving the peptide an overall neutral charge in solution. The cation-exchange paper, which uses cellulose phosphate as the cation-exchanger, will only bind to peptides which have an overall positive charge. So, only peptides with more than one basic residue will bind well to the cation exchange paper and therefore give meaningful data.[36] Also, peptides with additional positively charged sidechains might be expected to bind even stronger than peptides with two positively charged sidechain.

Overall, a correlation can be observed between peptide bioactivity and the number of basic sidechains in the peptide. Figure 7.4 shows a graph of peptide activity as a function of the number of arginines or lysines for the corresponding peptide. Clearly, even though there is variability of activity amongst peptides with the same number of basic sidechains, it appears that there is an underlying positive correlation between peptide activity and the number of basic sidechains in the peptides. We argue that peptides with fewer basic sidechains are unable to bind as well as longer peptides with

more basic residues, and so this particular assay method is inadequate for evaluating these libraries of peptides.

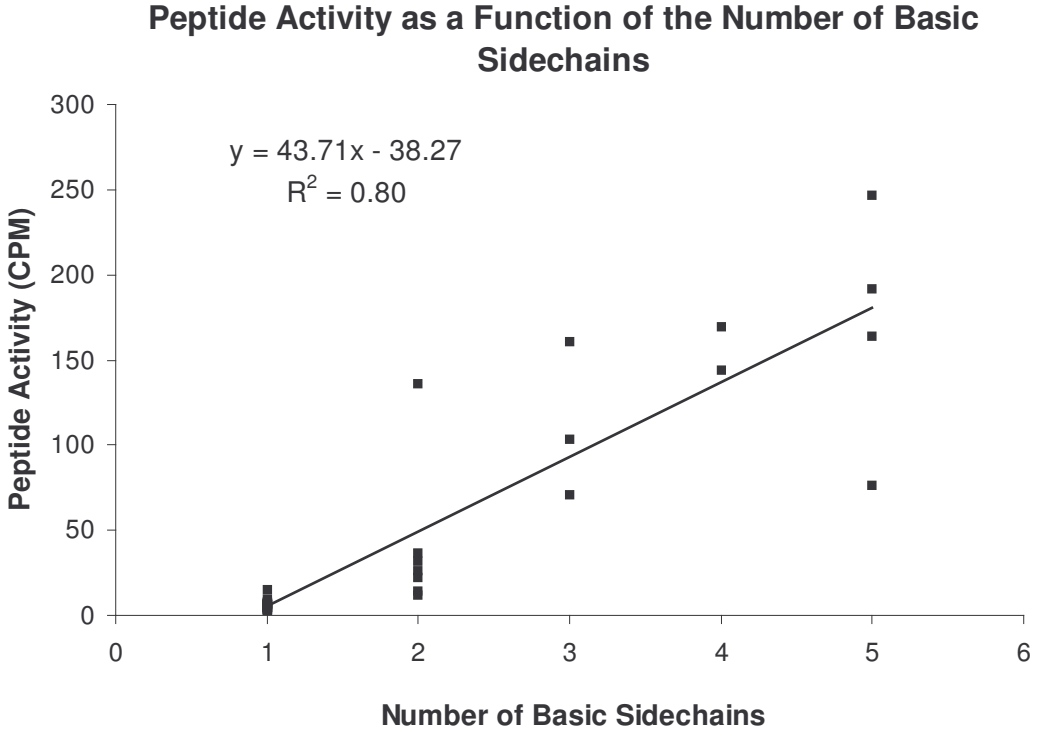

Figure 7.4: The relationship between peptide activity and basic sidechain count.

So, are the peptides in Library 2 being phosphorylated or not? Since **7.1** has five basic sidechain residues, it would be expected to bind to the cation exchange paper regardless of its phosphorylation level. However, serine phosphorylation is not possible. At the same time, the small peptides from Library 2 would also be expected to bind to the paper if they were not phosphorylated. Since the activities of **7.1** and the peptides from Library 2 differ so much, it appears that the peptides from Library 2 are not binding to the cation exchange paper at all. This implies that the peptides from Library 2 are indeed being phosphorylated. We therefore propose that the reason that the peptides from Library 2 give such apparently weak activities is because they are being phosphorylated by Chk1, which actually precludes binding to the cation exchange paper. Thus, the

activities of peptides from Library 2 are all below that of **7.1**, which is representative of a peptide with no sidechain phosphorylatable by Chk1. Only further testing with a different assay method would verify this proposal.

At the same time, we can observe some sequence length-activity dependence for peptides that have three or more basic sidechains. The activities of **7.7**-**7.10**, and **7.14**-**7.15** are significantly less active than similar peptides which are longer (i.e. **7.2-7.5**, **7.12**), while still remaining more active than peptides in Library 2. Based on the presence of basic sidechains in these peptides, we can safely say that these peptides evidently do not fit the substrate requirements of Chk1 as well as longer peptides like **7.2**. It might be possible that useful substrates require a longer sequence in order to have the best binding between substrate and enzyme. We believe that this work demonstrates that there are intermolecular forces between the residues further away from the site of phosphorylation that may not be residue specific, yet may play an important role in substrate-enzyme interactions. These non-specific interactions would not be elucidated by study of 15-residue peptides, where the interactions would be present for all peptides (such as in the work of Hutchins *et al.*[30]). Yet, once shorter peptides are analyzed, and these interactions are varied, their significance becomes more pronounced.

At this point, because the short peptides tested for Chk1 activity do not have significant activity as substrates in our assays, we are unable to conclude that any of the shorter sequences could be used as a motif for the design of a simpler bioassay. Previous work in the area of designing simplified kinase assays for protein kinases A and C showed that attaching an amino acid with a fluorescent, metal chelating sidechain to a peptide, could allow for the detection of phosphorylation by fluorescence. The peptides

consisted of either 5 or 10 residues connected by a 2-residue β-turn to the fluorescent amino acid Sox (**7.43**).[37] Based on our findings with Chk1, more work will be needed to see if phosphorylation by Chk1 can be detected with short substrates by this method.

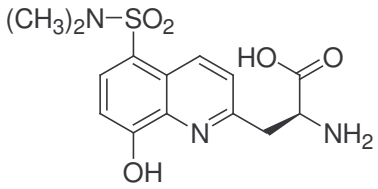

7.43: Sox

7.3 Experimental Section

7.3.1 Peptide Synthesis

All peptides were synthesized by use of standard solid-phase peptide synthesis with Fmoc-protected amino acids. The resin was initially swelled by the addition of CH_2Cl_2, followed by washing with NMP. After deprotection of the resin with 20% piperidine in NMP and washing with NMP, coupling reactions were performed by the following general procedure: 3 equivalents each of HOBT, HBTU, and the Fmoc-amino acid were dissolved in NMP and added to the resin, and agitated for 45 min. After NMP washing of the resin, 10% Ac_2O-10% DIEA solution in CH_2Cl_2 was added and agitated for 20 min. After washing with NMP, 20% piperidine in NMP was added to deprotect the amino acid coupled to the resin. This procedure was repeated until the peptide had the desired length. Once the final residue was coupled, the Fmoc group was removed by 20% piperidine in NMP, washed with NMP, and 10% Ac_2O-10% DIEA solution was added to cap the N-terminus of the peptide. The resin was washed with NMP, followed by ethyl ether, and dried under nitrogen. After drying, a 95:2.5:2.5 solution of TFA:H_2O:TIPS was added to cleave peptides from the resin and to deprotect the peptide

sidechains. The cleavage step was agitated for 2 hours. The TFA solution was then eluted from the reaction vessels, and the crude peptides were precipitated by addition of cold ether. The peptides were centrifuged, and the supernatant was pipetted away. This was repeated three times for each peptide. The crude peptides were off-white solids that turned into greenish oils upon exposure to air, apparently from uptake of water. (This change was reversible by dissolving the crude samples in DMSO, followed by lyophilization.) The remaining TFA was removed under a stream of nitrogen.

7.3.2 Peptide Purification, Characterization, and Sample Preparation

All peptides were purified by reverse phase C_{18} HPLC (Vydac, 250 mm × 10mm, 300 Å pore size, 5 μm particle size) using either an isocratic elution of 2:8 acetonitrile:water ratio, with 0.1% TFA as a modifier, or a gradient elution of 17%-25% $MeCN_{(aq)}$ with 0.1% TFA as a modifier over 25 min. All major components from each crude peptide product were collected.

The identities of the desired peptides were confirmed by MALDI-TOF mass spectrometry. The major component of each purification was characterized, and in nearly every case was identified as the desired peptide. In two cases, the major components did not correspond to the desired peptides; thus, minor components purified from the crude mixtures were subsequently identified as the desired peptides by MALDI-TOF MS.

MALDI-TOF analysis was performed using a Kratos PCKompact SEQ V1.2.0 instrument operating in a linear mode. Peptides were diluted to approximately 200 μM in water. A saturated solution of dihydroxybenzoic acid in acetonitrile was prepared as a matrix. For sample analysis, 5 μL of matrix solution was added to a slot on a MALDI

analysis plate. From the peptide solution, 5 μL was added to the matrix droplet. This droplet was allowed to dry. Upon drying, the sample plate was loaded into the instrument and analyzed. The laser intensity was adjusted for each sample to achieve the best signal-to-noise ratio, while the instrument scanned over a range of laser angles. The mass information was smoothed using the instrument software. The instrument was calibrated using a synthetic Chk1 substrate peptide kindly provided by Dr. Felicia Etzkorn.

To prepare solutions of peptides with known concentrations for bioassay, peptide stock solutions were analyzed by UV spectrophotometry and diluted accordingly. The value of the molar absorptivity for each peptide was assumed to be approximately equal to that of tyrosine, which is $\varepsilon = 1{,}420\ cm^{-1} \cdot M^{-1}$ at 274 nm. A stock solution of each peptide was prepared using ultrapure water, and a 1:15 diluted sample was prepared. The UV absorbance for each diluted sample was measured, and the concentration of the stock solution was determined. With this information, a sample of each peptide was prepared at a concentration of 1.0 mM by dilution of the stock solution. These solutions were submitted for the Chk1 bioassay.

7.3.3 Chk1 Assay Conditions

The Chk1 bioassay was performed by Mr. Ian Auckland in the laboratory of Dr. Jill Sible in the Department of Biology at Virginia Tech, and the procedure is summarized here for completeness. First, an aqueous stock solution of ATP was prepared. To prepare a stock solution for 50 samples, the solution included: 50 μL of 0.1 M EGTA (ethylene glycol-bis(2-aminoethylether)-*N,N,N′,N′*-tetraacetic acid); 20 μL of 1

M HEPES (pH 7.5); 15 µL of 1 M $MgCl_2$; 1 µL of 1 M DTT (dithiothreitol); 20 µL 10 mg/mL BSA (bovine serum albumin); 20 µL of 10 µM ATP; 1 µL of 250 µCi/mL [γ-^{32}P]-ATP; and 673 µL of H_2O. Next, 2 µL of 1mM peptide substrate solution was added to a 1.5 mL centrifuge tube, and 18 µL of the radioactive ATP stock solution was added. Finally, 1 µL of 80 nM Chk1 (Upstate) was added to the centrifuge tube for a final concentration of approximately 4 nM of Chk1. The solution was briefly vortexed, and the reaction was allowed to proceed for 20 minutes in a 27^{o}C waterbath.

At the end of the reaction time, 20 µL of 50% glacial acetic acid was added to terminate the reaction, and the sample was vortexed. From this mixture, 30 µL was taken and spotted onto a pre-cut square piece of P81 cellulose phosphate cation-exchange chromatography paper (Whatman). This sample is allowed to dry. The paper squares were then placed in a metal wire basket and soaked in 75 mM phosphoric acid, 10 mL of solution per square. This wash was performed in the following sequence: one wash for five minutes to remove the majority of the [γ-^{32}P]-ATP present on the paper, and three washes at 15 minutes each to complete the wash. After a final five-minute wash in acetone, the squares were allowed to dry. The dry squares were then placed into scintillation vials, 4 mL of scintillation cocktail was added, and the radioactivity of the samples was measured by a Cerenkov counter. Peptides were tested either as single samples or in duplicate. The radioactivity is reported in counts per minute from the Cerenkov counter.

References for Chapter 7

1. Hartwell, L.H.; Weinert, T.A. Checkpoints: Controls that Ensure the Order of Cell Cycle Events. *Science* **1989**, *246,* 629-634.

2. Novák, B.; Sible, J.C. Tyson, J.J. "Checkpoints in the Cell Cycle." In: *Nature Encyclopedia of Life Sciences*. London: Nature Publishing Group, 2002. Accessed from http://www.els.net/, February 20, 2005. [doi:10.1038/npg.els.0001355].

3. Uziel, T.; Lerenthal, Y.; Moyal, L.; Andegeko, Y.;Mittelman, L.; Shiloh, Y. Requirement of the MRN complex for ATM activation by DNA damage. *EMBO J.* **2003**, *22*, 5612-5621.

4. Paull, T.T.; Rogakou, E.P.; Yamazaki, V.; Kirchgessner, C.U.; Gellert, M.; Bonner, W.M. A Critical Role for Histone H2AX in Recruitment of Repair Factors to Nuclear Foci after DNA Damage. *Curr. Biol.* **2000**, *10*, 886-895.

5. Stewart, G.S.; Wang, B.; Bignell, C.R.; Taylor, A.M.R.; Elledge, S.J. MDC1 is a Mediator of the Mammalian DNA Damage Checkpoint. *Nature* **2003**, *421*, 961-968.

6. Deng, C.-X.; Wang, R.H. Roles of BRCA1 in DNA Damage Repair: a Link Between Development and Cancer. *Hum. Mol. Genet.* **2003**, *12*, R113–R123.

7. Scully, R.; Puget, N.; Vlasakova, K. DNA Polymerase Stalling, Sister Chromatid Recombination and the BRCA Genes. *Oncogene* **2000**, *19*, 6176-6183.

8. Fabbro, M.; Savage, K.; Hobson, K.; Deans, A.J.; Powell, S.N.; McArthur, G.A.; Khanna, K.K. BRCA1-BARD1 Complexes Are Required for p53Ser-15 Phosphorylation and a G_1/S Arrest following Ionizing Radiation-induced DNA Damage. *J. Biol. Chem.* **2004**, *279*, 31251-31258.
9. Iliakis, G.; Wang, Y.; Guan, J.; Wang, H. DNA Damage Checkpoint Control in Cells Exposed to Ionizing Radiation. *Oncogene* **2003** *22*, 5834-5847.

10. Helt, C.E.; Cliby, W.A.; Keng, P.C.; Bambara, R.A.; O'Reilly, M.A. Ataxia Telangiectasia Mutated (ATM) and ATM and Rad3-related Protein Exhibit Selective Target Specificities in Response to Different Forms of DNA Damage. *J. Biol. Chem.* **2005**, *280*, 1186-1192.

11. Hollstein, M.; Sidransky, D.; Vogelstein, B.; Harris, C.C. p53 Mutations in Human Cancers. *Science* **1991**, *253*, 49-53.

12. Steinman, H.A.; Hoover, K.M.; Keeler, M.L.; Sands, A.T.; Jones, S.N. Rescue of Mdm4-deficient Mice by Mdm2 Reveals Functional Overlap of Mdm2 and Mdm4 in Development. *Oncogene* **2005**, 1-6. Advance online publication.

13. Maya, R.; Balass, M.; Kim, S.-T.; Shkedy, D.; Leal J.F.M., Shifman, O.; Moas, M.; Buschmann, T.; Ronai, Z.; Shiloh, Y.; Kastan, M.B.; Katzir, E.K.; Oren, M. ATM-dependent Phosphorylation of Mdm2 on Serine 395: Role in p53 Activation by DNA Damage. *Genes Dev.* **2001**, *15*, 1067-1077.

14. Obaya, A.J.; Mateyak, M.K.; Sedivy, J.M. Mysterious Liaisons: the Relationship Between c-Myc and the Cell Cycle. *Oncogene* **1999** *18*, 2934-2941

15. Uto, K; Inoue,D.; Shimuta, K.; Nakajo, N.; Sagata, N. Chk1, but not Chk2, Inhibits Cdc25 Phosphatases by a Novel Common Mechanism. *EMBO Journal* **2004** *23*, 3386-3396.

16. Chen, M.-S.; Ryan, C.E.; Piwnica-Worms, H. Chk1 Kinase Negatively Regulates Mitotic Function of Cdc25A Phosphatase Through 14-3-3 Binding. *Mol. Cell. Biol.* **2003**, *23*, 7488-7497.

17. Uto, K; Inoue, D.; Shimuta, K.; Nakajo, N.; Sagata, N. Chk1, but not Chk2, Inhibits Cdc25 Phosphatases by a Novel Common Mechanism. *EMBO J.* **2004**, *23*, 3386-3396.

18. Xiao, Z.; Chen, Z.; Gunasekera, A.H.; Sowin, T.J.; Rosenberg, S.H.; Fesik, S.; Zhang, H. Chk1 Mediates S and G_2 Arrests through Cdc25A Degradation in Response to DNA-damaging Agents. *J. Biol. Chem.* **2003**, *278*, 21767-21773.

19. Zhou, J.; Ahn, J.; Wilson, S.H.; Prives, C. A role for p53 in base excision repair. *EMBO J.* **2001**, *20*, 914-923.

20. O'Neill, T.; Giarratani, L.; Chen, P.; Iyer, L.; Lee, C.-H.; Bobiak, M.; Kanai, F.; Zhou, B.-B.; Chung, J.H.; Rathbun, G.A. Determination of Substrate Motifs for Human Chk1 and hCds1/Chk2 by the Oriented Peptide Library Approach **2002**, *277*, 16102-16115.

21. Ng, C.P.; Lee, H.C.; Ho, C.W.; Arooz, T.; Siu, W.Y.; Lau, A.; Poon, R.Y.C. Differential Mode of Regulation of the Checkpoint Kinases CHK1 and CHK2 by Their Regulatory Domains. *J. Biol. Chem.* **2004**, *279*, 8808-8819.

22. Liu, Q.; Guntuku, S.; Cui, X.-S.; Matsuoka, S.; Cortez, D.; Tamai, K.; Luo, G.; Carattini-Rivera, S.; DeMayo, F.; Bradley, A.; Donehower, L.A.; Elledge, S.J. Chk1 is an Essential Kinase that is Regulated by Atr and Required for the G_2/M DNA Damage Checkpoint. *Genes Dev*. **2000**, *14*, 1448-1459.

23. Krämer, A.; Mailand, N.; Lukas, C.; Syljuåsen, R.G.; Wilkinson, C.J.; Nigg, E.A.; Bartek, J.; Lukas, J. Centrosome-associated Chk1 Prevents Premature Activation of Cyclin-B–Cdk1 Kinase. *Nature Cell Biol.* **2004**, *6*, 884-891.

24. Rhind, N.; Russell, P. Chk1 and Cds1: Linchpins of the DNA Damage and Replication Checkpoint Pathways. *J. Cell Sci.* **2000**, *113*, 3889-3896.

25. Bartek, J.; Lukas, J. Chk1 and Chk2 Kinases in Checkpoint Control and Cancer. *Cancer Cell* **2003**, *3*, 421-429.

26. Castedo, M.; Perfettini, J.L.; Roumier, T.; Yakushijin, K,; Horne, D.; Medema, R.; Kroemer, G. The Cell Cycle Checkpoint Kinase Chk2 is a Negative Regulator of Mitotic Catastrophe. *Oncogene* **2004**, *23*, 4353-4361.

27. Erdal, H.; Berndtsson, M.; Castro, J.; Brunk, U.; Shoshan, M.C.; Linder, S. Induction of Lysosomal Membrane Permeabilization by Compounds that Activate p53-independent Apoptosis. *Proc. Natl. Acad. Sci. U.S.A.* **2005**, *102*, 192-197.

28. Garber, K. New Checkpoint Blockers Begin Human Trials. *J. Nat. Can. Inst.* **2005**, *97*, 1026-1028.

29. Dai, Y.; Rahmani, M.; Pei, X.Y.; Khanna, P.; Han, S.I.; Mitchell, C.; Dent, P.; Grant, S. Farnesyltransferase Inhibitors Interact Synergistically with the Chk1 Inhibitor UCN-01 to Induce Apoptosis in Human Leukemia Cells Through Interruption of Both Akt and MEK/ERK Pathways and Activation of SEK1/JNK. *Blood*, **2005** *105*, 1706-1711.

30. Hutchins, J.R.A.; Hughes, M.; Clarke, P.R. Substrate Specifcity Determinants of the Checkpoint Protein Kinase Chk1. *FEBS Lett.* **2000**, *466*, 91-95.

31. Chapman, E.; Wong, C.H.; A pH Sensitive Colorometric Assay for the High-Throughput Screening of Enzyme Inhibitors and Substrates: A Case Study Using Kinases. *Bioorg. Med. Chem.* **2002**, *10*, 551-555.

32. Suganuma, M.; Kawabe, T.; Hori, H.; Funabiki, T.; Okamoto, T. Sensitization of Cancer Cells to DNA Damage-induced Cell Death by Specific Cell Cycle G_2 Checkpoint Abrogation. *Cancer Res.* **1999**, *59*, 5887-5891.

33. Fields, C.G.; Lloyd, D.H.; Macdonald, R.L.; Otteson, K.M.; Noble, R.L. HBTU Activation for Automated Fmoc Solid-Phase Peptide Synthesis. *Peptide Res.* **1991**, *4*, 95-101.

34. Pipkorn, R.; Boenke, C.; Gehrke, M.; Hoffmann, R. High-throughput Peptide Synthesis and Peptide Purification Strategy at the Low Micromol-scale Using the 96-well Format. *J. Peptide Res.* **2002**, *59*, 105-114.

35. Bayer, E.; Eckstein, H.; Hägele, K.; König, W.A.; Brüning, W.; Hagenmajer, H.; Parr, W. Failure Sequences in the Solid Phase Synthesis of Polypeptides. *J. Am. Chem. Soc.* **1970**, *92*, 1735-1738.

36. Robbins, J.C., Whatman Inc., personal communication.

37. Shults, M.D.; Imperiali, B. Versatile Fluorescence Probes of Protein Kinase Activity. *J. Am. Chem. Soc.* **2003**, *125*, 14248-14249.

VIII. Appendix

^{1}H and ^{13}C NMR spectra are included on the following pages for all purified natural products reported in the previous chapters.

Stelliferin riboside (**2.6**)

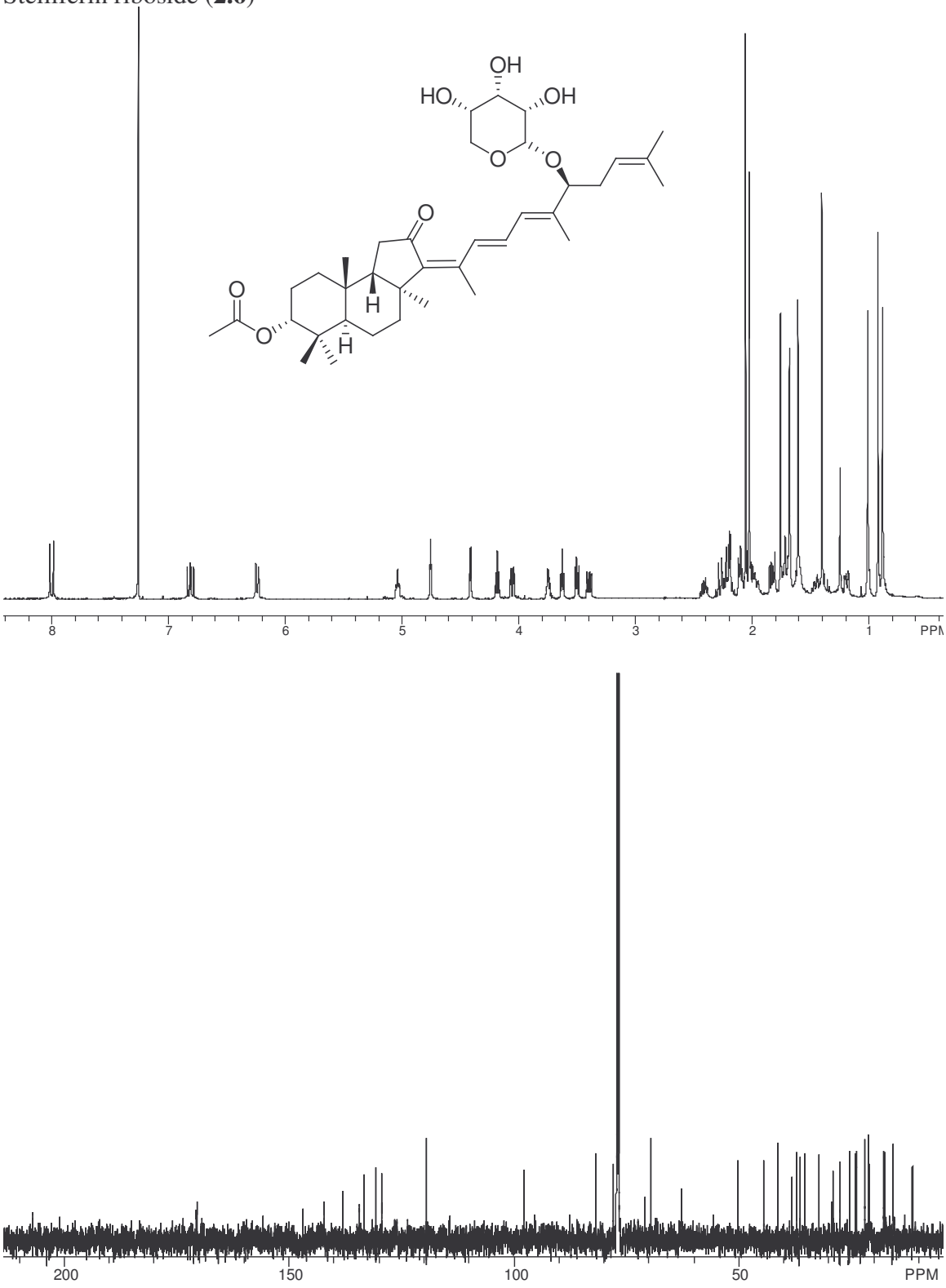

3-*epi*-29-acetoxy-stelliferin E (**2.7**)

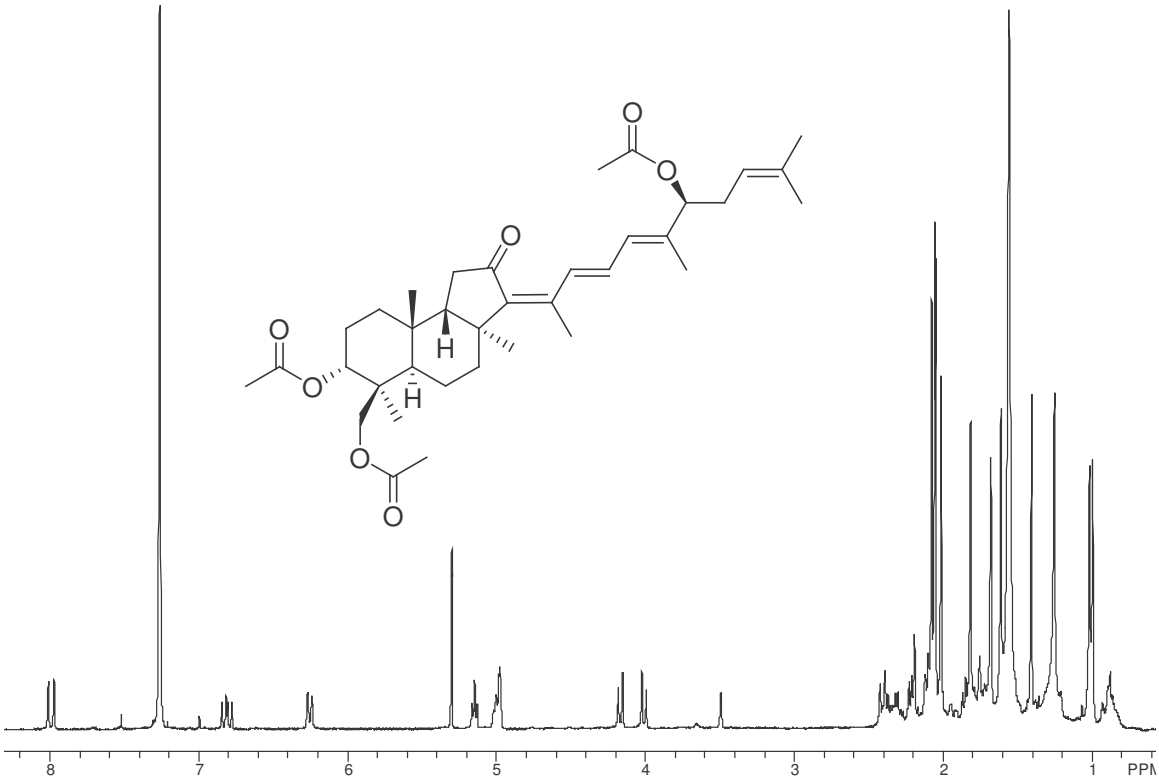

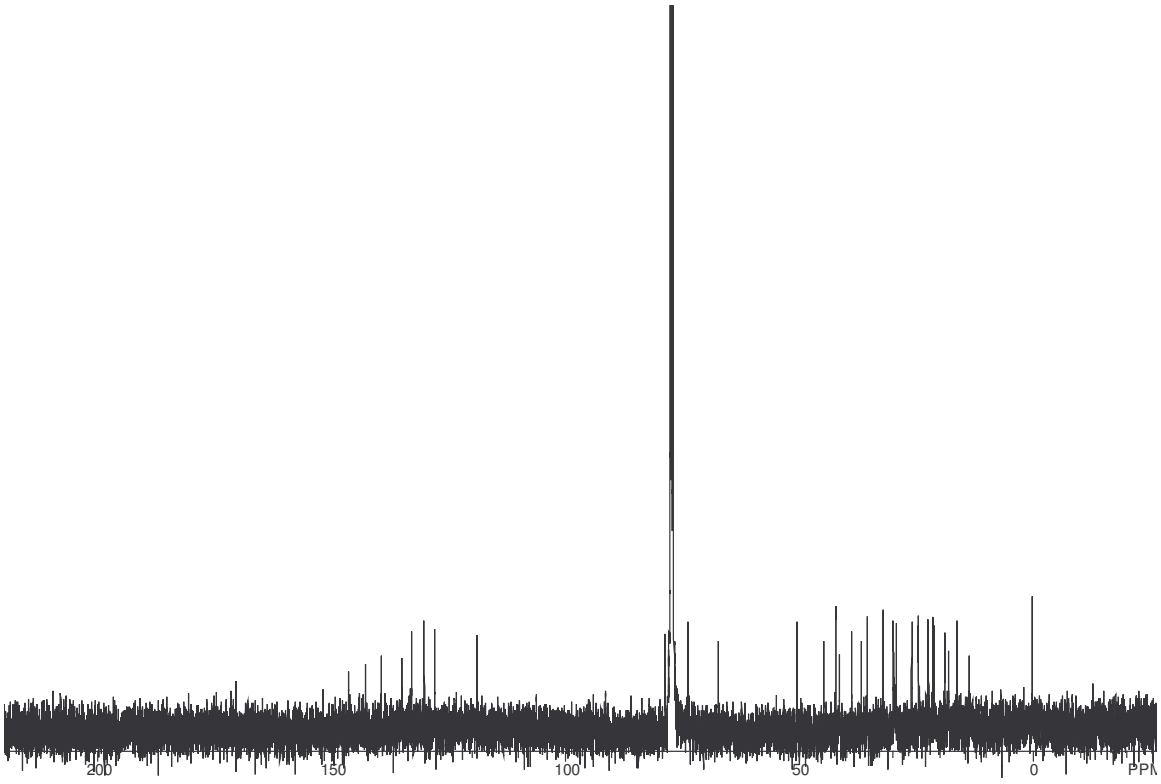

Stellettin J (**2.8**)

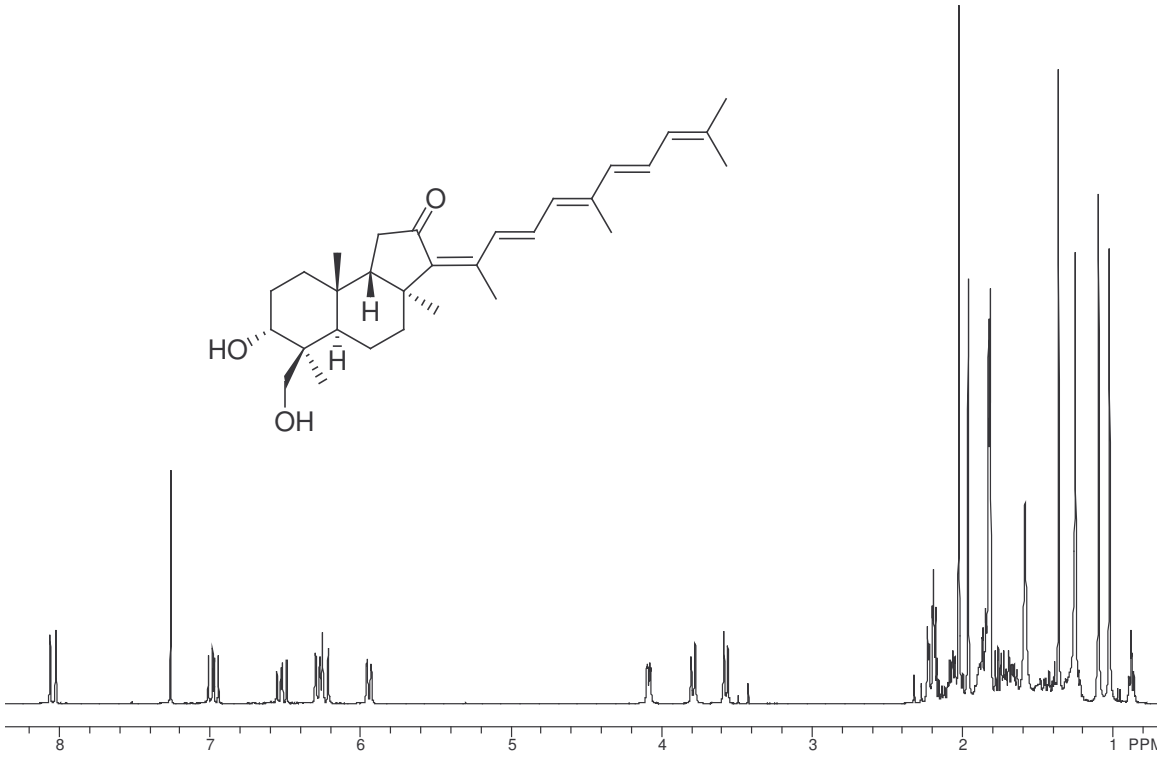

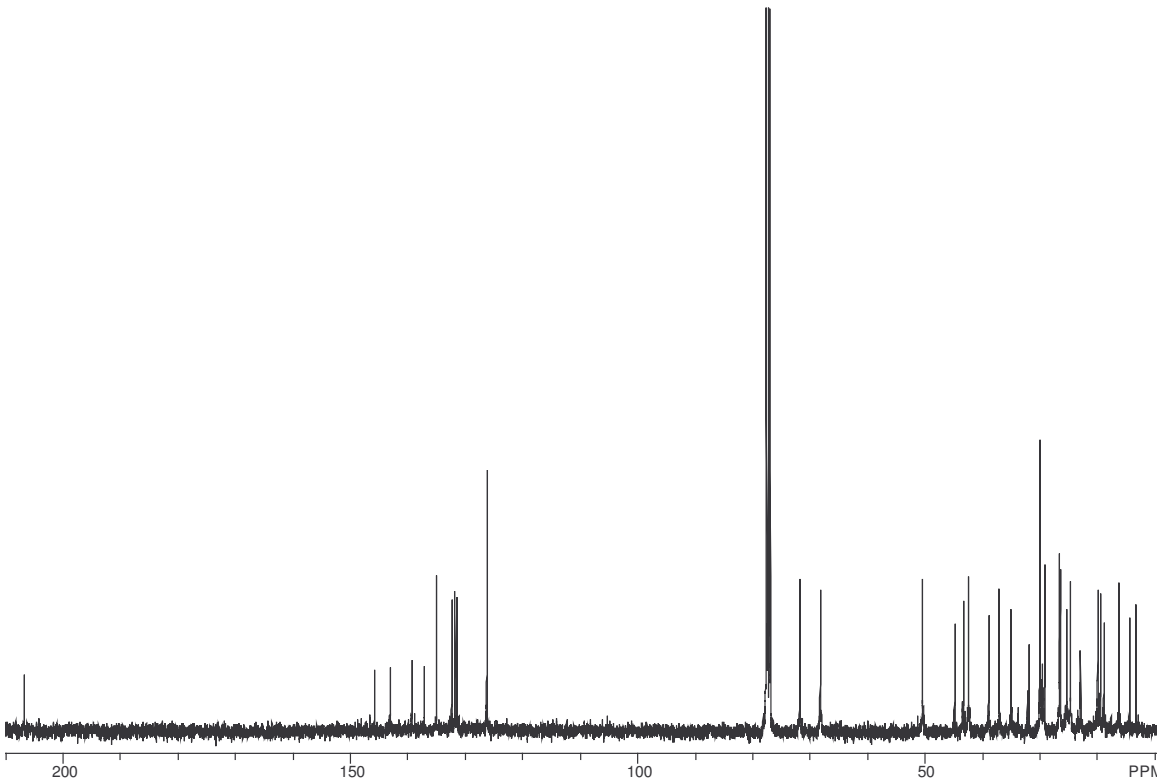

Stellettin K(**2.9**)

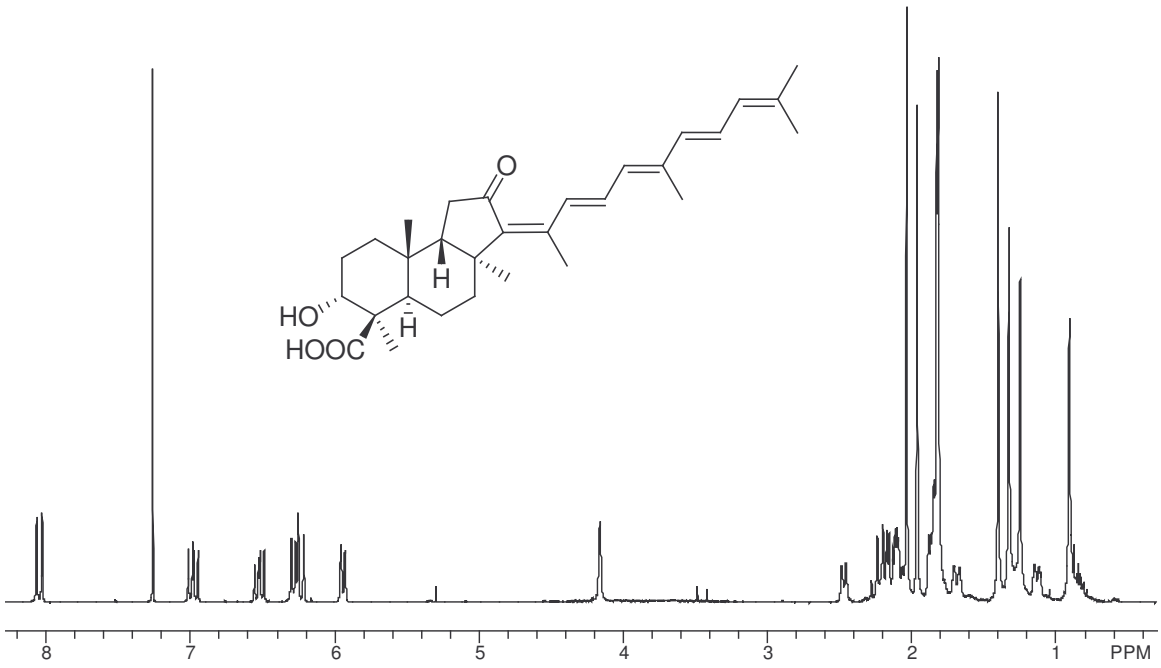

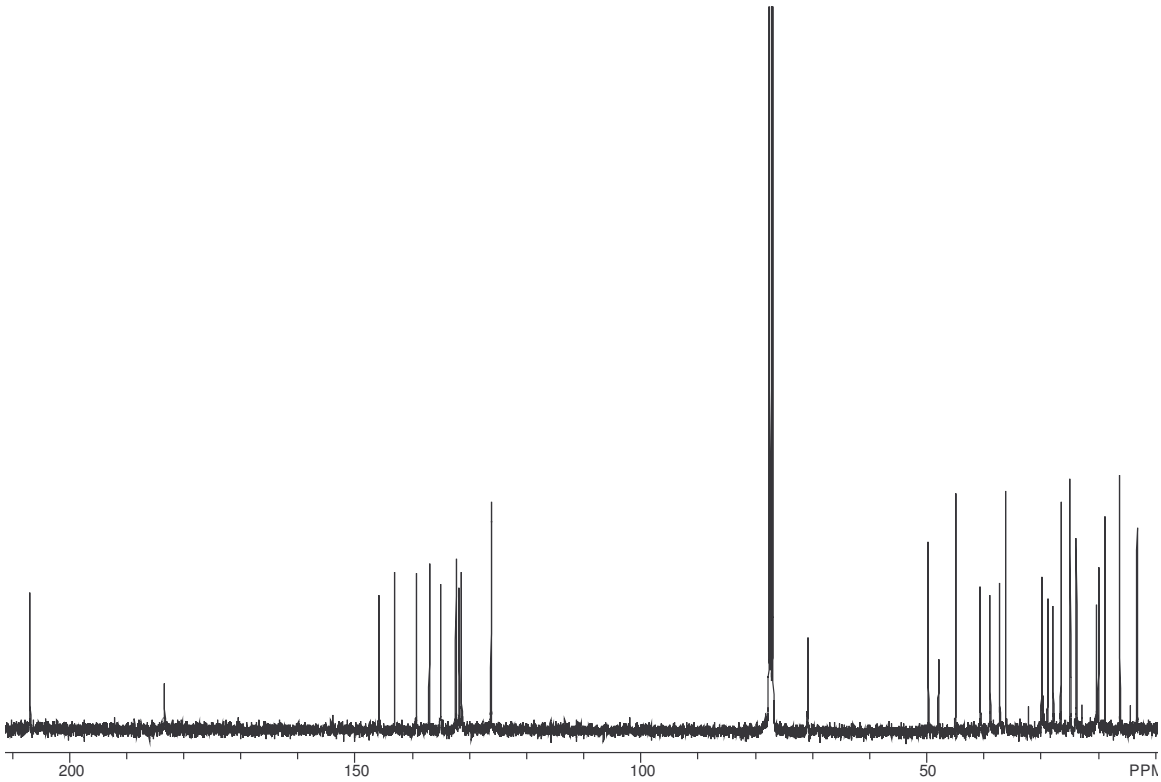

Heteronemin (**3.8**)

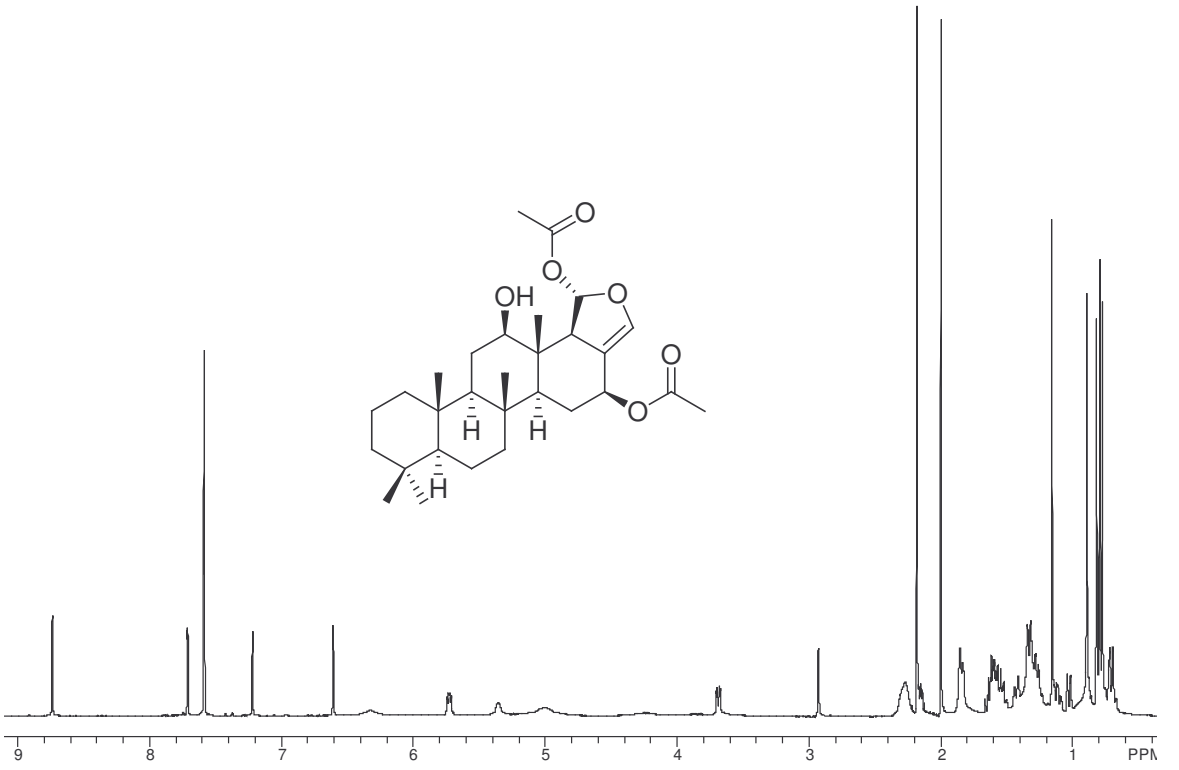

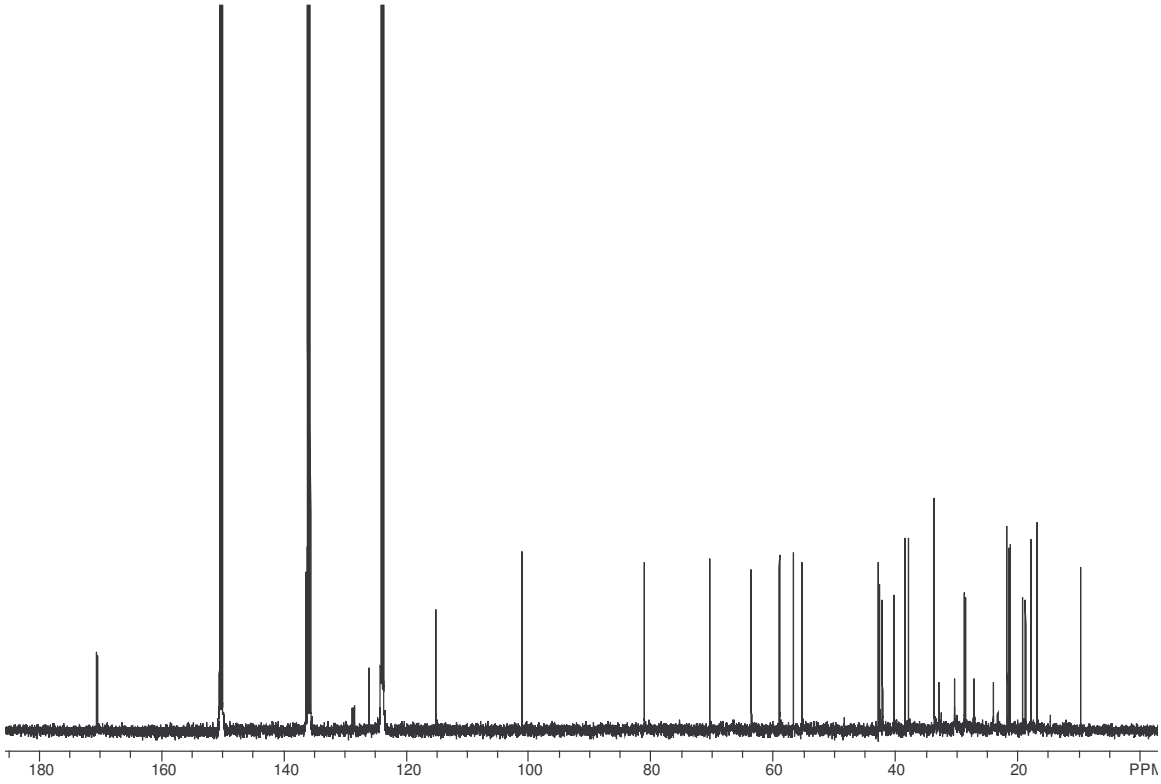

Heteronemin acetate (**3.12**)

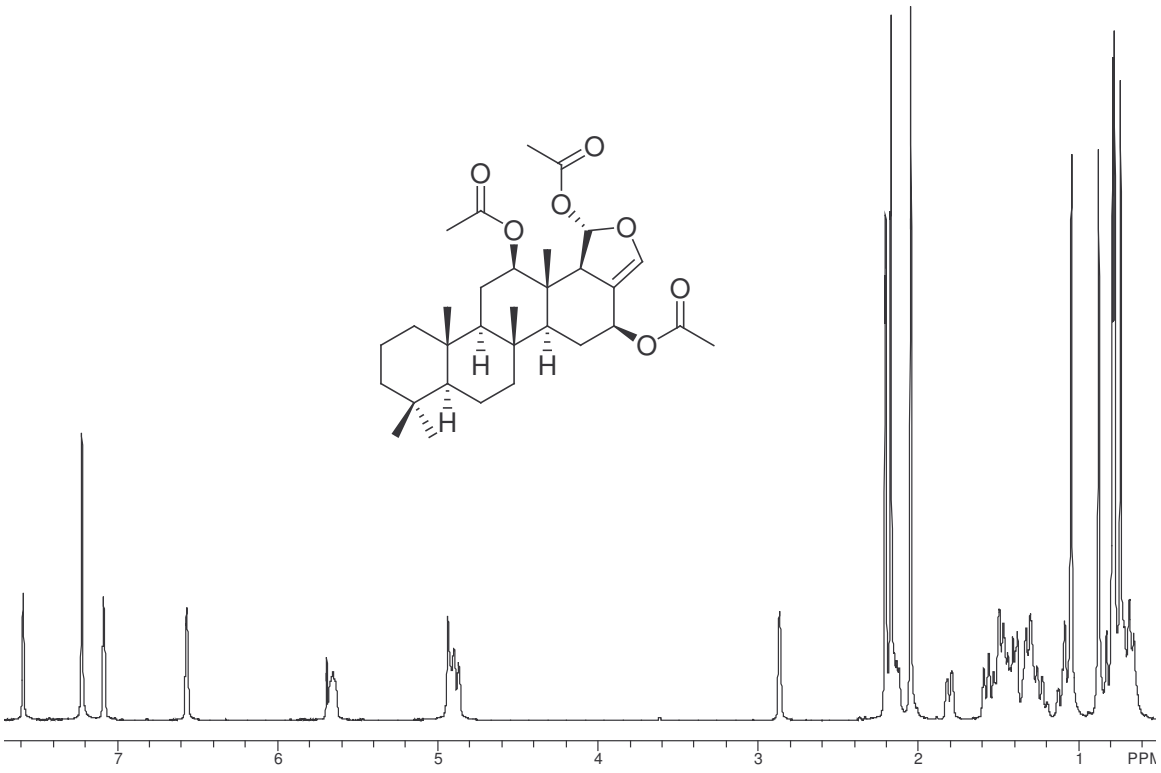

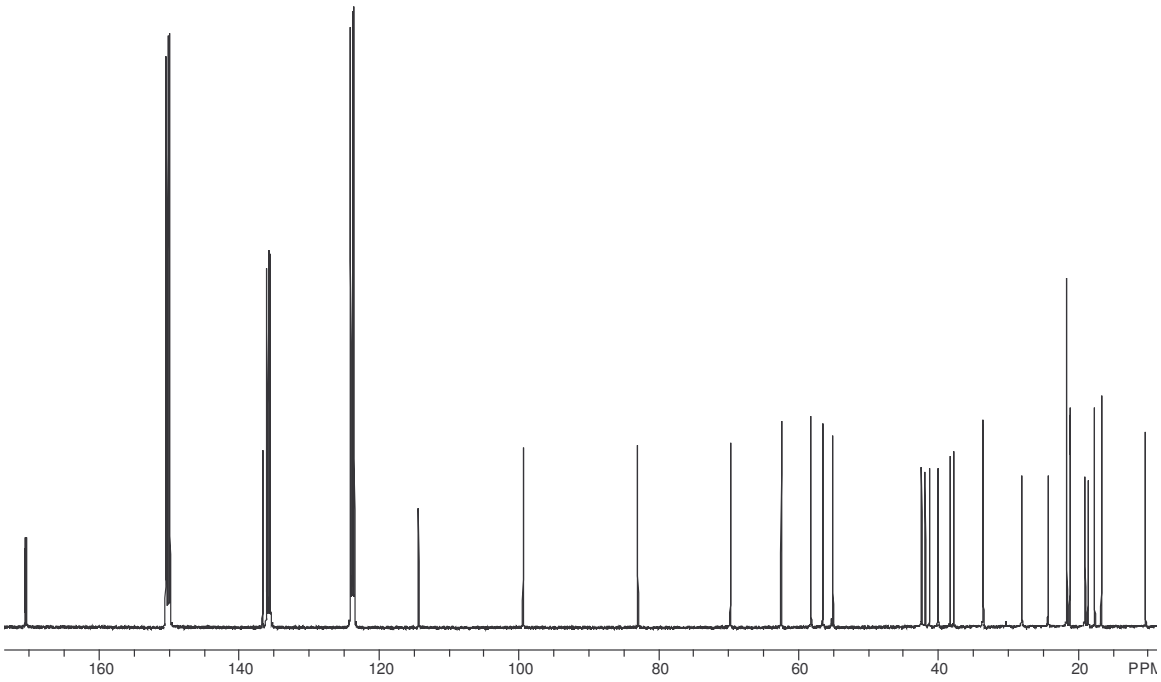

Heteronemin ketone (**3.13**)

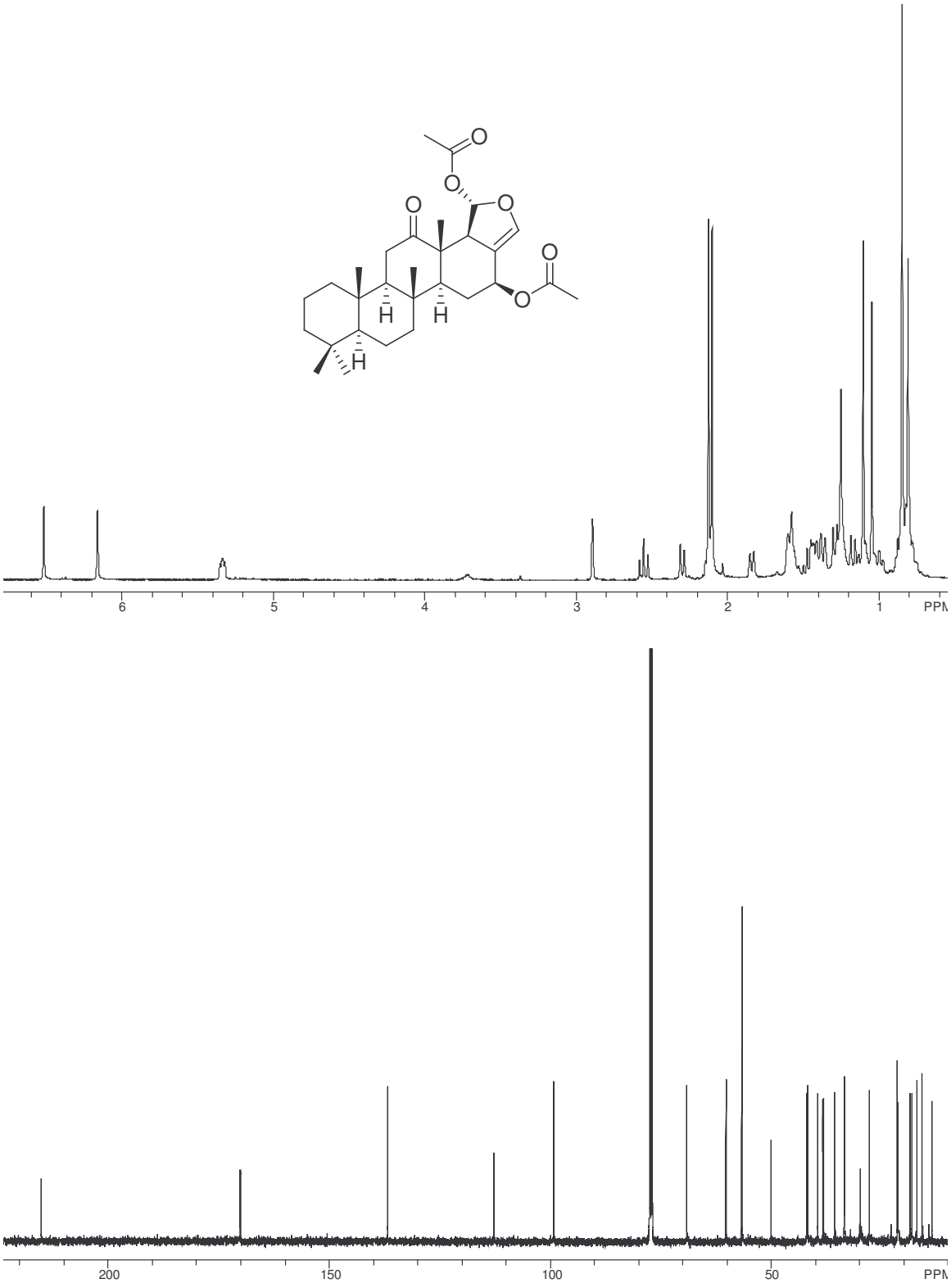

12-Deacetyl-12,18-diepiscalaradial (**3.14**)

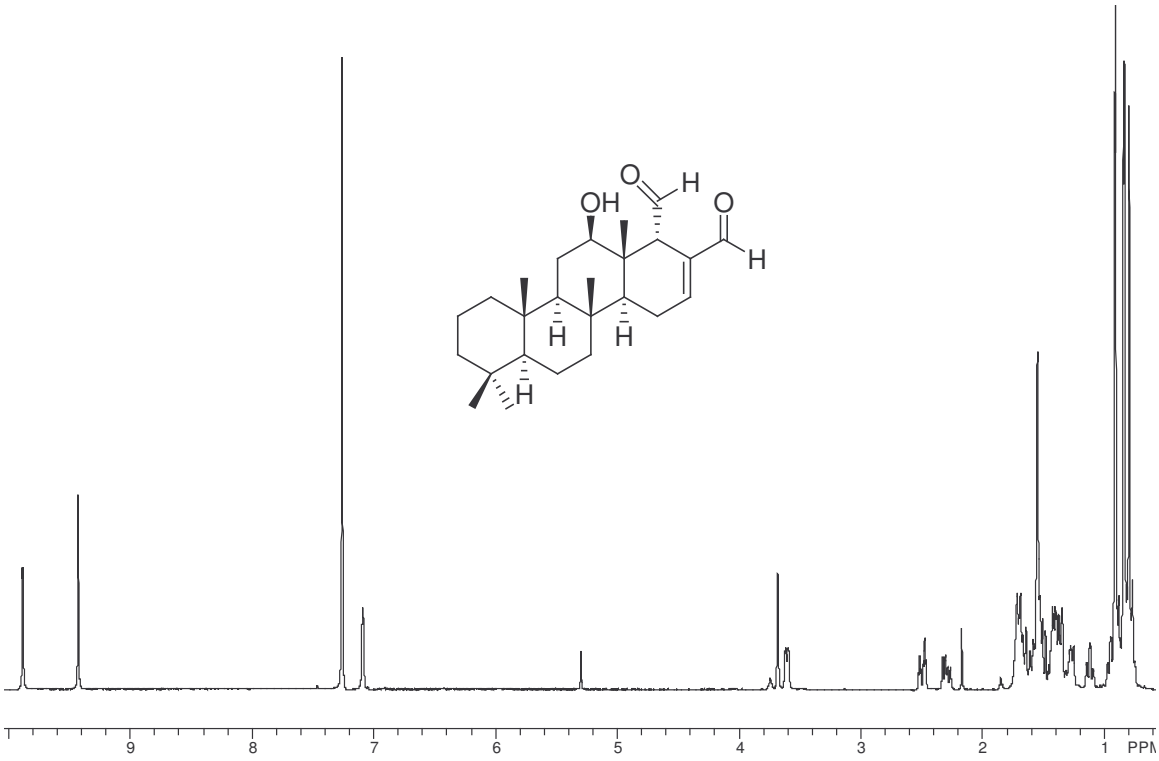

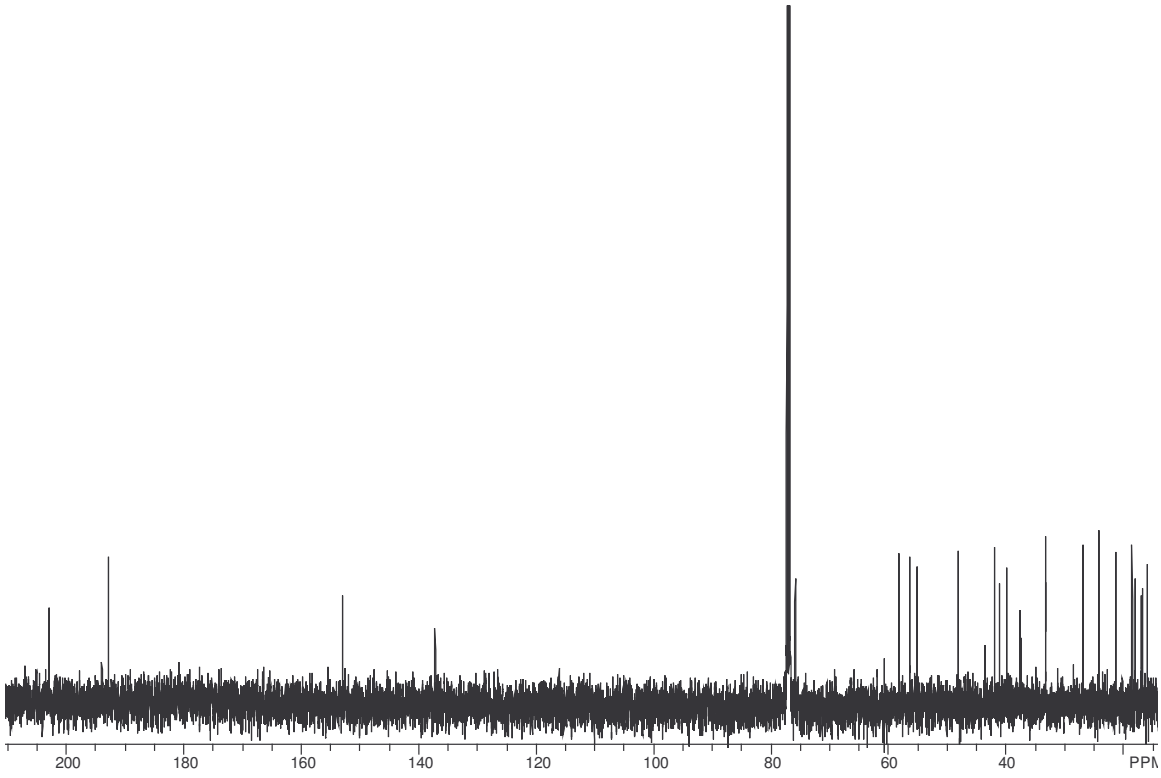

15,16-Dehydrosesterstatin 3 (**3.15**)

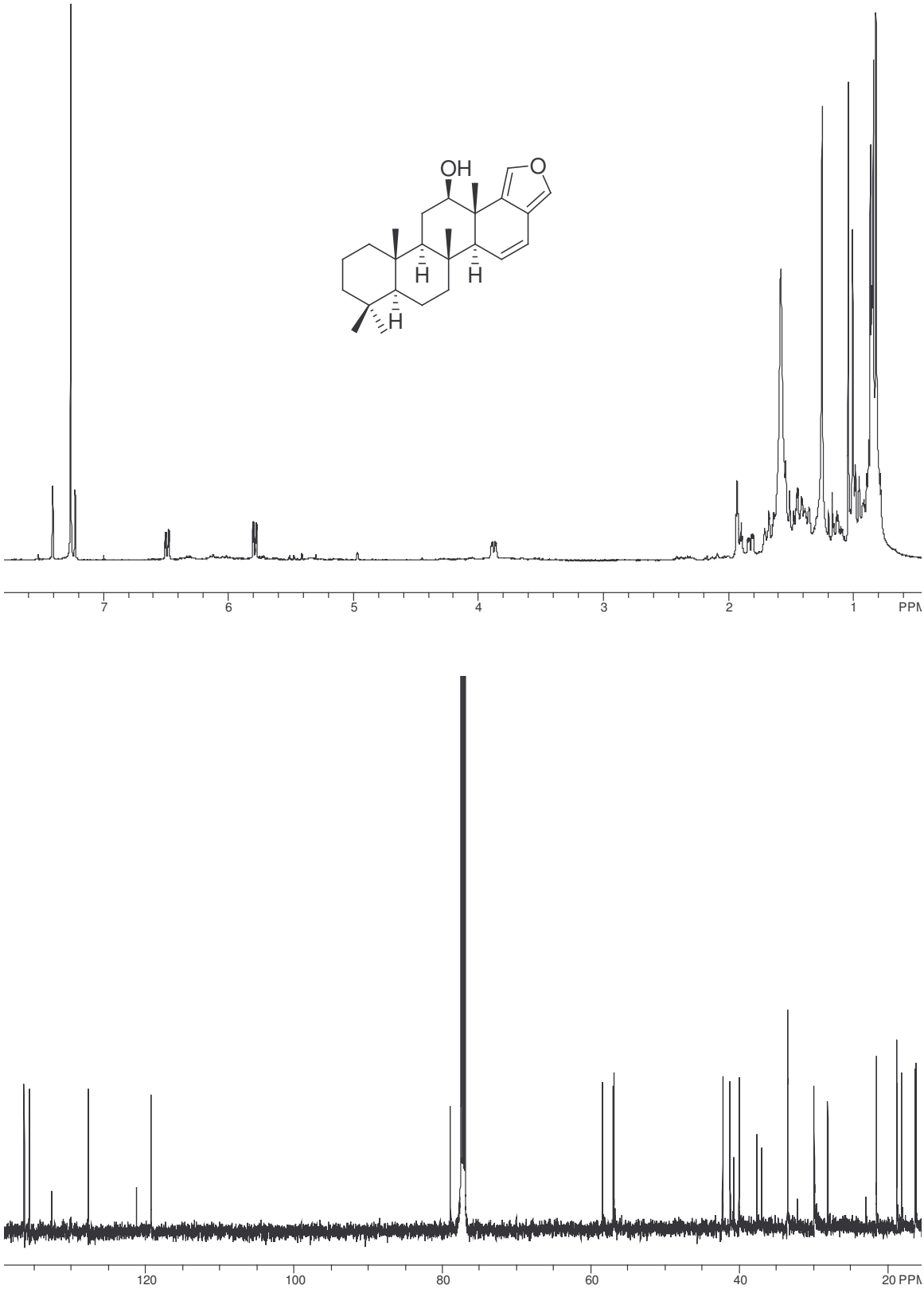

Mixture of Sulfated triterpenoids (**4.2** and **4.3**)

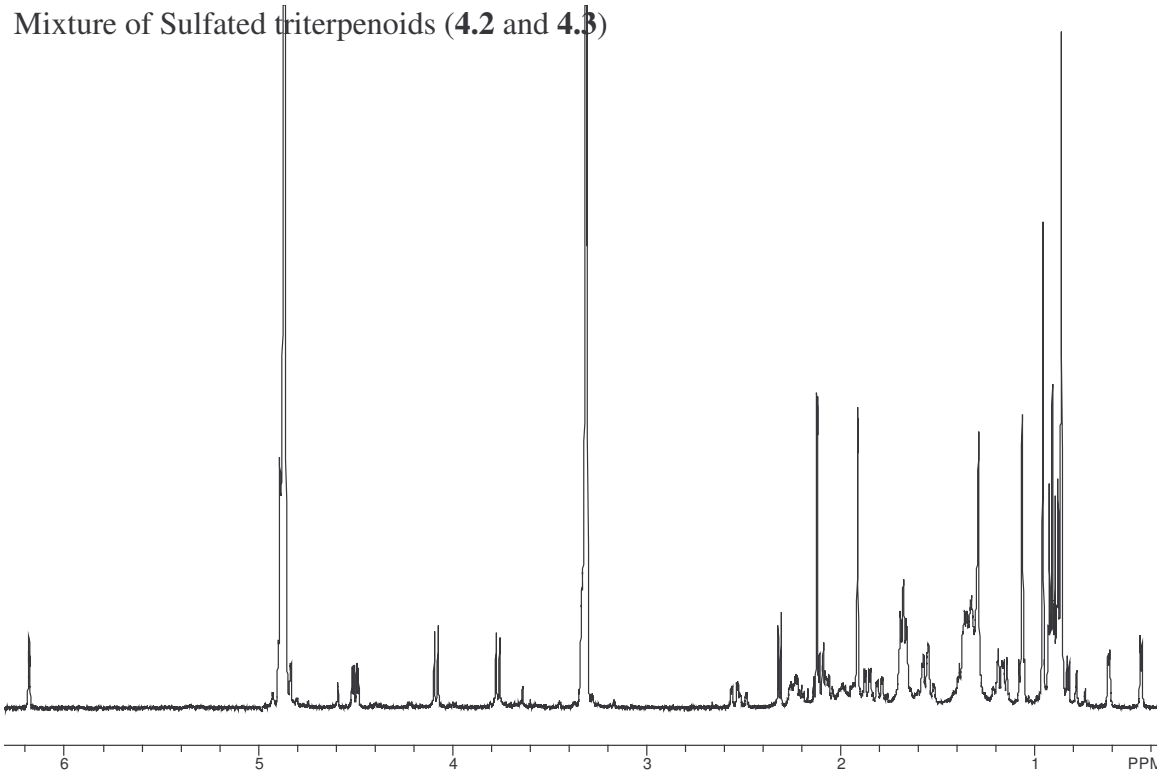

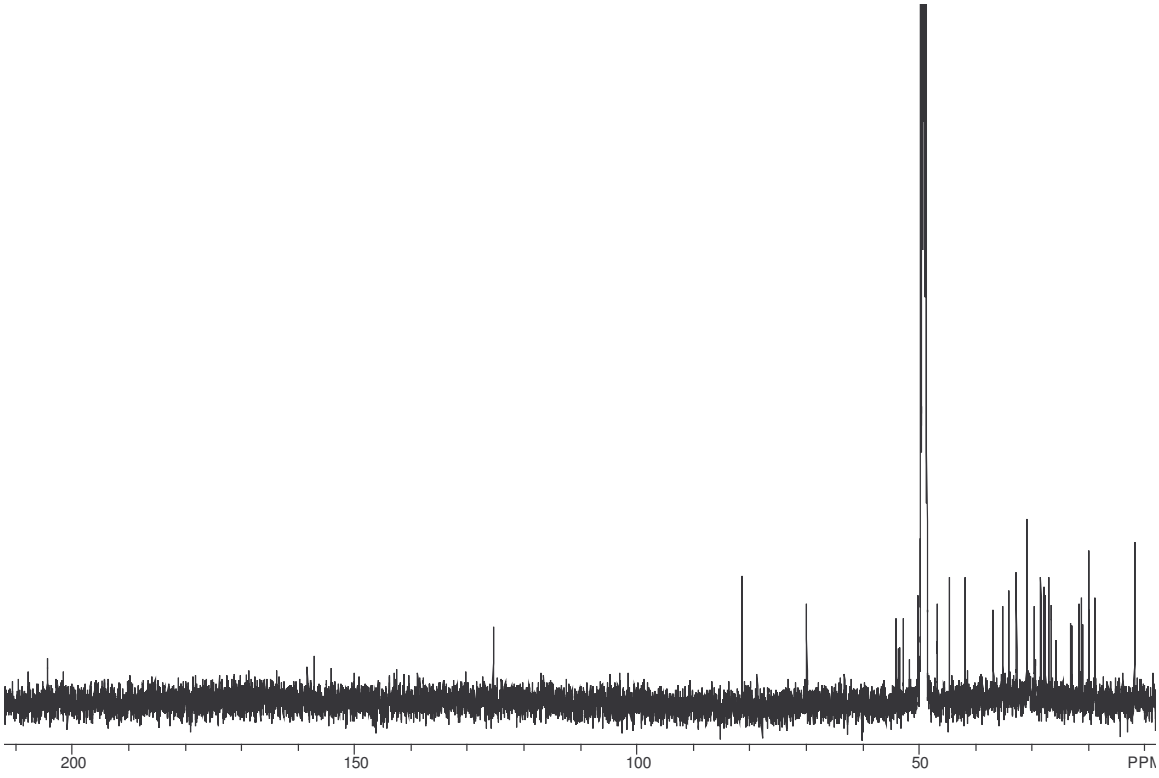

Oleanolic acid (**5.2**)

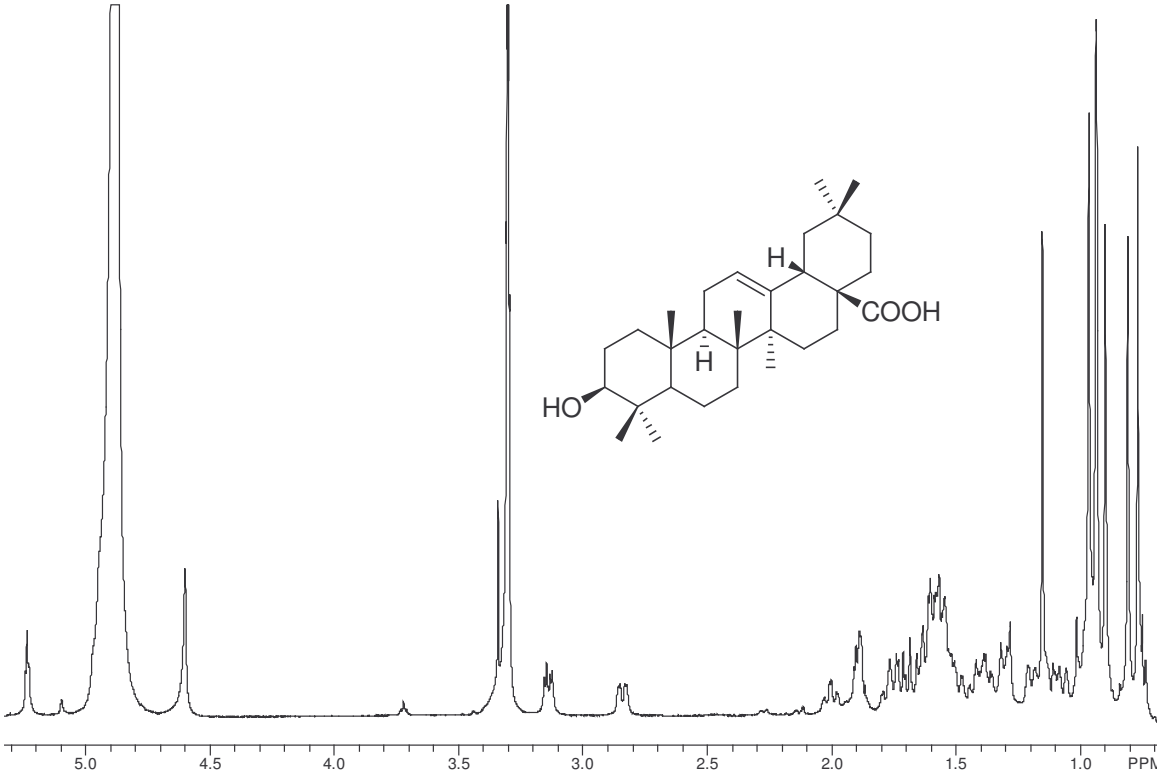

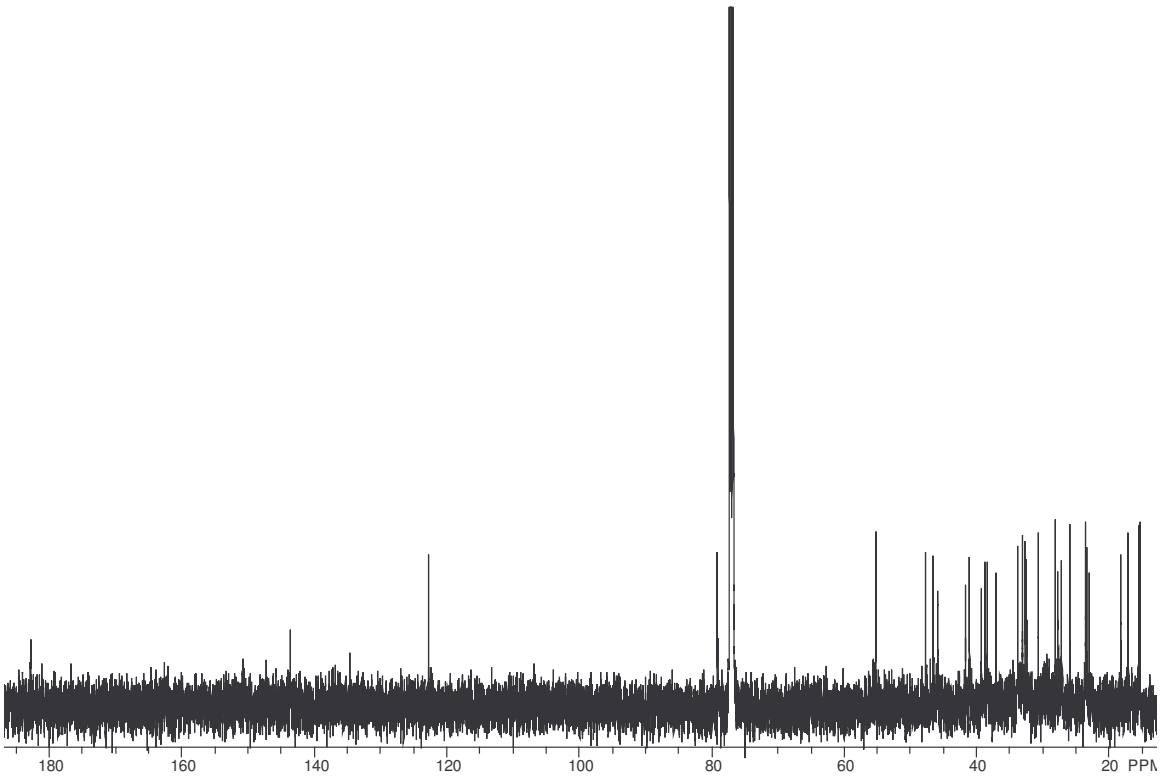

3-*O*-*p*-(*E*)-coumaroyloleanolic acid (**5.3**)

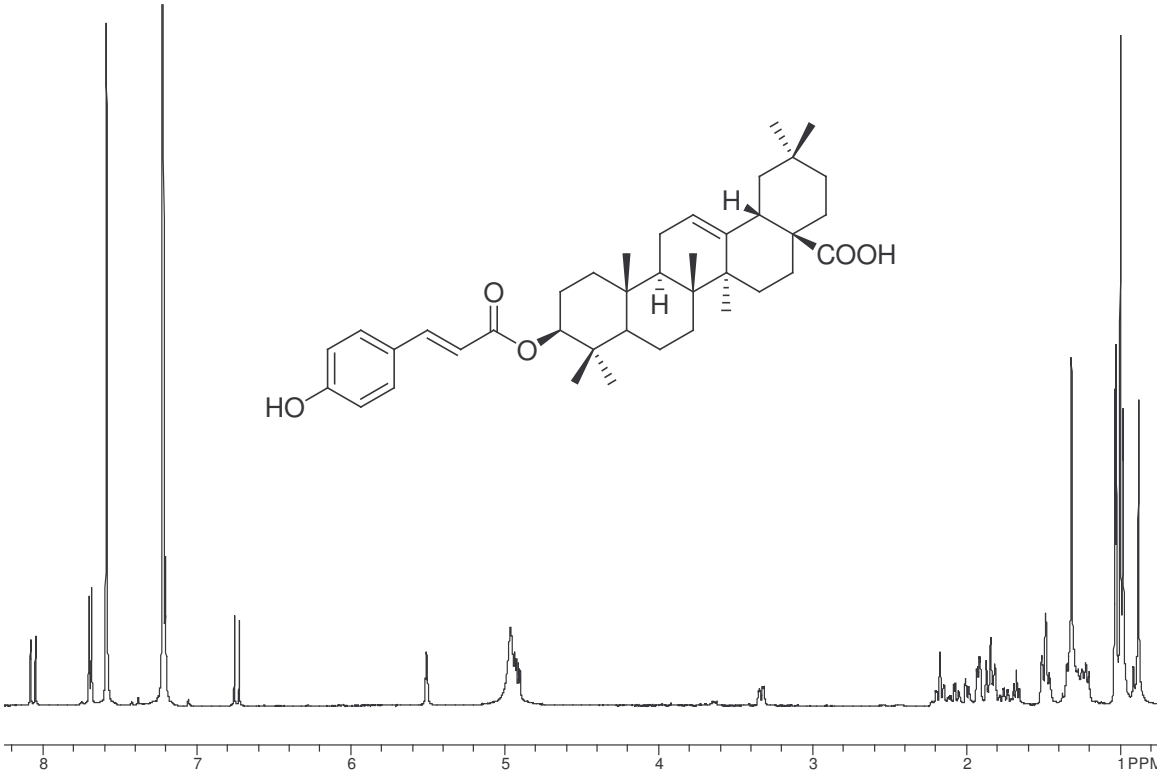

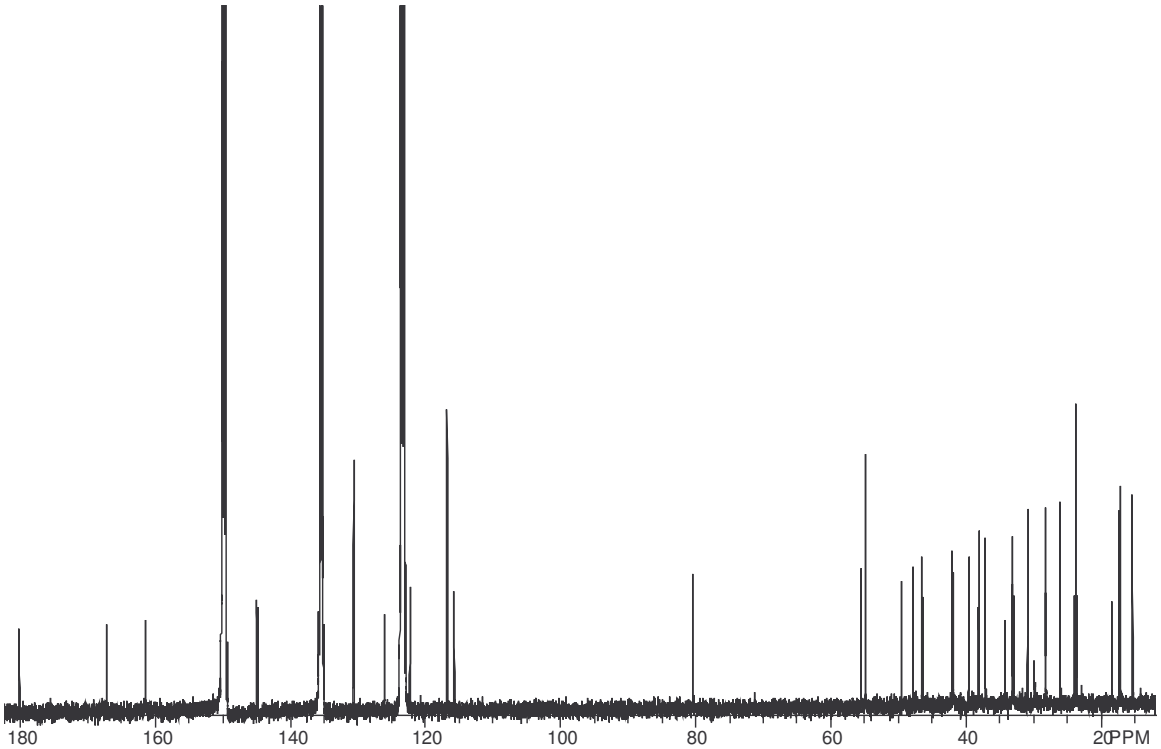

3-*O*-(*E*)-feruloyloleanolic acid (**5.4**)

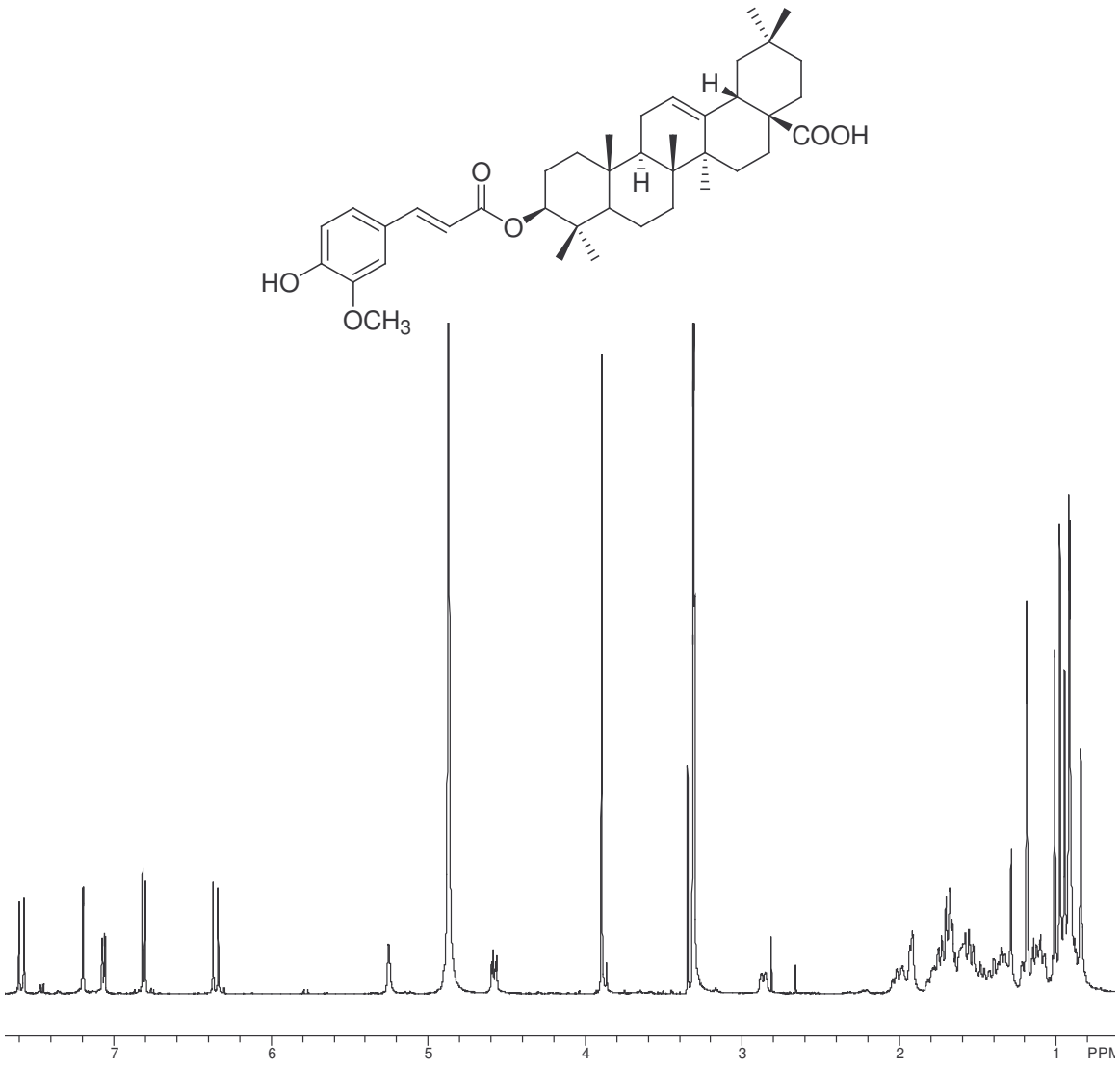

Vita

Jason Anderson Clement was born in Shelby, NC on March 12, 1978, to Carol T. and Ronald J. Clement, Sr., and he was raised in Lincolnton, NC. Jason graduated second in his class from Lincolnton High School in 1996. As a National Merit Scholarship finalist in 1996, Jason received a full scholarship to attend Western Carolina University in Cullowhee, NC. Jason performed research as an undergraduate, working with Dr. Royce S. Woosley in quantifying the volatile terpenoid contents of Canadian and Carolina Hemlock trees found in western North Carolina and in the Shenandoah Valley of Virginia. Jason graduated summa cum laude from Western Carolina University in 2000 with a B.S. in chemistry.

In 2000, Jason received a Cunningham Fellowship from the Department of Chemistry at Virginia Polytechnic Institute and State University (Virginia Tech), and he entered graduate studies there in chemistry. Jason worked in the laboratory of Dr. David G.I. Kingston studying potential antitumor natural products. In 2005, he received a Graduate Research Award from the Department of Chemistry at Virginia Tech, and he was awarded his Ph.D. that same year.

Jason is a member of the American Chemical Society (organic section), Phi Kappa Phi, Phi Lambda Upsilon, and he was a founding member of the Graduate Christian Fellowship at Virginia Tech. Jason is married to Dr. Ella C. Clement, and they have a daughter, Anna I. Clement.